SUPERIOR COURT OF WASHINGTON FOR KING COUNTY

RYAN M. PSZONKA, et al.,	
	No. 14-2-18401-8 SEA
Plaintiffs,	
	EXPERT OPINION REPORT OF
v.	DR. MARVIN R. PYLES, Ph.D., P.E.
SNOHOMISH COUNTY, et al.,	DR. J. DAVID ROGERS, Ph.D., P.E., P.G., C.E.G., C.HG.
Defendants.	DR. JONATHAN D. BRAY, Ph.D., P.E., NAE
TIM WARD, et al.	DR. ARNE SKAUGSET, Ph.D., R.P.F.
Plaintiffs,	DR. RUNE STORESUND, D.Eng., P.E., G.E.
v.	DR. GUNNAR SCHLIEDER, Ph.D., R.G., C.E.G.
SNOHOMISH COUNTY, et al.,	
Defendants.	JUNE 30, 2016
GREGORY REGELBRUGGE, et al.,	
Plaintiffs	
v.	
STATE OF WASHINGTON, et al.,	
Defendants	

1) Executive Summary

This report presents our expert opinions with respect to the SR 530 Landslide litigation. This report is part of a series of reports that chronicled the progress of the expert team, assembled by the Attorney General (AG) of Washington, to understand the cause(s) of the SR 530 Landslide (State of WA Expert Team). We previously prepared a preliminary report in May of 2015 and an interim report in January 2016.

The State of Washington Expert Team expresses condolences to all the families who lost loved ones in the tragic March 22, 2014 SR 530 Landslide event. The State Route (SR) 530 Landslide of March 22, 2014 (SR 530 Landslide) was a slope failure of unparalleled proportions in the United States. A major motivation of our in-depth investigation was to identify opportunities to advance the state of the practice so that lessons learned from this tragedy may help improve our societal ability to leverage our available methods, personnel, and financial resources to help prevent catastrophic losses like this from occurring in the future.

Our opinions are based on a review of previously available published information, execution of a site-specific subsurface exploration program, installation of site-specific instrumentation, a suite of geotechnical laboratory tests, extensive geologic field mapping at the site, and engineering analyses. Based on our site-specific evaluations, we present these opinions:

A. Forest management activities on Whitman Bench in the vicinity of the SR 530 Landslide did not produce a significant difference in throughfall during water year 2014 and, therefore, were not causative factors of the SR 530 Landslide.

B. Precipitation falling on Whitman Bench is hydrologically disconnected from the SR 530 Landslide in space and time and, therefore, was not a causative factor of the landslide.

C. The crib wall and settling pond were not causative factors of the SR 530 Landslide.

D. The geologic complexity of the SR 530 Landslide site precluded any reasonable predictability of the timing of a long-runout landslide within the perspective of a human lifetime.

E. The presence or absence of the 2006 debris field does not make a material difference in the runout of the SR 530 Landslide.

1   We are confident in the opinions that we express herein. However, the compressed schedule dictated

2   by the court has necessitated that much of our work be fast-tracked. As a result, this opinion report

3   should not be considered a final report. We have not yet achieved an objective set forth by the

4   Attorney General; which is to develop an unequivocal determination of the causation of the SR 530

5   Landslide. From a public policy perspective, we see continuing this work and preparation of a future

6   final report as important to the people of the State of Washington.

7

8

9

2) Table of Contents

15

16

1 **APPENDICES**

2

3 APPENDIX A – Precipitation Summary and Throughfall on Whitman Bench

4 APPENDIX B – Field Exploration

5 APPENDIX C – Geotechnical Instrumentation

6 APPENDIX D –Geotechnical Laboratory Testing

7 APPENDIX E – Engineering Properties of Soils

8 APPENDIX F – SR 530 Landslide Geologic Mapping & Cross Sections

9 APPENDIX G – Tree Displacement Mapping

10 APPENDIX H – Avulsion Analyses

11 APPENDIX I – Groundwater Evaluations

12 APPENDIX J – Slope Stability Studies

13 APPENDIX K – Runout Evaluations

14 APPENDIX L – J. David Rogers Declaration

15 APPENDIX M – Standard of Care

3) Nature of Involvement

The members of the expert team that prepared this report were retained by the State of Washington's Attorney General Office to formulate expert opinions in relation to the following questions associated with the State Route (SR) 530 Landslide that occurred on March 22, 2014:

1. The causation of the SR 530 Landslide;
2. The predictability of the SR 530 Landslide in the time frame of pertinent DNR FPA approvals;
3. The predictability of the runout of the SR 530 Landslide; and
4. The impact of pertinent DNR approved timber harvests on the Whitman Bench with regard to the causation of the SR 530 Landslide.

4) Credentials and Compensation

Please refer to our previous reports for our credentials and compensation.

Since our last report, we have added the expertise of Dr. Kenichi Soga. Dr. Kenichi Soga is Chancellor's Professor at the University of California, Berkeley. He obtained his BEng and MEng from Kyoto University in Japan and PhD from the University of California at Berkeley. He was Professor of Civil Engineering at the University of Cambridge before joining UC Berkeley in 2016. He has published more than 300 journal and conference papers and is co-author of "Fundamentals of Soil Behavior, 3rd edition" with Professor James K Mitchell. His current research activities are Infrastructure sensing, performance based design and maintenance of underground structures, energy geotechnics, and geotechnics from micro to macro. He is a Fellow of the UK Royal Academy of Engineering and a Fellow of the Institution of Civil Engineers. He is recipient of many awards including George Stephenson Medal and Telford Gold Medal from the Institution of Civil Engineers and Walter L. Huber Civil Engineering Research Prize from the American Society of Civil Engineers. He is compensated at a rate of $250/hr for review/consultation and $450/hr for testimony at trial/deposition.

5) Plaintiff Contentions

The Plaintiffs have put forth a suite of theories and hypotheses. The State of WA Expert Team extracted those theories as best they could be interpreted from the submitted complaints and stated them as hypotheses in the June 1, 2015 preliminary report (1) and our January 22, 2016 Interim Report (2). Subsequent to our Interim report (2), Plaintiffs introduced additional expert reports that presented a

1 new hypothesis that the presence of the 2006 debris field (and settling pond) as a result of the

2 construction of the crib wall, exacerbated the magnitude of the runout such that without the presence

3 of the 2006 debris field, the landslide runout would have been limited to the North Fork of the

4 Stillaguamish River.

5

6 Table 1 presents a summary of our interpretation of the Plaintiff contentions and highlights which

7 Plaintiff Expert addresses each contention. These contentions, as interpreted by the State of WA Expert

8 Team, include:

9

10   A. [Throughfall]   The increase in precipitation throughfall as a result of forest management

11   results in a direct increase in groundwater that destabilized the SR 530 Landslide;

12   B. [Seepage] The SR 530 Landslide failure mechanism was driven by unconfined gravitational

13   seepage emanating from an increase in precipitation throughfall;

14   C. [Erosion]   Erosion by the North Fork of the Stillaguamish River at the toe of the SR 530

15   Landslide foot destabilized the slope, which resulted in the SR 530 Landslide;

16   D. [Ponds] Construction of settling ponds at the foot of the SR 530 Landslide, for the purposes

17   of reducing sediment input to benefit fisheries, destabilized the slope, resulting in the SR

18   530 Landslide;

19   E. [Foreseeable] Stability analyses performed before the SR 530 Landslide, with subsurface

20   information available at the time, demonstrated, within the standard of practice, that the

21   landslide was going to occur and endanger the Steelhead Haven neighborhood; and

22   F. [2006 Debris] The continued presence of the 2006 debris fan (and settling pond) as a result

23   of the construction of the timber crib wall, exacerbated the magnitude of the runout such

24   that without the presence of the 2006 debris field, the landslide runout would have been

25   limited to the North Fork of the Stillaguamish River.

26
27

1 *Table 1: Summary of Plaintiff Contentions and contributing Plaintiff Experts*

Expert	Plaintiff Contentions					
	A: Throughfall	B: Seepage	C: Erosion	D: Pond	E: Foreseeable	F: 2006 Debris
Benoit, Jean	N.A.	N.A.	✓	✓	✓	✓
Bolton, Susan	N.A.	✓	N.A.	N.A.	N.A.	N.A.
Flowers, Gary	✓	✓	✓	✓	✓	✓
Hungr, Oldrich	N.A.	N.A.	N.A.	N.A.	✓	N.A.
Link, Timothy	✓	✓	N.A.	N.A.	N.A.	N.A.
Loaiciga, Hugo	✓	✓	N.A.	N.A.	N.A.	N.A.
McShane, Dan	N.A.	✓	✓	✓	✓	✓
Pitre, Christian	✓	✓	N.A.	N.A.	N.A.	N.A.
Porter, Michael	N.A.	N.A.	N.A.	N.A.	✓	N.A.
Sias, Joan	✓	✓	N.A.	N.A.	N.A.	N.A.
Stevenson, Matt	N.A.	N.A.	N.A.	N.A.	N.A.	N.A.
Tompkins, Mark	N.A.	N.A.	✓	✓	N.A.	N.A.

2 (N.A.) No statement relative to the respective plaintiff's contention; (✓) Statement made relative to the respective

3 plaintiff's contention.

4

5 While a number of Plaintiff experts submitted reports, not all experts opined directly on causation,

6 runout consequences, or foreseeability of the event (runout distance and timing). Table 2 summarizes

7 our understanding of which Plaintiff Expert explicitly addresses SR 530 Landslide (a) evaluation of

8 causation; (b) consequences associated with the landslide runout once the slide has been 'triggered,'

9 and (c) the foreseeability of the SR 530 Landslide.

10

11 *Table 2: Plaintiff Expert Opinion Mapping*

Expert	SR 530 Causation	SR 530 Runout	SR 530 Foreseeability
Benoit, Jean	N.A.	✓	✓
Bolton, Susan	N.A.	N.A.	N.A.
Flowers, Gary	cites Loaiciga	N.A.	N.A.
Hungr, Oldrich	✓	✓	✓
Link, Timothy	N.A.	N.A.	N.A.
Loaiciga, Hugo	✓	N.A.	N.A.
McShane, Dan	N.A.	✓	✓
Pitre, Christian	N.A.	N.A.	N.A.
Porter, Michael	N.A.	✓	✓
Sias, Joan	N.A.	N.A.	N.A.
Stevenson, Matt	N.A.	N.A.	N.A.
Tompkins, Mark	N.A.	N.A.	N.A.

12 (N.A.) No statement relative to the SR 530 Landslide; (✓) Statement made relative to the SR 530 Landslide.

1

As noted in our previous reports, the Hazel Landslide is a different landslide complex from the SR 530 Landslide (Figure 1). The pre-existing Hazel Landslide was constrained to the eastern portion of the SR 530 Landslide, and had been active, at a minimum, for decades. It emanated from a much lower elevation profile (its upper surface being near El. + 700 feet), and consisted primarily of prehistoric landslide debris from an older, and much larger, landslide complex. The SR 530 Landslide which included Hazel Landslide debris, extended to the west and north of the limits of the Hazel Landslide, with its upper surface at a much higher elevation (~El. +890 feet). The majority of the soils involved were intact prior to the failure of March 22, 2014, not having experienced any previous landslide disturbance. These two landslides appear to have different footprints, different soil compositions, different groundwater regimes, and were mechanistically different.
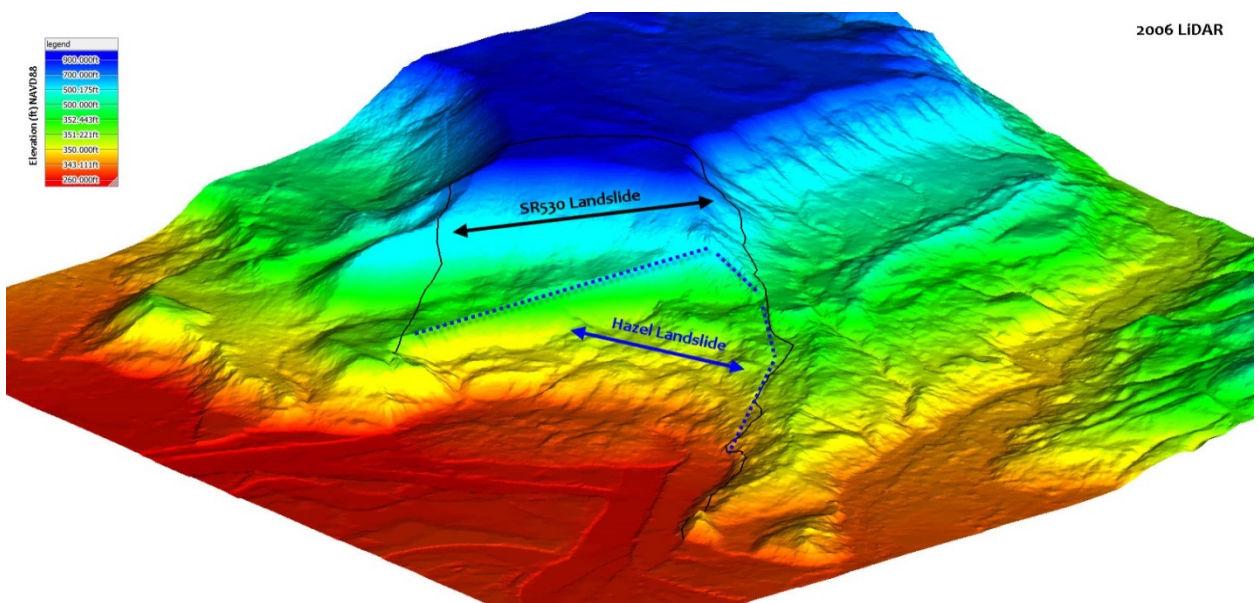
Figure 1: Overview of Hazel Landslide complex vs. SR 530 Landslide.

6) SR 530 Landslide Investigation Program

Our site-specific characterization programs included an extensive evaluation of topography (1951-present), geology, geomorphic site changes, historical aerial imagery review, subsurface seepage, weather, geologic field mapping, subsurface exploration, geotechnical laboratory testing, instrumentation (rain gages, inclinometers, vibrating wire piezometers), and engineering analyses. Our work focused on Whitman Bench as well as within the main body of the 2014 SR 530 Landslide. Unfortunately, we were not authorized to access the debris field south of the North Fork of the Stillaguamish River and north of SR 530. The general timeline of our work is summarized in Table 3.

1

Table 3: Timeline of State of WA Expert Team Investigation

Investigation Activities	Time Period
Rainfall instrumentation	November 2014 – June 2016
Field exploration planning	May 2015 – July 2015
Field exploration & field mapping	July 2015 – December 2015
Subsurface Instrumentation	August 2015 – June 2016
Geotechnical laboratory testing	August 2015 – June 2016
Groundwater analyses	January 2016 – June 2016
Slope stability analyses	May 2016 – June 2016
Runout analyses	May 2016 – June 2016
Final Expert Report	June 2016

6.1 Throughfall Instrumentation

Twenty eight rain gauges were installed to quantify the rainfall on the Whitman Bench and the throughfall under the different aged forest stands. The rain gauges were all Onset RG 3 tipping bucket rain gauges with a six inch orifice and a resolution of 0.01 inches of rainfall. Each rain gauge was mated with a HOBO Pendant event data logger. The rain gauges were installed by attaching them to metal 'T' fence posts with two hose clamps. The rain gauges were installed so that the orifice was level and, nominally, 4.5 feet above the ground.

Twenty four rain gauges were installed in three transects of eight rain gauges each. Each transect was located in a different age class of stand in the vicinity of the scarp of the SR 530 landslide (Figures A-1 through A-4). The transects were located parallel to the edges of the forest stands and, nominally, a distance of three tree heights into the stand from the forest edge. The first rain gauge in each transect was located a random distance between 0 and 50 feet from an arbitrarily chosen starting point. Each subsequent gage was installed at an interval of 50 feet. The first 21 rain gauges, seven gages in each of the three transects, were installed on November 20, 2014. An eighth rain gauge was added to each transect on December 4, 2014.

Four rain gauges were installed in a recent clearcut approximately 1 ½ miles north of the slide scarp (Figure A1-A4). These rain gauges were installed in the open and measured gross rainfall, not throughfall or net rainfall. These rain gauges were installed to allow the gross rainfall on Whitman Bench to be

referenced to other area rain gauges such as the rain gauges at Oso, Arlington, and Darrington. The first rain gauge was installed on November 20, 2014. A second rain gauge was installed on December 4, 2014. Two subsequent rain gauges were installed on April 20, 2015.

6.2   Field Exploration Planning

The field exploration program was generally outlined in May of 2015 and envisioned a series of exploratory borings on Whitman Bench, borings in Upper Headache Creek Basin, and borings within the main body of the SR 530 Landslide. Site reconnaissance efforts were conducted in June and July 2015 to identify potential access routes onto the body of the SR 530 Landslide. The Attorney General's office arranged, in conjunction with the Washington Department of Transportation (WSDOT), to access Whitman Bench and the main body of the slide. Authorization to access the slide area for subsurface exploration was not granted until July 2015. Our field exploration program began immediately upon available access to the site.

6.3   Field Exploration & Mapping

6.3.1   Subsurface Exploration

Drilling for subsurface exploration began on Whitman Bench in mid-July 2015. Simultaneous drilling by two drill rigs shifted to the main body of the slide in mid-September 2015 and continued through early October 2015. Drilling activities included in-situ soil testing (Cone Penetration Tests and SPT blow counts, etc.), subsurface soil sampling, installation of vibrating wire piezometers (for measurements of piezometric head), and installation of slope inclinometer casings (to record slope movements). Drilling with one drill rig resumed on Whitman Bench following completion of drilling on the main body of the SR 530 Landslide in October 2015 and was completed in December 2015.

As-completed locations are shown in Figure 2 and summarized in Table 4. Note that Figure 2 also shows the location of H-1vwp-14, which was a deep exploratory boring completed by WSDOT in 2014, prior to initiation of this field exploration program.

1 *Table 4: Summary of exploration points for SR 530 Landslide*

Boring Location	Exploration Point	Ground Elev (ft)*	Boring Depth (ft)	Start Date	End Date
EB-01	EB-01vwp-15	865.34	129.7	7/24/2015	7/26/2015
EB-01	CPT-01-15	~865.5**	32.6	7/27/2015	7/27/2015
EB-02	EB-02vwp-15	867.40	594.0	10/15/2015	12/10/2015
EB-02	SP-01vwp-15	~867.4**	116.0	10/13/2015	10/14/2015
EB-03	EB-03vwp-15	890.30	141.4	7/14/2015	7/16/2015
EB-04	EB-04si-15	537.37	281.5	9/16/2015	9/22/2015
EB-04	EB-14vwp-15	537.93	280.0	9/24/2015	9/29/2015
EB-04	CPT-17-15	537.67	157.3	10/1/2015	10/1/2015
EB-05	EB-05si-15	497.08	155.0	10/6/2015	10/8/2015
EB-06	EB-06vwp-15	867.54	279.0	10/27/2015	11/3/2015
EB-07	EB-07si-15	412.25	151.0	10/1/2015	10/2/2015
EB-07	H-18vwp-15	412.37	60.5	10/7/2015	10/7/2015
EB-08	EB-08vwp-15	847.29	240.0	10/20/2015	10/22/2015
EB-09	EB-09si-15	378.94	145.5	9/16/2015	9/18/2015
EB-09	H-13vwp-15	379.53	120.5	9/21/2015	9/23/2015
EB-09	CPT-19-15	378.3	53.3	10/7/2015	10/7/2015
EB-10	EB-10vwp-15	863.32	140.7	7/16/2015	7/21/2015
EB-11	EB-11vwp-15	832.53	76.5	7/22/2015	7/22/2015
EB-12	H-12si-15	438.06	176.0	9/23/2015	9/24/2015
EB-12	H-15vwp-15	437.59	131.0	9/29/2015	9/29/2015
EB-12	CPT-16-15	438.05	100.9	9/30/2015	9/30/2015

*Vertical datum is NAVD88, units of feet (see "osobh102315 revised.xlsx" for WSDOT Survey Results)
**Position not surveyed, but estimated based on adjacent boring location.
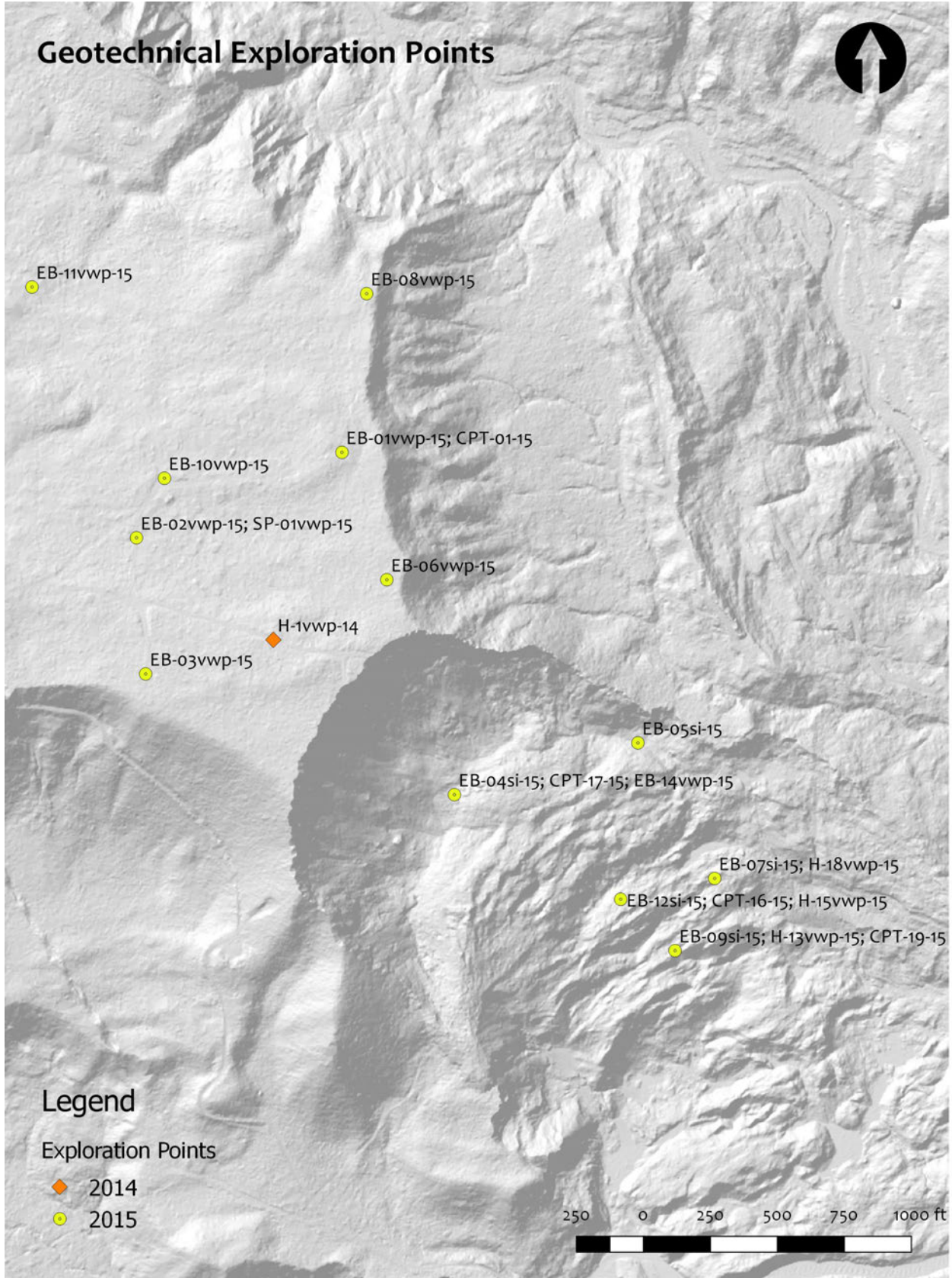
2

Figure 2: Locations of completed exploratory borings and CPTs.

6.3.2　Field Mapping

The interpretation of the regional and more site-specific glacial geology and stratigraphy is based on a diverse suite of information, including remote sensing data, direct field observations, published field observations by others, geologic literature and geologic maps, and personal communication with people familiar with the regional surficial and glacial geology. A detailed discussion of the field mapping activities is presented in Appendix F.

6.3.3　SR 530 Landslide Surface of Rupture

The surface of rupture was found exposed in the lower western portion of the slide source area, and was identified in the borings installed in the slide area. In some of the borings, identification of the location of the surface was unequivocal, as the surface represented the transition from high stratigraphic units (recessional outwash) into much lower stratigraphic units (glacio-lacustrine silt and clay), as shown in Figure 3. In other borings, the determination was made on the basis of an abrupt transition from disturbed/distorted laminae in the fine-grained glacio-lacustrine units to horizontally laminated material. In a few other borings, the determination was more difficult. However, in no case was any evidence of shearing or disruption consistent with the presence of the surface of rupture evident in the materials obtained from below El. +310 feet.

In the exposures in the lower western source area (Figure 4 & Figure 5), the surface of rupture is located on and barely within the Bear Lake Sand, transitioning upslope within a few tens of feet into the lowermost portion of the glacio-lacustrine silt and clay. In some exposures of the SR 530 Slide Surface of Rupture, Recessional Outwash is found on undisturbed Bear Lake Sands or on horizontally laminated fine-grained glacio-lacustrine unit. At other exposures, other stratigraphic units were exposed in contact with the Bear Lake Sands. These exposures were all located above El. +310 feet.

Figure 3: Surface of rupture delineated at contact of recessional sand and glacio-lacustrine silt and clay in boring EB-04si-15.

Surface of Rupture

Native, undisturbed Bear Lake Sands

Surface of Rupture

1
2 *Figure 4: View of surface of rupture exposure with clay shear zone at top of Bear Lake Sands (photo taken on*
3 *10/23/2015 at 48.282N;121.848W, looking SW).*
4

5
6 *Figure 5: View of glacio-lacustrine silt and clay exposure of surface of rupture (photo taken 10/23/2015 at*
7 *48.282N; 121.848W, looking N).*

6.4   Subsurface Instrumentation

Two instrumentation approaches were employed as part of our geotechnical exploration program: groundwater levels based on vibrating wire piezometers (VWP), and slope movement detection using traversing-type inclinometers. Details regarding specific instruments, configuration of data collectors and data transmission, and calibration sheets, are presented in the WSDOT report (3). Weekly updates were extracted from the data logger by WSDOT personnel and then distributed to the State of Washington Attorney General's office to the designated parties (the State of Washington Expert Team being one of those designated parties). Data collection from the inclinometers occurred in October 2015, January 2016, and April 2016.

6.5   Geotechnical Laboratory Testing

Geotechnical analysis of the SR 530 Landslide is an important component to understanding causation. In addition to slope geometry and stratigraphy, soil unit properties, such as unit weight, shear strength, and hydraulic conductivity are necessary components. As the SR 530 Landslide involved cohesionless granular soils as well as cohesive fine grained soils, both field and laboratory testing programs were required. Laboratory tests included index tests, gradation tests, specific gravity tests, consolidation tests on fine grained soils, direct shear tests parallel and perpendicular to soil laminations, triaxial tests in both compression and extension, torsional ring shear tests, and hydraulic conductivity tests. In addition, hydraulic conductivity was inferred from consolidation tests and the consolidation phase of triaxial tests. A catalog of geotechnical testing is presented in Appendix D and laboratory test results are presented in the Appendix D support materials.

7) Conceptual Model of SR 530 Landslide Failure Sequence

Based on the collected site-specific evidence, our expert team developed a working conceptual model of the failure sequence for the SR 530 Landslide. This conceptual model has yet to be fully vetted, but all of our analyses to date support the developed concept. We subdivided the failure area into four movements: M1, M2, M3, and M4. M1 consists of the body of the Hazel Landslide, which is an assemblage of past slide debris, glacio-lacustrine blocks, some disaggregated till blocks, and advance outwash (primarily silt and fine-grained sand). M2 consists of the midslope bench, M3 comprises the Whitman Bench segment, and M4 is the block of till that dropped from the northeast corner of the slide limits. A plan view of the four movement areas is shown in Figure 6. Figure 7 shows a view of the M4
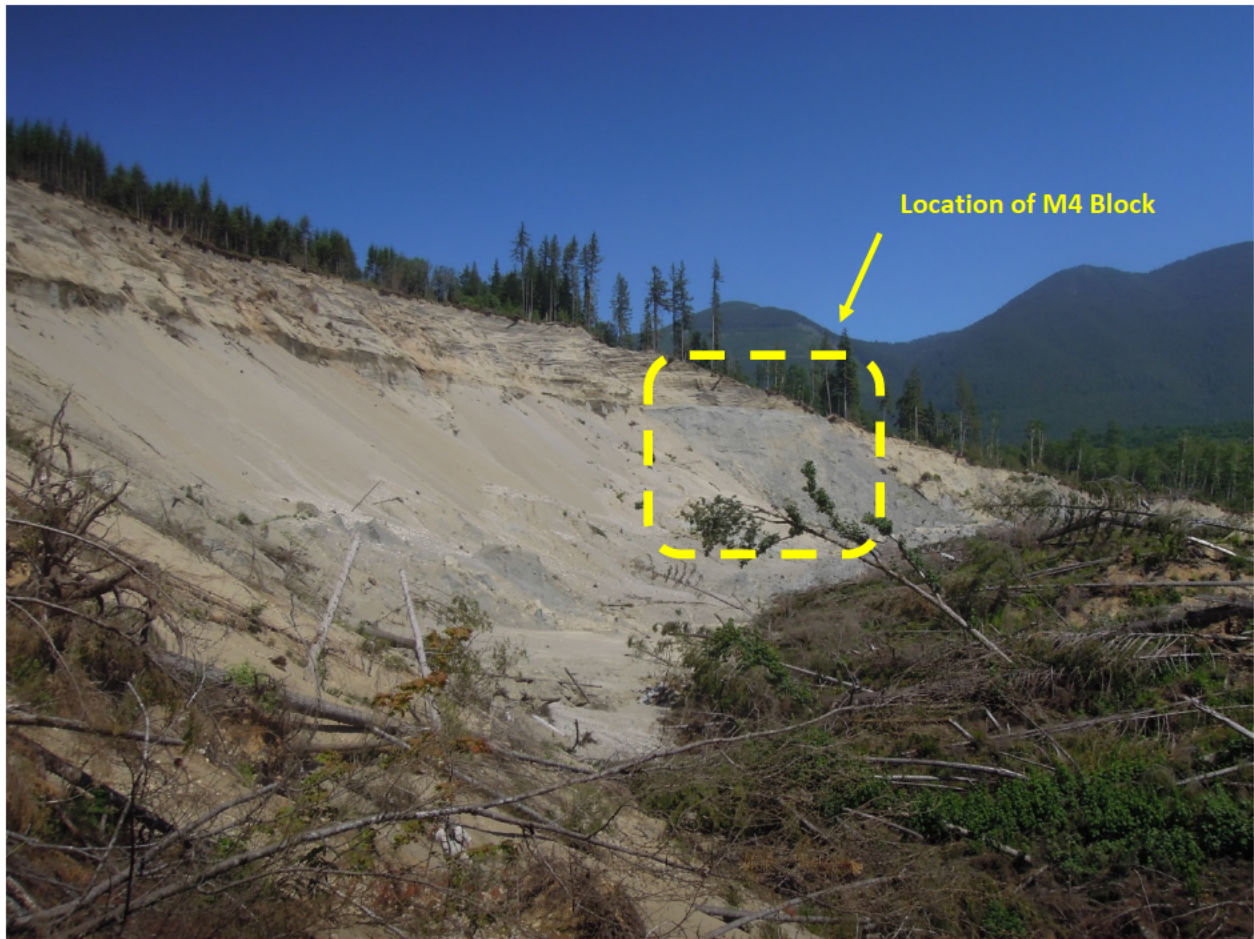
1   block source area looking from the western margins of the slide.   Figure 8 shows a cross-sectional

2   representation of the composition of the four movement sequences.
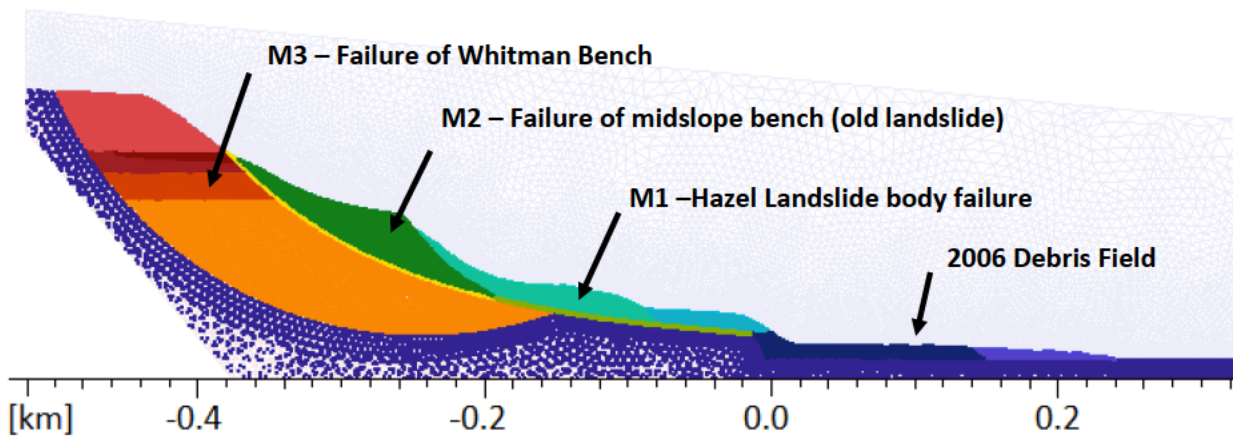
3
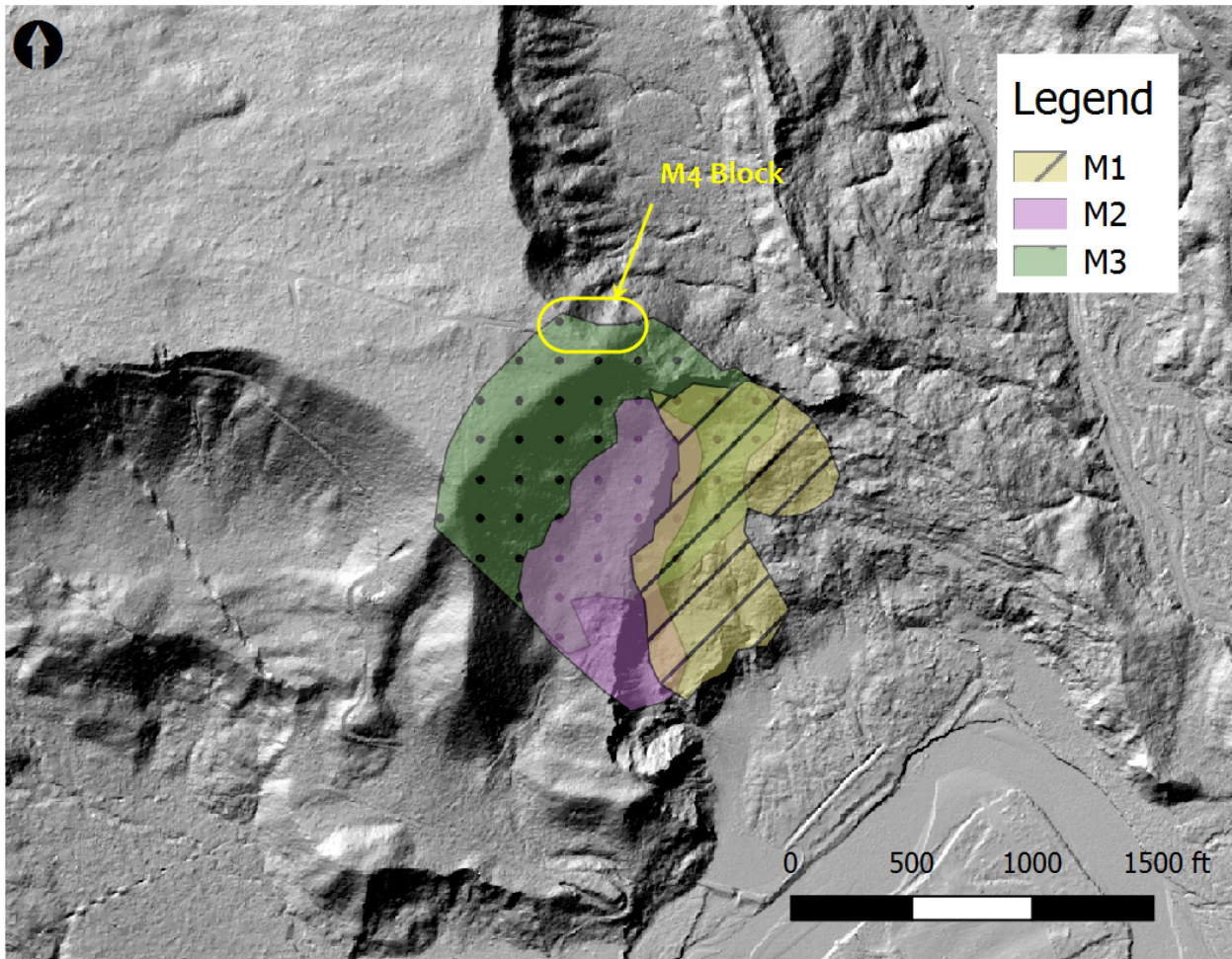
4

5   *Figure 6: Map of conceptual movement sequences M1, M2, M3, and M4.*

1

2   *Figure 7: View towards M4 block, as seen from western margin of the head scarp graben.*

3

4

5   *Figure 8: Overview of SR 530 Landslide movements sequences M1, M2, and M3. Note that M4 is not depicted.*

6

8) Basis for Opinions

Our opinions presented are based on a review of previously available published information, execution of a site-specific subsurface exploration program, installation of site-specific instrumentation, a suite of geotechnical laboratory tests, extensive field mapping at the site, and engineering analyses.

We are confident in the opinions that we express herein. This said, responding to the Attorney General's charge goes well beyond addressing the litigation issues associated with the SR 530 Landslide. The expert team is made up of professionals who have an obligation to our respective professions and to the State's under which we are licensed.

Much of the work necessary to complete the subsurface field exploration, geologic mapping, installation and monitoring of field instrumentation, laboratory testing, interpretation of laboratory test results, and analyses of seepage, stability, and runout of the SR 530 landslide should occur in sequence, with moderate overlap in some cases. The compressed schedule dictated by the court has necessitated that much of this work proceed in parallel, beginning with limited or partial data and numerous parameter estimates. To the degree possible, as data have come on line from one phase of the study, we have entered it into what should have been the next phase, but were in reality, being done in parallel. As a result, this effort should not be considered a final report.

We anticipate continued work to refine the analyses and to ensure correspondence between the various phases of the investigation. We have not achieved an objective put forth by the Attorney General; which is an equivocal determination of the causation of the SR 530 Landslide. Based on the available data, and reasonable inferences from our analyses, we have eliminated a number of the causation hypotheses. However, we have not fully reduced all of the available data and have not identified with sufficient certainty the primary cause(s) of the March 22, 2014 SR 530 Landslide. From a public policy perspective, we see this work and a final report that will be forthcoming important to the people of the State of Washington.

Based on our detailed site-specific evaluations performed to date, we offer the following opinions:

8.1   Precipitation and Throughfall

It is our opinion that in 2014 the difference in throughfall between the different aged stands on Whitman Bench were not significantly different and thus timber harvest on Whitman Bench was not a causative factor for the SR 530 landslide. This opinion is based on the following:

8.1.1   Lack of significant differences in throughfall

In 2004, 8.5 acres of the forest on the Whitman Bench was harvested in a wedge-shaped clearcut and approximately ½ acre of that area became part of the SR 530 Landslide in 2014. Removal of a forest canopy decreases interception, which increases the amount of net precipitation that reaches the forest floor. In 2014, at the time of the SR 530 Landslide, the area was a nine year old, harvest regenerated Douglas-fir forest. As we interpret it, the Plaintiffs contend that the increase in net precipitation to the forest floor due to reduced interception from the nine-year old Douglas-fir forest resulted in an increase in groundwater that was hypothesized to exacerbate the causal factors triggering the SR 530 Landslide.

In order to ascertain the influence of the nine-year old Douglas-fir forest on the SR 530 Landslide, a network of 24 rain gauges were installed in the three different age class forests on the Whitman Bench in the vicinity of the scarp of the SR 530 Landslide. The objective of the rain gauge network was to quantify the magnitude of the throughfall for the three age classes of Douglas-fir forest. The rain gauges were arrayed in three transects of eight rain gauges, one transect for each of the forest age classes. Throughfall was measured at all the gauges throughout the winter rainy season for water years 2015 and 2016.

Throughfall for each of the forest age classes was analyzed using a simple one-way analysis of variance. The parameters analyzed were 21 day and 42 day throughfall duration for Water Year[1] (WY) 15 and WY 16. The analysis of variance showed that for both throughfall parameters and water years the differences in the average throughfall between the different forest age classes were not significantly different. Thus, the clearcut from 2004, which at the time of the SR 530 Landslide was a nine-year old Douglas-fir forest, which had no impact on the amount of throughfall or net precipitation that reached the forest floor on the Whitman Bench in the vicinity of the SR 530 scarp.

---

[1] The term "water year" in reports that deal with surface-water supply is defined as the 12-month period beginning October 1, for any given year through September 30, of the following year (http://water.usgs.gov/nwc/explain_data.html).

These data and analysis are for WY 15 and WY 16. The throughfall values for the different-aged forest classes during March 2014 when the SR 530 Landslide occurred are not known precisely. However, there is no plausible reason to believe that a similar analysis for the 2014 water year would yield a different outcome than the outcomes calculated for WY 15 and WY 16. Thus, there is no compelling reason to believe that the 2004 clearcut on the Whitman Bench had any impact on the SR 530 Landslide. A detailed analysis of the data is presented in Appendix A.

8.1.2 March 2014 was not an extreme precipitation month

The ruling hypothesis for landslide events is that they are initiated by rainfall. It stands to reason that an extreme event like the SR 530 landslide would be assumed to be initiated by extreme rainfall. No long term rain gauge was available at the location of the SR 530 landslide so the rain gauge at Darrington (data available at www.climate.washington.edu/maps/maps.php) was used to evaluate rainfall for the SR 530 landslide. The 21- and 42-day duration rainfall for the Darrington rain gauge on March 22, 2014 was 15.79 and 26.89 inches, respectively. The 21 day rainfall at Darrington is reported to have a return period of 98.6 years (4) and 88 years (5). However, these recurrence intervals are for the unique time period that ends on March 22. When evaluated on an annual basis the recurrence interval for the 42 day rainfall is 2.9 years and for the 21 day rainfall it is 2.1 years (Henn et al 2015). Neither of these return periods constitutes extreme events. They are only slightly wet of average. The 21- and 42-day average throughfall for the Whitman Bench can be estimated from the rain gauge network installed on Whitman Bench and the Oso rain gauge (https://fortress.wa.gov/ecy/eap/flows/regions/state.asp). These values are 13 and 19 inches, respectively, which are 18 % and 29 % less than the values reported for Darrington. A more thorough discussion of this topic is presented in Appendix A.

8.2 Seepage

It is our opinion that precipitation falling on Whitman Bench is hydrologically disconnected from the SR 530 Landslide in space and time and, therefore, was not a causative factor of the landslide. This opinion is based on the following:

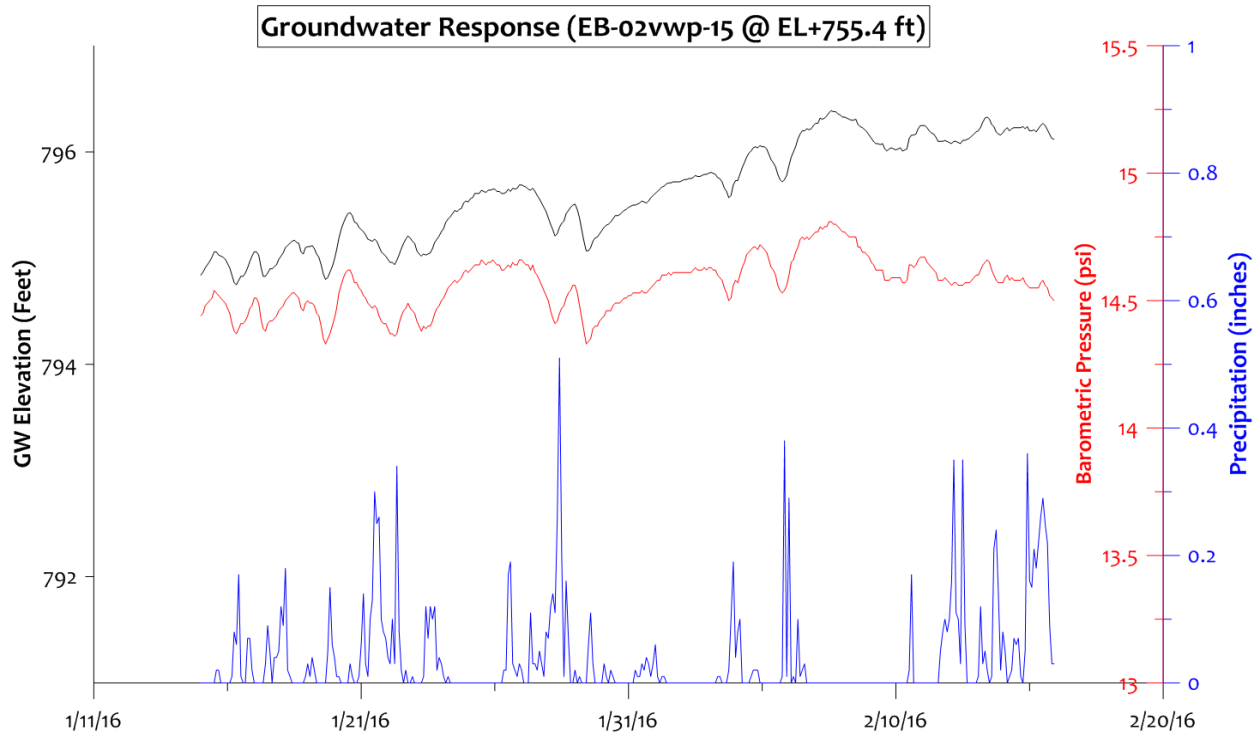### 8.2.1 Lack of groundwater response to precipitation events on Whitman Bench

Groundwater monitoring performed on Whitman Bench shows that there is no immediate response in the unconfined aquifer following precipitation events. We observed a gradual seasonal fluctuation in the groundwater data (Figure 9), where the groundwater level increases in elevation, reaches a peak value, and then starts to decline. Immediate responses in groundwater elevation due to barometric

1   pressure variations were observed (Figure 9 and Figure 10). The data do not support any immediate

2   groundwater response due to infiltration.
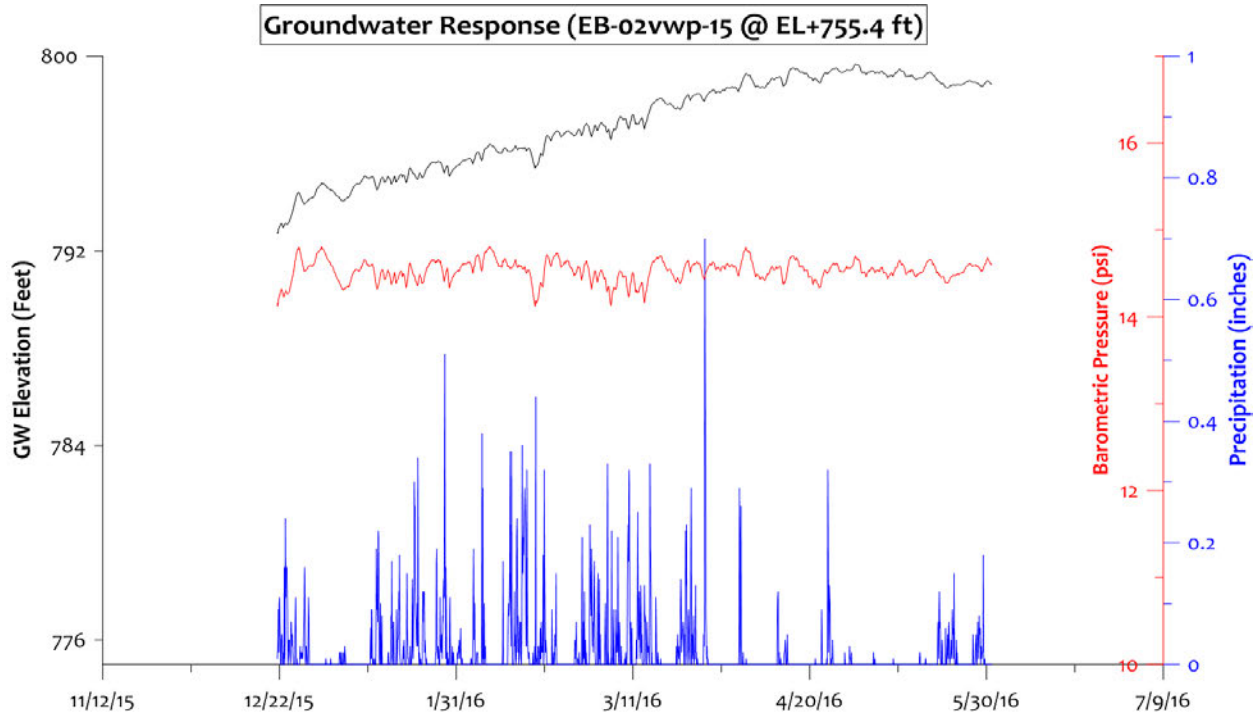
3

4   *Figure 9: Seasonal 'increase' in groundwater elevation.*

5

6
7   *Figure 10: Immediate groundwater response to barometric pressure compared with no discernable immediate*
8   *response to precipitation events.*

8.2.2 Whitman Bench is hydrologically disconnected from the SR 530 landslide in space and time

Eight exploratory borings were drilled into the Whitman Bench (see Figure 2). At each of these exploratory borings a layer of glacial till and/or silt was encountered at 80 to 130 feet below grade at the base of the recessional outwash. The fact that the glacial till or silt acts as an aquitard is evident because at each exploratory boring a perched water table was encountered (see Appendix I). The perched water table in conjunction with the till layer shows that the till layer is an aquitard and a barrier to the downward percolation of rainfall that falls on the bench. Furthermore, piezometers located at depths below the glacial till show no direct response to rainfall (see Appendix I).

The perched water table on top of the glacial till does appear to respond to rainfall, however the response is muted, lagged, and has a periodicity. The local elevation of the water table is at a minimum in the late fall. It builds during the winter rainy season and reaches a maximum in the spring. The water table drains throughout the spring and summer to again reach a minimum in the fall (Figure 11). The time lag in the response shown in Figure 11 is apparent given the pattern of maximum 21 day and 42 day rainfall amounts which occur between late November and Early January. The groundwater peak is subdued, but appears to occur in the late March through April time frame.
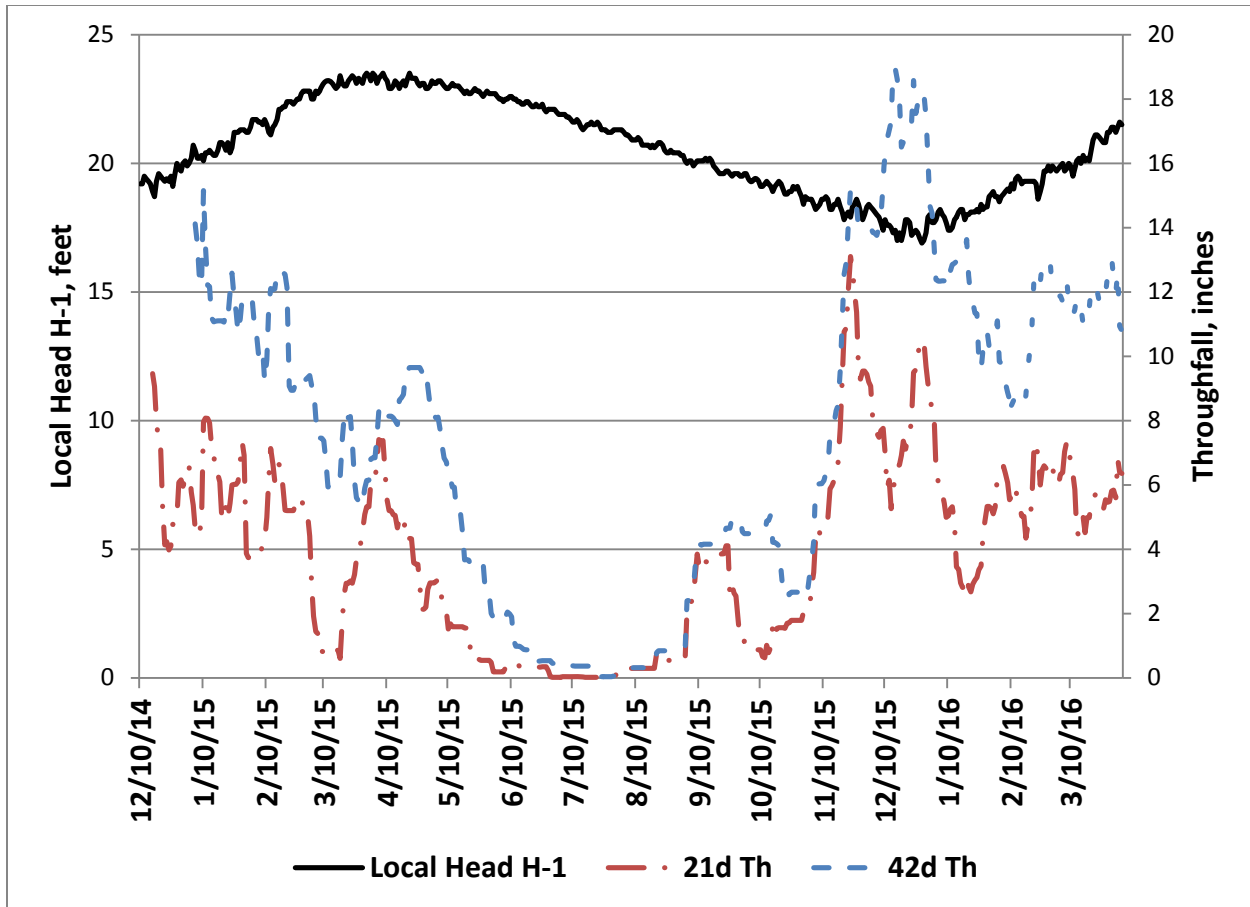
Figure 11: A graph of local head in feet at H-1 with the 21 day and 42 day throughfall on Whitman Bench.

8.2.3   No immediate GW influence in lacustrine unit beneath WB that made up Surface of Rupture of SR 530 landslide

The piezometer data from the fall 2014 boring advanced by WSDOT reveal that glacial till underlies the recessional outwash sand and gravel that makes up the surface strata on Whitman Bench. This till acts as an aquitard preventing downward seepage of water that infiltrates the ground surface beneath the 12-year old, 27-year old, and 80+ year old forest stands on Whitman Bench.   The till is also blanketed with a low permeability sandy silt, which also behaves as an aquitard. The piezometer measurements show a gravitational water table perched near the base of the recessional sands that generally slopes to the east (Figure 12), which is consistent with the observation of springs along the Upper Headache Creek Basin erosional escarpment. While minor seepage is evident in the SR 530 scarp, there is no indication the minor seeps in the scarp are of the magnitude of seepage observed exiting the recessional outwash strata along the Headache Creek escarpment, which drains into the Headache Creek basin.

1   The groundwater monitoring data collected to date suggests that shallow groundwater percolating

2   through the recessional outwash gravels and sands flows off to the east, concentrating to the center of

3   the Upper Headache Creek Basin. The groundwater data does not support flow towards the SR 530

4   Landslide main scarp. Therefore, the Miller-Sias model (6) (7) of assumed groundwater flow is not

5   supported by site-specific data.

6
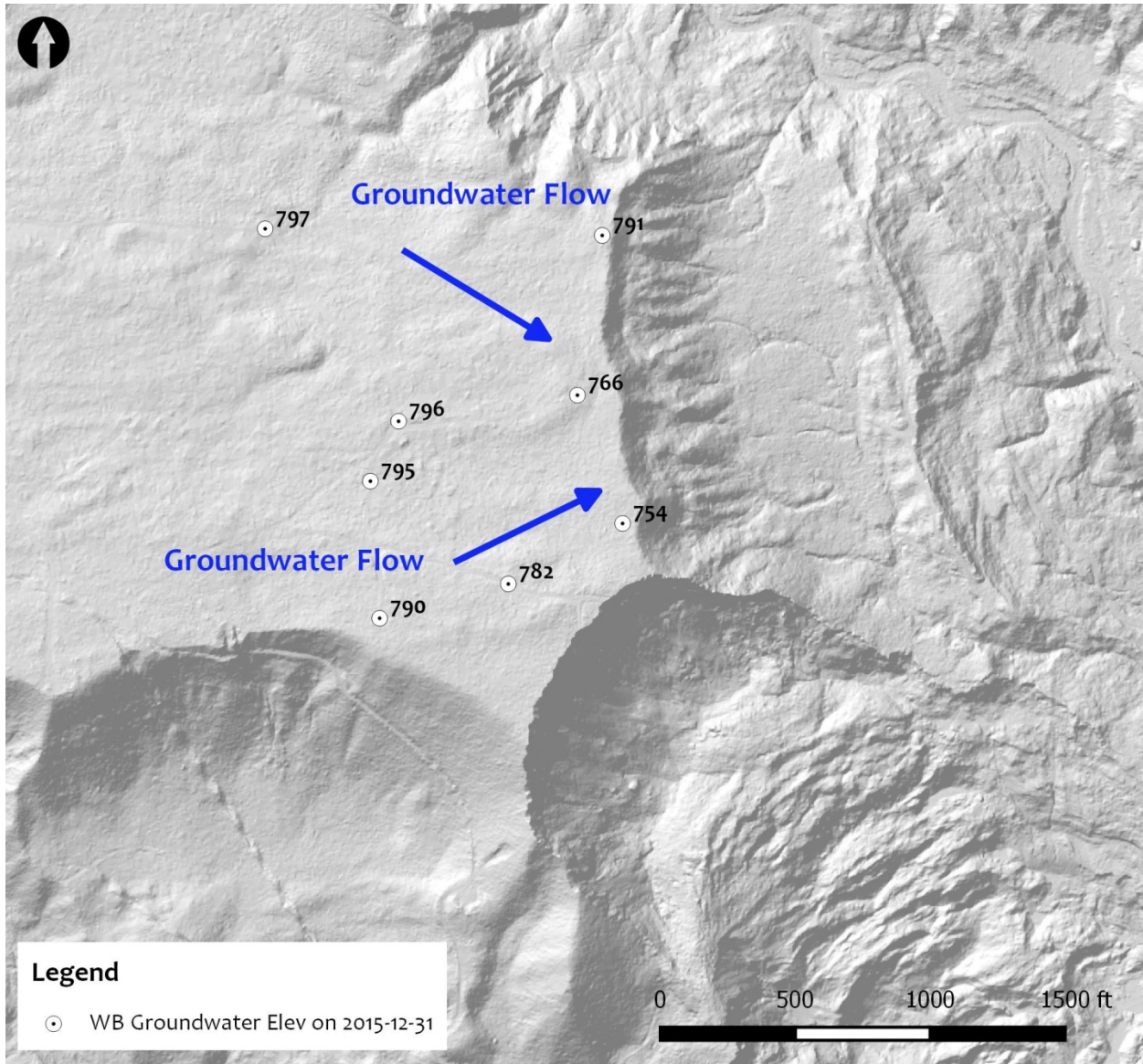
7
8   *Figure 12: Groundwater flow based on elevations of groundwater surface from instruments installed in Whitman*
9   *Bench (elevations reported at noon on 12/31/2015).*

10

1   Additional evidence of the lateral, rather than downward movement of groundwater can be gleaned

2   from the response to precipitation recorded by the piezometers installed in the recessional outwash

3   sands and gravels that cap the Whitman Bench and piezometers installed below the silt/till Aquitards.

4

5   As indicated above, WSDOT boring H-1vwp-14 indicates that the piezometric pressure below the till is

6   less than that above the till, confirming that the silt/till serves as an aquitard, perching groundwater

7   within the base of the Recessional Outwash underlying the Whitman Bench. The silt and till layers form

8   an effective aquitard, which restricts downward percolation and redirects said seepage off towards the

9   east, likely flowing upon the low permeability horizons. Hence, precipitation landing on Whitman Bench

10   and percolating down to the groundwater table appears to drain towards Headache Creek Basin, not

11   downward through the till, and not directly toward the SR 530 Landslide.

12

13   We note that the work of Miller and Sias (7) (6), specifically invoked in the Plaintiff's complaints, which

14   purported to be specific to the SR 530 Landslide site, equated water that reached the ground to

15   groundwater, and considered modeled increases in groundwater to occur everywhere. That is, the

16   entire area analyzed by Miller and Sias, which included the area of the SR 530 Landslide, was considered

17   to be forested on the one hand, and clearcut on the other. The reason for pointing this out should be

18   apparent in that the clearcut timber harvest that occurred in the fall of 2004 on the Whitman Bench was

19   only ~8.5 acres in area, out of a total area of some 1100 acres comprising the Whitman Bench. This

20   means that the 2004 harvest only involved about eight-tenths of one percent of the bench area.

21

22   As discussed in our previous reports, three problems are apparent from the deficiencies in the work of

23   Miller and Sias. First, the clearcut harvest occurred in 2004 and the SR 530 Landslide did not occur until

24   2014. Second, since only a small portion of the area of the Whitman Bench was clearcut harvested, any

25   increase in rainfall reaching the ground surface in the area of the clearcut, must be dispersed laterally,

26   toward the landslide, in order to determine its impact. Third, in order for any increase in infiltrated

27   water to influence the SR 530 Landslide mass, it must flow downward, through the soil profile to a depth

28   sufficient to increase the pore water pressure at the elevation of the surface of rupture at the base of

29   the 2014 Landslide mass. None of these factors was considered in the work of Miller and Sias, making

30   their work irrelevant to the actual cause of the SR 530 Landslide.

1 ### 8.2.4 GW response in slide debris is directly linked to precipitation

2 Based on our instrumentation (vibrating wire piezometers) over the last winter season (2015-2016), a

3 direct relationship was observed between precipitation and groundwater response in the SR 530

4 Landslide debris. Figure 13 shows precipitation and piezometer records for piezometers installed in the

5 slide debris for the period between October 2015 and April 2016.

6
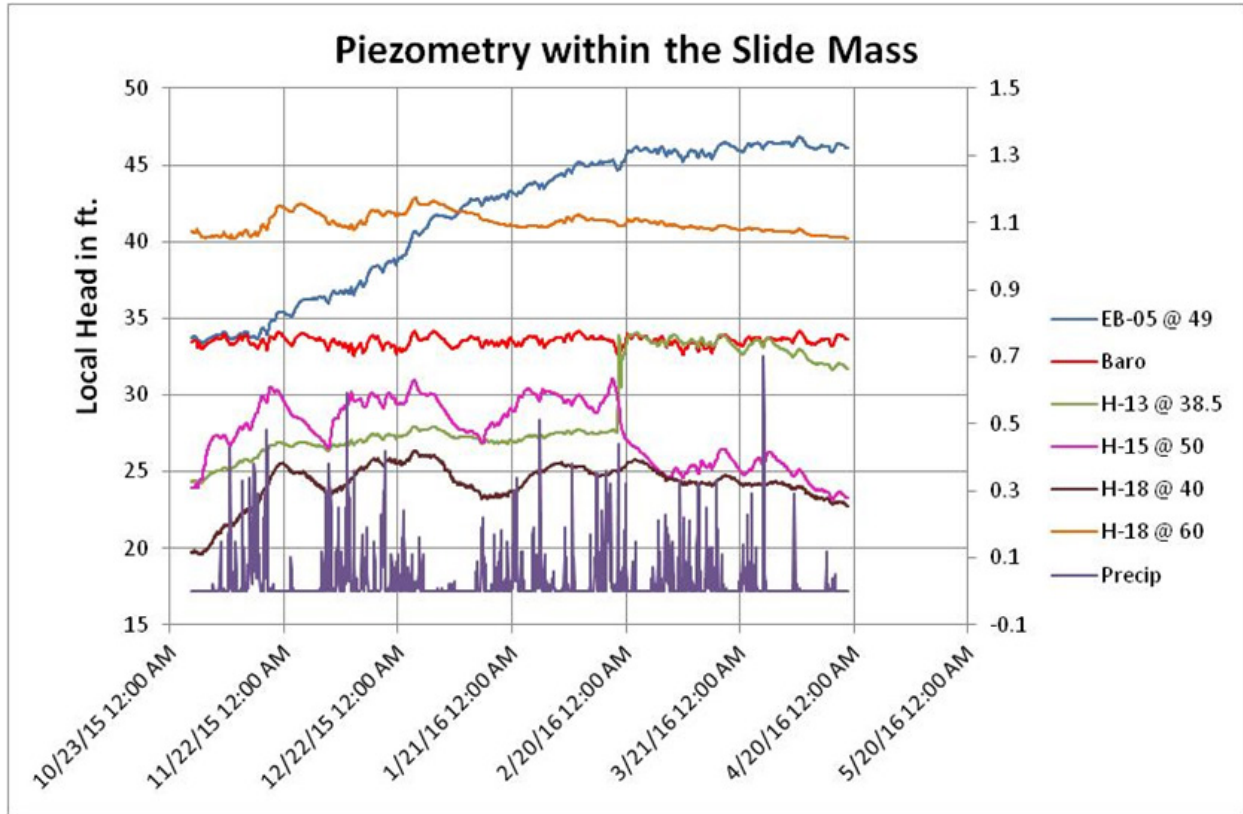
7

8 *Figure 13: Piezometer response within the slide debris to precipitation during the 2015-2016 winter season.*

9

10 ### 8.2.5 Minimal seepage from Headache Creek Basin

11 Water was observed to seep from the Headache Creek basin into the body of the Hazel Landslide. This

12 seepage is only a fraction of the overall water within the Hazel Landslide area and much of the seepage

13 is directly connected to a stream system that drains to the Stillaguamish River. Based on our multiple

14 excursions into the Headache Creek basin, the "floor" of the basin is primarily low permeability fine-

15 grained glacio-lacustrine material with a veneer of sand and silt (Figure 14). As a result, the amount of

16 water retained within Headache Creek Basin is minimal (no significant storage capacity within the glacio-

17 lacustrine materials) and any water that enters the basin, either as throughfall or seepage from

18 Whitman Bench, which appears to runoff rather quickly.

1

2 Based on our field observations, approximately 1/3 of the Headache Creek basin water discharges to the

3 north, into upper Rollins Creek. The remaining 2/3 discharges to Rollins Creek via Headache Creek. We

4 judge that less than 20 percent of the 2/3 southern discharge might seep into the left lateral escarpment

5 of the Hazel Landslide area. Higher flows will rapidly drain out of the system due to the lack of

6 permeable soil to provide water storage.

7

8 As noted earlier, water seeping into the body of the old Hazel Landslide, drains to the Stillaguamish

9 River as surface flow. This is a result of the presence of low permeability glacio-lacustrine and advance

10 silts and fine-grained sandy soils on the Hazel Landslide body.
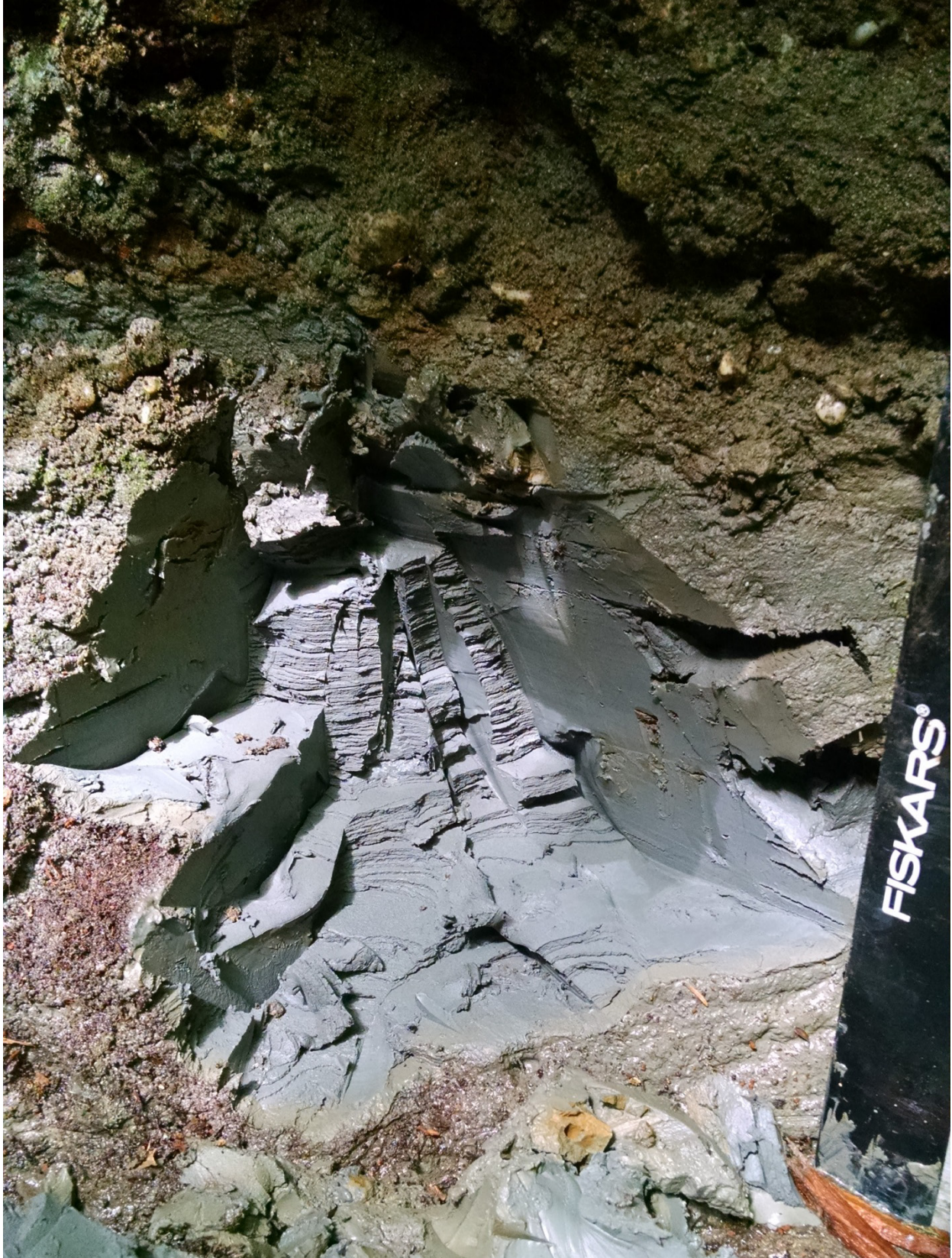
Figure 14: Exposed very low permeability laminated glacio-Lacustrine clay beneath a thin veneer of sand and gravel in Headache Creek, just above the left lateral escarpment of the SR 530 Landslide.

8.2.6   Seepage from west margin and mid slope bench

The volume of observed interflow (springs) from the midslope bench onto the west body of the Hazel Landslide body is much greater than the seepage from Headache Creek into the east side. Historic aerial photos (Figure 15 through Figure 23) show active discharge from the west portion of the Hazel Landslide body. This discharge has also been removing sediment and transporting it into the North Fork of the Stillaguamish River, where it is then flushed away. This sediment removal caused by the western seepage, is very likely a primary factor in slope destabilization, rather than seepage derived from Headache Creek basin. Note that the 1952 Shannon map (8) calls this western creek out as 'Slide Creek.' The Shannon map also shows contours that indicate Mudflow Creek likely extends up to the northeast corner of the midslope bench.
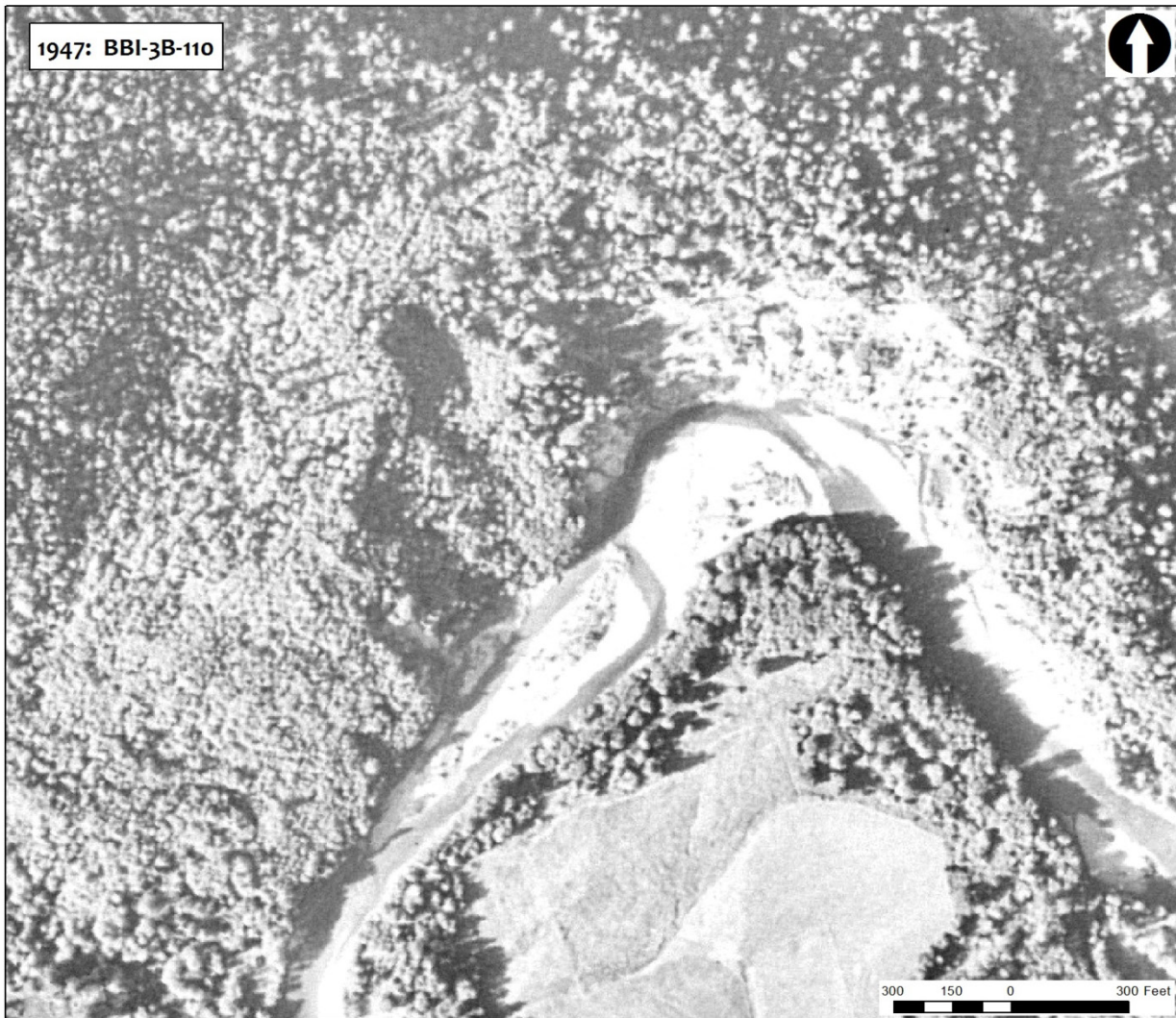
Figure 15: Aerial photo from 1947 showing active deposition of material eroded from Slide Creek that has forced the river to the southern shore, with a pioneer channel reforming at the base of the Bear Lake Sand deposit.
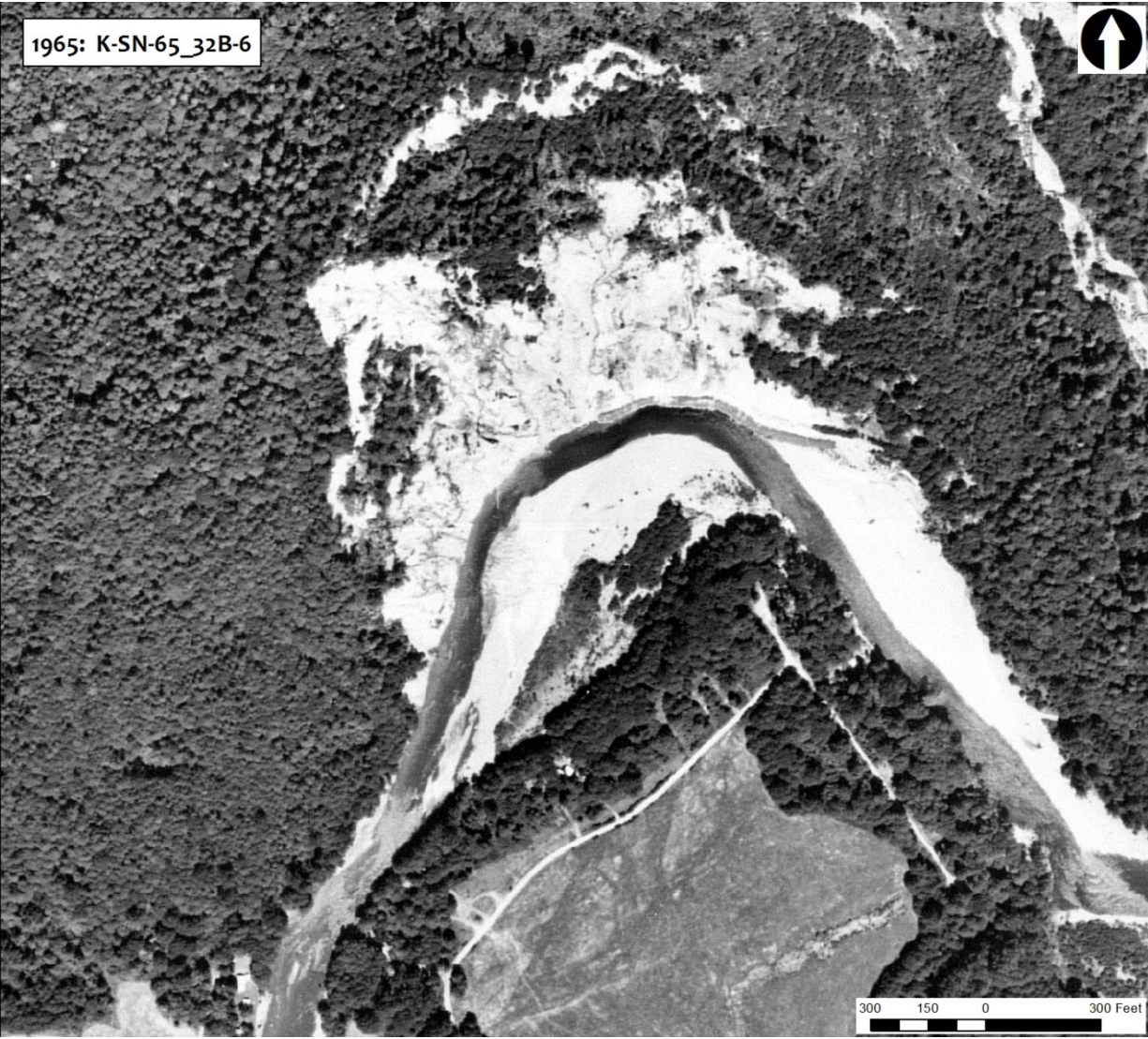
Figure 16: Aerial image from 1965 that shows 'turbid' water at the mouth of Slide Creek. Notice also that the river channel is 'pinched' at this location due to active deposition of sediment.

2003: NWC2003

1

2   *Figure 17: Aerial photo from 2003 showing active deposition from Slide Creek.*

2003: NWC2003

1

2   *Figure 18: Close-up view of the 2003 aerial image, showing recent deposits from Slide Creek.*

1

2 *Figure 19: 2009 aerial image showing active sediment deposition from Slide Creek, into the sedimentation pond.*

2009: NAIP2009

160 80 0 160 Feet

Figure 20: Close up view of active sediment deposition observed in the 2009 aerial image.

2012: 13840E4628N

Figure 21: 2012 aerial image showing continued active deposition in the sedimentation pond.

Figure 22: Close-up of the 2012 aerial image showing recent sediment deposition from Slide Creek into the sedimentation pond.

1

2 *Figure 23: Continued deposition of material eroded by Slide Creek, following the 2014 SR 530 Landslide (photo*
3 *taken in April 2016).*

8.3 Erosion

5 We previously concluded, as explained in the Declaration of Dr. J. David Rogers of November 5th, 2015

6 (Appendix L), that the North Fork (NF) of the Stillaguamish River did not trigger the SR 530 Landslide

7 because: (a) the surface of rupture of the SR 530 Landslide is located around El. +310 to +320 feet, which

8 is well above the river level of approximately El. +270 to +280 feet; and (b) the NF Stillaguamish River

9 was laterally disconnected by approximately 600 feet from the SR 530 Landslide initial surface of rupture.

10

11 We also found (Appendix L) that the settling pond had no impact on triggering the SR 530 Landslide,

12 because (a) the toe of the surface of rupture of the SR 530 Landslide is located around El. +310 to +320

13 feet, well above the settling pond, situated at approximately El. +275 feet, (b) the presence of

14 permeable "Bear Lake Sands," which abuts the settling pond, would not result in saturated conditions

15 that propagate 'uphill' into the glacio-lacustrine silt and clay deposits; rather any hydrostatic pressures

16 resulting from the settling ponds would tend to 'drain' either side of the settling pond; and (c)

17 groundwater data from the piezometer network installed in the Bear Lake Sands indicates groundwater

levels consistent with river level. As a result, there is no viable physical mechanism by which surface runoff in the settling pond could have elevated pore water pressures within the 2014 SR 530 Landslide situated well above the settling pond.

We also concluded (Appendix L) that the timber crib wall had no impact on triggering the SR 530 Landslide because none of the three potential Crib Wall impacts: (1) elevating groundwater levels above the landslide's basal surface of rupture so as to decrease the stability of the slope; (2) increasing flow velocities of the Stillaguamish River so as to exacerbate bank undercutting and erosion; and (3) the Crib Wall provides support for the slope by creating a 'toe berm' that acts as a 'door stop' to keep the hillside propped up are feasible; line up with the available physical evidence.

8.4 Predictability

As we interpret it, the Plaintiffs' experts contend that stability analyses performed before the SR 530 Landslide, with subsurface information available at the time, demonstrated, within the standard of practice that the landslide was going to occur and endanger the Steelhead Haven neighborhood.

To date, we have been unable to identify any previous stability analyses for the Hazel Landslide or the SR 530 Landslide that were based on any site-specific data, which would be required for a meaningful slope stability evaluation. We have only seen speculative slope stability analyses utilizing hypothetical site characterization models, based wholly upon assumptions.

Predicting catastrophic events such as the SR 530 Landslide is extremely challenging. There are four aspects of such predictions that together have rendered this type of problem largely intractable. First, a purely deterministic assessment of slope stability [using existing geomechanics procedures] requires knowledge of subsurface stratigraphy, material properties, and groundwater conditions, and these variables are costly to obtain and always include some uncertainty (which is important to estimate). Second, overlaying the time dependency of risk on the mechanics aspect of stability that comes from a deterministic stability assessment requires a quantitative assessment of climate based variables and relatively steady state earth processes. Third, prediction of the severity of an event – what makes it catastrophic – is not possible for most situations. Fourth, the result of a prediction must be meaningful to individuals and society as a whole such that action on the part of those individuals and society is

compelling. A brief comment about each of these components of an actionable, meaningful prediction follows.

8.4.1 Deterministic assessment of slope stability

The stratigraphy, material properties, hydrology, and groundwater conditions at a particular site are necessary for a mechanistic evaluation of slope stability. Each site is different and details matter. A comprehensive site investigation program, supplemented with analytical studies, and interpreted with engineering judgment grounded in theory, experience, and consideration of the shortcomings of each component of the assessment are required. The high resolution ground surface of a slope may be obtained from a LiDAR survey, but LiDAR became commercially available only in the last 15 to 20 years. Subsurface conditions important to mechanistic stability analysis, such as stratigraphy and the strength of the various strata, can only be obtained via site-specific field investigation. Further, the groundwater regime at the site has base level and seasonal components that may require multiple years of record to understand. Moreover, each of the components of the subsurface characterization has spatial and temporal variability that must be considered.

Limit Equilibrium slope stability analysis dates back to the mid 1800's when Alexander Colin published, "Landslides in Clay." It is the most common approach in the analysis and design of slopes. Limit Equilibrium analysis combines mechanics with descriptions of physical and engineering properties of the soil or rock material that makes up a slope. The rigor with which the mechanics of a slope is represented along with the rigor used to represent the engineering properties [primarily shear strength] of the soils that make up a slope determines the relative accuracy of the method. One of the reasons for the popularity of Limit Equilibrium Slope Stability Analysis is that the end result can usually be related via a simple explanation to lay-people, as well as to knowledgeable professionals. The Factor of Safety of a slope that results from limit equilibrium stability analysis can be viewed as the degree of stability with numbers greater than 1.0 representing stable states, and higher values representing more stable conditions than lower values.

As simple as the factor of safety concept is, it can be easily misused and misunderstood. Factor of safety calculations are used for analysis of existing slopes and in the design of slopes. When used in the slope design process, a computed factor of safety less than 1.0 means that one or more components of the slope are not adequate to prevent failure when the slope is constructed. The slope could be too steep or too high, the soil that makes up the slope could be too weak, or there could be too high a

groundwater level in the slope. Of course it could also be combinations of the listed items. A computed factor of safety less than a threshold value points to the need to improve the design by changing one or more of the items listed. A designer will go through a process of varying the slope, the soil strength, or the groundwater level until an acceptable computed factor of safety results. Then the slope can be built to match the parameters used in the design computations with the result being a "stable slope" with an acceptable factor of safety. Things are different for a natural slope.

Special consideration must be used when computing a factor of safety for an existing (or 'natural') slope. The slopes in the area of the SR 530 landslide all naturally existed prior to their failure. This means that prior to failure, the factor of safety had to be at least a little bit greater than 1.0; otherwise, the slope would have already failed. If you conduct a factor of safety calculation for the Hazel Landslide slope prior to the January 2006 landslide and you get a value of factor of safety that is less than "one," it means that something in your calculations is incorrect. We put "one" in quotes here to emphasize the lack of precision in the analyses.

The same thing is true for the SR 530 Landslide – at the onset of the failure, the correct computed factor of safety must be very close to "one." So, a computed factor of safety of the Hazel Landslide slope prior to the 2006 failure of FS=0.6 for example, means that that slope either could not have existed (which it obviously did), or one or more of the input parameters to the analysis were incorrect. We note that computed factors of safety for an existing slope greater than "one" are not necessarily correct because there can be errors in the input parameters in these cases as well. But, at least a computed factor of safety greater than "one" for a stable slope can be a correct reflection of the stability. A computed factor of safety less than "one" for an existing slope is simply incorrect. The biggest unknown factor in most stability analyses of natural slopes is the temporal distribution of pore water pressures.

8.4.2   Overlaying the temporal component

Overlaying the temporal component, as implied above, groundwater conditions may have a time depended component that is seasonal. In addition to this, groundwater is driven by climate which has a random characteristic over time that cannot be predicted from day to day or from year to year. What can be done is to evaluate the probability that an extreme event will occur, but this is often not a prediction in terms of the human time frame (most engineering assessments are limited to considering a 75 t0 100 year design life). Other temporal changes that can affect slope stability include erosion that changes slope geometry, and weathering of soils and rocks.

8.4.3 Severity of an event

A small landslide on a hillslope in mountainous forested terrain may have no direct impact on any people. A much larger landslide, such as the SR 530 Landslide, can clearly be deadly, and yet the stability mechanics and temporal probability components that must be considered in prediction are the same. The toll of the SR 530 Landslide was so high because of the distance the landslide debris traveled, or the "runout" of the slide. Other cases of previous long runout slides in the Stillaguamish Valley have been identified. The Rowan slide to the west of the SR 530 Landslide site ran out all the way across the valley as did other slides, but (1) they occurred long ago in terms of the human time frame (>100 years), and (2) they had long runouts totally independent of any modern human activities, such as timber harvesting or the construction of crib walls or sedimentation ponds. Evaluating the runout distance was done post-hoc in the case of the SR 530 Landslide via several different methods, but the analytical techniques for estimating runout are neither commonly taught to geotechnical engineers, nor recognized within the geotechnical profession and have not been used in prediction. So, even if we had known from stability analyses that the SR 530 Landslide, a landslide much larger than the historic Hazel Landslide, was unstable with an uncomfortably high likelihood of occurrence, we would not have been able to predict the runout with any level of confidence, except to say that some large slides in the Stillaguamish valley have runout and crossed the valley. Many other landslides in the Stillaguamish valley have not runout across the valley, during prehistoric time (>150 to 200 years ago). Even with the hindsight today, we do not know with scientific certainty how many existing or future landslides in the Stillaguamish valley have the potential to runout long distances.

8.4.4 Meaningful prediction

In human terms, what constitutes a meaningful prediction? It has been predicted that a Cascade Subduction Zone earthquake and tsunami has a 30 percent chance of occurring in the next 50 years. Are individuals moving their families to safer ground beyond the predicted Tsunami inundation zone? Is society banding together to relocate critical structures, such as firehouses, police stations, hospitals, and schools to safer ground? Not really, and yet, this is a prediction that is as certain as predictions can be in the earthquake business. The potential consequences of a Cascade Subduction Zone earthquake in terms of death and destruction are largely recognized. In the landslide business, we cannot yet achieve this level of prediction. Large destructive landslides often surprise us. We can assess some landslide hazards based on geologic signature – and this is what the plaintiffs' experts have termed "prediction." But most often we do not have the means to make predictions that have actionable meaning to people. It is a worthy research goal to develop valid and reliable methods for predicting landslide activity that

are meaningful so that meritorious warnings can be issued. Unfortunately, to date, the state of the

practice has not achieved the required level of certainty in predictions.

An important component of any prediction is the standard of practice to be used by the professionals

making the prediction. Mechanistic stability analysis of a natural landslide might be considered part 1 of

a landslide prediction. Mechanistic stability analysis requires knowledge of (1) slope geometry, (2)

subsurface stratigraphy, (3) physical and engineering properties of all the potentially involved strata, and

(4) groundwater flow patterns that can be used to estimate pore water pressures throughout the

potentially involved strata.

Detailed slope geometry such as that obtained from LiDAR was available for the SR 530 Landslide area as

early as 2003, but this type of information was not included in the standard of practice until sometime

later in the 2010's. Subsurface stratigraphy at depth can be mapped in some cases by site specific

geophysical methods, but in general, establishing stratigraphy and measuring soil properties requires

drilling and sampling with field and laboratory tests to follow in conjunction with surface and subsurface

geologic mapping. Characterizing groundwater flow patterns and the associated pore water pressures

that are necessary for stability analysis of natural landslides requires numerous piezometer installations

in bore-holes that are distributed in plan and in depth, again coupled with geologic interpretation.

Although a limited amount of investigation of the Hazel Landslide area was done following a couple of

the movement events of that slide, none of this work was done for the SR 530 Landslide area, and

therefore, no prediction within the bounds of the standard of practice for engineering geology and

geotechnical engineering was possible. Conducting a stability analysis for the purpose of predicting a

natural landslide without benefit of the investigation outlined above and the data from that

investigation is unlikely to produce a plausible and defensible prediction that is actionable.

8.5   2006 Debris

Our analyses found that the presence or absence of the 2006 debris field does not result in a material

difference in the runout extents of the SR 530 Landslide. This opinion is based on the following suite of

evidence.

8.5.1   Empirical Evidence

Empirical evidence, largely based on publications made public subsequent to the SR 530 Landslide, from

the North Fork of the Stillaguamish River Valley suggests that an SR 530 Landslide event that initiates at

1   a Whitman Bench elevation may cross the valley floor. Recent studies by others ((9), (10), (11)) have

2   identified historic and pre-historic runout events in the North Fork of the Stillaguamish Valley (Figure 24,

3   Figure 25, and Figure 26). Landslides that involve materials similar to the SR 530 Landslide include the

4   Rowan slide, which has been mapped to extend across the valley floor. There is no evidence that a

5   debris field was in place below this long runout landslide at the time it occurred. Certainly, there were

6   no crib walls or sedimentation ponds present at the time of this pre-historic slide.

7
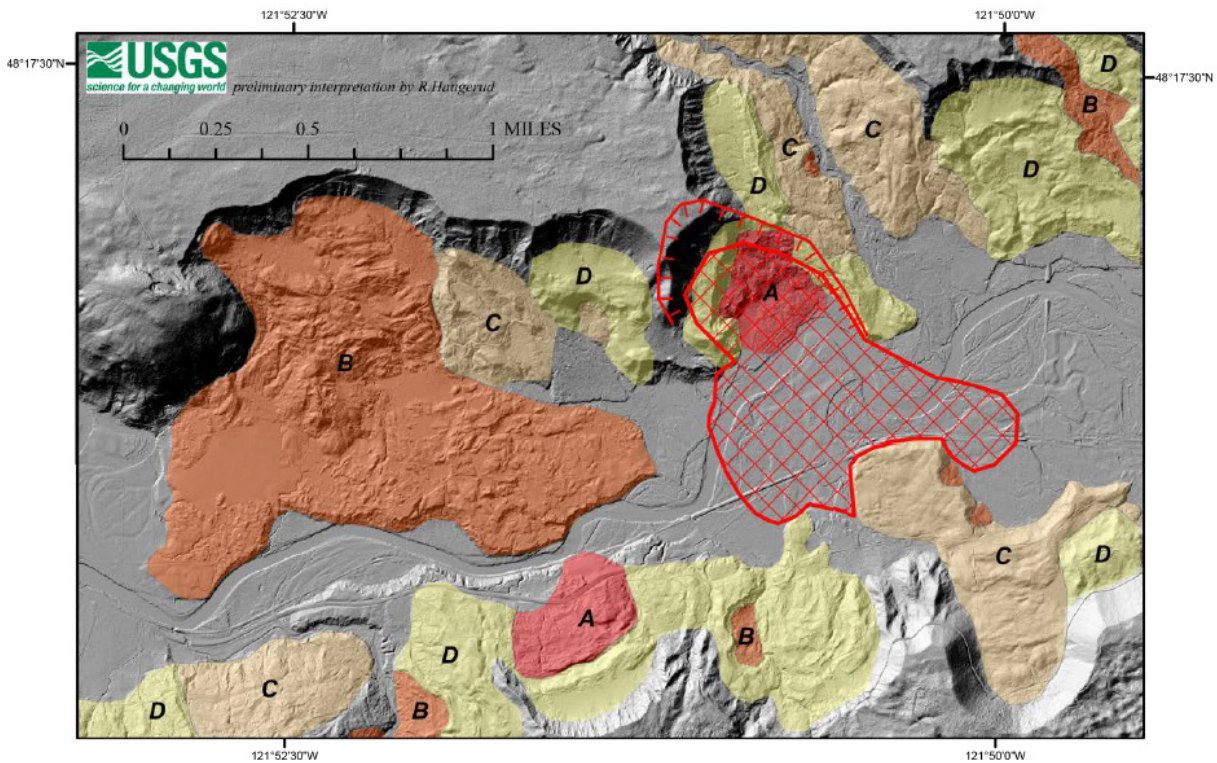
Figure 2. Shaded-relief image calculated from the 2013 lidar survey. Colored areas show older landslide deposits, distinguished by their relative age: A, youngest to D, oldest. The red cross-hatched area marks the approximate extent of deposits from the March 22, 2014, landslide.

8

9   *Figure 24: Landslide deposits as mapped by Haugerud of USGS (9) published after the 2014 SR 530 Landslide.*

10
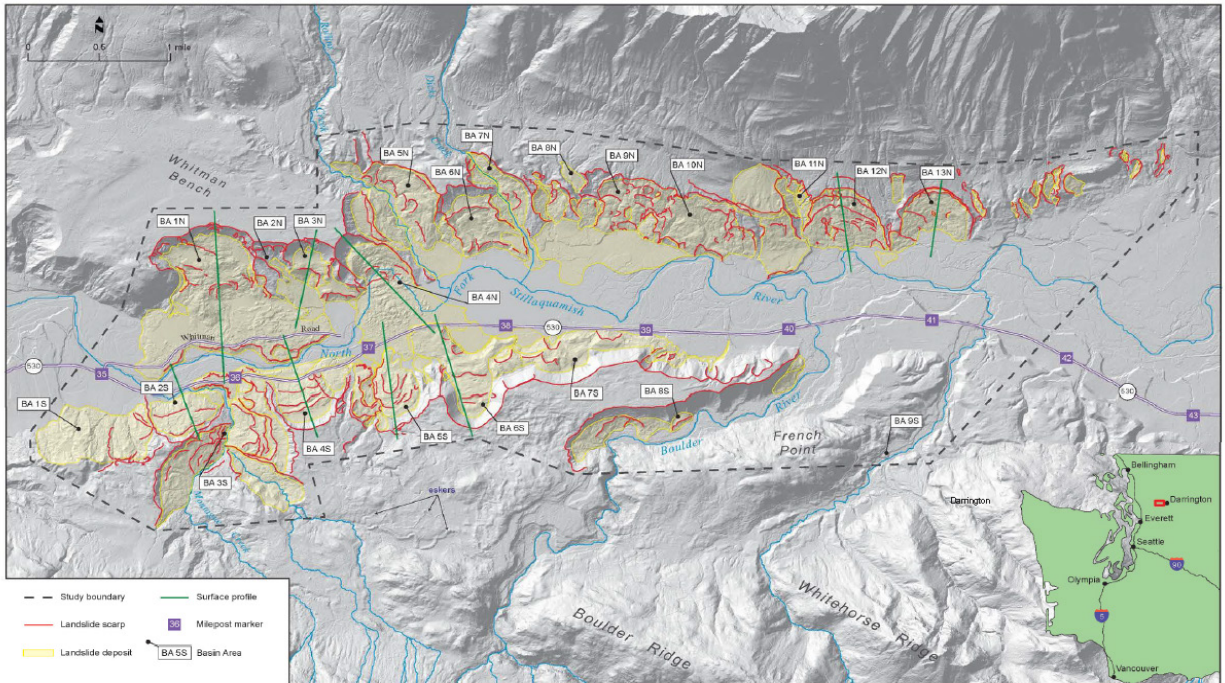
Figure 1A. Map of the study area showing interpreted LiDAR hillshade and basin areas. Hillshade mosaic compiled from 2010, 2013, and 2014 bare-earth LiDAR data obtained from Snohomish County, the Tulalip Tribes of Washington, and WSDOT, respectively.

Figure 25: Landslides as mapped by Gerstel and Badger (10) published after the 2014 SR 530 Landslide.
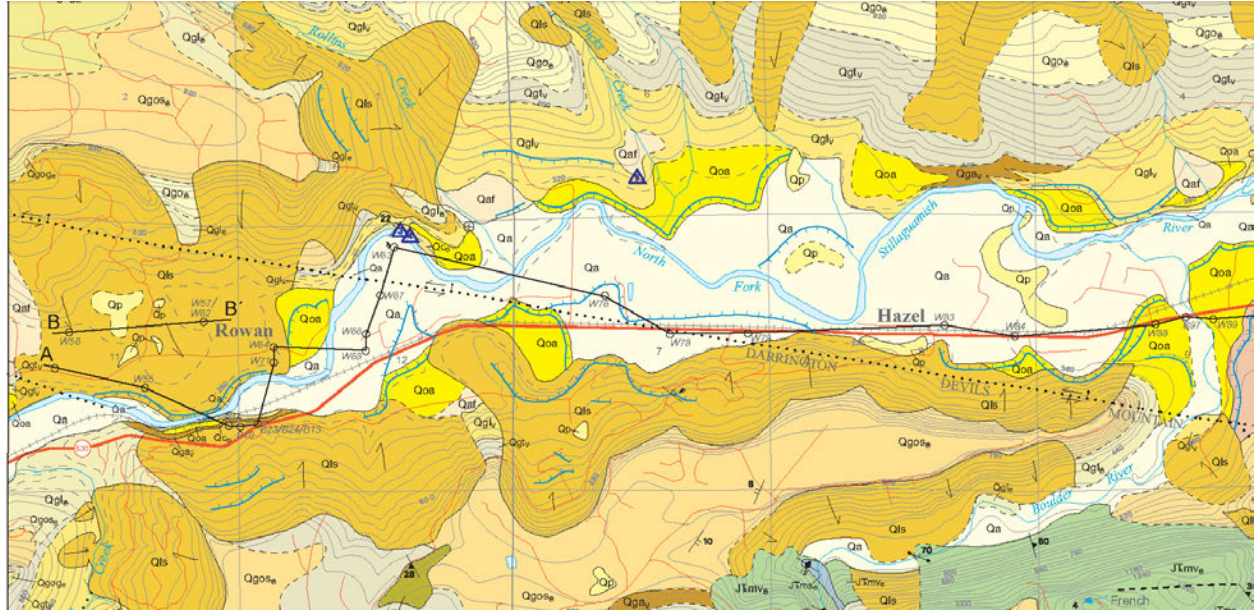
Figure 26: Quaternary age landslides (Qls) as mapped by Dragovich et al (11), released in 2003.

8.5.2   Similar runout with different soils

The western side of the Hazel Landslide, and hence the materials in the debris field differ significantly from those in the eastern side of the Hazel Landslide, and its resulting debris field. Shannon (8) noted this difference and identified the primary earth/water movements in the western side as "Slide Creek" and the primary earth/water movements in the eastern side as "Mudflow Creek." The western side of

1 the Hazel Landslide is dominated by cohesionless soil types (e.g., non-plastic coarse sands and gravels);

2 whereas the eastern side of the Hazel landslide is dominated by cohesive soil types (e.g., plastic silts and

3 clays). Photographs of representative soils in each side of the Hazel landslide are shown in Figure 27.

4

5 *Figure 27: Western side of the landslide complex shown at the left and eastern side of the landslide complex*
6 *shown on the right.*

7

8 Previously presented photographs in Figure 17, Figure 18, and Figure 22 show the different

9 characteristics of the debris material below the western side of the Hazel Landslide and its eastern side.

10 This is a result of the differing characteristics of the material in the western and eastern parts of the

11 Hazel Landslide source area discussed previously. The materials in the western side of the 2006 debris

12 field and in the area in the vicinity of the sedimentation pond are largely alluvial deposits derived from

13 erosion of the materials in the western portion of the slide area. The clayey and silty materials in the

14 eastern side of the 2006 debris field are largely mudflow deposits derived from the eastern part of the

15 source area.

16

17 Although the soil characteristics of the western and eastern sides of the 2006 debris field differ

18 significantly, the 2014 SR 530 Landslide ran out similarly to the west and east as it traveled across the

19 2006 debris field and then across the valley. If the 2006 debris field had been a primary factor in the

20 length of the runout, the differing soils characteristics of its western side and eastern side should have

21 made a difference in the distance of the runouts on each side of the 2014 SR 530 Landslide. Since there

22 was no appreciable difference in the runout distances, it is not likely that the 2006 debris field was a

23 factor in the long runout distance of the SR 530 Landslide.

24

Additionally, it is plausible that had the 2006 debris field not been present, the M1 material would have slid off the Hazel Landslide slope, landing in the river creating a temporary debris field. Our analysis of the seismic record from 2006 found that an M1-type movement does not register a signal on the seismic record. Thus it is possible for a modest volume of M1 type material to have moved prior to larger scale movements (M2, M3, and M4). The M1 material would have been comprised primarily of Advance silts and fine-grained sands, with a consistency that would have made it mobile. Due to the mobility of the M1 material, it is also plausible that even with the presence of the 2006 debris field, the M1 material partially flowed down slope and initially covered the 2006 debris and this is the material that the later SR 530 Landslide earth movements (i.e. M2 and M3) moved across.

8.5.3   Quantitative Runout Analyses

The runouts of the 2006 Hazel Landslide and the 2014 SR 530 Landslide were back-analyzed by Dr. Kenichi Soga using the material point method (MPM) to assess if the MPM models of these landslides could capture the key observed characteristics and distances traveled by the landslide debris during these two events (see Appendix K). After these two runout events were captured sufficiently well with the MPM models, the potential effects of the presence or absence of the 2006 debris field below the toe of the surface of rupture of the SR 530 Landslide was investigated. The MPM model that was calibrated to capture the observed runout of the SR 530 Landslide was rerun with all modeling aspects identical to the calibrated SR 530 Landslide analyses, with the exception that the 2006 debris field was removed completely and the North Fork of the Stillaguamish River reoccupied its former position before the January 2006 Hazel landslide. Thus, the primary objectives of the MPM analyses were to ascertain if the MPM models could capture and provide insight into the differing runout distances traveled by the 2006 Hazel Landslide debris and the SR 530 Landslide debris, and to investigate if the presence of the 2006 debris field significantly affected the runout distance traveled by the SR 530 Landslide debris.

The adopted MPM model was able to capture the observed distance of the 2006 Hazel Landslide runout (Figure 28). Moreover, the MPM model that was calibrated to capture the observed distance of the 2006 Hazel Landslide runout was also able to capture the general characteristics and runout distance of the SR 530 Landslide (Figure 29). Therefore, the actual runout distance of the SR 530 Landslide is captured well with these analyses, which are, in turn, consistent with the 2006 Hazel Landslide analyses. We are confident that the MPM model is capturing the basic physics involved in the slope runout problem using reasonable estimates of soil stratigraphy, slope and surface of rupture geometry, and engineering properties of the component materials.
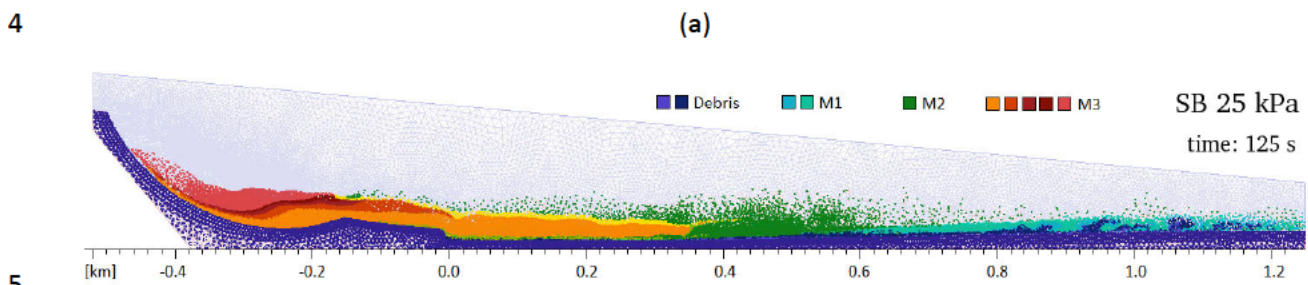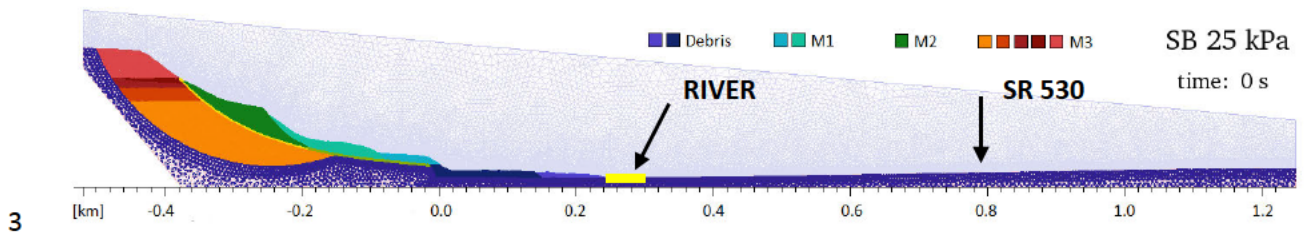
t = 0 s
M1
M2

(a)

t = 53 s
M1
M2

(b)
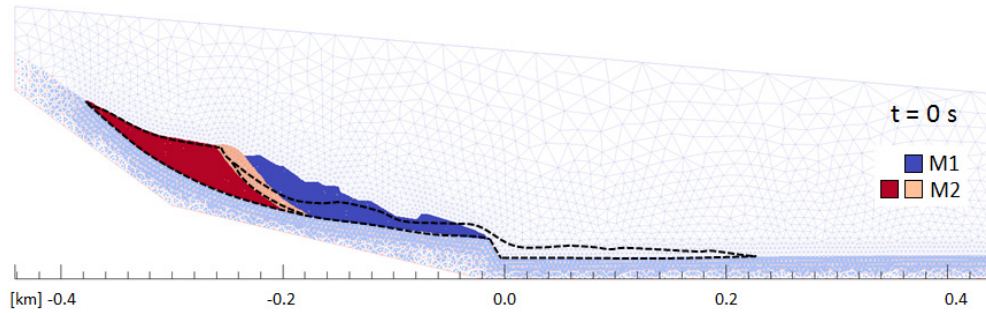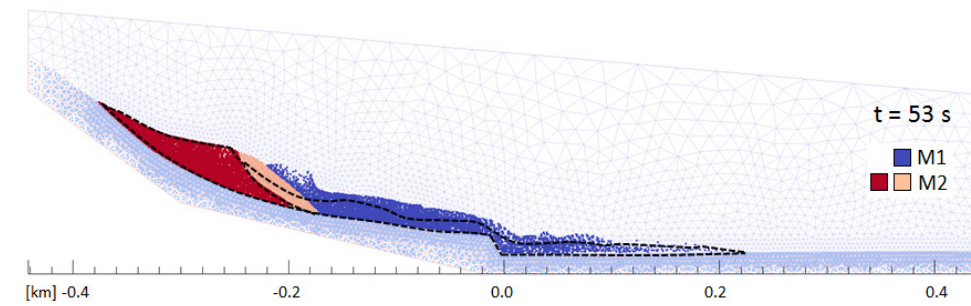
Figure 28: (a) Initial landslide geometry, and (b) final landslide geometry for the 2006 Hazel Landslide runout. The observed final topography of the 2006 Hazel Landslide runout is indicated with a dashed line (Appendix K).

With the calibrated MPM runout analyses of the SR 530 Landslide capturing the key characteristics of the observed runout including its long runout distance, the calibrated SR 530 Landslide MPM model could be used with confidence to investigate the potential effects, if any, of changes in the landslide geometry such as the absence of the 2006 debris field at the bottom of the slide. The MPM model that was calibrated to capture the observed distance of the 2006 Hazel landslide runout and the general characteristics and observed runout distance of the SR 530 Landslide was rerun with only one change, which was the removal of the 2006 debris field between the toe of the landslide and the North Fork of the Stillaguamish River, to investigate the potential effects of the absence of the debris field at the bottom of the slide. The simulated runout behavior of the hypothetical case where there is no 2006 debris field below the toe of the landslide was similar to the simulated runout behavior of the actual SR 530 Landslide case (compare Figure 30 with Figure 29). In both analyses, the SR-530 Landslide debris runout distances were essentially the same. In both cases, the debris ran out across the valley floor. Therefore, the calibrated SR-530 Landslide MPM runout analyses fully support the opinion that the

1   presence or absence of the 2006 debris field did not make a material difference in the runout of the SR

2   530 Landslide.

3   (a)

4

5

6   (b)

7   *Figure 29: (a) Initial landslide geometry, and (b) final landslide geometry for the SR 530 Landslide runout for the*
8   *calibrated MPM baseline model case (see Appendix K).*

9

10

11 (a)

12

13 (b)
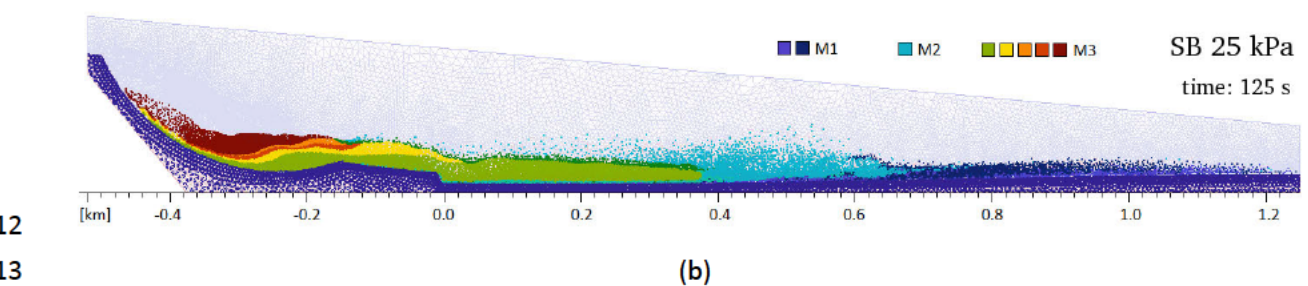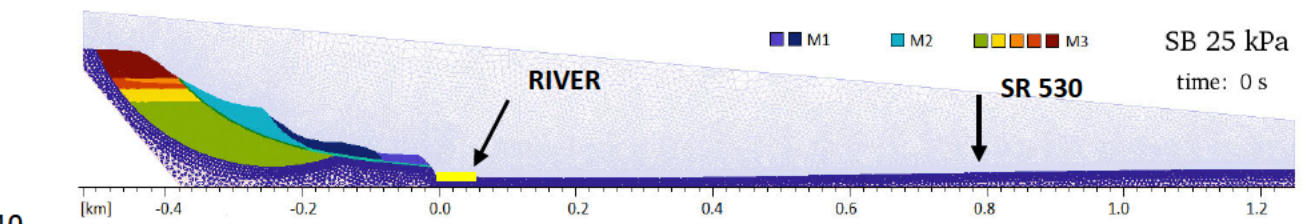
14 *Figure 30: (a) Initial landslide geometry, and (b) final landslide geometry for a hypothetical case wherein the*
15 *2006 debris field does not exist at the time of the SR 530 Landslide (see Appendix K).*

16

17 The key difference between the runout distances of the 2006 Hazel Landslide and the actual SR 530

18 Landslide appears to be the larger and higher combined mass of the M1/M2 sliding mass and the "push"

received from the much larger M3 sliding mass. The larger landslide mass coupled with much of it initiating from a higher starting elevation produced the long runout of the SR 530 Landslide. Removal of the debris field does not change the calculated results appreciably. The presence or absence of the 2006 debris field is found to be unimportant in these runout analyses

9) Reservation

We reserve the right to clarify, amend and/or supplement our observations and forthcoming opinions based on development of additional information as this case proceeds. We reserve the right to provide rebuttal opinions at the appropriate time to contentions or expert opinions that may be disclosed by the Plaintiffs in this case.

1 This Expert Opinion Report submitted on behalf of AG Experts submitted on June 30, 2016 by:

2

30 June 2016

_____

DR. MARVIN R. PYLES, Ph.D., P.E.

_____

DR. J. DAVID ROGERS, Ph.D., P.E., P.G., C.E.G., C.HG.

_____

DR. JONATHAN D. BRAY, Ph.D., P.E., NAE

_____

DR. ARNE SKAUGSET, Ph.D., RPF

_____

DR. RUNE STORESUND, D.Eng., P.E., G.E.

_____

DR. GUNNAR SCHLIEDER, Ph.D.

1

2

10)   Works Cited

1. **Rogers, J. David, et al., et al.** *Preliminary Expert Report, Superior Court of Washington for King County, No. 14-2-18401-8 SEA, June 1, 2015 .* 2015.

2. **Rogers, J. David, et al., et al.** *Interim Expert Report, Superior Court of Washington for King County, No. 14-2-18401-8 SEA, January 22, 2016.* 2016.

3. **Washington State Department of Transportation, (WSDOT).** *Geotechnical Data Report; SR 530 Landslide: Geotechnical Study. Prepared for and under the direction of the Office of the Attorney General.* 2016.

4. **Keaton, Jeffrey R., et al., et al.** *The 22 March 2014 Oso Landslide, Snohomish County, Washington.* s.l. : Geotechnical Extreme Events Reconnaissance (GEER), 2014.

5. **Henn, B., et al., et al.** Hydroclimatic Conditions Preceding the March 2014. *J. Hydrometeor.* 2015.

6. *Deciphering large landslides: linking hydrological, groundwater and slope stability models through GIS. Hydrological Process., 12, 923-941 (1998).* **Miller, Dan J. and Sias, Joan.**

7. **Miller, Dan and Sias, Joan.** *Environmental Factors Affecting the Hazel Landslide, Level 2 Watershed Analysis, Hazel Landslide, Washington.* 1997.

8. **(Shannon), William D. Shannon & Associates.** *Report on Slide on North Fork Stillaguanish River near Hazel, Washington.* 1952.

9. **Haugerud, Ralph A.** *Preliminary Interpretation of Pre-2014 landslide Deposits in the Vicinity of Oso, Washington; U.S. Geological Survey Open File Report 2014-1065.* 2014.

10. **Gerstel, Wendy J. and Badger, Thomas C.** *Reconnaissance Mapping and Characterization of Landslides Along State Route 530 Between Mileposts 35 and 41, Snohomish County, Washington. Report to Washington Department of Transportation Geotechnical Office.* 2014.

11. **Dragovich, Joe D., et al., et al.** *Geologic Map of the Mount Higgins 7.5-minute Quadrangle,Skagit and Snohomish Counties, Washington, WA Department of Geology & Earth Resources.* 2003.

12. **USGS.** *USGS 12167000 NF STILLAGUAMISH RIVER NEAR ARLINGTON, WA.*

13. **Riemer, M.F., Collins, B.D., Badger, T.C., Toth, C.** *Geotechnical soil characterization of intact Quaternary deposits forming the March 22, 2014 SR-530 (Oso) landslide, Snohomish County, Washington: U.S. Geological Survey Open-File Report 2015-1089, 17 p.* 2015.

14. **Allstadt, Karen.** *Interactive comment on "Seismology of the Oso-Steelhead Landslide" by C. Hibert et al., Nat. Hazards Earth Sys. Sci. Discuss, 2, C3274-C3283.* 2015.

15. **Hibert, C., C. P. Stark, and G. Ekstrom.** *Seismology of the Oso-Steelhead Landslide, Nat. Hazards Earth Sys. Sci. Discuss, 2, 7309-7327.* 2014.

16. **Iverson, R. M., D. L. George, K. Allstadt, M. E. Reid, B.D. Collins, J.W. Godt, C.M. Cannon, C.S. Magirl, R.L. Baum, and J.A. Coe.** *Landslide mobility and hazard: implications of the 2014 Oso disaster, Earth and Planetary Science Letters, 412, 197-208.* 2015.

17. **Miller, Dan.** *Hazel/Gold Basin Landslides: Geomorphic Review Draft Report.* 1999.

18. **Benda, Lee, Thorsen, Gerald W. and Bernath, Stephen.** *Report of the I.D. Team Investigation of the Hazel Landslide of the North Fork of the Stillaguamish River (F.PA. 19-09420).* 1988.

19. **Radbruch-Hall, Dorothy, Roger B. Colton, William E. Davies, Ivo Lucchitta, Betty A. Skipp, and David J. Varnes.** *Landslide Overview Map of the Conterminous United States, USGS Open-File Report 97-289.* 1982.

20. **Duncan, J.M., and Wright, S.G.** *Soil Strength and Slope Stability.* 2005 : John Wiley & Sons, Inc., Hoboken, New Jersey.

21. **Badger, Tom.** *Personal communications regarding ongoing WSDOT Phase 1 Investigation of the SR-530 landside hazards.* 2015.

22. **(DNR), State of Washington Department of Natural Resources.** *How much do you know about landslides in Washington State?* 2009.

23. **Tech, Tetra.** *Snohomish County; Natural Hazard Mitigation Plan Update; Volume 1: Planning-Area-Wide Elements.* September 2010.

24. **Schuster, R.L. and R.J. Krizek, Eds.** *Landslides: Analysis and Control, Special Report 176 of the National Academy of Sciences.* 1978.

25. **King City Sheriff #2345.** *Photograph taken March 24, 2014.*

26. **Miler, Dan.** *Power Point from Lecture: "The Hazel Landslide: Deja Vu all over again.".* 2014.

27. **Harding, David J.** *Data Product Description for NASA-USGS LiDAR Mapping Projects: West Rainier, Northern San Andreas, Darrington-Devis Mountain, and Mt. Saint Helens.* 2005.

28. **TerraPoint LLC.** *Mt_Higgins_Meadow_Mtn.* 2003.

29. **Watershed Sciences Inc (WSI).** *2013 Tulalip LiDAR Project.* Corvalis, OR : s.n., 2013.

30. —. *Tulalip LiDAR; Technical Data report - Delivery 2.* Corvalis, OR : s.n., 2013.

31. **Spatial, Quantum.** *2014 Stillaguamish LiDAR, Including Oso.* 2014.

32. **Quantum Spatial.** *Oso Landslide/Stillaguamish River LiDAR, Technical Data Report.* 2014.

33. **Turner, A. Keith and Schuster, Robert L. (eds).** *Landslides, Investigation and Mitigation; Special Report 247.* Washington, D.C. : Transportation Research Board, National Research Council, 1996.

34. **USACE.** *Slope Stability EM 1110-2-1902.* s.l. : U.S. Army Corps of Engineers, 2003.

35. **Ecology, Washington State Department of.** Washington State Well Log Viewer. *Washington State Department of Ecology.* [Online] 2016. [Cited: 08 30, 2015.] https://fortress.wa.gov/ecy/waterresources/map/WCLSWebMap/.

36. **LaHusen, Sean R., et al., et al.** Surface roughness dating of long-runout landslides near Oso, Washington (USA), reveals persistent postglacial hillslope instability. *Geology.* 2015.

37. **Hood, Darden.** Letter to Mr. Tom Badger; RE: Radiocarbon Dating Result For Sample EB-04-15-226. Miami : Beta Analytic, Inc., 2015.

38. **Puget Sound Lidar Consortium.** Darrington (North Fork Stillaguamish) USGS/NASA survey. *Puget Sound Lidar Consortium.* [Online] Puget Sound Lidar Consortium. [Cited: 10 01, 2015.] http://pugetsoundlidar.ess.washington.edu/lidardata/restricted/filegeodatabase/darrington/index.html.

39. **USGS.** The National map. *Elevation Products (3DEP).* [Online] USGS. [Cited: 10 01, 2015.] http://viewer.nationalmap.gov/basic/?basemap=b1&category=ned,nedsrc&title=3DEP%20View.

40. **Dreger, Douglas S.** *Personal Communications.* 2015.

41. *Forest interception studies in the United States.* **Zinke, PJ.** [ed.] W. E. Sopper and H. W. Lull. New York : Pergamon Press, 1967, International Symposium on Forest Hydrology, pp. 137-161.

42. **Rothacher, J.** Net precipitation under a Douglas-fir forest. *Forest Science.* 1963, Vol. 9, 4, pp. 423-429.

43. **Rowe, L. K., Marden, M. and Rowan, D.** Canopy and litter interception of rainfall by hardwoods of eastern United States. *Water Resources Research.* 1965, Vol. 1, 2, pp. 193-206.

44. **Rutter, A. J., et al., et al.** A predictive model of rainfall interception in forests, 1. Derivation of the model from observations in a plantation of Corsican Pine. *Agricultural Meteorology.* 1971, Vol. 9, pp. 367-384.

45. **Keim, R. F. and Skaugset, A. E.** A linear system model of dynamic throughfall rates beneath forest canopies. *Water Resources Research.* 2004, Vol. 40.

46. *QGIS-A Free and Open Source Geographic Information System.*

47. **Washington State Department of Transportation, (WSDOT).** *Oso Slide April 2014 Static US Feet - Ground Based LiDAR Survey.*

48. —. *Oso Slide March 2015 Static US Feet - Ground Based LiDAR Survey.*

49. —. *Oso Slide Sept 2015 Static US Feet - Ground Based LiDAR Survey.*

50. **Storesund, Rune.** *Western Margin Ground-Based LiDAR Survey (Sept 2015).*

1   51. —. *SR 530 Headscarp Ground-Based LiDAR Survey (Sept 2015).*

2   52. **Thorsen, Gerald W.** *Memorandum - Landslide of January 1967 which diverted the North Fork of the*

3   *Stillaguamish River near Hazel.* Olympia : Washington Department of Natural Resources; Geology &

4   Earth Resources Division, 1969.

5   53.

6

7

APPENDIX A

Precipitation Summary and Throughfall on Whitman Bench

The ruling hypothesis for these types of landslides is that while there are many causal factors, they are triggered by extreme rainfall. Further, it is expected that the extreme nature of the rainfall will match the extreme nature of the landslide. In other words, if the SR 530 landslide was caused by rainfall then that rainfall should also be an extreme event. The rain gauge closest to the location of the landslide was the Oso rain gauge (http:\\fortress.wa.gov\eay\eap\flow). It is administered by the Washington Department of Ecology, is about three miles from the slide, and is at the elevation of the valley bottom. There were five years of record for that rain gauge, water years 2012 to 2016. On March 22, 2014, the 21 day (21d) and 42 day (42d) duration rainfall was 13.15 and 19.93 inches, respectively. These values were not the maximum 21d and 42d values for the year but they were, in essence, the same. The maximum 21d rainfall was 13.16 inches and occurred on March 21, 2016. The maximum 42d rainfall was 20.09 inches and occurred on March 29, 2014. During the five year record for the Oso rain gauge the 21d rainfall was 13.05 inches in WY 2012 and 13.88 inches in 2016. These values are either slightly more than (13.88 inches) or about the same as (13.05 inches) the March 22, 2014 value. Similarly, for the 42d rainfall the March 22, 2014 value of 19.93 inches was, in essence, matched or exceeded in every year of record; 19.52 inches in WY 2012, 21.73 inches in 2013, 20.02 inches in WY 2014, and 21.87 inches in WY 2016. So the March 22, 2014 values of rainfall were not unique or extreme for this part of Washington.

It is possible to assign values of 21d and 42d throughfall to the Whitman Bench for March 22, 2014. Average daily throughfall can be calculated by taking the average of the 24 throughfall gages on the Whitman Bench for each day. Then the 21d and 42d average daily throughfall can be calculated. Once the 21d and 42d throughfall is calculated the maximum value of each parameter can be determined. These values can be compared to similar duration rainfall values for the appropriate date for the Oso rain gauge. Simple ratios can be determined to compare Oso rain gauge values to Whitman Bench throughfall values. Then, using these ratios the 21d and 42d average throughfall values for the Whitman Bench on March 22, 2014 can be calculated from 21d and 42d rainfall values for the Oso rain gauge. The 21d and 42d average throughfall for the Whitman Bench on March 22, 2014 was approximately 13 and 19 inches, respectively. The values that were used to characterize the rainfall for the SR 530 landslide on March 22, 2014 are from the Darrington, Washington (www.climate.washington.edu/maps/maps/php) rain gauge and are 15.79 inches and 26.89 inches for the 21d and 42d rainfall, respectively. The throughfall values for Whitman Bench and the rainfall values for the Darrington rain gauge have a difference of 3.79 inches or 18 percent less for the 21d rainfall and a difference of 7.89 inches or 29 percent less for the 42d rainfall. The rainfall that fell at Darrington is much more than the average throughfall on the Whitman Bench, just under half again as much. The difference in the Darrington rainfall and the Whitman Bench throughfall are due to differences in elevation and topography and the Whitman Bench values include interception loss while the Darrington values are for an open rain gauge.

In their paper, Henn et al 2015 report a return period of 88 years for the 21d rainfall for the Darrington rain gauge for the time period ending March 22. The 42d rainfall similarly has a large (>20 yr) return period. But these values are for the unique time period that ends on March 22. For landslide processes, it makes more sense to consider these rainfall amounts as they occur on an annual basis. From Henn et al 2015, for Darrington return periods:

40   *"When considered relative to annual maximum accumulations, the 2014 accumulations*

41   *are necessarily less unusual. For windows of less than 1 yr, the return periods peak at 2.9*

42   *yr for the 42-day accumulation, indicating that the 2014 accumulations were barely*

43   *above the median annual maximum 42-day precipitation accumulation."*

44   When considered based on an annual basis the 21d rainfall for Darrington on March 22, 2014 had a

45   return period of about 2 years (Henn et al 2015). So the rainfall amounts that fell in the vicinity of the

46   Oso landslide prior to March 22, 2014 are not extreme.

47   Furthermore, the Hazel Slide does not require an extreme value of rainfall to move. The Hazel Slide

48   moved or "failed" on January 7, 1967 and on January 25, 2006. Rainfall values for the Darrington rain

49   gauge were not available for those dates so rainfall values from the Concrete Pipeline Fish Station

50   (www.climate.washington.edu/maps/maps.php) were used. For January 7, 1967 the 21d and 42d rainfall

51   for the Concrete Pipeline Fish Station rain gauge were 5.38 and 7.46 inches, respectively. For January 25,

52   2006 the 21d and 42d rainfall for the Concrete Pipeline Fish Station rain gauge were 12.51 and 23.41

53   inches, respectively. For March 22, 2014, these values were 11.45 inches and 19.69 inches, respectively.

54   The 21d and 42d rainfall for the 1967 movement of the Hazel slide were both less than half of the March

55   22, 2014 values. For the 2006 movement of the Hazel slide, both rainfall durations were greater than the

56   values for March 22 2014.

57   For January 7, 1967 the 21d and 42d rainfalls for the Arlington rain gauge were 4.53 and 10.56 inches,

58   respectively. For January 25, 2006 the 21d and 42d rainfalls for the Arlington rain gauge were 5.91 and

59   11.38 inches, respectively. On March 22, 2014 the 21d and 42d rainfall amounts for the Arlington rain

60   gauge were 7.28 and 12.25 inches, respectively. All four of the rainfall parameters associated with the

61   movement of the Hazel slide in 1967 and 2006 were less than these same parameters for March 22,

62   2014. None of these values are considered extreme, yet the Hazel Slide moved. The Hazel Slide has

63   always moved in the winter during regional, wet mantle storms. So winter rainfall is needed as a

64   necessary condition for the slide to occur. These same rainfall conditions occur during most winters in

65   western Washington but the Hazel Slide has moved only every 10 or 15 years. So the rainfall is a

66   necessary condition for failure to occur, but it doesn't appear to trigger the failure.

67   **Throughfall**

68   In 2004, 8.5 acres of the forest on the Whitman Bench was harvested in a wedge-shaped clearcut.

69   Approximately ½ acre of that area became part of the SR 530 landslide in 2014. Removal of a forest

70   canopy decreases interception, which increases the amount of net precipitation that reaches the forest

71   floor. As we interpret it, the Plaintiffs contend that the increase in net precipitation to the forest floor

72   due to reduced interception that results from clear-cut timber harvest results in a direct increase in

73   groundwater. In this appendix, the effect of the different age classes of forest on throughfall on the

74   Whitman Bench is quantified.

75   There are three distinct age classes of forest on the Whitman Bench in the vicinity of the scarp of the SR

76   530 landslide. The youngest age class is mentioned above. That stand is a Douglas-fir forest that was

77   approximately nine years old when the SR 530 landslide occurred. As of the writing of this report it is a

78 12-year old harvest-regenerated Douglas-fir forest that developed as a result of reforestation after the
79 2004 clearcut. The majority of the forest in the vicinity of the SR 530 scarp is a harvest-regenerated
80 Douglas-fir forest that developed from a large clearcut in 1988. Thus, that stand was, nominally, 27
81 years old when the slide occurred. Finally, there is an older age class of Douglas-fir forest that occupies
82 the edge of the bench where the slope falls off steeply. This stand was approximately 80 years old when
83 the slide occurred. The objective of this project was to quantify the throughfall for each of these three
84 different age class Douglas-fir forests.

85 **Methods**

86 Twenty eight rain gauges were installed to quantify the rainfall on the Whitman Bench and the
87 throughfall under the different aged forest stands. The rain gauges were all Onset RG 3 tipping bucker
88 rain gauges with a six inch orifice and a resolution of 0.01 inches of rainfall. Each rain gauge was mated
89 with a HOBO Pendant event data logger. The rain gauges were installed by attaching them to metal 'T'
90 fence posts with two hose clamps. The rain gauges were installed so that the orifice was level and,
91 nominally, 4.5 feet above the ground.

92 To quantify throughfall under the three age classes of forest stand, 24 rain gauges were installed in
93 three transects of eight rain gauges each. Each transect was located in a different age class of stand in
94 the vicinity of the scarp of the SR 530 landslide (Figures A1-A4). The transects were located parallel to
95 the edges of the forest stands and, nominally, a distance of three tree heights into the stand from the
96 forest edge. The first rain gauge in each transect was located a random distance between 0 and 50 feet
97 from an arbitrarily chosen starting point. Each subsequent gage was installed at an interval of 50 feet.
98 The first 21 rain gauges, seven gages in each of the three transects, were installed on November 20,
99 2014. An eighth rain gauge was added to each transect on December 4, 2014.

100 Four rain gauges were installed in a recent clearcut approximately 1 ½ miles north of the slide scarp
101 (Figure A1-A4). These rain gauges were installed in the open and measured gross rainfall, not throughfall
102 or net rainfall. These rain gauges were installed to allow the gross rainfall on Whitman Bench to be
103 referenced to other area rain gauges such as the rain gauges at Oso, Arlington, and Darrington. The first
104 rain gauge was installed on November 20, 2014. A second rain gauge was installed on December 4,
105 2014. Two subsequent rain gauges were installed on April 20, 2015.

106 All of the rain gauges were calibrated when they were received before they were installed on Whitman
107 Bench. The rain gauges were removed in July 2015 and recalibrated. Once they were recalibrated they
108 were reinstalled on site on September 26, 2015. They are all still installed and collecting data as of the
109 date of this report.

110 Data was downloaded from the rain gauge network on a frequent but irregular basis. Data downloads
111 were scheduled for time periods directly after storms because storm data was the most valuable and
112 the rain gauges were most vulnerable to damage and need maintenance after storms. There were seven
113 data downloads in WY 15 between November 2014 and July 2015. There were eight data downloads in
114 WY 16 between October 2015 and May 2016. There were the normal problems associated with field

115   data collection that included stuck tipping buckets, dead batteries, and plugged funnels but no data was
116   lost from the data loggers.

117   **Throughfall Data Analysis**

118   The first step in the analysis of the throughfall data was to select the parameters to analyze. The
119   parameters chosen were the maximum throughfall for the 21-day (21d) and 42-day (42d) durations
120   calculated on a daily time step. The reasons for the choice of these parameters are several. The Oso
121   landslide was an extreme event. It was certainly greater than a once in a generation or once in a lifetime
122   event. It was, most likely, a once in a millennium event. If rainfall is to be hypothesized as a triggering
123   mechanism then by necessity the rainfall that occurred prior to the slide must also occur as a low
124   frequency/high return period event. The frequency of occurrence was determined for a number of
125   rainfall durations (28) following the Oso landslide (See Geer Report and Henn et al 2015). The two
126   durations that had the highest return periods were the 21d and 42d. There is no evidence in the
127   literature that these two rainfall durations are special and in any way uniquely correlate with the
128   occurrence of large, deep-seated landslides. They were used in this analysis simply because of the high
129   return period for these two durations that was reported for the rainfall that preceded the occurrence of
130   the SR 530 landslide.

131   Further, if 21d and 42d duration rainfall/throughfall amounts are used for analysis, then the data will
132   come from rainfall that occurs in the middle of the winter during regional, wet-mantle storms. During
133   regional wet-mantle storms in winter deciduous hardwoods are in a leaf-off condition. If rainfall
134   durations become long enough they start to move outside of the window of leaf-off conditions for
135   hardwoods. For example, rainfall that occurs in the fall before leaves are dropped and rainfall that
136   occurs in the spring after leaf-on will result in more interception than would occur in the winter during
137   leaf off conditions. The analysis was carried out for conditions that were similar to the conditions that
138   occurred prior to the SR 530 landslide, namely winter, wet-mantle storms. Thus, the 21d and 42d
139   durations were used to simulate those conditions.

140   One way analysis of variance was carried out for the throughfall amount on the day that the maximum
141   21d and 42d throughfall occurred in water years 2015 and 2016. The null hypothesis was that the
142   average throughfall for the three age classes of forest are equal and the alternative hypothesis is that
143   they are not equal.

144        $H_0: \mu_{12 \text{ yr std}} = \mu_{27 \text{ yr std}} = \mu_{80 \text{ yr std}}$

145        $H_a: \mu_{12 \text{ yr std}} \neq \mu_{27 \text{ yr std}} \neq \mu_{80 \text{ yr std}}$

146   The maximum for the average daily throughfall for the 21d duration in WY 2015, in our dataset,
147   occurred on December 10, 2014. The overall average for that date for the 20 rain gauges used in the
148   analysis was 9.40 inches. The averages for the different age class stands were: 9.56 inches for the 12-
149   year old stand (6 gages), 10.10 inches for the 27-year old stand (7 gages), and 8.57 inches for the 80-year
150   old stand (7 gages). The averages of the throughfall or the three different aged stands were not
151   significantly different at the 95 % confidence level.

152   The maximum for the average daily throughfall for the 42d duration in WY 2015, in our dataset,
153   occurred on January 1, 2015. The overall average for that date for the 20 rain gauges used in the analysis
154   was 14.82 inches. The averages for the different age class stands were: 15.26 inches for the 12-year old
155   stand (6 gages), 16.07 inches for the 27-year old stand (7 gages), and 13.21 inches for the 80-year old
156   stand (7 gages). The averages of the throughfall for the three different aged stands were not
157   significantly different at the 95 % confidence level.

158   The data analyzed for the maximum 21d and 42d throughfall in WY 2015 for the rain gauges on the
159   Whitman Bench may not have been the annual maximum for that location. The rain gauges were
160   installed and began operating on November 20, 2015. Data for analysis could not be used until 21 and
161   42 days after that date. The values of maximum 21d and 42d throughfall are, in fact, the maximum in
162   our database for WY 2015. The data for the Oso rain gauge was interrogated to determine whether or
163   not the annual maximum 21d and/or 42d rainfall occurred before the rain gauges on the Whitman
164   Bench were installed. The maximum 21d rainfall for the Oso rain gauge occurred on November 9, 2014
165   and the maximum 42d rainfall occurred on November 30, 2014. Thus, it is likely that the annual
166   maximum 21d and 42d throughfall on Whitman Bench in WY 2015 occurred before the rain gauges were
167   installed or before they were installed long enough to generate the requisite duration data. However,
168   the throughfall values used in the analysis are the maximum values in the data set for WY 2015.

169   The maximum for the average daily throughfall for the 21d duration in WY 2016 occurred on November
170   17, 2015. The overall average throughfall for that date for the 24 rain gauges used in the analysis was
171   13.10 inches. The average throughfall for the different age class stands, all based on eight rain gauges
172   were: 13.28 inches for the 12-year old stand, 12.61 inches for the 27-year old stand, and 13.43 inches
173   for the 80-year old stand. The averages throughfall for the three different aged stands were not
174   significantly different at the 95 % confidence level.

175   The maximum of the average daily throughfall for the 42d duration in WY 2016 occurred on December
176   8, 2015. The overall average throughfall for that date for the 24 rain gauges used in the analysis was
177   18.97 inches. The average throughfall for the different age stands, all based on eight rain gauges, were:
178   20.06 inches for the 12-year stand, 18.40 inches for the 27-year old stand, and 18.44 inches for the 80-
179   year old stand. The averages of the throughfall for the three different aged stands were not significantly
180   different from each other at the 95 % confidence level.

181   Analysis was carried out for 21d and 42d duration throughfall for WY 2015 and WY 2016. The null
182   hypothesis was that the average throughfall for the three different aged forests were equal. The
183   alternative hypothesis was that they were not equal. For both water years and throughfall durations the
184   null hypothesis was not rejected (see attached ANOVA tables). Thus, there is no statistically significant
185   difference in the amount of throughfall that was measured under the canopies of the three different age
186   forests. For the area on the Whitman Bench in the vicinity of the scarp of the SR 530 landslide, forest
187   management had no effect on throughfall.

188

189   Table A-1: Water Year 2015 – Maximum 21-day Rainfall Duration

Treatment	2004 CC	27-yr stand	80-yr stand
	9.45	8.39	8.56
	9.32	12.72	6.63
	7.6	8.93	8.98
	12.4	11.08	7.55
	7.72	9.26	8.41
	10.84	11.49	8.54
		8.36	11.33
Total	57.33	70.73	60.00
Sample size (n)	6	7	7
Mean	9.56	10.10	8.57

190

191   Grand Total: G = 188.06 inches

192   Total number of observations = 6 + 7 + 7 = 20

193   Grand mean = 9.403 inches

194

195   Table A-2: Analysis of Variance Table

Source of Variation	d. f.	Sum of Squares	Mean Square	F value (calc.)
Total	19	54.33		
Among samples	2	8.42	4.21	1.56
Within samples	17	45.91	2.70	

196

197   Calculated F value: $F_{2, 17}$ = 1.56

198   Tabular F value: $F_{.05, 2, 17}$ = 3.59[1]

199        $F_{2, 17}$ = 1.56; $F_{.05, 2, 17}$ = 3.59

200   1.56 < 3.59 (p = 0.2388)[2] Thus, fail to reject the H_0.

201   There is no statistically significant difference between the means of the three treatments

202   [1] Table A5, Petersen, Roger G., Exercises in Statistical Inference, OSU Bookstores, Inc. 1975.

203   [2] p-value calculator GraphPad; http://graphpad.com/quickcalcs/PValue1.cfm

204   Table A-3: Water Year 2015 – Maximum 42-day Rainfall Duration

Treatment	2004 CC	27-yr stand	80-yr stand
	15.18	12.06	12.13
	14.80	19.77	6.61
	12.13	14.18	14.16
	20.02	17.70	11.70
	11.77	15.61	14.04
	17.64	18.39	14.57
		14.80	19.25
Total	91.53	112.50	92.45
Sample size (n)	6	7	7
Mean	15.26	16.07	13.21

205

206   Grand Total: G = 296.48 inches

207   Total number of observations = 6 + 7 + 7 = 20

208   Grand mean = 14.82 inches

209

210   Table A-4: Analysis of Variance Table

Source of Variation	d. f.	Sum of Squares	Mean Square	F value (calc.)
Total	19	210.97		
Among samples	2	30.31	15.15	1.43
Within samples	17	180.66	10.63	

211

212   Calculated F value: $F_{2, 17}$ = 1.43

213   Tabular F value: $F_{.05,2, 17}$ = 3.59[1]

214          $F_{2, 17}$ = 1.56; $F_{.05, 2, 17}$ = 3.59

215   1.43 < 3.59 (p = 0.2667)[2] Thus, fail to reject the H_0.

216   There is no statistically significant difference between the means of the three treatments

217   [1] Table A5, Petersen, Roger G., Exercises in Statistical Inference, OSU Bookstores, Inc. 1975.

218   [2] p-value calculator GraphPad; http://graphpad.com/quickcalcs/PValue1.cfm

219   Table A-5: Water Year 2016 – Maximum 21-day Rainfall Duration

Treatment	2004 CC	27-yr stand	80-yr stand
	11.62	10.73	12.45
	11.79	14.22	11.67
	9.66	10.54	13.65
	15.41	13.77	11.87
	12.32	11.74	12.56
	12.83	14.69	13.98
	13.15	11.79	15.35
	19.42	13.40	15.90
Total	106.20	100.88	107.43
Sample size (n)	8	8	8
Mean	13.28	12.61	13.43

220

221   Grand Total: G = 314.51 inches

222   Total number of observations = 3(8) = 24

223   Grand mean = 13.1 inches

224

225   Table A-6: Analysis of Variance Table

Source of Variation	d. f.	Sum of Squares	Mean Square	F value (calc.)
Total	23	100.01		
Among samples	2	3.03	1.52	0.33
Within samples	21	96.98	4.62	

226

227   Calculated F value: $F_{2, 21}$ = 0.33

228   Tabular F value: $F_{.05,2,17}$ = 3.59[1]

229        $F_{2, 21}$ = 0.33; $F_{.05,2, 21}$ = 3.47

230   0.33 < 3.47 (p = 0.7240)[2] Thus, fail to reject the H_0.

231   There is no statistically significant difference between the means of the three treatments

232   [1] Table A5, Petersen, Roger G., Exercises in Statistical Inference, OSU Bookstores, Inc. 1975.

233   [2] p-value calculator GraphPad; http://graphpad.com/quickcalcs/PValue1.cfm

234   Table A-7: Maximum Rainfall for 42-day Duration - Water Year 2016

Treatment	2004 CC	27-yr stand	80-yr stand
	17.37	14.75	17.23
	17.63	21.35	16.10
	16.49	15.34	18.57
	22.86	19.83	16.44
	20.00	17.56	17.39
	19.49	21.67	18.67
	18.80	17.39	21.08
	27.90	19.30	22.03
Total	160.48	147.18	147.51
Sample size (n)	8	8	8
Mean	20.06	18.40	18.44

235

236   Grand Total: G = 455.17 inches

237   Total number of observations = 3(8) = 24

238   Grand mean = 18.97 inches

239

240   Table A-8: Analysis of Variance Table

Source of Variation	d. f.	Sum of Squares	Mean Square	F value (calc.)
Total	23	190.36		
Among samples	2	14.40	7.20	0.86
Within samples	21	175.96	8.38	

241

242   Calculated F value: $F_{2, 21}$ = 0.86

243   Tabular F value: $F_{.05,2,17}$ = 3.47[1]

244        $F_{2, 21}$ = 0.86; $F_{.05,2, 21}$ = 3.47

245   0.86 < 3.47 (p = 0.4375)[2] Thus, fail to reject the H_0.

246   There is no statistically significant difference between the means of the three treatments

247   [1] Table A5, Petersen, Roger G., Exercises in Statistical Inference, OSU Bookstores, Inc. 1975.

248   [2] p-value calculator GraphPad; http://graphpad.com/quickcalcs/PValue1.cf

References

249

250 Henn B, Q Cao, DP Lettenmaier, CS Magirl, C Mass, JB Bower, M St. Laurent, Y Mao and S Perica. 2015.
251 Hydroclimatic conditions preceding the March 2014 Oso landslide. American Meteorological Societ, DOI:
252 10.1175/JHM-D-15-0008.1
253
254 Keaton, Jr, J Wartman, S Anderson, J Benoit, J deLaChapelle, R Gilbert, and D Montgomery. 2014. The 22
255 March 2014 Oso Landslide, Snohomish County, Washington. GEER Report, July 22, 2014.
256
257

258
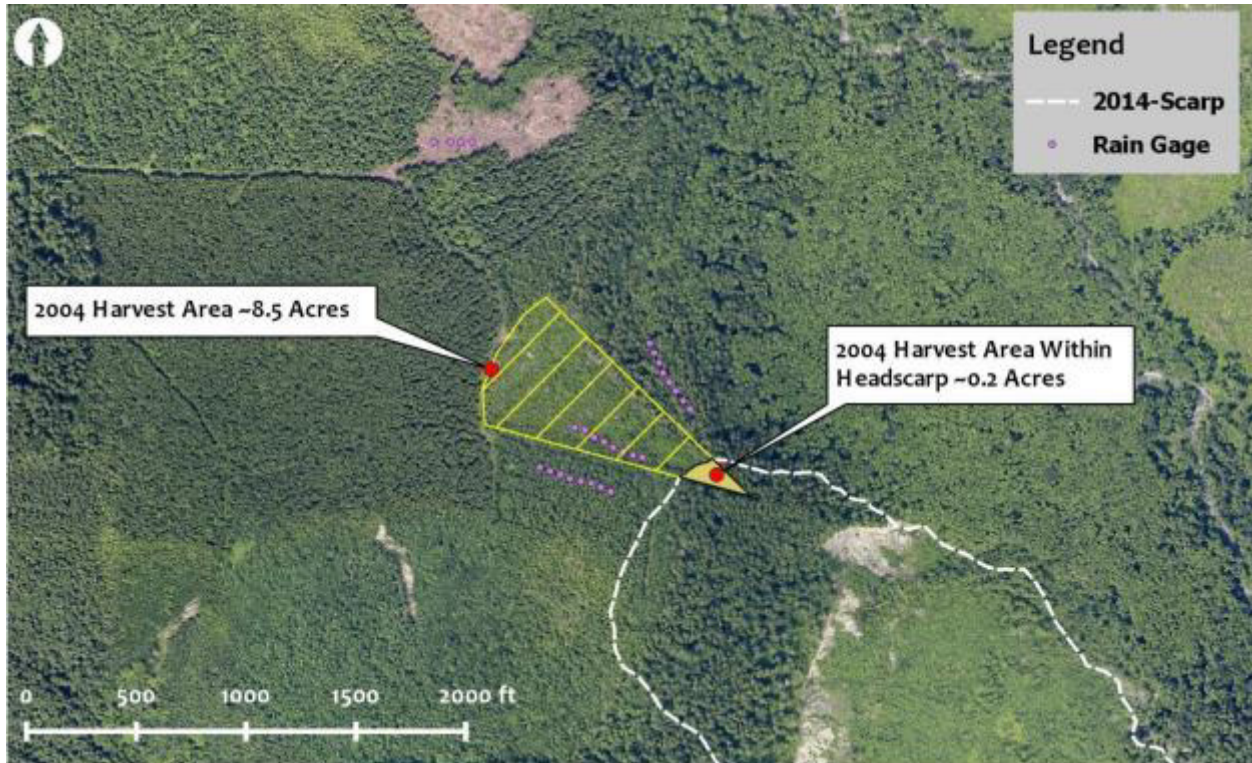
259
260 *Figure A-1: Overview of rain gage locations with 2012 aerial Image basemap.*

261
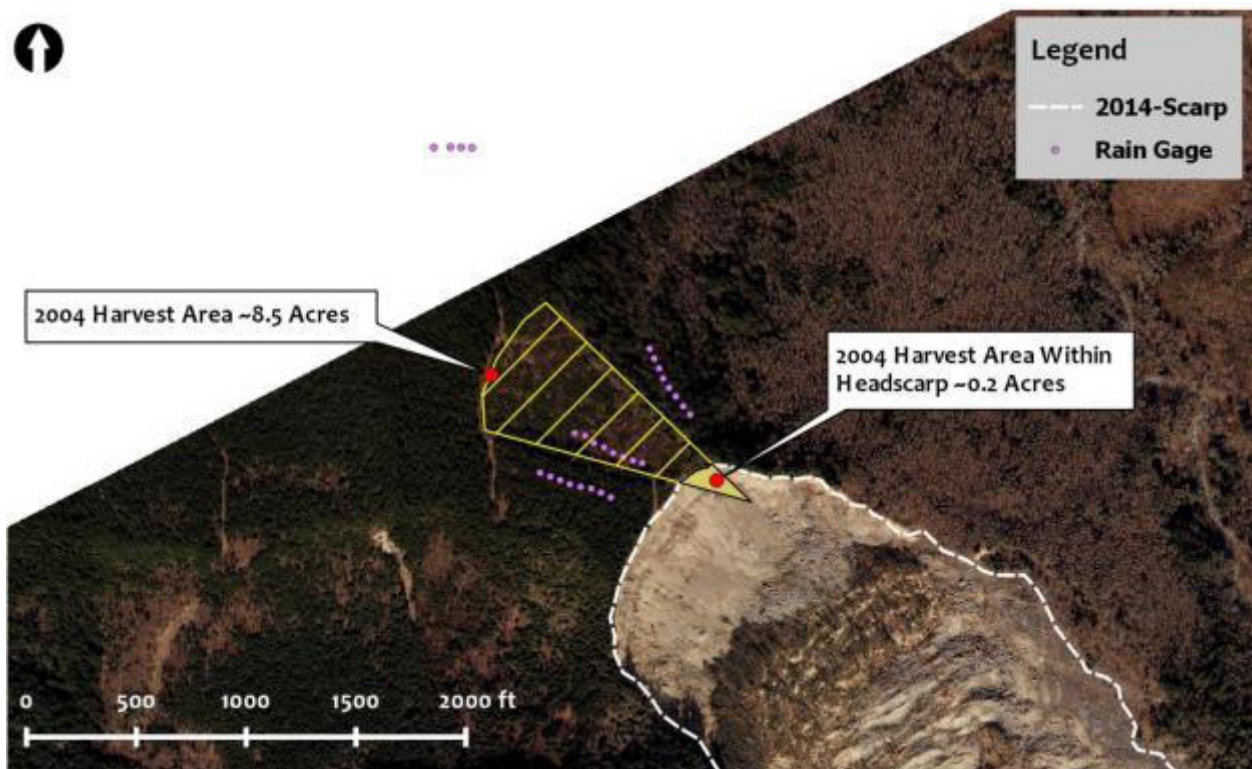
262
263 *Figure A-2: Overview of rain gage locations with 2014 (post slide) aerial Image basemap.*

264

265
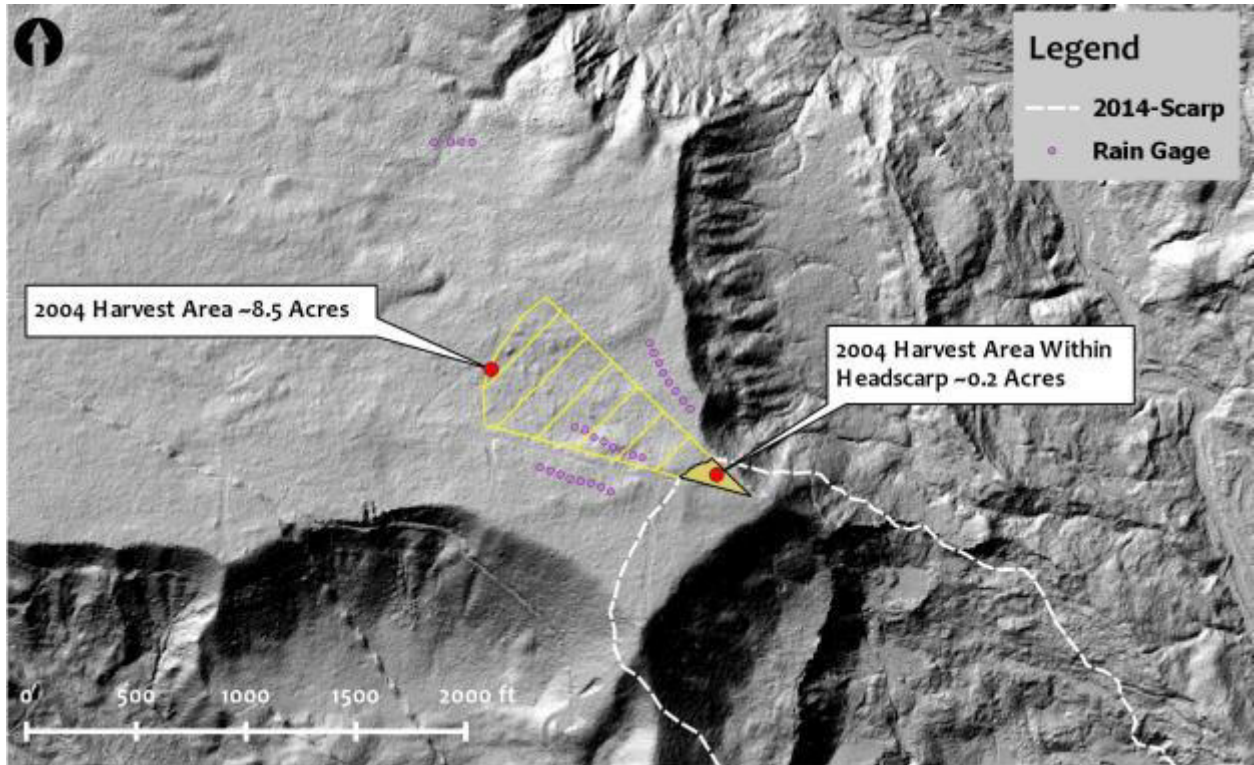
Figure A-3: Overview of rain gage locations with 2013 Aerial LiDAR hillshade basemap.

266
267
268
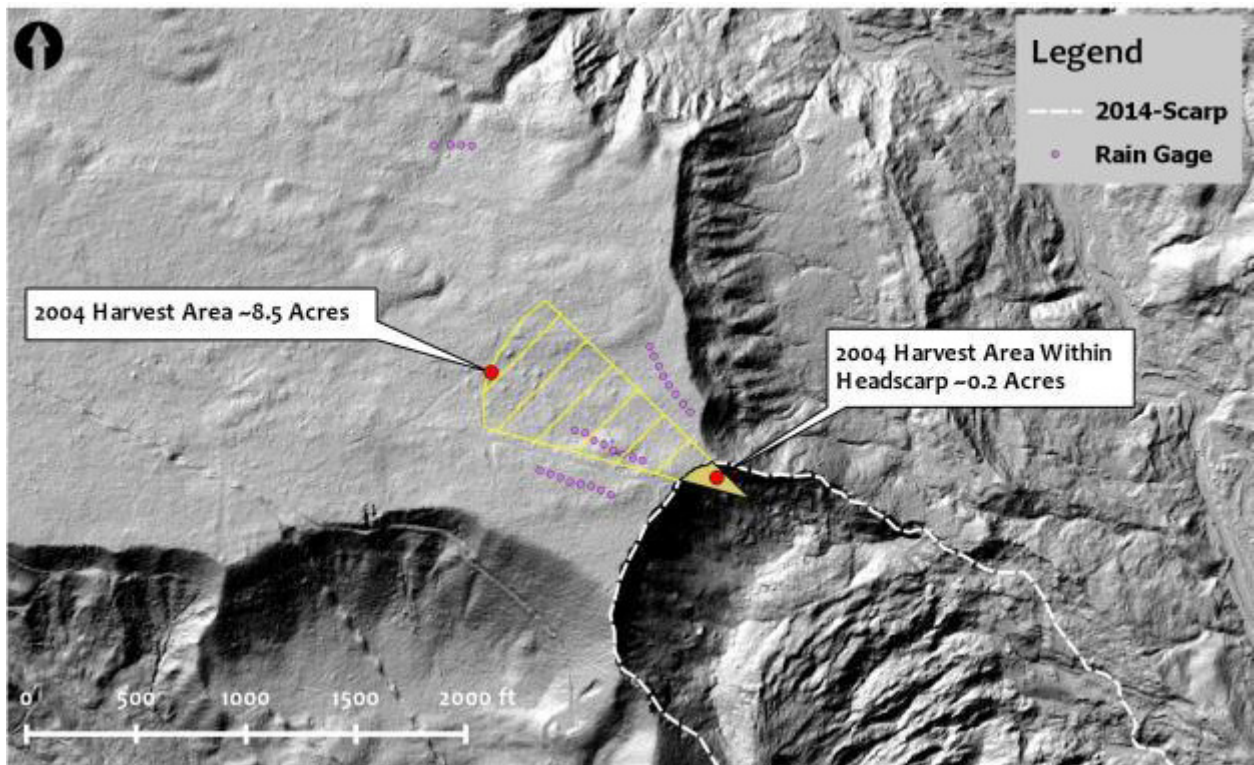
Figure A-4: Overview of rain gage locations with 2014 Aerial LiDAR hillshade basemap.

269
270

271

APPENDIX B

Field Exploration

1   Drilling for subsurface exploration began on Whitman Bench in mid-July 2015. Simultaneous drilling by

2   two drill rigs shifted to the main body of the slide in mid-September 2015 and continued through early

3   October 2015. Drilling activities included in-situ soil testing (Cone Penetration Tests and blow counts,

4   etc.), soil sample collection, installation of vibrating wire piezometers (for measurements of piezometric

5   head), and installation of slope inclinometer casings (necessary to record slope movements). Drilling

6   with one drill rig resumed on Whitman Bench following completion of drilling on the main body of the

7   SR 530 Landslide in October 2015 and was completed in December 2015.

8

9   Supporting information included in the electronic support documents include:

10   • Final geotechnical exploration report completed by WSDOT titled "Geotechnical Data Report, SR

11   530 Landslide: Geotechnical Study" and dated May 2016. *We note that there are a number of*

12   *discrepancies contained in this report and our interpretations are not constrained to the*

13   *information as presented in this report>.*

14   • Copy of survey results from WSDOT survey of exploration points at the site.

15   • Photos of soil samples taken during drilling of the soil borings.

16   • Copies of the original field logs as completed by the WSDOT inspectors.

17   • Photographs of cores received at WSDOT geotechnical laboratory.

APPENDIX C

Geotechnical Instrumentation

Two instrumentation approaches were employed as part of our geotechnical exploration program: groundwater levels based on vibrating wire piezometers (vwp), and slope movement detection using traversing-type inclinometers. Details regarding specific instruments, configuration of data collectors and data transmission, and calibration sheets, are presented in Appendix C. VWP instruments generally collect data every two hours. Weekly updates are extracted from the data logger by WSDOT personnel and then distributed to the State of Washington Attorney General's office for distribution to the designated parties (State of Washington Expert Team being one of the designated parties).

WSDOT initiated the process of instrument installation during execution of the exploratory borings as part of the 2015 campaign (WSDOT previously installed instruments as part of the 2014 work performed on Whitman Bench). The WSDOT instrumentation team then connected the individual stations to central data loggers, after the majority of the installations were complete. The first batch of data came online in late October 2015. The last set of instruments was connected to the base stations in late December 2015. Field data quality control efforts began in earnest following receipt of the February 22nd piezometer data report. It emphasized in our January 22nd Interim Report that observing groundwater conditions through a full wet season was essential to understanding the groundwater system. A number of questions arose during review of the data, and through development of answers to those questions and review by the full expert team, a protocol for acceptance and rejection of piezometer data was developed. Finalization of the quality control protocols occurred after receipt of the April 18th piezometer data report which allowed updating of the records through the winter high precipitation season. Details of the quality control protocol and interpretation of the piezometer records are presented in Appendix I. Fortunately, piezometric level changes over time are moderate enough that changes since the April 18th data set are not likely to be significant from a geotechnical analysis perspective.

Supporting information included in the electronic support documents include:
- Data collected from the VWP instruments (as well as two rain gages).
- Inclinometer data from EB-04si-15; EB-05si-15; EB-07si-15; EB-09si-15; and H-12si-15.
- (from Appendix B support materials) Final geotechnical exploration report completed by WSDOT titled "Geotechnical Data Report, SR 530 Landslide: Geotechnical Study" and dated May 2016.
  <We note that there are a number of discrepancies contained in this report and our interpretations are not constrained to the information as presented in this report>.

APPENDIX D

Geotechnical Laboratory Testing

1 Geotechnical analysis of the SR 530 Landslide is an important component to understanding causation

2 and runout consequences. In addition to delineating slope geometry and stratigraphy, characterizing

3 the engineering properties of the soil units (e.g. unit weight, shear strength, and hydraulic conductivity)

4 are also necessary components of the evaluation. Since the SR 530 Landslide involved both cohesionless

5 granular soils as well as cohesive fine grained soils, both a field and laboratory testing program was

6 required. Field tests consisted of driven Standard and Oversized Penetration Tests, and Cone

7 Penetration tests. Laboratory tests included index tests, gradation tests, specific gravity tests,

8 consolidation tests on fine grain soils, direct shear tests both parallel and perpendicular to soil

9 laminations, triaxial tests in both compression and extension, torsional ring shear tests, and hydraulic

10 conductivity tests. In addition, hydraulic conductivity was inferred from consolidation tests and the

11 consolidation phase of triaxial tests.

12

13 Our stratigraphic interpretation of the SR 530 Landslide includes prehistoric failure surfaces that we

14 infer to be in glacio-lacustrine silt and clay, landslide debris from the Hazel slide, intact glacio-lacustrine

15 silt and clay, and intact sections of glacial advance silt and sand, glacial till, and recessional outwash sand

16 and gravel. We could not sample these materials directly, because they are now failed and no longer in

17 place. Instead, we did extensive sampling from boring EB-02 located on the Whitman Bench, and

18 sampling from beneath the SR 530 surface of rupture in borings located on the slide area.

19

20 The high plasticity, over-consolidated fine-grained glacio-lacustrine unit beneath the upper sand/gravel,

21 till, and outwash sand units is the primary stratigraphic unit tested for shear strength, because much of

22 the surface of rupture of the SR 530 Landslide appears to lies within this unit. Thus, this unit is the

23 primary focus of the geotechnical laboratory testing program. Over-consolidated, high plasticity glacial

24 silts and clays are particularly susceptible to strength loss, which could help explain the cause of the

25 rapid movement and long runout length of the SR 530 Landslide. The stability assessment of the SR 530

26 Landslide is largely governed by the shear strength of the soil materials that failed during the SR 530

27 Landslide movement. Thus, strength data of the soil materials collected along the surface of rupture and

28 within the SR 530 Landslide mass are essential to perform realistic slope stability analyses.

29

30 We have employed several strength tests to comprehensively evaluate the shear strength of over-

31 consolidated silt and clay materials. Torsional Ring Shear (TRS) tests are used to evaluate fully softened

32 and residual effective friction angles of the glacio-lacustrine silt and clay. When combined with Direct

33 Shear (DS) test data that captures the peak friction angles of the silt and clay materials, a nearly

34 complete picture of the effective shear strength of the fine-grained glacio-lacustrine unit can be

35 discerned. The shear strength of the rhythmically bedded, mostly laminated, glacio-lacustrine deposit is

36 likely anisotropic. Thus, some of the Direct Shear (DS) tests have been performed with non-horizontally

37 oriented test specimens to evaluate anisotropy.

38

39 The stress-strain responses of the soil materials are important as well, because the materials potentially

40 involved in the 2014 Landslide likely achieved their peak, fully softened, and residual strengths at

41 different times as the landslide deformed. Therefore, a series of triaxial (TX) tests have been performed

42 to characterize the nonlinear, stress-dependent stress-strain response of the key stratigraphic horizons.

43 Stress-strain strength anisotropy has also been evaluated by performing TX compression and TX

44 extension tests.

45

46 In addition to strength testing of the fine-grained glacio-lacustrine unit, stress history has been

47 investigated through a series of consolidation tests. Soil response depends significantly on the soil's

48 stress history (i.e., whether it has never felt a higher stress than it is feeling currently, or if it is over-

49 consolidated because it once felt a stress higher than what it is feeling currently). These test results,

50 along with estimates of the in situ state of the fine-grained glacio-lacustrine unit, are essential

51 components of the numerical simulations of the SR 530 Landslide.

52

53 Lastly, soil units other than the fine-grained glacio-lacustrine unit, also require strength characterization.

54 In particular, the surface of rupture was found within the sand unit beneath the fine-grained glacio-

55 lacustrine unit at one location. The Cone Penetration Tests (CPT), Standard and Over-sized Penetraton

56 Tests, and index testing are being used to estimate the shear strength of these units, because

57 "undisturbed" sampling of sands and tills was not possible. However, our team believes there are

58 sufficient field data and robust correlations available to develop reasonable estimates of the strength of

59 these soil units.

60

61 Supporting information included in the electronic support documents include:

62 • Geotechnical test results from Cooper Testing Laboratories, located in Palo Alto, California.

63 • Geotechnical test results from Geotesting Express, located in Acton, MA.

64 • Geotechnical test results from UC Berkeley, located in Berkeley, CA.

65   • Carbon-dating via WSDOT contract laboratories.

66   • Minerology evaluations by Dr. Ann M. Hagni.

67

APPENDIX E

Engineering Properties of Soils

APPENDIX E – ENGINEERING PROPERTIES OF SOILS

Soil Units and Stratigraphy

The generalized stratigraphy of the Whitman Bench and the Hazel slide before the March 22, 2014 SR-530 landslide is shown in Figure E-1. The generalized stratigraphy is based on the geologic studies and fieldwork performed as part of this study. After describing the geometry of the soil stratigraphy in this section, the results of the field and laboratory testing program are used to develop preliminary estimates of the engineering properties of key soil units, which are shown in Table E-1. These estimates of engineering soil properties are revised slightly based on the slope stability calibration analyses discussed in Appendix J.
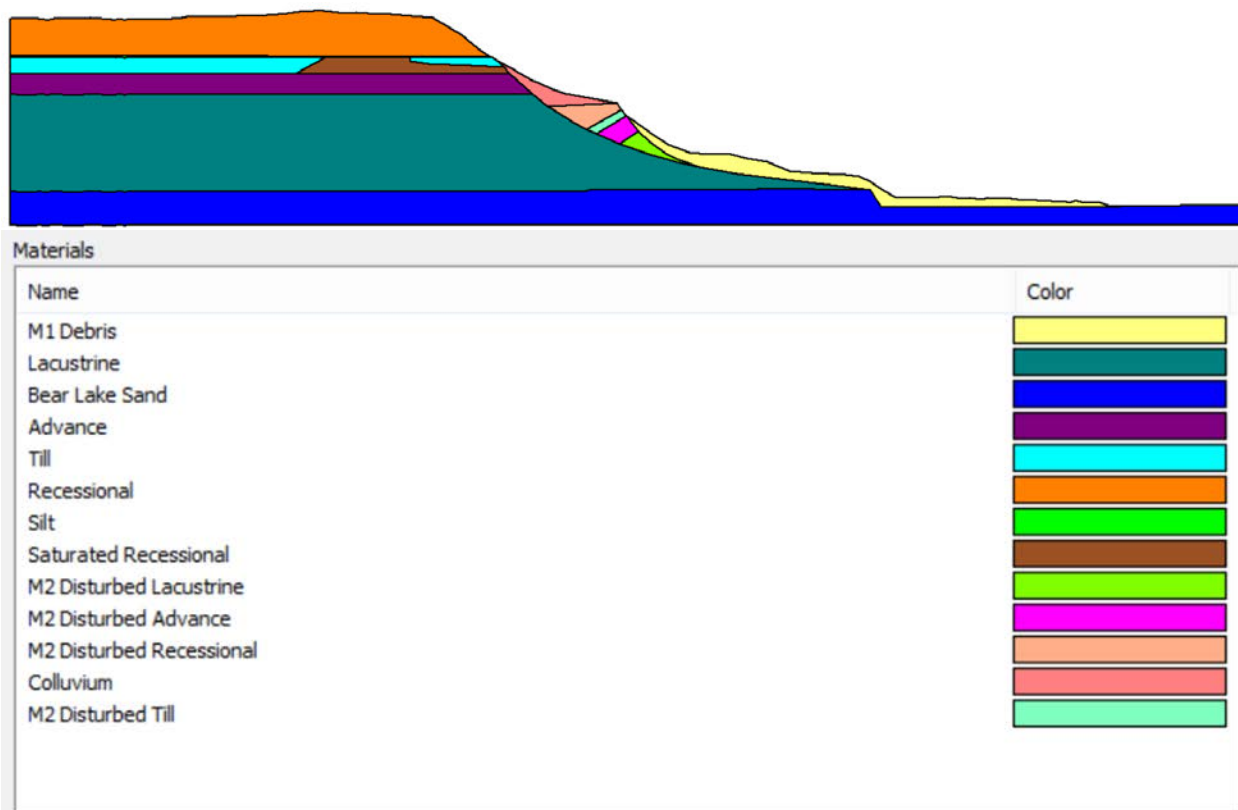
Figure E-1: Generalized stratigraphy of Whitman Bench and the Hazel slide before the 2014 SR-530 landslide.

At the top of the Whitman Bench there are recessional materials that are composed of largely sand and gravel in its upper part (shown as orange and designated in Table E-1 as Unit 1a if above the groundwater level and as Unit 1b if below the groundwater level). The recessional sand and gravel unit overlie a recessional silt layer (shown in bright green, which is difficult to see in Figure E-1 because it is relatively thin; it is designated as Unit 2 in Table E-1). The recessional sand, gravel, and silt materials overlie till (shown in light blue, which is designated as Unit 3 in Table E-1). Although the till does appear to be a widespread strata in the Whitman

bench, there is evidence of a discontinuous area where the till is missing in the SR 530 headscarp. In this area, the saturated recessional sand and gravel material (shown in brown; which is designated as Unit 1b in Table E-1) was found, so it is depicted in the cross section where it was observed. The advance silt and sand unit (shown in purple in Figure E-1 and designated as Unit 4 in Table E-1) appears to underlie these units across the area of the Whitman Bench shown in Figure E-1.

The advance materials cover the lacustrine clay and silt unit (shown in greenish gray and designated as Units 5a, 5b, 6a, 6b, 6c, and 6d in Table E-1). The lacustrine clay and silt unit is a key soil unit that is over 300 feet thick. Because of its importance, its thickness, and its variability, it was divided into several subunits. The upper one-third of the lacustrine unit was noticeably siltier. However, as with the rest of the lacustrine unit, there were both silt and clay layers within it. Thus, Units 5a and 5b of Table E-1 are used to describe it. The lower two-thirds of the lacustrine unit was noticeably clayier; however, it too contained clay and silt layers, thus there are separate subunits for the clay layers and silt layers within it. Additionally, the vertical effective stresses acting within that part of the lower lacustrine clay and silt unit under Whitman Bench were significantly higher than those acting within that part of the unit under the Hazel landslide. Thus, subunits of the lower part of the lacustrine clay and silt unit were used to capture these differences. There was often insufficient data to differentiate the engineering properties of the subunits of the lacustrine clay and silt unit. However, the subunits were maintained to recognize potential differences that could be identified in the future.

The Bear Lake sand unit (shown in blue and designated as Unit 7a where under the Whitman Bench and Unit 7b where under the Hazel landslide) is the lowest unit characterized at the site in this study.

The mid-slope bench, which is also referred to as the M2 slide material of the 2014 SR-530 landslide, consists of five materials: 1) disturbed recessional sand and gravel that is treated as cohesionless colluvium, 2) disturbed recessional sand and gravel, 3) disturbed till, 4) disturbed advance outwash silt and sand, and 5) disturbed lacustrine clay and silt (see legend of Figure E-1). The M2 landslide debris is designated as Unit 8a (above the groundwater level) and Unit 8b (below the groundwater level) in Table E-1. There was insufficient laboratory testing to differentiate the subunits of M2 at this stage of the study. During the slope stability calibration analyses (shown in Appendix J), the individual subunits listed above were used with soil properties based in part on their parent intact material strengths.

The 2006 Hazel slide debris is also referred to as the M1 slide debris when above the toe of the surface of rupture and as the debris field material when below the toe of the surface of rupture (both shown as yellow in Figure E-1). The debris field material differed noticeably form the M1 slide material, because it was significantly more disrupted after falling off the toe of the surface of rupture of the Hazel slide atop the Bear Lake sand unit. Thus, the debris field material was assigned significantly lower strength values than the M1 slide debris material. Additionally, the eastern sides of the M1 slide debris and debris field materials differed noticeability from their western sides. Thus, the M1 slide debris material was categorized as Unit 9a on its eastern side and as Unit 9b on its western side in Table E-1. The debris field material was categorized as Unit 10a on its eastern side and as Unit 10b on its western side in Table E-1.

Table E-1. Estimated Engineering Properties of Soils

Unit #	Material	Unit Weight (pcf)	OCR	cu residual (ksf)	φu residual (deg)	c' TXC peak (ksf)	φ' TXC peak (deg)	c' DS peak 90 to bed (ksf)	φ' DS peak 90 to bed (deg)	c' DS peak (ksf)	φ' DS peak (deg)	c' softened (ksf)	φ' softened (deg)	c' residual (ksf)	φ' residual (deg)	cu/σv' TXC	φu TXC (deg)	cu/σv' TXE	φu TXE (deg)	cu/σv' DSS	φu DSS (deg)
1a	Recessional Sand and Gravel above GWT	120	1.0	_	_	0	43	_	_	_	_	_	_	_	_	_	_	_	_	_	_
1b	Recessional Sand and Gravel below GWT	130	1.0	_	_	0	43	_	_	_	_	_	_	_	_	_	_	_	_	_	_
2	Recessional Silt	125	1.0	_	_	0	38	_	_	_	_	_	_	_	_	_	_	_	_	_	_
3	Till	140	2.0	_	_	2	40	_	_	_	_			_	_	_	_	_	_	_	_
4	Advance Outwash Silt and Sand	125	1.5	_	_	0	38	_	_	_	_	_	_	_	_	_	_	_	_	_	_
5a	Upper (one-third) Lacustrine Clayey Silt	125	1.3	_	_	0	30	0	26	0	22	0	20	0	12	0.41	0	0.31	0	0.35	0
5b	Upper (one-third) Lacustrine Silty Clay	125	1.3	_	_	0	30	0	26	0	22	0	20	0	12	0.41	0	0.31	0	0.35	0
6a	Lower Lacustrine Clayey Silt under Bench	125	1.3	_	_	0	30	0	26	0	22	0	20	0	12	0.41	0	0.31	0	0.35	0
6b	Lower Lacustrine Silty Clay under Bench	125	1.3	_	_	0	30	0	26	0	22	0	20	0	12	0.41	0	0.31	0	0.35	0
6c	Lower Lacustrine Clayey Silt under Slide	125	1.5	_	_	0	30	0	26	0	22	0	20	0	12	0.41	0	0.31	0	0.35	0
6d	Lower Lacustrine Silty Clay under Slide	125	1.5	_	_	0	30	0	26	0	22	0	20	0	12	0.41	0	0.31	0	0.35	0
7a	Bear Lake Sand under Bench	130	1.3	_	_	0	40	_	_	_	_	_	_	_	_	_	_	_	_	_	_
7b	Bear Lake Sand under Slide	130	1.3	_	_	0	40	_	_	_	_	_	_	_	_	_	_	_	_	_	_
8a	M2 Slide Debris above toe of slide above GWT	115	1.0	0.15	0.0	0	26							0	12						
8b	M2 Slide Debris above toe of slide below GWT	115	1.0	0.15	0.0	0	26							0	12						
9a	Eastern M1 Slide Debris above toe of slide	115	1.0	0.08	0	_	_					0	20	0	12						
9b	Western M1 Slide Debris above toe of slide	115	1.0	0.10	0	_	_					0	20	0	12						
10a	Eastern 2006 Debris Field below toe of slide	115	1.0	0.04	0	_	_							0	12						
10b	Western 2006 Debris Field below toe of slide	115	1.0	0.05	0	_	_							0	12						

Note: 1 ksf = 1000 psf = 47.87 kPa

Basis of the Estimates of the Engineering Properties of Soils in Table E-1

The engineering properties of soil presented in Table E-1 are based on our interpretation of the results of the field and soil laboratory testing programs described in Appendices B and D of this report, which were made available to our team as of 1 May 2016. Many of the laboratory tests presented in Appendices D were not available to the team by 1 May 2016, so we based our preliminary estimates of the engineering properties of soils on data that were available at that time to enable the groundwater, slope stability, and run-out analyses to commence. Additional laboratory test results were examined to identify potential inconsistencies with our preliminary estimates of soil properties, but there was insufficient time due to the compressed time schedule allowed by the court to integrate all laboratory test data in a comprehensive manner. This shortcoming is compensated for in this study by relying on the back-analyses of important field observations such as the stability of the Hazel landslide before the January 2006 landslide and the initiation and run-out of the January 2006 Hazel landslide to adjust the engineering properties of key soil units if required and judged reasonable to do so (see Appendices J and K).

Soil unit weights are estimated based on the soil descriptions and field tests (e.g., blow counts) delineated on the field logs and the laboratory soil density measurements on selected soil samples.

Stress history characterization (i.e., overconsolidation ratio) is based primarily on the oedometer tests performed on laboratory specimens of the lacustrine clay and silt materials and estimates of the in situ state of effective stress prior to the 2014 SR-530 landslide. The characterization of the site geology provided the primary means for estimating the stress history of other units in which oedometer tests were not or could not be performed. The characterization of the site geology also provided additional information on the stress history of the lacustrine clay and silt materials.

The shear strength of the soil units were characterized through several types of laboratory tests and through correlations with field tests. The best quality samples (as characterized by the oedometer tests, visually observations, and field notes on sampling) were used in the laboratory tests on "undisturbed" soil specimens. No sample is perfectly undisturbed, thus as is convention, the word is placed within quotation marks. The SHANSEP technique was employed for some of the strength testing to address in part the sample disturbance issue.

Consolidated-Undrained (CU) Triaxial Compression (TXC) and Triaxial Extension (TXE) tests with and without pore water pressure measurements for slow and rapid tests, respectively, were used primarily to characterize the Mohr-Coulomb (M-C) effective stress strength parameters (c', ϕ') and total stress (undrained) strength parameters (c_u, ϕ_u) of the lacustrine clay and silt unit. With an estimate of the in situ vertical effective stress and the measured effective confining stress in the laboratory, undrained shear strength ratios (c_u/σ_v') were developed for the TXC and TXE stress paths. The Direct Simple Shear (DSS) strength parameters were estimated as being intermediate of the TXC and TXE strength parameters. Both the Bjerrum recompression technique and the SHANSEP procedure were used to evaluate soil strength of soil specimens consolidated to an estimate of the in situ vertical effective stress and of soil specimens consolidated to an estimate of the soil's in situ overconsolidation ratio after achieving normalized behavior, respectively.

Fully softened and residual shear strength parameters for the lacustrine clay and silt unit were developed based on the results of the Torsional Ring Shear tests performed on soil specimens consolidated to several effective normal stresses at high water content for the fully softened strength and after extensive shearing for the residual strength.

Consolidated-Drained (CD) Direct Shear (DS) tests provided estimates of peak shear strength of the lacustrine clay and silt unit for both test specimens oriented parallel and orthogonal to the predominantly horizontal layering of the clay and silt materials of this unit. At this stage of the study, preference was given to use of c' = 0 values, which is representative of the low c' values indicated in many of the DS tests. However, many later DS tests also indicate that these soils have high c' values. For example, a subset of the DS test data for low to intermediate normal effective stresses found that weaker soils within the unit had c' = 400 psf and ϕ' = 27°, which exceeds the DS strength values listed in Table E-1. Thus, during the slope stability calibration analyses nonzero c' values were used if required to achieve initial pre-failure stability. Some sensitivity analyses were performed using higher c' values to evaluate the sensitivity of the slope stability results to the differing soil strength characterizations produced by the DS tests.

The program *CPeT-IT* (v.1.7.6.42 by GeoLogismiki Geotechnical Software, 2007) was used to evaluate the results of the cone penetration tests (CPTs) presented in Appendix D. The CPTs provide estimates of correlated engineering soil properties that are only directly applicable for the conditions at the time of the test. The CPT measurements are useful, because they are nearly continuous and provide estimates of the undrained shear strength of clayey soils.

CPT 16-15 appears to have penetrated displaced slide debris overlying intact material that is composed largely of lacustrine clay and silt materials. The undrained shear strength (c_u) is estimated (using N_{kt} = 14) to be within the range of 1000 psf to 2000 psf in part of the upper part of the slide debris, c_u is estimated to be between 2700 psf and 3500 psf directly above the surface of rupture (which is at Elev. 381 ft), and c_u is greater than 6000 psf below the surface of rupture. CPT 17-15 appears to have penetrated primarily intact lacustrine clay and silt materials below the surface of rupture (which is at Elev. 403 ft), but it was advanced only 21.5 ft below Elev. 401.8 ft. The undrained shear strength of this material is estimated to be largely within the range of 6000 psf to 7000 psf. CPT 19-15 appears to have penetrated displaced slide debris overlying intact material that is composed largely of lacustrine clay and silt materials. The undrained shear strength is estimated to be between 1500 psf to 2000 psf directly above the surface of rupture (which is at Elev. 339 ft), and c_u is greater than 6000 psf 10 feet below the surface of rupture.

TXC peak strengths of units not tested in the laboratory were estimated based on correlations with the field tests (e.g., blow counts) and through engineering judgment. For example, the TXC peak effective friction angle of the recessional sand and gravel material of Unit 1a and Unit 1b were developed using empirical correlations presented by Duncan (2004; "Friction Angles for Sand, Gravel and Rockfill," *Kenneth L. Lee Memorial Seminar Notes*, Long Beach, CA, April 28) based on the relative density, effective confining stress, and coefficient of uniformity of these materials, where the relative density was estimated based on the penetration resistances (i.e., blow counts) from the field work.

The effective residual shear strengths of the M1 slide debris and debris field materials were characterized assuming they were similar to the measured values of the lacustrine clay and silt unit (i.e., $\phi' = 12^{\circ}$). Similarly, the effective residual shear strengths of the M2 slide debris materials were characterized assuming they were similar to the measured values of the lacustrine clay and silt unit (i.e., $\phi' = 12^{\circ}$). Analogous to what was assumed for the M1 slide debris and debris field materials for the, the fully softened shear strength of these materials were characterized assuming they were similar to the measured values of the lacustrine clay and silt unit (i.e., $\phi' = 20^{\circ}$). The effective friction angle of the M2 slide debris material at this stage of the study was assumed to be 26° based on engineering judgment. However, this value was not used, because the slope stability calibration analyses were able to model the different subunits of the M2 slide debris material using partially reduced strength estimates of the intact units (see Appendix J).

Estimating the residual undrained shear strengths (c_u) of the M1 slide debris and debris field materials was challenging, because there was little data available to characterize these materials as they had been removed from area of the SR-530 landslide site that access was provided to our team. It was assumed that these materials were of high water content and consequently of low residual undrained shear strength. Case histories of liquefaction flow slides (e.g., Idriss and Boulanger 2008 "Soil Liquefaction During Earthquakes," EERI Monograph, Oakland, CA) provide a lower bound estimate of the undrained residual shear strength of the weakest of these soils, which was assumed to be the eastern side of the highly disrupted debris field soils (i.e., c_u = 40 psf). This value is also approximately equal to the undrained shear strength of a fully remolded clayey soil at its liquid limit. The western side of the disrupted debris field was sandier and stronger (as evident in aerial photographs of these alluvially deposited materials located on the western side of the debris field) so it was assigned a c_u value of 50 psf. The less disrupted eastern and western sides of the M1 slide debris materials were assigned undrained residual shear strengths twice the lower bound values (i.e., 80 psf and 100 psf, respectively). These values are within the middle to of the range of the undrained residual shear strength of liquefied material with low blow counts (i.e., $N_{1,60cs-Sr} < 6$). The M2 slide debris material was considerably stronger than the M1 materials, so its liquefied undrained residual shear strength was assumed to be approximately 150 psf, which is still a relatively low value of undrained residual shear strength based on case histories of liquefaction-induced flow slides (e.g., see Idriss and Boulanger 2008).

Basis of the Estimates of Other Engineering Properties of Soils

Other engineering properties of soil, which are not presented in Table E-1, are required in supporting analyses of the slope stability and run-out studies. For example, values of the hydraulic conductivity of key soil units are required in the seepage analyses (Appendix I), and values of the post-failure reduced undrained shear strengths of partially remolded landslide debris are required in the run-out analyses (Appendix K). These values are estimated based the results of the available laboratory tests presented in Appendix D and through correlations with field tests discussed in Appendix B. The rationale for the use of the selected best estimate and upper/lower bound estimate values of the engineering properties of these soils is discussed when they are presented in other parts of this report.

APPENDIX F

SR 530 Landslide Geologic Mapping & Cross Sections

Geologic Setting

The data developed during the field exploration program indicate that the stratigraphy and distribution of many of the geologic materials are extremely complex. This complexity is illustrated in a section of the materials exposed in the main scarp of the SR 530 Landslide (see Figure 23 and Figure 24; Appendix E). As outlined below, much of the complexity of the site is related to the origin of the Whitman Bench. The different units were formed, either in close proximity to ice margins, or in direct contact with the ice during one or more glacial episodes of the Pleistocene epoch. In these ice-marginal environments extremely complex stratigraphic relationships can be developed, as one sequence of deposition truncates another . Thus, overly simplistic "layer cake" geologic interpretations, as presented to date in the various literature describing the SR 530 Landslide site, do not adequately characterize this site for meaningful assessment of the factors contributing to the disastrous event of March 22, 2014.
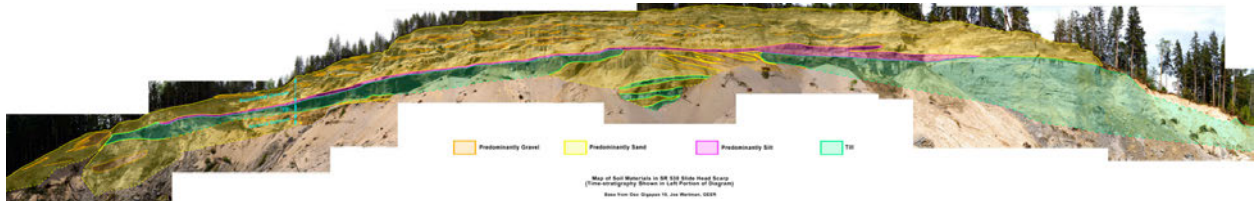
Figure 1: Mapping of geologic units exposed in the main scarp of the SR 530 Landslide.
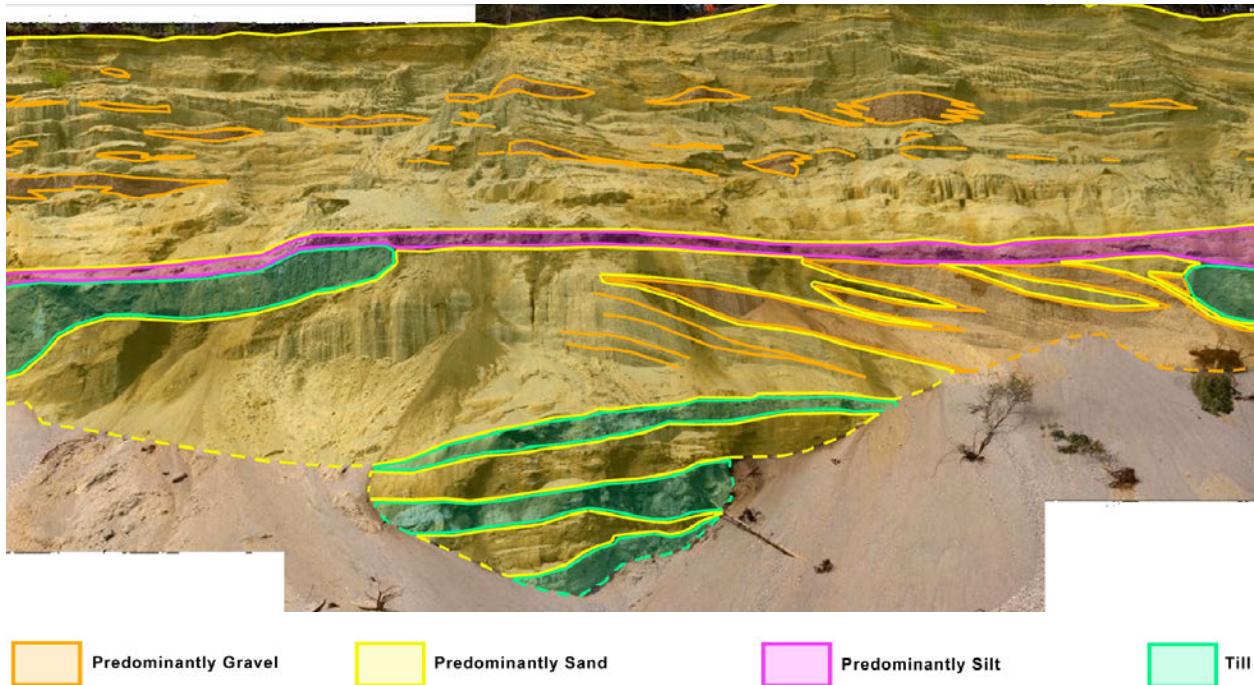
Figure 2: Close-up view of the central portion of the SR 530 Landslide main scarp, showing the stratigraphic complexity.

Methods

The interpretation of the regional and site-specific glacial geology and stratigraphy is based on a diverse suite of information, including remote sensing data, direct field observations, published field observations by others, geologic literature and geologic maps, and personal communication with people familiar with the surficial and glacial geology of the region.

Remote Sensing

For the regional context, the interpretation of glacial features was gleaned from remote sensing data, consisting of LiDAR and Digital Elevation Model (DEM) hill shade images ((4) (8) (9) (10)), and augmented by observations on Google Earth. Similarly, the geomorphology of the vicinity of the SR-530 slide was also developed largely from LiDAR hill shade images and aerial photos. Utilization of such methods for initial surficial geologic mapping is standard practice for geologists. Extensive field verification of the interpretations of the geomorphic features observed via these methods was initially limited by the time requirements of the subsurface exploration program at the site, and later, by inclement weather and court-imposed deadlines. However, in the immediate vicinity of the slide, many of these interpretations - such as the presence of kettles on the Whitman Bench and on its unnamed counterpart on the south side of the North Fork Stillaguamish Valley (where eskers were also identified), have been confirmed by field observations of exposures and/or by subsurface exploration data developed by others (e.g. WSDOT).

Other remote sensing data utilized for mapping of the slide features include high-resolution aerial ortho-photography obtained by WSDOT in the days following the March 22, 2014 event, video and still photos obtained by first-responders and the Snohomish County Sheriff's Department following the 2006 and 2014 slope movements, and pre-slide historic aerial photography from diverse sources, including Snohomish County and other entities. In addition, the oblique aerial photography of Robert Tart provides significant insights into the characteristics and distribution of materials between 2002 and the post-2014 event.

Field Mapping

The post-2014 stratigraphy at the site was developed from direct observations of exposures in the main and lateral scarps of the 2014 landslide, in the blocks which moved during 2014 and 2015/16, and from observations of the materials penetrated by our exploratory borings in 2014-15. Inclement weather was prevalent during much of the 2015/16 wet season, which resulted in dangerous site conditions that often precluded completion of detailed mapping of the displaced blocks on the north side of the river. Despite requests through the Attorney General's office, permission to access the debris field on the south side of the river was not granted by relevant property owners. Therefore, observations on the "south" side of the river were limited to vantage points from the "north" bank of the river using binoculars. In those areas we were able access (north of the present river channel), our field methods consisted of observations of stratigraphic relationships of different geologic materials, field classification of these materials using ASTM Method D-2488 (Visual-Manual Procedure), observations of cross-bedding/foreset dip directions, stratigraphic contacts, failure surface and bedding attitudes, and qualitative observations of the type and provenance of lithologies present in the different geologic units.

Locations of field observations and pertinent photo-documentation were recorded using a GPS-equipped iPad Mini in Avenza PDF Maps utilizing the high-resolution geo-referenced aerial photo obtained by WSDOT on March 24, 2014. Where necessary, more exact elevations of key locations were obtained from Terrestrial LiDAR mapping performed on the slide deposit by Storesund Consulting and WSDOT. Additional photo-documentation was obtained using an Olympus Tough TG-310 14-Megapixel camera.

Subsurface Exploration

Members of the State's expert team were present at the drill sites during the majority of the time drilling and sampling operations were conducted at the site by WSDOT. Exceptions included portions of borings EB-01vwp-15, EB-02vwp-15, EB-02sp-15, and EB-10vwp-15. For those portions of borings EB-02vwp-15, EB-03vwp-15, EB-04si-15 (+ EB-14vwp-15), EB-05si-15, EB-06vwp-15, EB-07si-15 (+EB-18vwp-15), EB-08vwp-15, EB-09si-15 (+EB-13vwp-15), and H-12si-15 (+EB-15vwp-15), where a member of the expert team was present, they observed the sampling, visually inspected the samples, and photographed most samples not collected in brass tubes. The main focus of the observations included the determination of material properties, including Unified Soil Classification System group names per ASTM D-2488 (Visual Manual Procedure), consistency/compactness (from penetration rate sampling and isolated measurements of Unconfined Compressive Strength/Shear Strength using a pocket penetrometer/Torvane), bedding/stratification/lamination characteristics and degree of deformation/dip of these features, where applicable, color, consistency, plasticity state, and moisture/saturation conditions, where possible.

Other Information

Information on shallow geology within the valley of the North Fork Stillaguamish River in the vicinity of the slide was also obtained from water well logs on file with the Washington Department of Ecology (11). The precise locations of select water wells in the Steelhead Haven neighborhood was determined from Snohomish County Planning and Development records, such as site plans submitted with building permit applications.

Results

Geologic Units

Previous publications regarding the geology and stratigraphy of the site and immediately surrounding area include the Geologic Map of the Mount Higgins Quadrangle, Washington (Dragovich, 2003). At the site of the SR 530 Landslide, the map indicates that Whitman bench is comprised of the following stratigraphic units (in order of increasing age):

➢ **Qls: Landslide complexes (Holocene)---**Diamicton with soft sand, silt, and (or) clay matrix; contains locally derived, angular to subangular clasts and may contain some rounded clasts from older Quaternary deposits; poorly sorted and unstratified; includes deep-seated (slump-earthflows) and shallow (debris flows and torrents) landslides. Some landslides may have been initiated during removal of ice buttressing during late Pleistocene deglaciation or may be seismically induced….

➢ **Qgoe: Recessional outwash (Pleistocene)---**Sand, gravel, and sandy cobble gravel with rare boulders; loose; clasts are subrounded and commonly polymictic; contains interlayered thin to laminated beds of sandy silt and silt, particularly where grading to unit Qgle; non- to well stratified; typically contains meter-thick, subhorizontal beds normally crudely defined by variations in cobble, gravel, and sand content. Pebble imbrication, scour, and local low-amplitude trough and other cross-bedding features indicate deposition in braided river and deltaic environments. Some deposits were isolated ice-contact deposits, as indicated by the occurrence of rare flow and (or) ablation till lenses and near-ice sedimentary structures…

➢ **Qgle: Recessional glaciolacustrine deposits (Pleistocene)---**Clay, silt, sandy silt, and sand with local dropstones; gray to light gray to blue-gray; weathered to shades of brown; well-sorted; loose, soft, or stiff; nonstratified to laminated; varve-like rhythmite beds about 0.4 in. thick and laminated beds of silt to sand common; locally contains ball-and-pillow structures; rare sand dikes; common dropstone clast types include granite and greenstone; deposited in glacial lakes impounded by receding glacial ice and locally interfingers with recessional outwash

➢ **Qgtv: Till (Pleistocene)---**Nonstratified, matrix-supported mixture of clay, silt, sand, and gravel in various proportions with disseminated cobbles and boulders; compact or dense; mottled dark yellowish brown to brownish gray, grayish blue, or very dark gray; matrix commonly consists of silty fine to coarse sand with or without clay; includes Canadian-provenance and locally derived clasts; where overlying bedrock, up to 90 percent of basal clasts are excavated from underlying bedrock; generally a few yards thick, but can range from a discontinuous veneer to several tens of feet; forms a patchy cover over much of the study area; overlies bedrock in elevated alpine settings but forms a conformable layer in glacial-terrace and low valley-bottom settings and thus mantles topography…; consists largely of lodgment till but may locally include flow till…

➢ **Qglv**: **Advance glaciolustrine deposits (Pleistocene)---**Clay, silt, silty clay, and silty fine sand with local drop stones; blue-gray or gray, weathered to pale yellowish brown; locally contains thick beds of structureless, clast-rich diamicton that may be flow till or iceberg melt-out contact zones; also, locally contains lenses and beds of fine- to medium-grained sand; stiff or dense; well sorted. Bedding varies widely from structureless to thinly bedded to laminated and most

commonly consists of 0.4 to 1.6 in. thick rhythmite beds (probable varves) that are normally graded from silty clay to fine sand. Rhythmite bedding is locally interrupted by thin to thick beds of sand or silty fine sand. Soft-sediment and (or) ice-shear deformational features include contorted bedding, overturned folds, and flame structures. Overturned fold geometries are consistent with east-southeast-directed ice shear during ice advance up the major river valleys….

➢ **Qco: Deposits of the Olympia nonglacial interval (Pleistocene)**---Gravel, sand, silt, clay, peat, and rare diamicton; compact to very compact, well-sorted, and very thinly to thickly bedded; disseminated organic material, logs or wood fragments are common….

The GEER report identifies essentially the same units as being present and observed in the main and lateral scarps of the SR 530 slope movement. Similarly, the USGS/UC Berkeley/WSDOT report "Geotechnical Characterization of Intact Quaternary Deposits Forming the March 22, 2014 SR-530 (Oso) Landslide, Snohomish County, Washington" identifies the same stratigraphy (in order of increasing stratigraphic position): Deposits of Olympia nonglacial Interval, Advance glaciolacustrine deposits of Vashon Stade, Advance outwash of Vashon Stade, Till of Vashon Stade, and Recessional outwash of Everson Interstade.

BLS: Bear Lake Sand (Formerly "Olympia Beds")

The oldest (lowest) of the stratigraphic units penetrated by some of the exploratory borings on the Whitman Bench and in the 2014 slide area consists of a deposit of sand which, at EB-09, is at least 90 feet thick (the boring was terminated prior to reaching the bottom of the unit). This same unit is exposed at several locations, including extensive portions of the lower left lateral scarp of the slide, and along the lower right lateral scarp of the slide, and was exposed during the summer/fall of 2015 at the base of the steep slope below dormant slide deposits in the west-central portion of the source area. The latter exposure was subsequently covered by slide deposits which moved more than 100 feet during the 2015/16 wet season. The other exposures were not significantly affected by these latest slope movements at the site. The unit was also exposed along the west bank of Rollins Creek in one location.

The elevation of the upper contact of this unit varies from 310' to 325' above mean sea level (NAVD 88). The upper contact is higher in the southeastern and eastern portions of the exposures and borings, dropping to the northwest and west.

At all locations where this unit is exposed, the cross-bedding dips to the north and west, or towards the northern valley side. The sand also contains interbeds of laminated silt and clay, irregularly spaced throughout the entire thickness of the deposit. The exposed upper portions of the unit consist of horizontally to fore-set bedded very fine-grained to fine-grained sand with a salt-and-pepper appearance, resulting in an overall light to medium gray color in the areas where the unit was affected by the 2014 slide event (western and west-central exposures). In the eastern exposure along the left margin of the slide, the unit is a tan color.

The ten or more feet of the sand unit exhibits laterally extensive interbeds of rhythmically bedded gray, light greenish-gray, and nearly black clay. The thickest of these interbeds was observed to have been thrusted, with formation of recumbent folds. The thrust direction appears to have been from the NNE or NE (see site photos). This clay interbed was tested with a pocket penetrometer and shown to have a UCS >>4.5 tsf (>>9,000 psf). In places, the sandy portions of the BLS contain isolated rounded rip-up clasts of the intercalated rhythmically bedded clay/silt.

Based on information developed by WSDOT in 2014, the BLS also underlies at least part of the unnamed bench forming the counterpart of Whitman Bench on the south side of the North Fork Valley. WSDOT boring H3-VWP-14, installed in 2014 through a slope movement deposit on the south side of the valley, suggests that the BLS is present at that location also, with an elevation of approximately 322' for the top of the unit.

The elevations of the top of the BLS and thickness (rounded to nearest 0.5') penetrated in the borings are presented in the following table. None of the borings performed to date penetrated this unit:

Boring	Top elev.	Thickness Drilled
H1-VWP-14	312.0'	70.5'
H3-VWP-14	332' (?)	48.0' (?)
EB-02VWP-15	312.5'	39.0'
EB-04SI-15	312.5'	56.0'
EB-14VWP-15	313.5'	54.0'
EB-07SI-15	323.5'	62.0'
EB-09SI-15	324.5'	91.0'
EB-13VWP-15	324.5'	65.5'
EB-12SI-15	319.0'	57.0'
EB-15VWP-15	319.5'	13.0'

FGL: Fine-grained Glacio-lacustrine Unit

At all locations observed, and in the exploratory borings extending to the required depth, the Bear Lake Sand is overlain by a rhythmically bedded or laminated fine-grained soil unit, which is generally dominated in the lower portions by fat clays (CH), and in the upper portions, contains more lean clay and silt. The contact of the Fine-grained Glacio-Lacustrine unit (FGL) with the underlying Bear Lake Sand is abrupt wherever it was encountered, although there appear to be clay interbeds within the Bear Lake Sand near the contact with the FGL.

The FGL is a nearly 300-foot thick deposit of rhythmically bedded or laminated silt and clay. Laminations are mostly on the order of 1/32nd to 1/8-inch thick. Some of the unit, especially in the lower portions, is rhythmically bedded, with individual beds on the order of 1/8 to 1/2-inch thick. Each bed is usually a fining-upward couplet, with silt near the bottom and clay near the top. The overall characteristics of the material range from an elastic Silt (MH), to a lean clay (CL) and, especially in the lowest portions, a fat Clay (CH). However, it appears that individual laminae may well range from Silt (ML) at the bottom to fat Clay (CH) at the top of the lamina. X-Ray Diffraction analyses revealed that the CH materials include smectite clays, including montmorillonite.

In the lower portions of the unit some rhythmite beds are light greenish-gray, alternating with very dark gray to black layers. In the thinner-bedded upper portions of the unit, the material is generally a more uniform color across sequences of rhythmite beds, although there are lighter greenish-gray and darker gray intervals containing numerous individual beds per even-colored section. In the thinner-bedded sections, the presence of the rhythmites is often detectable only from the texture of "split" samples. When cut with a knife, the presence of the thin-bedded rhythmites is essentially undetectable.

The unit also contains isolated "drop stones," which are pebbles or cobbles ice-rafted on the lake and then dropped into the fine-grained deposits, as the ice-floes either capsize or melt. The unit has often been referred to in previous reports (14) as "Blue Clay."

The upper contact of the FGL, where present and undisturbed by glacial processes, is generally gradational with the overlying "Advance Outwash." However, at several locations (EB-04, EB-05, EB-07, EB-09, and H-12) the upper portion of the unit is truncated, either due to slope movement, or due to previous erosion/modification, even in areas where no slope movement has occurred in recorded history. However, where present and unmodified, the upper contact is generally located at elevations ranging from approximately 600 to 630 feet. Precise location of the upper contact with the Advance Outwash is not possible due to the broadly gradational nature of the contact. The overall thickness of the FGL is around 300 ft, making it the largest unit documented at the site.

It should be noted that due to the small thickness of individual beds/laminae, and the amount of material required to perform index testing (Atterberg limits etc.), it is likely that several rhythmites are required to obtain the material for each test. This obscures the apparent change in gradation and index properties across individual rhythmite beds/laminae, which appear to represent a fining-upwards sequence; often ranging from silt near the bottom to clay at the top, or from lean clay at the bottom to fat clay at the top.

AO: Advance Outwash

Of all the units in the stratigraphic column, the Advance Outwash (AO) exhibits the most variable characteristics, both vertically and laterally. Generally, the unit is finer-grained in the eastern portions of the Hazel/SR-530 slides, and sandy to even gravelly in the central and western portions of the slide area.

In exposures along the eastern margin and in failure blocks within the eastern portion of the slide on the north side of the post-2014 river alignment, the AO unit is comprised largely of silt (MH to ML), sandy silt, and a few feet of silty sand near the top of the unit. The thickness of the upper silty sand increases westward, from less than 10 feet directly below the till in the eastern blocks just north of the river, to more than 20 feet in the central and western blocks in the same position relative to the river.

The east-west dichotomy is even more apparent in the current main and side scarps of the SR-530 Slide. In the western portion of the main scarp of the slide, the AO unit consists of a thick sequence of foreset bedded medium to coarse and even pebbly sand with intercalated gravel beds. Foreset beds are generally dipping east to southeast, often with gravelly layers separating fore-set-bedded strata. Bedding is off-set and disrupted in portions of the deposit. In places, gravel was observed in contact with sand along surfaces, dipping 80 degrees into the present slope (to the west).

In the central and eastern portions of the main scarp of the SR-530 Slide, the AO unit is mostly covered by talus. An exception is the central portion of the main scarp, where an approximately 75-ft. high exposure of the unit was observed. The lower half of the exposure reveals three layers of till, consisting of a gravelly diamicton with a gray fine-grained matrix, separated by sandy outwash. This package has an apparent dip to the southwest or west. The upper half of the exposure is comprised of a sand-and-gravel deposit which dips into the slope (apparent dip to the north or northwest). Actual dip angles could not be measured due to unsafe conditions in this area (the recessional outwash is constantly raveling from above). The sand-and-gravel deposit extends eastward for at least 15 ft from the center, with the top contact conformable with the top of the till exposed in the main scarp, on the east and west side of the AO deposit. Equivalent materials (sand-and-gravel) were not observed in the failure blocks on the north side of the river, below the main scarp.

In the northeast portion of the main scarp, a significant portion of the AO unit is replaced by a thickened till section, the lower portion of which is covered with talus. As a result, it is not possible to determine the thickness of AO in that area. The following table summarizes the unit thicknesses revealed in the borings that penetrated this stratigraphic interval:

Advance Outwash Contact Elevations and Thickness (in feet)

Boring	Top Elev.	Bottom Elev.	Thickness	Comments
H1-VWP-14	674	599	75	
EB-02vwp-15	653.5	596.5	57	
EB-06VWP-15	686.5	624	62.5	
EB-07SI-15	+/-422.5	372.5	+/-50	In slide mass, top excavated for road.
EB-08VWP-15	-	-	-	Not present between Till and FGL

Till Complex (lodgement till, flow till, and deformation till)

Three types of till were found at different locations and at different levels in the stratigraphy. In this context, all materials which either originated directly from the ice or were significantly disturbed, or deformed by the ice, are classified as till.   The reason for referring to this unit as a "till complex" is the fact that at several exposures and borings, stratified drift up to several tens of feet thick, is interbedded (sometimes as blocks several tens of feet across) with two or more layers of diamict till.

Volumetrically, the most important type is lodgement till, which formed in direct contact with the presumed bottom of the glacier(s) by mixing of sediment sources of widely varying grain sizes (from silt/clay to sand, gravel, and boulders). The matrix of the lodgment till at this site is generally gray to greenish gray, and it contains numerous subangular to well-rounded gravel, cobbles to boulders, some of which are shaped and striated. Cobbles in this material are generally of rather muted colors, and dominated by lithologies known to be present within a few miles of the site. Lithologies include dark gray to black mudstones, olive green to grass-green greenstone, pinkish to brown clastic sedimentary rocks (usually sandstone) to meta-sedimentary rocks, phyllites, schists and associated milky quartz-vein materials, and minor coarse-grained intrusive igneous rocks, mostly of intermediate composition. The thickest till unit visible in the main scarp of the SR-530 Slide is comprised mostly of lodgement till.

Materials of a composition similar or identical to the lodgement till, but present as layers only a few feet thick, intercalated in otherwise stratified, more sorted outwash deposits, or present in thicker layers

with internal stratification or irregular layering, are interpreted as flow tills. Flow tills are created when till generated in contact with ice forms mudflows or slides off the ice and is deposited, either in a body of water, or on the ground, some distance from the ice margin. Till of this type was found in the lower portion of the AO unit exposed in the central portion of the main scarp (identifiable as flow till only due to the +/-5 ft-layers separated by stratified outwash) and in the lower, crudely stratified portion of the massive section of till, exposed in the NE portion of the main scarp. It is possible that some of the thinner till sections encountered in the borings also originated as flow till, but verification of the actual origin (lodgement vs. flow till) of these layers is not possible in the limited exposure afforded by samples from borings.

Deformation till is another type of till observed at this site. It consists of severely sheared and deformed Fine-grained Glacio-Lacustrine silt/clay, however, lacking admixture of materials of other grain sizes (sand or gravel). This material was only found in borings in the eastern portion of the site, both in the 2014 slide area and in borings on the Whitman Bench. The deformed material is characterized by blocky structure, with slickensides on 3-dimensional mass planes of separation, distorted laminations/rhythmites, and light colored silt and very fine sand partings, which often cut across original stratification, and are frequently deformed in flame structures.

Rotated till blocks and associated recessional outwash are present beneath horizontally bedded outwash in the eastern portion of the main/side scarp of the SR-530 Slide at lat/long 48.2867/-121.8499. The till, although mantled under 5 to 10 feet of colluvium, underlies the ridge forming the divide between the Hazel/SR-530 Slides and Rollins Creek, to an elevation of approximately 575', where it pinches out against the Advance Outwash lying beneath it.

Till complex (without the Deformation till of the FGL unit) elevations and thicknesses in the borings on Whitman Bench are summarized in the following table:

Boring	Top Elev.	Bottom Elev.	Tot. Diamict Thickn.	Tot. Strat. Thickn.	Tot. Thickness
H1-VWP-14	760.0'	674.0'	46.5'	49.5'	96.0'
EB-02vwp-15	754.0'	653.5'	66.0'	34.5'	100.5'
EB-06vwp-15	733.5'	686.5'	27.0'	20.0'	47.0'
EB-08vwp-15	771.0	632.0'	104.5'	34.5'	139.0'

RO: Recessional Outwash

Based on observations in the main scarp of the SR-530 landslide, on the failed blocks in the debris field north of the river, and in the borings, the bulk of the Recessional Outwash (RO) consists of sand and gravel lying on a basal silt layer, which ranges from a few feet to around 10 feet thick. Additional minor silt lenses are also present in the lower portion of the unit.

In the exposures in the main scarp of the SR-530 Slide, the sand and gravel portion of the unit exhibits foreset cross-bedding in the lower two thirds of the unit with trough-cross-beds in the upper portion. In nearly all cases, cross-bed dip directions indicate easterly sediment transport at the time of deposition. Gravelly portions appear to be more concentrated in the western and central portions of the main scarp, while very few gravel lenses were observed in the eastern portion.

Larger cobbles in the RO consist to an estimated 70 to 80 percent or more of "exotic" lithologies such as granitic or other felsic igneous rock types, mostly of Canadian provenance.

Due to its stratigraphic position (the prominent unit capping the Whitman Bench), the RO was penetrated by all of the borings installed on the bench, and the upper portions of the unit were found in several of the borings installed on the slide itself. The following table summarizes elevations and thickness of the RO observed in the borings.

Recessional Outwash Contact Elevations and Thicknesses Observed in the Borings

Boring	Top Elev.	Bottom Elev.	Thickness	Comments
H-1VWP-14	891.9'	759.9'	132'	
EB-01VWP-15	865.3'	736.3'	129'	
EB-02VWP-15	867.5'	754.0'	113.5'	
SP-01-15	867.0'	752.5'	114.5'	
EB-03VWP-15	890.3'	762.8'	127.5'	
EB-04SI-15	431.9'	401.4'	30.5'	Slide Debris, Top Buried, Bottom Truncated
EB-05SI-15	489.1'	447.0'	42.1'	Slide Debris, Top Buried, Bottom Truncated
EB-06VWP-15	867.5'	733.5'	134.0'	
EB-08VWP-15	847.3'	770.8'	76.5'	
EB-10VWP-15	863.3'	760.8'	102.5'	
EB-11VWP-15	832.5'	765.5'	67.0'	

Radio-carbon Dating

A small piece of woody debris or peat was found in EB-04SI-15 at an elevation of 309.5 ft, near the top of the Bear Lake Sand, and was subsequently submitted for C-14 dating. The result was an infinite date (greater than 43,500 YBP).

Other Observations/Information

In-place FGL, consisting of horizontally laminated "blue clay" was found in the channel of Headache Creek at lat/long 48.2864/-121.8471 (elev +/-529').

The multi-crested ridge along the eastern edge of the bench in the Headache Creek basin is comprised of brown silty sand with occasional cobbles. The ridge top slopes southward at approximately 5%.

Surfaces of Rupture/Separation

Surfaces of Rupture or Separation were found at several locations, in exposures at the surface and interpreted from the cores/samples obtained from the borings. Historically, exposed failure surfaces were also inferred from information provided by previous researchers and other parties that studied the site prior to the SR-530 Landslide (Shannon & Associates, Thorsen, Benda, Bob Tart, etc.).

The SR-530 Surface of Rupture/Separation was observed at several locations, summarized in the following table:

Location/Designation	Latitude	Longitude	Elevation	Surface of
West-Central Gully	48.2824	-121.8488	310-314'	Rupture
East Margin Gully	48.2839	-121.8453	+/-340'	Rupture
West Margin	48.2828	-121.8502	+/-437'	Dipping NW. Rupture
West Margin	48.2825	-121.8505	+/-519'	Separation
River @ Road # 1	48.2811	-121.8412		Separation
River @ Road # 2	48.2811	-121.8408		Separation
River @ Road # 3	48.2812	-121.8417		Separation
Drag Fold	48.2798	-121.8399		Separation

In addition, an ancient surface of rupture/separation was located in the lowermost portion of the west margin at numerous points, from lat/long 48.2813/-121.8488 to 48.2820/-121.8489.

As discussed by Thorsen, photographically documented by Mr. Tart in the 2006 slide scarp, and observed in the exposures of the remainder of the former mid-slope bench in the lower western margin of the SR-530 Slide, the former mid-slope bench consisted mostly of back-rotated slope movement blocks, in which the formerly horizontally deposited soil units of the Whitman Bench were dipping northward, at angles up to 30 or nearly 45 degrees. At least four back-rotated blocks can be identified in the Tart photos. In general, it appears on the photos as if the depressions created by the back-rotation of the blocks have been filled by shallow-dipping to nearly horizontal outwash deposits.

Interpretation of Depositional Environments and Apparent Age of Geologic Units

Bear Lake Sand

Whereas this sand unit has previously been interpreted (12) to be of "Olympia" age, meaning it was deposited during the interglacial period preceding the Fraser Glaciation, this origin seems somewhat in doubt. During an interglacial period (such as today), the Stillaguamish River is transporting large quantities of gravel, cobbles, and boulders, some of which are 2+ feet in diameter. One would expect the river to have moved similar material during the last significant interglacial period. However, no such material is to be found at that level in this vicinity. Instead, the Bear Lake Sand consists of a deposit of sand more than 90 feet thick, with minor laminated silt and clay interbeds, which is suggestive of a deltaic deposit formed in a standing body of water. The USCS soil classifications for these materials vary from poorly graded Sand (SP) to well-graded Sand (SW), silty Sand (SM), with more minor Silt (ML), elastic Silt (MH), and lean Clay (CL). The deposit lies well above current sea-level (top of unit at 310 to 325 feet elevation), precluding deposition in an estuarine environment. We infer, therefore, that this sandy soil must have been deposited in a deltaic environment in a body of standing water.

Given that a marine environment can be all but ruled out due to the elevation of the deposit, a freshwater lake origin must be assumed. We have chosen to name this inferred former body of water "Bear Lake." The hypothesis requires the presence of a dam to impound a lake. Several scenarios for forming the dam can be envisioned. These include, at a minimum, a landslide dam, a moraine dam, an ice dam farther down the NF Stillaguamish River Valley formed by the Puget Sound Lobe, or an ice dam formed by a local alpine glacier extending across the NF Stillaguamish River Valley.

Of these, the first two appear implausible. In recent geologic history, the only landslides in the valley capable of damming the North Fork originate in the glacial drift along the sides of the valley. These deposits would not have been present at the time of the deposition of these sands which underlie and, therefore, pre-date deposition of the Whitman Bench.

A moraine dam is similarly implausible, as the NF of the Stillaguamish River is a powerful river, which would likely have removed such a dam in short order, draining the lake. Therefore, glacial damming is the most likely scenario for forming the lake in which the sand was deposited. This, however, could not have occurred during a significant interglacial period, but rather would have occurred during the onset of a glacial stade of an as yet undetermined age.

There is no physical evidence that the top of the Bear Lake Sand was subject to weathering, soil formation, or significant erosion which might have removed weathering features or paleosols. Where exposed in outcrop, the top of the sand is essentially horizontal and the elevation varies by no more than 15 feet across an area almost 1,200 ft wide. Therefore, the top of the Bear Lake Sand is not interpreted as an unconformity.

In this scenario, deposition of the Bear Lake Sand was terminated when the lake level rose significantly, due to closure of a lower spillway by the advancing Puget Sound Lobe, or due to an increase in the elevation of a local ice-lobe dam across the valley. This would have placed the head of the delta significantly upstream of the Whitman Bench, precluding sand from reaching the area. The dam appears to have been of variable height, which can be inferred from the clay beds intercalated within the sand.

This is another piece of evidence that the lake level was likely not controlled by a moraine or landslide dam, but rather, impounded by a glacial ice dam of varying height through time.

There are two possible ice sources for damming the NF Stillaguamish River Valley. One consists of the local alpine glaciers advancing down French Creek from the Whitehorse Mountain massif, which could have reached and crossed the North Fork valley. This ice dam likely would not have been high, placing the head of the delta of the North Fork relatively close to the Whitman Bench, which would explain the dominance of sand in the deposits. Where a river enters a lake, gravel is the first material to be deposited as the water velocity decreases. Sand is transported farther out into the standing water, and suspended sediments, such as silt and especially clay, are usually dispersed across the lake as turbidity, settling onto the floor of the lake, much farther from the head of the submerged delta.

In this case, for some time, sand was the dominant material deposited in the vicinity of what later became the Whitman Bench, which suggests that the location of sediment input into the lake was not very far removed, but sufficiently far to have dropped its gravel bedload closer to its source. The time frame required for deposition of more than 90 feet of sand with some intercalated silts and clays is impossible to determine with the available information.

The lack of soil development or scouring on the top of the Bear Lake Sand also implies that little time elapsed between deposition of the sand and the change in the lake level that resulted in deposition of the Fine-grained Glaciolacustrine unit. The Fine-grained Glaciolacustrine sequence has been interpreted by previous researchers as a deposit of the Fraser Glaciation and, possibly, the Vashon Stade. No evidence was developed during this investigation to cast any doubt on these interpretations.

The fact that there was essentially no hiatus in deposition between these two units implies that the BLS is not significantly older than the FGL unit, and may be as young as the Frazer Glaciation, or even Vashon Stade (approximately 18,000 – 13,000 YBP).

The main evidence contrary to this hypothesis are three radio-carbon dates obtained from wood fragments, possibly within these sands, by Dragovich (12), and one very small wood fragment found near the top of the BLS in EB-04. The samples collected by Dragovich produced C-14 ages of 35,040 +/- 450 and 38,560 +/- 640 YPB, and the fragment from EB-04 indicates an "infinite" age, older than approximately 43,500 years (13).

A possible solution to this discrepancy is re-mobilization of older "Olympia Age" interglacial slough deposits containing woody debris, by glaciers advancing down the NF Stillaguamish River or Sauk River Valleys at the onset of the Fraser Glaciation. The "old" wood was then re-deposited in the younger deltaic sediments.

One point which might support the re-sedimentation hypothesis is that the wood dated by Dragovich et al in 2003 (12) was reportedly collected from deposits located close to river level (around elevation 260') (personal communication). The wood fragment in EB-04 was found very close to the top of the sand unit, at an elevation around 310 ft, or 50 feet higher than river elevation. Yet, the material obtained from stratigraphically higher (presumed younger) deposits provided an older C-14 date than the wood from lower (presumed older) strata.

Given that the sand may not be part of the Olympia Interstade, our expert team determined that it was appropriate to assign the unit a local stratigraphic name and, for purposes of this assessment, it has been designated the "Bear Lake Sands." The actual age must, at this point be considered indeterminate.

Fine-grained Glacio-Lacustrine Unit

It is possible that transition from deposition of the Bear Lake Sands to the FGL occurred in this vicinity when the water level of the lake deepened as a result of the Puget Sound Lobe blocking the mouth of the Stillaguamish River. Given the fact that elevation of the Puget Sound Lobe ultimately reached an altitude of around 4,100 feet near the mouth of the Stillaguamish River, it was capable of damming a lake with a relatively high pool elevation. The lake level would have been controlled by the elevation of the lowest available spillway. The limited time available to complete this investigation has made it impossible to verify the probable location of such spillways.

Raising the lake level in the NF Stillaguamish River Valley would have resulted in moving not only the North Fork delta, but also deltas deposited by smaller side tributaries far up their respective valleys. As a result, once the lake level rose significantly, deposition of sand would have ceased in the vicinity of the current Whitman Bench, to be replaced by deposition of finer-grained, suspended components of the outwash flow.

Given the approximately 300-ft thickness of the FGL, and the thickness of individual laminae, which is on average probably less than 1/8", it is very unlikely that each lamination represents a year, as that would imply a total time of deposition around 28,800 years. These laminations most likely do not represent "varves" (annual laminae). Instead, each lamina, or rhythmite probably represents an individual depositional event in the lake, or possibly, portions of the lake. The latter deduction is also supported by the fact that in some portions of the unit, the laminae consist of interbedded lighter greenish-gray and darker gray to black layers. The distinctly different colors imply at least two sediment sources contributing material to the lacustrine deposits. Given the colors, it is also appears that these sediment sources were of local origin, based on bedrock lithologies (mud-stone and green stone sources), rather than exotic (distant) sources.

Once the termini of the glaciers advanced toward the current location of Whitman Bench, shrinking the lake, the sediment sources (outwash streams) would have become much closer, resulting in more coarse-grained sediment reaching this vicinity. This would explain the observed transition from exclusive deposition of silt and clay rhythmites to thicker bedded and coarser grained strata of the Advance Outwash.

Advance Outwash

This unit is located between the fine-grained glacio-lacustrine silts and clays and the overlying till, while portions of the unit may also be integrated into the till complex. It is also the most laterally variable unit, in terms of its variable composition. In those borings on the Whitman Bench which extend below the till, the unit consists mainly of silt, sandy silt, silty sand, and sand. However, in the western exposures of the 2014 Landslide main scarp (Figure 23), the unit consists predominantly of sand and gravel. In the remainder of the main scarp, much of this unit is covered by sand and gravel "talus" collecting at the base of the headscarp from raveling of the recessional outwash.

In the western main scarp, the unit consists of cross-bedded coarse-grained poorly-graded sand with frequent thin and discontinuous layers of pebbles and cobbles. At one location in the west-central portion of the exposure, a deposit of well-sorted light-colored pebbles to small cobbles, more than 10 feet thick, terminates against the sand along a surface dipping at 80 degrees. Similar off-sets were observed throughout the deposit, indicating that this unit was deposited as ice-contact stratified drift, where the shifting and melting ice caused collapse of the material deposited on or against the ice. Large-scale cross beds in the western portion of the main scarp appear to dip at shallow angles to the southeast. Similar apparent dips (eastward component) were observed in silty coarse gravel beds located directly beneath the till, in the west central portion of the 2014 main scarp. The constant raveling of the younger recessional outwash materials lying above the till negates access to much of the 2014 main scarp, so direct measurements of these units' attitudes (strike and dip) were not possible.

In the center of the main scarp, the lowermost exposed "Advance Outwash" consists of a couple of layers of what appears to be till, a few feet thick, separated by thin bands of sandy outwash. These tills occur several tens of feet below the general elevation of the principal till unit, prominently exposed along much of the 2014 Landslide main scarp. It is likely that these till layers represent "flow till." Above the apparent flow tills exposed near the center of the 2014 main scarp is a deposit of stratified sand and gravel, which forms a high point near the center of the main scarp (Figure 24), replacing the lodgement till present east and west of this outcrop. Apparent dips on individual strata are toward the east on the east side, and to the west on the west side of the deposit. The actual dip appears to be to the north-northwest. Given the attitude of the bedding, this deposit is interpreted as part of a delta, and the sediment source would have been on the valley side. The prevalence of light-colored "exotic" pebbles and cobbles in the deposit indicates that the northern ice-marginal drainage of the glacial lobe extending up the Stillaguamish River Valley from the Puget Sound Lobe was the likely source.

In the central and east-central portion of the main scarp, this sand-and-gravel delta replaces the main deposit of lodgment till present east and west of those exposures. However, this coarse-grained deltaic deposit was not found in either of the borings drilled by WSDOT in late 2014, less than 300' behind the 2014 main scarp. Given the slope angle of the beds forming the deposit, and its thickness, the top of the delta could not have extended significantly farther to the northwest (under the Whitman Bench) than the present main scarp.

Whereas the AO unit is dominated by deltaic deposits of sand and gravel of probable exotic origin in the western and central portions of the main scarp, it appears to consist mostly of dark gray silty sand and silt in the eastern portions of the site. This is deduced mainly from the composition of the unit in EB-07si-15 and in the failure blocks located on the north side of the river in the eastern portion of the slide area. Stratigraphic relationships are largely preserved in these slide blocks, although they have undergone significant deformation.

Till

The thickness of the till is highly variable across the 2014 main scarp and in the recent borings extended through the unit on the Whitman Bench. In the eastern portion of the main scarp, the total till complex, consisting of several layers of apparent flow till overlain by a massive lodgement till, is in excess of 100 feet thick. In H-1VWP-14, the till complex was 86 feet thick, consisting of several layers of diamict separated by stratified outwash; in EB-02VWP-15 it consisted of two layers of diamict separated by interbedded sand and gravel, with the entire package totaling 100.5 feet. In EB-06VWP-15, the unit was

53 feet thick, and in EB-08VWP-15 it also consisted of two layers separated by bedded sands and gravel, totaling 139 feet. As discussed above, no till is present for approximately 150 to 200 feet laterally across the center of the 2014 main scarp, and immediately to the east. To the west of the center of the main scarp, the lodgement till layer is never more than 30 feet thick, with the predominant thickness between 20 and 25 feet. It thins to less than 20 feet in the westernmost portion of the 2014 main scarp, and is truncated against a steeply southward dipping discontinuity. The lower portions of the headscarp are covered by later collapse debris and talus, and it is not possible to determine if additional till strata are present within the stratified drift below the lodgement till.

 Deformation till was encountered in several borings below either the diamict till complex (EB-06VWP-15 and EB-8VWP-15), or below apparent failure surfaces (EB-05SI-15 and EB-07SI-15). The deformation till was also encountered in H1-VWP-14, where there are reports of "distorted sand laminae" and occasional slickensided surfaces to elevation 505 ft, or 287 ft below the bottom of the diamict till complex. There are no such descriptors for the FGL in EB-02VWP-15, but samples were obtained from this boring below the till almost exclusively in brass tubes, which would preclude observation of such deformation.

As a result, it is apparent that the actual influence of glacial overriding on the fabric of the materials underlying Whitman Bench extends significant distances below the stratigraphic position of the obvious diamict till complex.

Recessional Silt

At most places along the exposed 2014 main scarp and in the borings on the Whitman Bench, a Silt/Sandy Silt/Silty Sand unit was encountered, either directly above the till or, in the center of the main scarp, lying upon the sand-and-gravel delta. The unit is dark brown to dark gray in color in outcrop and dark greenish blue in the borings. It appears to form an aquitard, where active seeps were observed in the main scarp of the 2014 Landslide. It is probable that this unit formed in a relatively small ice-marginal lake above the Whitman Bench, prior to the time when the sand-and-gravel delta of the recessional outwash had pro-graded (filled in the lake) to this location.

Recessional Outwash

The youngest unit at the site consists of what has been called "Recessional Outwash." This unit consists mostly of sand with localized concentrations of gravel. The stratification of the unit appears to be near-horizontal, but many of the strata are internally cross-bedded, either as foreset or trough crossbeds. Apparent dips of the crossbeds are generally to the east. Gravel is present mostly in the western and central portions of the main scarp, and is essentially absent in the exposures along the eastern part of the 2014 main scarp.

Because the overwhelming majority of the gravel in the unit is comprised of granitic and other exotic lithologies found primarily in British Columbia, it appears that this unit was deposited primarily by the northern ice-marginal drainage of the arm of the Puget Sound Lobe extending up-valley in the North Fork Stillaguamish valley, or coming through the topographic trough in which Lake Cavanaugh is now located.

The unit has been ascribed a Vashon Stade age by previous researchers, and no evidence to the contrary was found during this assessment. However, it is interesting to note that, on the equivalent of the

Whitman Bench along the southern valley side, the unit appears to be <u>overlain</u> by eskers. Similar features are present on Whitman Bench northwest of the area of investigation. This would imply that glacial ice was present on top of the benches at some time after deposition of the "recessional outwash." Given the compressed timeline imposed on our assessment, it was not possible to further investigate this somewhat enigmatic stratigraphic relationship.

Glacial Context

Based on our recent mapping of glacial geomorphic features in the area, including the Cultus Mountains, Skagit, Sauk, and North Fork Stillaguamish Valley, the stratigraphy of the Whitman Bench and surrounding area appears to be the result of complex interaction of at least four different ice streams/sources during the Fraser Glaciation (approximately 30,000 to 10,000 years before present [YBP]), and possibly, only the latest significant glacial advance of that glaciation (the Vashon Stade, 18,000 to 13,000 YBP). Due in large part to the recent availability of higher-quality LiDAR-derived digital elevation models of the surrounding area, it has been possible to map glacial depositional and scour features resulting from the interaction of glaciers with the landscape. These features mainly include moraines, flutes, drumlins, eskers, and otherwise glacially "streamlined" substrate. The resulting map is included with this appendix as electronic shape files.   And from these features, ice flow directions and ice sources can be inferred.

The apparent ice sources include an arm of the Puget Sound Lobe of the Cordilleran Ice Sheet extending up the North Fork of the Stillaguamish; an arm of the more southern portion of the Cordilleran Ice Sheet extending down the North Fork Valley from highlands of the Northern Cascades to the east; an arm of the local Cultus Mountains ice sheet originating on the Skadulgwas Pk./Mt. Higgins massif (just over 5,000' elevation) immediately NE of the site, and extending through Rollins Creek; and, possibly, an alpine glacier from the White Horse massif (just under 7,000' elevation) located southeast of the site, extending across the North Fork valley from French Creek.

The relatively complex interaction through time of the four ice streams converging onto the area of the Whitman Bench is likely the result of micro-climatic influences of the Cordilleran Ice Sheet when interacting with the prevailing westerly winds coming off the Pacific Ocean. During the initial stages of a glaciation, the higher mountains to the north and east of the Whitman Bench area (Cultus Mountains and the crest of Northern Cascades) caused significant orographic precipitation, which, when falling predominantly as snow, results over time in formation of large amounts of glacial ice.

However, the same condition occurs farther north, along the Cascade Range in British Columbia. The glaciers emanating from that area ultimately coalesced into the Puget Sound Lobe, which extended southward in the Puget Sound Lowland, towards Seattle and points south. Once that lobe reached a certain thickness and height, it started creating its own orographic effect, intercepting much of the moisture coming off the Pacific Ocean. This deprived the southern portions of the Cordilleran Ice Sheet and the glaciers originating around Whitman Bench of their snow supply, resulting in a collapse of the more local alpine glaciers and mountain ice sheets.

The opposite effect occurs upon initial recession of the Puget Sound Lobe, towards the end of larger-scale glacial events. As the elevation of the Puget Sound lobe drops due to melting along its base and edges, the topographic high points around Whitman Bench received more precipitation in the form of

snow, allowing the alpine glaciers to become the locally dominant ice sources, and possibly, even re-advance.

Current Understanding of Geologic Setting

The idea that several independent sediment sources were active at the time of the deposition of the sediments underlying the Whitman Bench was first developed when it became apparent that the composition of the gravel-size component in the till at the SR-530 Landslide area differed significantly from that of the gravel component of the overlying "recessional outwash" materials. The till contains an overwhelming majority (estimated at 80%+) of relatively local lithologies, whereas the overlying outwash contains a similarly overwhelming majority (also around 80%) of exotic lithologies, thought to be derived in large measure from bedrock sources in British Columbia (from the Frazer Glaciation).

Based on the distribution and orientation of lateral moraines on the northern side slopes of the North Fork (NF) Stillaguamish Valley, it appears that during much of the last glacial episode, ice flowed in a westerly direction east of Whitman Bench, and in an easterly direction west of Whitman Bench (Figure 25). Significant ice sources reaching the NF Stillaguamish River Valley were the White Horse Mountain massif southeast of the site (just under 7,000' elevation), and the top of Skadulgwas Peak and Mount Higgins, located immediately northeast and east-northeast of the site (maximum elevation just above 5,000'). Based on lateral moraine orientations, the "alpine" glaciers from White Horse Mountain appear to have flowed down the valleys of Boulder and French Creeks, while the western portion of the glacier from Skadulgwas Peak initially flowed northwestward, and then spilled southwestward into the Rollins Creek Valley, following that valley to the south.

Based on the location of the highest lateral moraines exposed along the south flank of Skadulgwas Peak, at the last glacial maximum the ice elevation on the north side of the NF Stillaguamish Valley was at least 4,500 feet. At Mt. Higgins, ice flowing southward from the Cultus Mountains into the North Fork valley deposited steeply plunging lateral moraines on the upper north slope of the North Fork valley.

The higher lateral moraines along the south face of Skadulgwas Peak are essentially flat-lying, indicating that there was very little surface slope on the glacial ice mass, at least in an East-West direction. Farther to both the east and the west, the lateral moraines appear to be sloping; with the moraines east of Skadulgwas Peak sloping westward, and the moraines on the valley sides west of Whitman Bench decreasing in elevation, eastward. This suggests that two arms of the Cordilleran Ice Sheet, flowing mostly around and partly over the Cultus Mountains, essentially 'met' at Whitman Bench, in the vicinity of which they were joined by the more local ice streams flowing down the Rollins and French/Boulder Creek drainages.
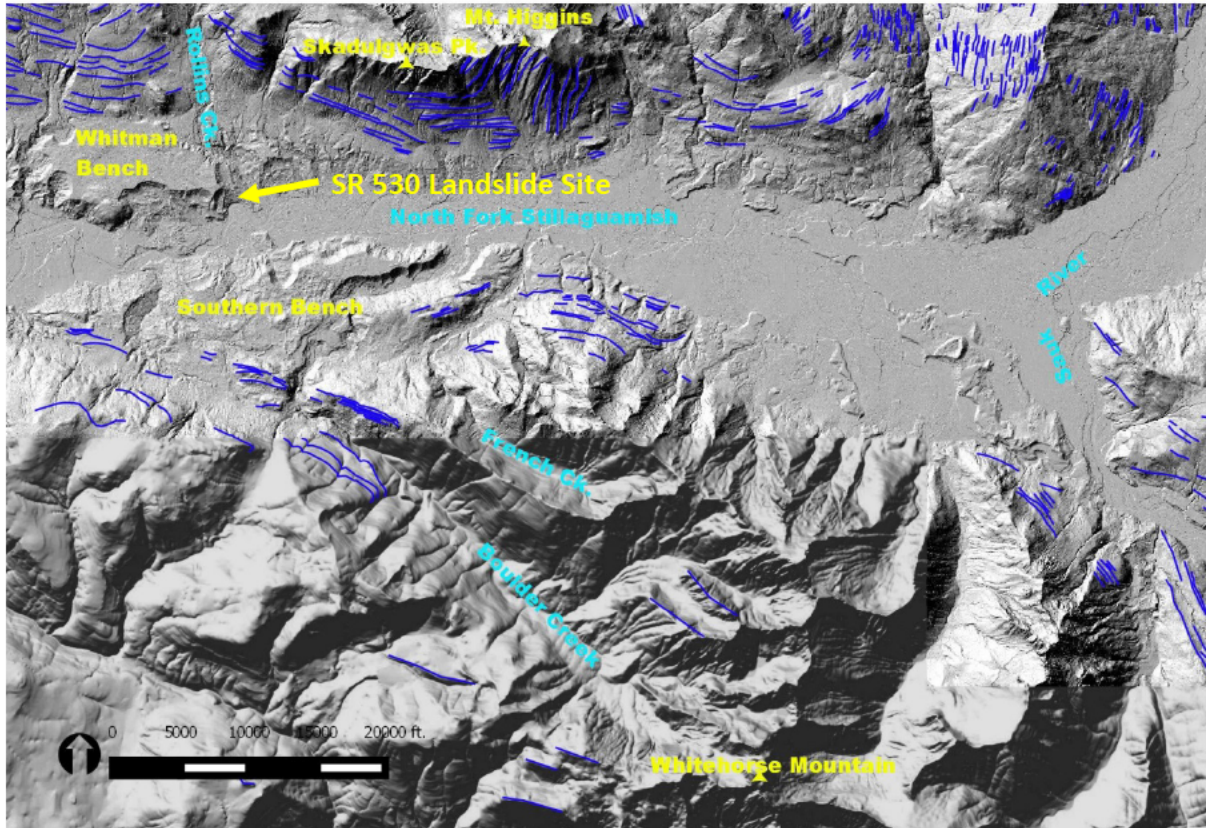
Linear glacial geomorphic features identified in the vicinity of Whitman Bench.

Based on the orientation of glacial streamlining in the area around and north of Lake Cavanaugh and farther to the northwest, the source of the ice entering the NF Stillaguamish Valley from the west and northwest was the eastern side of the Puget Sound Lobe. The source of the ice moving westward from the eastern portion of the NF Stillaguamish Valley would have been located east, north, and northeast of the present-day valley. It is not clear whether at times of significant glaciation, the Glacier Peak massif contributed ice to the NF Stillaguamish Valley through the Sauk drainage. Lateral moraines on the mountain directly southeast of Darrington indicate that the last glaciers in that vicinity flowed in a southerly direction, up the Sauk Valley. However, there is also geomorphic evidence, albeit more subdued, of ice moving northward through the Sauk Valley southeast of Darrington, likely during the earlier part of the last glaciation.

Based on the direction and cross-cutting relationships between the lower lateral moraines on the south flank of the Skadulgwas Peak- Mt. Higgins massif, the western ice source, or possibly the Rollins Creek lobe, appears to have outlasted the eastern ice source by a short time, and may have undergone minor re-advances during late Vashon Time. This is also indicated by evidence exposed along the south side of the NF Stillaguamish Valley in the vicinity of Boulder and French Creeks, where eskers (englacial outwash tunnel fills) were deposited on top of the outwash bench which forms the southern counterpart of the Whitman Bench in that area. An approximately 2% eastward slope of this depositional bench suggests that the youngest outwash there was deposited from the west, along the margins of the retreating western glacier (arm of the Puget Sound Lobe).

Kettle holes, which are closed-contour depressions resulting from melting of "dead ice" buried by outwash, are present on the Whitman Bench and its southern counterparts. This is evidence that most of the "recessional outwash" was deposited along the glacial margins rather than in a more distal pro-glacial outwash plain.

Origin of Lower Portions of Whitman Bench

The lower units underlying Whitman Bench include the Bear Lake Sands, Fine-grained Glaciolacustrine Unit, and the Advance Outwash. All of these units were deposited prior to the last glacial maximum of the Vashon Stade.

As outlined above, the Bear Lake Sands appear to have been part of a delta deposited by the North Fork Stillaguamish and/or its local tributaries (Rollins and French/Boulder Creeks) in an ice-dammed lake. The Bear Lake Sands can be shown to be present both under the eastern portion of Whitman Bench and under the bench on the south side of the North Fork valley, directly south of the SR 530 Slide. Therefore, the ice dam for the lake could have been either a local alpine glacier emanating from French Creek, or an arm of the Puget Sound Lobe blocking the valley, farther to the west. The down-valley extent of the sand and/or equivalent units, is not currently known. The lack of this information precludes an unequivocal decision regarding the source of the ice dam during deposition of the Bear Lake Sands.

Regardless of the configuration of the ice dam during deposition of the Bear Lake Sand, the intercalated very fine-grained silt and clay beds indicate that the height of the dam was variable, increasing at times to the point where the area of deposition of sand moved farther upstream, or at least upstream out of the vicinity of Whitman Bench. Such events appear to have become more frequent during the later stages of deposition of the Bear Lake Sand, as there are several silt/clay interbeds present in the uppermost 10 to 12 feet of the sand deposit.

Finally, the lake level rose to an elevation where deposition of sandy materials ceased completely in the vicinity of the later SR-530 Slide. It is possible that the deposition of the Fine-grained Glaciolacustrine sequence began when the Puget Sound Lobe grew sufficiently to close off one or more of the lower-elevation spillways on the south side of the North Fork Stillaguamish valley, west of Oso. A potential higher-elevation spillway was identified east of Arlington, starting in the Jim Creek valley at lat/long 48.2147/-121.9494, extending past Twin Lakes, Chain Lakes, and Barge Lake to a high point around 820 feet at lat/long 48.1602/-121.9290, and with an outlet to the South Fork Stillaguamish Valley near Mud Lake at lat/long 48.1435/-121.9285. For a significant time following this lake level rise, sediment kept in suspension in quiet water or transported via sub-aqueous mud flows (turbidity currents) on a very gently sloping lake floor reached the location of the future SR-530 Slide. The latter transport mechanism is indicated due to the large number of rhythmites making up the 300'+ section of FGL, which precludes each rhythmite representing an annual sedimentation cycle (varve). In addition, the fact that the rhythmite sequence often includes color changes between individual couplets implies different sources were contributing material during individual sedimentation events, rather than an overall homogenization, as would be expected during mixing of suspended sediments throughout the lake.

Both the Bear Lake Sand and Fine-grained Glaciolacustrine sequence were likely deposited over the entire width of the North Fork Valley. However, according to the logs for water wells extending to 100 or more feet in the more central portions of the valley, no materials fitting the description and

stratigraphic relationships of these units were encountered during drilling of these wells. "Till" was reported to be present in some of the water wells in Steelhead Haven. This indicates that the BLS and FGL units were never deposited in the center of the valley; were removed in the center of the valley by later glacial advance(s); or removed by river or subglacial drainage scour.

After an extended period of deposition of very fine-grained glaciolacustrine silts and clays, several of the glacial lobes in the valley advanced sufficiently far towards the site of the later SR-530 Slide to once again contribute coarser-grained materials, which comprise the Advance Outwash unit. In the eastern portion of the Hazel/SR-530 Slide area, the advance outwash consists mainly of an upward coarsening sequence of silts interbedded with fine sands and finally, mostly sand, nearly all of which is dark gray to light gray in color, implying a more local source, from the mudstones and meta-sedimentary rocks present in the Skadulgwas Pk./Mt. Higgins massif in the vicinity of Whitman Bench. Therefore, this portion of the Advance Outwash was likely deposited either from the glacial lobe of the Interior Cordilleran Ice Sheet extending down the North Fork Valley, or from the local alpine glacier in the Rollins Creek valley.

In the western portion of the slide area, materials deposited at the equivalent stratigraphic level consist of medium-to coarse-grained sand and gravel, which appears to have been deposited in an ice-contact delta complex. The latter conclusion is based on the fact that the sand and gravel show fore-set cross bedding, which is disrupted along several steeply dipping surfaces which place gravel in lateral contact with sand. Such features are generally interpreted as collapse structures resulting from shifting of ice, against which the sediments were originally deposited. The provenance of the gravel in this western portion is significantly more exotic (British Columbia) than the cobble and boulder content of the overlying till. Therefore, the northern ice-marginal drainage of the arm of the Puget Sound Lobe extending up the North Fork Valley, is the likely source for the deltaic sediments of the west side of the slide area.

The locus of deposition for the western delta appears to have shifted to the center of the slide area shortly prior to the advance of the glaciers that inundated the Whitman Bench area and resulted in deposition of the till complex over the site. In the center of the headscarp, a thick deposit of northward-dipping sand and gravel takes the place of the lodgement till present both to the east and west of the center. The light color of the gravel in this foreset-bedded central deposit implies an exotic provenance for the unit, which may also have been deposited by the northern ice-marginal drainage of the Puget Sound Lobe arm extending up the North Fork Valley.

The proximity of at least some of the glacial lobes to the later site of the Hazel/SR-530 Slides during the later portion of the deposition of the Advance Outwash unit, is also supported by the presence of flow till units within the Advance Outwash sequence in the center of the SR-530 main scarp, in the lower western side scarp, and the presence of till units (unknown whether flow till) intercalated with stratified glacial drift in several of the exploratory borings installed in Whitman Bench (H1-VWP-14, EB-02VWP-15, EB-06VWP-15, and EB-08VWP-15).

Kame Terrace Concept

There is a strong possibility that the uppermost portions (Recessional Outwash) of Whitman Bench and its southern counterpart formed as "kame terraces," during the later stages of glacial recession, when the ice level in the valley and vicinity had dropped from its high stand around 4,500 ft. nearly to the level of the top of the till (around 750 ft). In that scenario, the glacier extending westward up the North Fork valley from the Puget Sound lobe was occupying the central portion of the valley to current river level or even lower (there is evidence of till in some of the water well logs in the valley). The Recessional Outwash would have been deposited along the margins of this glacier. Evidence from lateral moraines in and adjacent to the middle and upper reaches of Rollins Creek indicate that the Rollins Creek glacier was, at that time, a significant tributary ice stream to the glacier occupying the central part of the North Fork valley.

A kame terrace origin for the Whitman Bench and others in its vicinity would obviate the necessity of evacuating an average of approximately one million cubic yards of material from a 10-mile stretch of the NF Stillaguamish Valley every year for the last 13,000 years. This represents the volume of material that would have been present if the benches were continuous across the valley, as inferred in papers recently published by some researchers ((7), (6)).

Of interest in this context is a C-14 date reported in Lahusen et al. (7) for a log buried in the fluvial terrace of the NF Stillaguamish River, which was over-run by the Rowan Landslide. The log was dated at 11,692+/-286 YBP, which would allow only approximately 1,300 years between final recession of the ice and the river reaching its current level in the valley. This appears to be an impossibly short time-frame for evacuation of so much material filling the valley, if the Whitman Bench and its southern counterpart had been continuous across the valley at the end of the Vashon Stade.

A kame terrace origin would also explain the apparent collapse of some portions of the till deposit in the eastern portion of the main scarp, where the collapsed blocks are buried under essentially flat-lying sand-and-gravel outwash, which is at a lower elevation (around 700 ft AMSL) than the exposed surface of Whitman Bench (around 890 ft AMSL). Collapse of the edge of kame terraces is a frequently observed phenomenon, as the melting ice removes lateral support from sediments, which were originally deposited in contact with the ice. The approximate configuration of this original pre-historic failure is labeled P-1 on cross sections 4 and 5 and on the accompanying GIS map. The actual extent of this failure is impossible to determine with the evidence available to date. It may have extended along the entire width of the southeast-facing slope of Whitman Bench, or been limited to the northeast part of the later Hazel/SR-530 Slide area.

A kame terrace collapse of portions of the upper edge of Whitman Bench also provides a plausible explanation for the origin of the former mid-slope bench, large portions of which were involved in the SR-530 Landslide in 2014. The deposits underlying this bench had been previously identified as ancient landslide blocks (Thorsen, 1988). Photos taken by Bob Tart and others of the post-2006 slide scarp indicate that these slide blocks were significantly back-rotated, along failure surfaces with steep apparent southwest dips separating individual blocks. However, the contacts of the soil units within the blocks are dipping in a northerly direction, rather than to the northeast, as would be expected from back-rotation only along the steeply southwest-dipping failures.

This discrepancy can be explained by invoking a pre-historic two-stage failure involving the same slide material. The first failure, involving the upper half of the bench deposit would have occurred toward the southeast, roughly in the fall line direction of the former SE slope of the Whitman Bench. This failure would have been in response to melting of the ice buttressing the slope on that side. The failure surface on which this movement occurred is labeled P-2 on Sections 6 through 12. It is also likely that the slide debris at least partially rode up onto the adjacent, melting glacier. The back-rotation of the top of the block(s) resulting from the movement on the P-2 surface would have been to the northwest.
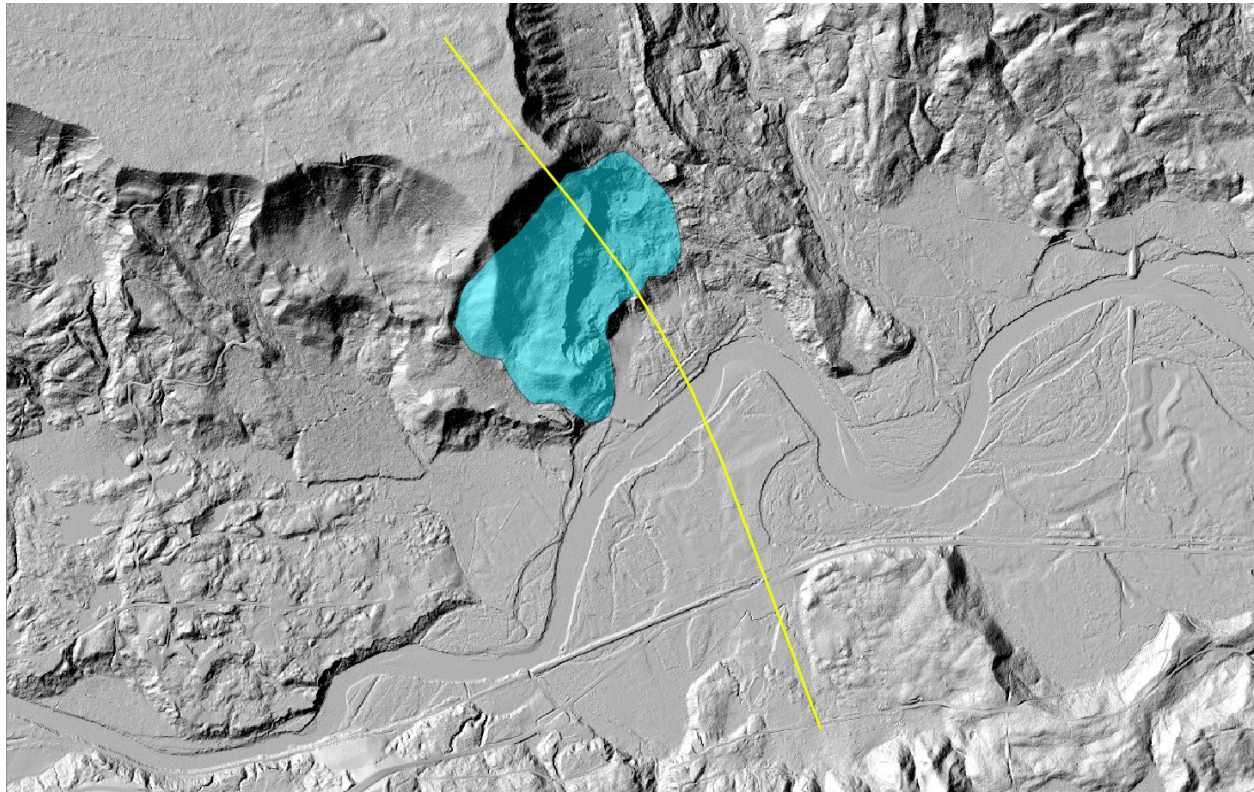
Approximate Extent of Ancient P-2 Failure Surface
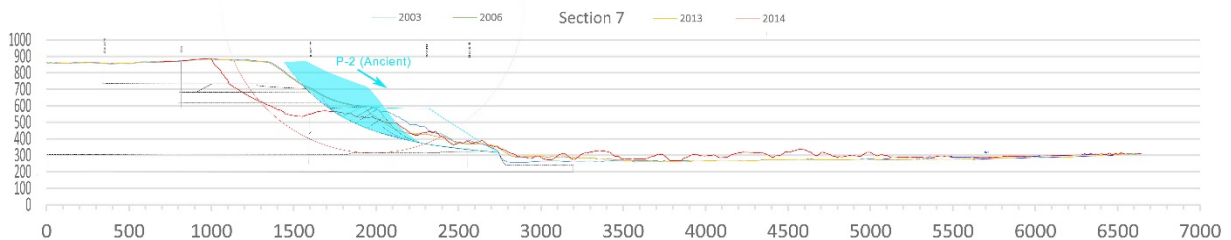
Mid-slope Bench Block Restored to its Inferred Pre-Kame-Terrace-Collapse Position

Due to the collapse of the Puget Sound Lobe of the Cordilleran Ice Sheet near the end of the Vashon Stade or possibly Everson Stade, it is probable that in this final stage of glacial recession, the Rollins Creek lobe, fed from the local, higher-elevation Skaldulgwas Pk./Mt. Higgins massif, would have been a more active ice source than the Puget Sound lobe. This conclusion is borne out by evidence of southwest-ward sloping lateral moraines higher on the west side of the Rollins Creek valley, which are tangential to lateral moraines of the Puget Sound Lobe arm extending down the valley in which Lake

Cavanaugh now lies. As a result, it is probable that the slope and flow direction of the glacier sitting at the base of the SE-facing slope of the Whitman Bench was to the southwest and west during the final stages of deglaciation.

A southwesterly slope on the ice below Whitman Bench would have re-directed the soil material involved in the second kame terrace failure (P-2) toward the southwest. It is probable that the portion of the failure located on the lower SE-facing slope of the Whitman Bench followed the erosional surface exposed by the melting and lowering of the ice surface in the valley. Headward-progressive southwesterly movement of the P-2 failure mass and extension of the slide mass in that direction would have resulted in the formation of the four landslide blocks observed in the Tart photos of the mid-slope bench, following the 2006 failure. The failure blocks would have been back-rotated to the northeast.

Therefore, where initial back-rotation during the southeastward first phase of the P-2 movement had resulted in northwesterly dip, further back-rotation of those surfaces to the northeast during the second phase of the P-2 movement then resulted in the steeper, northerly dip observed on the Tart photos.

As discussed above, both the P-1 and P-2 slope movements occurred immediately prior to the final deglaciation of the North Fork Stillaguamish valley. Further evidence of this is present in the form of draped and nearly horizontally bedded outwash sediments filling the closed-contour depressions left between the back-rotated upper surfaces of the former mid-slope bench failure blocks and the SE-facing slope of the portion of the Whitman Bench. Horizontally bedded sand-and-gravel requires streamflow moving alluvial material over and between the P-2 failure blocks at elevations ranging from approximately 485 to 600 ft, or nearly 300 to 400 ft below the top of the recessional outwash on the remainder of the Whitman Bench surface, but more than 200 feet above the current elevation of the North Fork Stillaguamish River.

As a result of both the P-1 and P-2 movements which were the direct and probably immediate result of removal of ice which buttressed the slope of the Whitman Bench at the end of the last glacial episode, the mid-slope bench block and the slope underlying the former Hazel slide movements were resting on pre-existing failure surfaces dipping at variable angles to the southeast or south-southeast. It appears that much of the "Hazel" slide movements occurred either directly on these surfaces or on parallel surfaces created over time by "abrasion" of material within the basal shear zone during the Hazel slope movements.

Final Glacial Events in the Vicinity of Whitman Bench

The final glacial events that can be documented in the geomorphology and geology in the immediate vicinity of Whitman Bench appear to have occurred in Headache Creek. Although the bench forming the main portion of the drainage basin for this creek has been mapped by others as a result of large-scale, deep-seated (rotational) slope movement, that interpretation is inconsistent with our site observations. The fact that horizontally laminated FGL is present in the channel of Headache Creek at lat/long 48.2864/-121.8471 (elev +/-529'), and at the north end of the Headache basin at lat/long 482916/-121.8496 (elev. =/- 510') demonstrates that the bench is underlain by in-place FGL, within the appropriate elevation range. Therefore, the bench on which Headache Creek flows cannot have originated as a slope movement block. Given the presence of the multi-crested ridge at the east edge of the bench, a more likely origin of the bench is partly as a higher-elevation floor of the Rollins Creek glacial trough, which was later modified by the ice-marginal drainage along the west side of the Rollins

Creek glacier. The ridge, which, where excavated by hand methods, consists of non-stratified silty sand with cobbles, and is interpreted as a late-recessional stage lateral moraine complex of the Rollins Creek glacier. The overall slope on the ridge (approximately 5% to the south) is consistent with this interpretation, as is the fact that the ridge is comprised of several partly over-lapping sub-parallel crests.

This re-interpretation of the origin of the geomorphic features in the Headache basin also implies that the local glaciers were the last to recede from the area of the Whitman Bench, which is consistent with a late-recessional southwest slope on the ice located southeast of Whitman Bench.

Observations Pertinent to SR-530 Slide Configuration and Sequence of Events

By necessity, a determination of which factors were important in the causation, initiation, and subsequent run-out of the March 22, 2014 SR-530 Landslide depends on an understanding of the configuration of the failure(s) in three dimensions, and an evolution of the failure through time. There are several lines of evidence which point to a certain sequence of events during the March 22, 2014 slide. These include evidence of where trees of identifiable species and height were located prior to and following the slide, where "intact forest floor" was located prior to and following the slide, the stratigraphy of the mid-slope bench as identifiable from photos prior to the slide, where the geologic units came to rest, as identifiable on high-resolution aerial photos, Giga-Pan photos taken by others (WSDOT and GEER), the seismic signals of the slide as measured at several stations in the vicinity, eyewitness reports, and observations of the surface of rupture and surface of separation in the slide area.

Tree Evidence

The tree evidence is described in Appendix G of this report. In summary, based on observations on air photos pre- and post-failure, most of the mass located on the south side of the river in the March 24, 2014 air photo appears to consist of a significant portion of the former mid-slope bench. This is based on the fact that a total of 693 segments of mature conifers can be identified in the post-slide photo. Of these, 75 are whole trees, 64 consist of large pieces of trunk with the tree tops, but lacking root balls, 497 consist of large trunk pieces with or without root-ball, but lacking the tree top, and 57 consist of trees with green limbs from the root ball to the top of the tree. The latter did not grow up in the interior of a dense stand but rather along the edge of such a stand, or in an area of scattered trees.

An edge of a dense stand was present only at the top of the 2006 Hazel Slide scarp and a few isolated live trees appear to have been present in two patches formed by Hazel slide blocks, immediately adjacent to the toe of the 2006 scarp. These are the only locations within the source area of the 2014 SR-530 slide where fully limbed, green conifers could have been present. 57 of these trees ended up in a zone located from roughly 300 to 500 ft south of the river, to a maximum distance of 1,600 ft south of the river, and just south of Hwy 530. Most of these fully limbed trees are located along the southern edge of the zone of greatest concentration of mature conifers. This indicates that the former mid-slope bench forms the largest portion of the mass covering the Steelhead Haven neighborhood on the south side of the post-failure river alignment.

Extension of the forest floor covering the surface of the transported mid-slope bench block appears to increase in a southerly direction. Close to the river, and directly south of the zone of over-riding by the gray material, only small patches of mineral soil are visible through the mat of needles, leaves and twigs forming the forest floor. However, this zone of mostly continuous forest floor ranges from only 100 to around 250 feet wide. To the south of there, the forest floor has significant gaps, generally arranged in more or less curvilinear segments of what appear to be slide block boundaries/scarps. This zone is approximately 250 to 300 feet wide (N-S). Beyond that, only small patches of intact forest floor are found, often associated with the root ball of a conifer.

Geologic Composition of the Former Mid-Slope Bench Blocks and Other Slide Debris

The portion of the former mid-slope bench block covered with more or less patchy forest floor is underlain by a light tan to tan mineral soil, which is consistent with the general appearance of the Recessional Outwash material observed in exposures on the north side of the river. This is also consistent with the apparent composition of the upper portion of the former mid-slope bench slide blocks, as shown on Bob Tart's photos taken after the 2006 Hazel Slide. These photos show both severely tilted and nearly flat-lying very light-colored stratified deposits consisting of sand and gravel.

In the Tart Photos, in all cases, the apparent Recessional Outwash in the mid-slope bench blocks is observed to be underlain by gray to dark gray soil units of varying "texture" or "morphology." Given the observations in the remaining western portion of the mid-slope bench, these units consist mostly of till and advance outwash (both silt and sand-and-gravel). Very little (less than five feet maximum) fine-grained glacio-lacustrine material (silt/clay or lean clay/ fat clay rhythmites, or the deformed and disrupted equivalent) was observed in the base of the ancient failure block remaining in the southwest margin of the failure area (site photos).

Gray hummocky areas were also observed in the post-SR-530-Slide deposits on the south side of the river, beyond the area underlain by apparent Recessional Outwash. In particular, this color of soil deposits is prevalent in the south-central area of the slide deposit, west of the north portion of the low hill which separates the eastern and western long-run-out lobes. Upon close inspection of the high-resolution air photo, it is apparent that the surface of most of these gray "hummocks" is covered with angular soil blocks. Similar, gray to dark gray hummocks covered in angular soil blocks are also present in the eastern long-run-out lobe, although in that area, much of the soil is located under muddy water in the 3-24-14 air photo. Based on observations on the north side of the river, such blocks are formed by either Till or Advance Outwash silt. Therefore, it is probable that these deposits represent the lower portions of the former mid-slope bench block(s).

More detailed mapping of the slide deposits was performed on the north side of the river, although this task could not be completed due to the inclement weather of the 2015/16 wet season, which resulted in hazardous conditions at the site, and later by the double murder of Monique Patenaude and Patrick Shunn which resulted in closure of the slide area for several weeks shortly after the weather improved at the end of March. By the time the closure was lifted by the Snohomish County Sheriff's office, it was too late to continue with the field work. The geologic mapping completed on the north side is included in the Discovery documents electronically as .KMZ files. In summary, much of the deposits in the eastern and central portion of the first row of slide blocks north of the river consists of a relatively thick section of gray to dark gray Silt, sandy Silt, and minor silty Sand of the Advance Outwash. A

discontinuous veneer of till blocks approximately 6 feet or less thick is present over the Advance Outwash in the easternmost portion, overlain by approximately 5 to 10 feet of recessional outwash, locally with isolated patches of forest floor and very few trees.

In the western portion, till is even more sparse, with only isolated smaller blocks of till under the Recessional Outwash covering the lower rows of slide blocks in that vicinity.

Recessional Outwash is conspicuously absent in the central portion of the first row of landslide blocks north of the river. This area is mostly underlain by Advance Outwash, consisting of Silt (ML to MH), sandy Silt, and smaller areas of gray silty very fine- to fine-grained Sand (SM). A couple of days after the March 22, 2014 event, the area was covered in numerous angular blocks, which, by September 2015 had decrepitated to rounded, steep-sided hummocks a few feet in diameter (see site photos). Larger till blocks are present on the back (N) side of this area, now partially submerged by the western arm of the largest pond that formed in the slide area, since the 2014 event.

Large quantities of Advance Outwash silt are/were also present in the slide block covering the area where the Bear Lake Sand cliff is located. The lower portion of this block consists of disturbed laminated fine-grained glaciolacustrine clay, which, in the fall of 2015, could only be found in small gullies eroded into the toe of the steep south side of the block. This portion of the block failed during the 2015/16 wet season, resulting in an extensive lobate flow deposit in the previous alluvial fan area, south of the block. The failure covered all of the previous exposures of glacio-lacustrine clay in this vicinity.

Besides the till cliff collapse deposit in the new main scarp "graben," the largest surficial deposits of till in the slide debris were observed upslope of EB-07SI-15, between that boring and EB-12SI-15, and on the slope between the latter boring and EB-09SI-15. Till pieces are also present on the top of the slide block west of EB-09SI-15, partially covered in Recessional Outwash. The originally angular till blocks were in the process of degrading and decrepitating in the fall of 2015, and this process has continued through the 2015/16 wet season.

Recessional outwash and forest floor patches are conspicuously absent from the area around EB-07SI-15 and EB-12SI-15 and for some distance downslope from there.

Failure Surface Exposures/Outcrops

A drag fold was observed from the right bank at the base of one of the larger slide blocks on the left (south/west) bank of the river at Lat/Long 48.2795/-121.8395. The drag fold is in apparent rhythmically bedded clay overlain by what appeared to be a blocky sandy silt, overlain by silt and an unknown thickness of till, which is overlain by Recessional Outwash (site photos PA051188 and PA051190 – 10/05/15). The drag fold is located immediately above the Surface of Separation, with the material below the failure surface consisting of alluvial gravel of the North Fork. Access to this area was precluded due to lack of permission of entry from local landowners.

The surface of separation was also observed at three locations on the north/east (right) bank of the river at approx. lat/long 48.2811/-121.8410, 48.2810/-121.8400, and 48.2812/-121.8412. In the first case, the failure surface separates brown silty sand alluvium from a sheared mixture of clay, silt, sand, and rounded cobbles (site photos PB061800 through -1812, 11/6/15). In the second case, the surface of separation is located a few feet higher, separating a brown silty sand (alluvium) from gray silt and lean clay (slide debris) (Photos PB061793 through -1798, also 11/6/15). In the third case, the failure surface separates alluvial gravel with tree roots below, from gray sandy Silt above (Site Photos SR 530 9-20-15 001 through -006). The tree roots at the surface of separation were mostly aligned parallel to the apparent movement direction of the slide.

The toe of the surface of rupture was extensively exposed last summer and fall at the confluence of the post-SR-530 Landslide "Slide Creek" and "Mudflow Creek" of Shannon and Associates (1952) in the vicinity of lat/long 48.2823/-121.8488, at elevations ranging from approximately 310 to 314 ft. Site photos of this area include the following: SR 530 9-20-15 051 through 109, P9210326 through P9210338, P9250814 through P9250821, IMG_0159 through IMG_0164, PA281685 through PA281689, PA291724 through PA291727, PB181847 through PB181879, and PB281943 through PB281947. Initial exposures showed the surface consisting of Recessional Outwash over Bear Lake Sands, with minor glaciolacustrine clay, smeared out along the surface. After additional erosion, later exposures in October and November 2015 showed the surface rising from the top of the Bear Lake Sands to within the rhythmically bedded fine-grained glaciolacustrine clay, located above the Bear Lake Sands. The surface had blocky, disrupted clay above it for a distance of 6 to 12 inches, and undisturbed rhythmically bedded clay/silt below. The surface of rupture within the clay formed the bed of the successor to "Mudflow Creek," upstream from a point located approximately 100 feet NW of the gully exposure. At the knick-point formed in the creek bed by the drop off the glaciolacustrine clay deposit, the failure surface had approximately 4 inches of highly sheared clay above the rhythmically bedded clay-silt sequence. Block samples of that material were carved and placed in wood boxes with paraffin for sealer, but the onset of inclement weather and rising creeks in the area precluded moving the heavy samples to the vehicles the day they had been packed. They were placed near the western margin of the slide for later retrieval. However, this area was subsequently buried during the winter under approximately 15 feet of 2015/16 slide debris and the samples were lost.

A very similar Surface of Rupture, or Surface of Separation, was exposed for a total length of approximately 280 feet in the lower portion of the western margin, centered on approximate lat/long 48.2815/-121.8487. As in the southern portion of the exposure in the creek valley side slopes and channel, this failure surface is located on Bear Lake Sand. The material immediately above the failure surface consists of sheared, blocky, disrupted glaciolacustrine clay. Site photos related to this exposure

include: IMG_0143, IMG_0147, IMG_0153 through 0158, and PB181824 through PB181832. At the southernmost exposure, near lat/long 48.2813/-121.8487, the surface dips 27˚ to the SW. For most of the exposure from there northward, the surface is essentially flat or dipping at a very low angle to the south or southwest.

Another Surface of Rupture was discovered in the west margin, between lat/long 48.2828/-121.8502 and 48.2827/-121.8502. Site photos related to this surface are P33312393, P3312394, P3312405 through P3312409, P3312417 through P3312431, P4012761 through P4012763, and P4282128 through P4282132. At the northeastern end of the exposure, the surface was located on silty Sand, and the material above the surface is sandy gravel. Less than 5 feet below the surface, the soil consists of a dark gray sandy Silt. The surface itself has a discontinuous layer of gray slightly sandy Silt, approximately 0.25" thick. The surface dips northward at approximately 35˚, although this angle should be treated as preliminary because no larger area could be cleaned for measurement on the steep slope in which it is exposed. At its southern end, this surface is coincident with the surface of separation located beneath the SR-530 Slide deposit on the western remnant of the mid-slope bench. The latter surface is described in the next paragraph.

A Surface of Separation extends northward from the southern tip of the SR-530 slide deposit on top of the western margin, located at lat/long 48.2822/-121.8504, to the end of the surface of rupture at 48.2827/-121.8502. Site photos related to this surface include: PB281938 through PB281942. This Surface of Separation is characterized by having Recessional Outwash (gravelly sand to sandy gravel) on top of a slightly uneven, sub-horizontal layer with brown soil and occasional plants/roots. The latter is interpreted as the former top soil developed on the mid-slope bench block remaining in-place, west and southwest of the west margin of the SR-530 Slide.

Another exposure of the Surface of Rupture was noted on the last visit to the site, along the eastern margin of the slide. Recent erosion in a small gully had exposed a failure surface on rhythmically bedded fine-grained glacio-lacustrine deposits. The location is at lat/long 48.2839/-121.8454. Site photos associated with this location include: P4292152 through P4292165. Portions of this surface of rupture located close to the adjacent slope of the eastern slide margin were dipping nearly 45˚ towards the southwest, and portions were nearly flat, with slickenside directions parallel to the overall movement direction (SE). The material above the surface of rupture consisted of blocky disrupted and sheared laminated silt/clay. The total shear zone, consisting of dark gray clay, was from half to one inch thick.

Surface(s) of Rupture in Borings

Surfaces of Rupture were encountered in all exploratory borings installed within the SR-530 Slide source area. The depths to and elevations of these surfaces in the borings where samples allow identification of such surfaces are summarized in the following table:

Boring #	Depth to Surface (ft.)	Elevation (ft. NAVD 88)
EB-04SI-15	134.5'	402.9'
H-14VWP-15	131.0'	406.9'
EB-05SI-15	50'	447.1'
EB-09SI-15	40.0'	338.9'
H-12SI-15	57 – 65'	374.1 – 382.1'
H-15VWP-15	56 – 65'	373.6 - 382.6'

Eyewitness Reports

Three first-hand witnesses of the slide were interviewed in November of 2015 by Dr. Schlieder. They included John Reed and the late Monique Patenaude and Patrick Shunn. Mr. Reed reiterated his previous statements regarding the sequence of events which he had previously provided to both GEER and the USGS. The USGS version of Mr. Reed's account is as follows:

"We obtained a key eyewitness account a few days after the event from a man who had been standing on a fluvial terrace just west of the DAF path, with a clear view overlooking the adjacent North Fork Stillaguamish River. The man was first alerted to the event by a roaring noise, which he described as similar to that of "low-flying aircraft." He could not see its cause, however, because terrain and trees blocked his view of the landslide source area. At this time he saw no landslide activity in the vicinity of the river. The initial noise gradually diminished, and tens of seconds passed before another loud noise developed and the man saw the river "tossed in the air," and "turning black" in color. He then saw "a wall of turbulent earth" moving southeastward, with a height he estimated as "100 feet overhead" and a speed he estimated as "100 miles per hour.""

GEER's description of John Reed's account is as follows:

"Eyewitness was in the front yard of their house on the north side of the Stillaguamish River when they heard a loud, prolonged scraping and noticed the brief fluttering of treetops on the lower bench of Mt. Higgins. "The noise sounded like a 747 (airplane) about to crash. It lasted about a minute and a half. It was loud." "When (the landslide) hit the water, it shot way up, way taller than the tallest trees. Then I saw this big black wall – it must have been more than 100 feet high – rise high above the neighborhood. The houses, in comparison, looked minuscule. It was unbelievable.""

"Eyewitness reports that when the landslide hit the river, it accelerated. They also report a period of relative quiescence between initiation and runout."

It is not apparent that anyone other than Dr. Schlieder spoke with the late Monique Patenaude and/or Patrick Shunn about their observations during the event. Their house is located west-southwest of John Reed's former residence. Mr. Shunn indicated that he was upstairs in an eastern room, when he heard a noise like low-flying fighter jets. However, when the origin of the noise did not significantly change for some time, it lead him to assume that an aircraft was in trouble. He went to the window and scanned the sky to the east. He did not see any aircraft, but after some time saw portions of the landslide through the trees, moving in the area of the neighborhood. He called to his wife Monique "landslide!" At the time, she was downstairs in the laundry room. She raced up the stairs in time to see large trees at the top of the ridge NE of their house falling over toward the south in rapid succession "Bam!, Bam!, Bam!"…

Inferred Configuration and Sequence of Movements of the Hazel/SR-530 Slides

As outlined above, at the end of deglaciation (around 13,000 YBP) following the Vashon and Everson Stades of the Frazer Glaciation, the upper portions of the SE-facing slope of Whitman Bench had

undergone slope movement as a result of removal of lateral support by the melting glacial ice of the Puget Sound and Rollins Creek lobes. Evidence for an initial partial rotational collapse of the uppermost portion of the terrace edge, involving only the Till and the Recessional Outwash exists only in the northeastern portion of the later SR-530 Slide. The surface along which this initial movement occurred has been designated P-1 for purposes of this report. The second movement (designated P-2) occurred on a southeast-facing erosional slope exposed by melting of the ice occupying the valley, initially moving much of the material comprising the upper part of the slope to the SE, and later in a SW direction, following the slope of the ice still present at the base of the hill. The southwesterly slope on that ice is inferred to have been the result of the local dominance of the Rollins Creek lobe during the latter stages of the collapse of the Puget Sound Lobe.

Both movements (to the southeast and southwest) left part of the failed kame terrace material sitting on the Bear Lake Sand at the base of the slope, with the bulk sitting on an ancient (+/-13,000 YBP) surface of rupture/separation on the part of the slope, underlain by the Fine-grained Glaciolacustrine sequence and Advance Outwash. The slope angle of the lower portion of the P-2 surface is defined by the location of the failure surface found in borings in EB-07SI-15, EB-09SI-15, and H-12SI-15, in exposures in the western gully area, and along the lower western margin of the slope movements.

From time to time, most likely in response to river erosion at the toe of the slope, portions of the Whitman Bench and the mid-slope bench block have failed during the last millennia. There are indications that the Rowan Slide, in close proximity to the Hazel/SR-530 slides was a similar large-scale rapid event involving a large portion of the south-facing slope of Whitman Bench east of the bedrock promontory located centrally along the south margin of the bench. Based on recent work by Lahusen et al. (2015), it is probable that this large-scale slide occurred within the last 1,000 years.

The Hazel Slide area has been historically documented to have been active from the early part of the 20th Century through 2006. The Hazel Slide involved an ever-growing area of the ancient kame terrace collapse landslide complex, sitting at the base of the SE-facing slope of Whitman Bench. Based on the fact that significant activity of the Hazel slide can, in large part be correlated to the times when the North Fork of the Stillaguamish has been at the base of the Bear Lake Sand cliff, it is probable that complete removal of the slide debris from previous Hazel Slides was often the initiating factor in further movements on P-2 and headward progression of the slide into the ancient mid-slope bench landslide complex.

In addition to removal of debris at the toe of the Bear Lake Sand cliff, material is removed from the slide area above the BLS cliff by erosion from Slide Creek (west side, always along the toe of the Hazel scarp), and Mudflow Creek (east side). Due to the different geologic materials comprising the east and west sides of the Hazel slide area, Slide Creek removes mostly cohesion-less sand and gravel (Recessional Outwash, coarse-grained Advance Outwash, and coarse-grained parts of the Till complex), and Mudflow Creek erodes mainly silty Advance Outwash, Till, and underlying Fine-grained Glaciolacustrine materials dominant in the eastern portions of the former mid-slope bench blocks.

Based on erosion rates of the debris field located south of the BLS cliff after the larger Hazel Slide events (as documented in historic aerial photos), near-complete removal of accumulated slide debris has taken from 15 to 25 years or more, depending on the size/volume of the movement. The largest such slide event documented on aerial photos occurred in 1967, and the resulting debris had not yet been completely removed by the North Fork Stillaguamish River by 2003.

Complete removal of the 1967 slide debris at the base of the BLS cliff by 2006 may have resulted in the January 25, 2006 Hazel Slide movement, which threatened to flood the Steelhead Haven neighborhood. Following the 2006 event, the historically documented efforts to limit the impact of the Hazel Slide on the anadromous fish habitat and fishery of the North Fork were propagated by construction of the timber crib wall along the north bank of the North Fork and a sedimentation pond for Slide Creek.

Minor activity can be documented in the Hazel Slide area above the BLS cliff and along its head scarp between the 2006 and 2013 LiDAR images. It is probable that this seemingly minor activity related to the old Slide and Mudflow Creeks resulted in the ultimate de-stabilization of the central and eastern portions of the ancient mid-slope bench landslide complex.

Two scenarios are possible for the initiation of the March 22, 2014 SR-530 Slide. The first scenario involves additional minor movement of the Hazel Slide material sitting in the source area above the BLS cliff. This may have removed sufficient lateral support from the toe of the remainder of the mid-slope bench to initiate movement of a large portion of this ancient slide deposit on the pre-existing failure surface P-2. For purposes of this report, such minor movement of the 2006 slide debris in the source area is designated M-1.
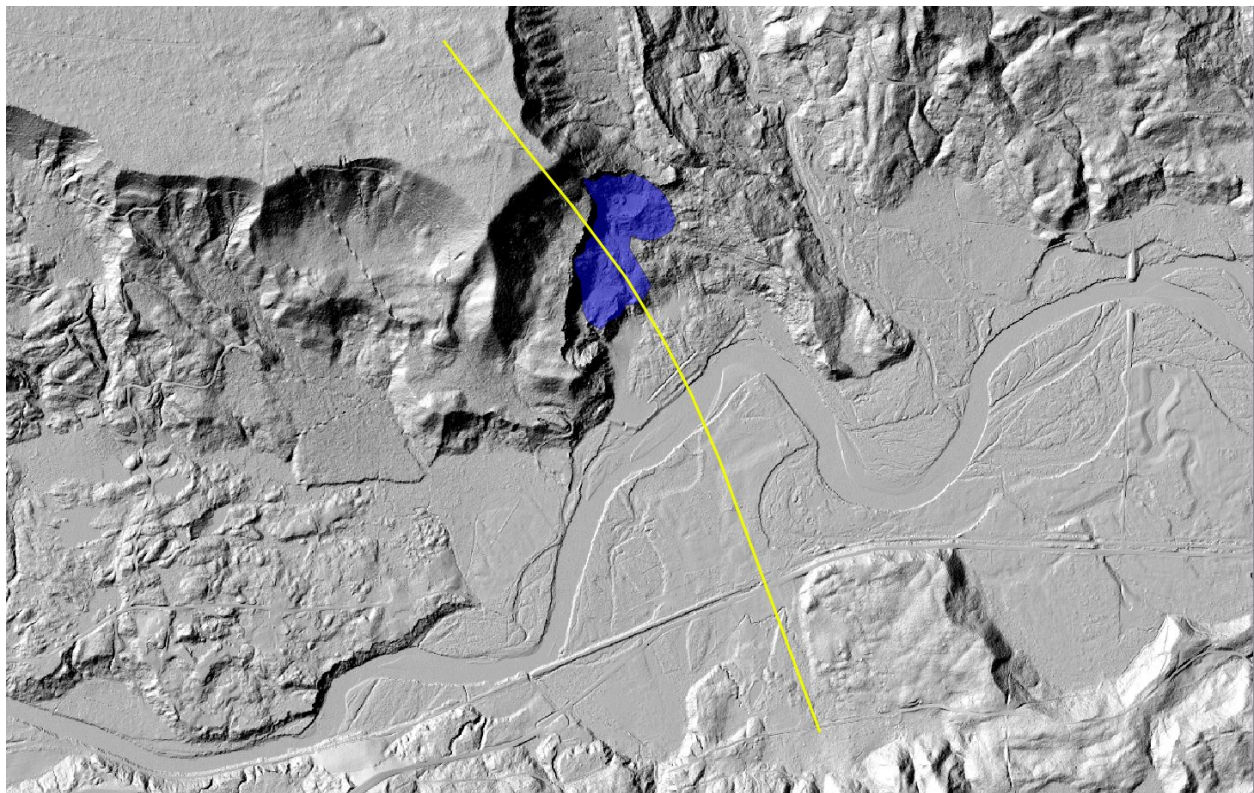
Approximate Extent of M-1 Movement During the SR-530 Slide Event.
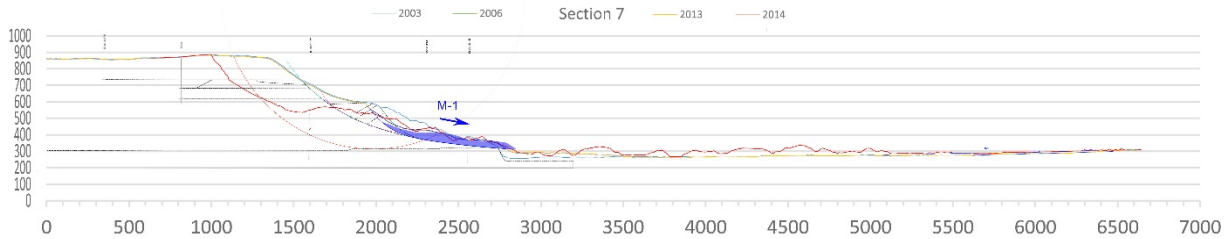
M-1 Movement on Lower Ancient P-2 Surface.

The second scenario only involves erosion of material from the toe of the SE facing Hazel scarp by Slide Creek. Significant deposition of alluvial material can be documented in the LiDAR between 2006 and 2013, both in the sedimentation pond and along the lower part of the course of Slide Creek, just upslope from there. This near-constant erosion may, in itself, have ultimately resulted in removal of sufficient lateral support at the toe of the mid-slope bench to initiate failure of a large portion of the remaining mid-slope bench blocks, along surface P-2.

Regardless of the actual scenario involved in initiation of the movement of large portions of the remainder of the mid-slope bench, this movement appears to have occurred largely on the steeper upper portion of the pre-existing ancient failure surface P-2. This movement (designated M-2 for purposes of this report) appears to have largely overridden the slide debris sitting in the 2006 Hazel slide source area above and below the BLS cliff. Evidence for this over-riding is the fact that none of the extensive alder brush covering the 2006 slide debris prior to the SR-530 Slide can be found at the appropriate locations of the deposit covering the valley floor post-2014. Therefore, it appears to have been ground up and incorporated into the slide deposit.
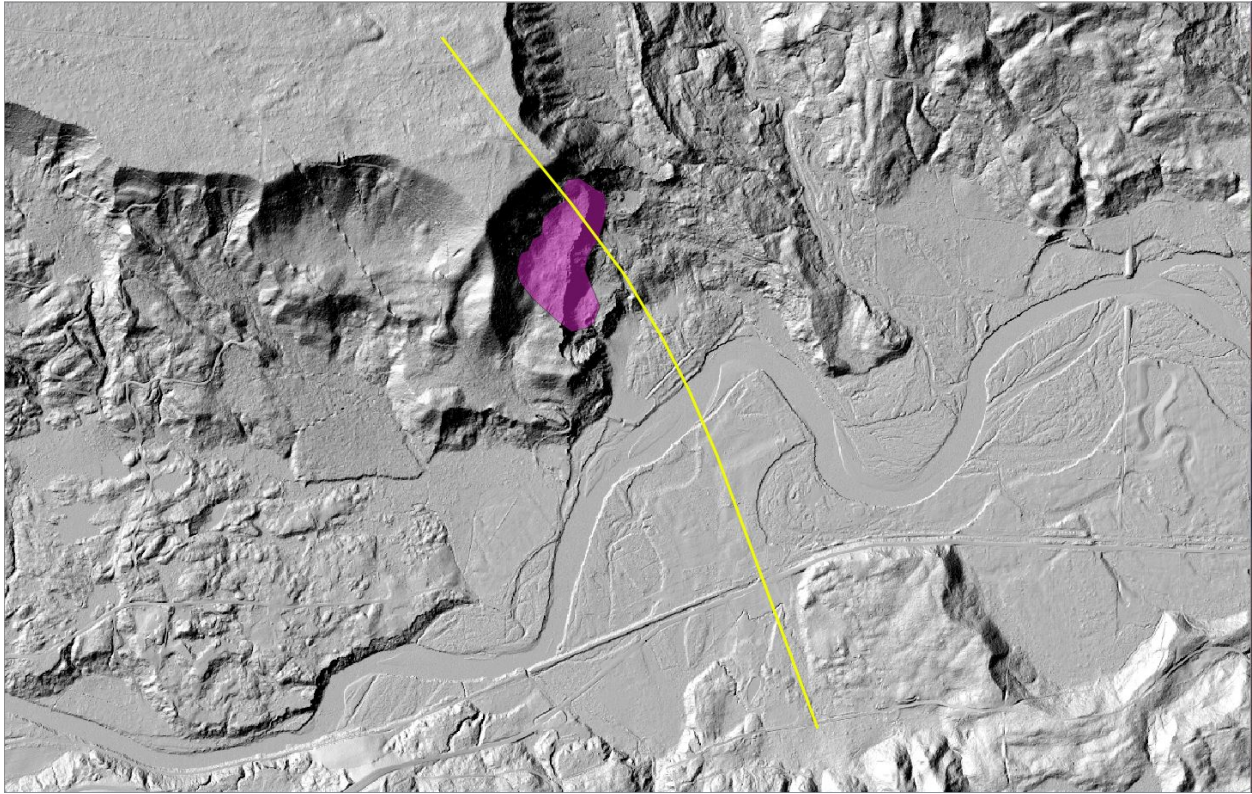
Approximate Extent of M-2 Movement, Involving the Central Portion of the Former Mid-slope Bench
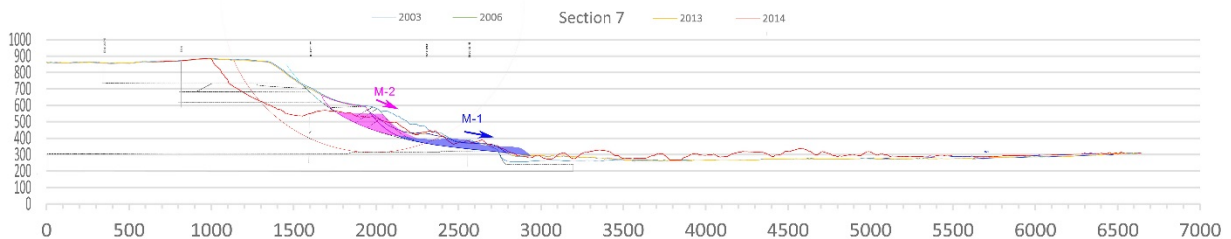
Initiation of M-2 Movement After Unloading of the Toe by M-1

Either scenario of initiation satisfies the requirement from the eyewitness accounts that a significant delay occurred between initiation of rapid, noisy movement of a relatively large soil mass covered with forest, and the time of arrival of that mass at the river, where it was observed by people looking from the west. Moreover, either scenario also satisfies the eyewitness accounts and physical requirements that the material be moving rapidly by the time it reached and crossed the river. This can only be achieved if the movement initiates higher on the slope and the mass has time and slope distance to accelerate from standstill to the "100 miles per hour," which may be a slight exaggeration, but indicates that it was moving rapidly by the time it came into Mr. Reed's field of view.

The Shunn/Patenaude account also corroborates John Reed's statements in that significant time passed between the initial, prolonged noise generated by the slide and the arrival of the slide in an area where it was visible to these eyewitnesses, and another time interval between the mass arriving at the river

and when the M-3 mass spilled over the western margin of the slide area to knock down trees at the top of the ridge. Mr. Shunn had to have time to wonder about the prolonged noise, look out the window and fail to see aircraft, then see the slide coming into view and alert Ms. Patenaude, who then had to run upstairs and arrive in time to see tall firs flattened by the spill-over of M-3 onto the west margin.

Based on both tree and forest floor distribution, pre- and post-SR-530 Slide, and the composition of the deposits covering the valley compared to those previously comprising the former mid-slope bench, it is this former mid-slope bench block that appears to have buried much of the central and southern portions of the Steelhead Haven neighborhood and significant portions of the area to the south of the highway (SR-530).

The initiation of rapid failure of the SR-530 Slide by acceleration of the former central portions of the mid-slope bench block is also consistent with the fact that an area of significant extent exists within the middle to lower portions of the later, larger M-3 slide mass, now forming the new mid-slope bench block and debris field north of the river, that has little or no forest floor cover or trees. The bare spot would have been produced by sliding on the M-2 surface in areas where this surface was sufficient steep to preclude deposition of the tail end of the sliding M-2 mass. Once the M-2 mass had slid sufficiently far to have reached the lower-sloping portions of the M-2 surface (identical, or nearly so to the P-2 surface), the sliding mass left a comet-trail-like veneer of Recessional Outwash over the lower part of the M-2 scarp, which was underlain by Till, Advance Outwash, and Fine-grained Glaciolacustrine material.

Movement of the M-2 mass instantaneously unloaded the toe of the Whitman Bench slope, resulting in rotational failure of the much larger M-3 mass. Given its comparatively large mass and elevation above the valley floor, this mass possessed significant potential energy, which, once moving, was converted to kinetic energy. Portions of this kinetic energy were imparted to the M-2 mass still moving on the slope below when it was struck from behind by the leading edge of the M-3 block. This ultimately resulted in propelling the combined M-2 mass and leading edge of the M-3 mass into the Steelhead Haven neighborhood, and flung the leading edge of the M-2 mass far beyond SR-530. It is also possible that the impact of the leading edge of M-3 on the backside of the moving M-2 block resulted in the acceleration of the M-2 mass when the leading portions of the M-2 block were already in view of John Reed, moving on the relatively flat portions of the valley floor in the vicinity of the river. This would be consistent with his report that the slide accelerated "when it hit the river."
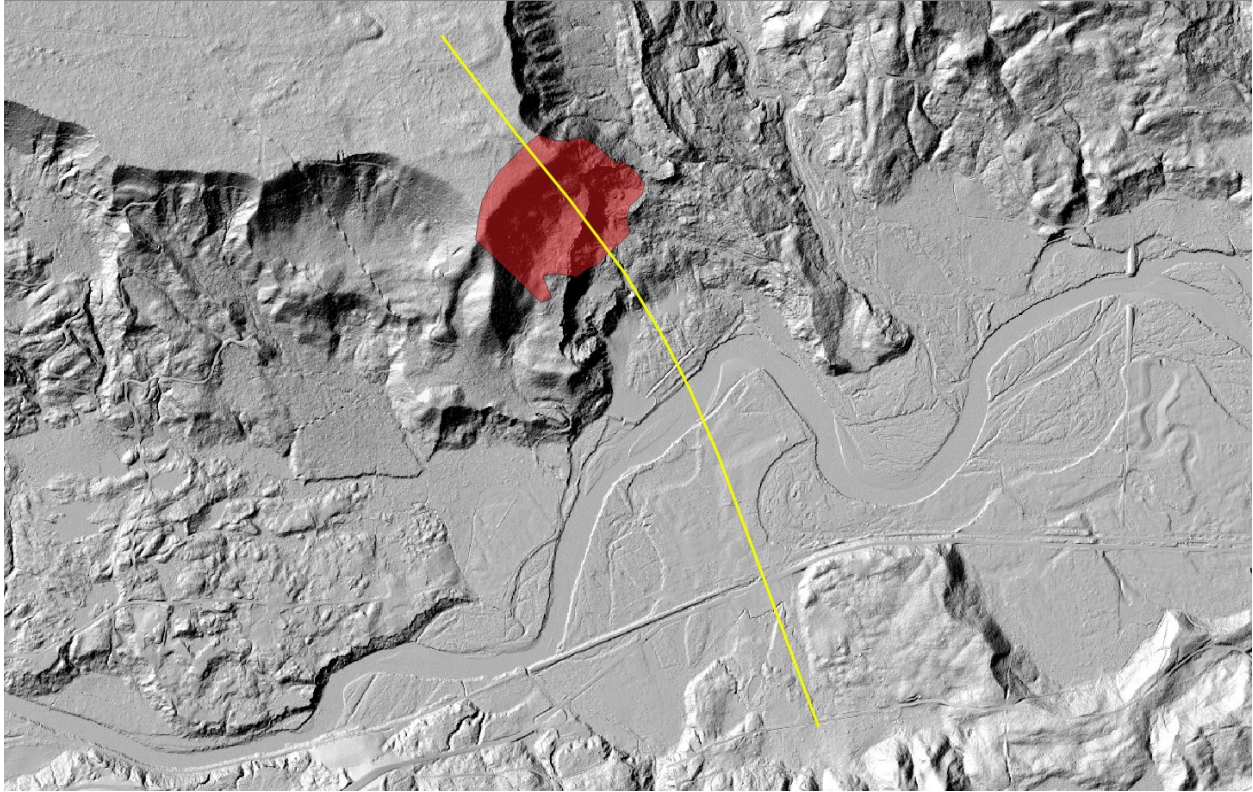
Approximate Extent of M-3 Movement
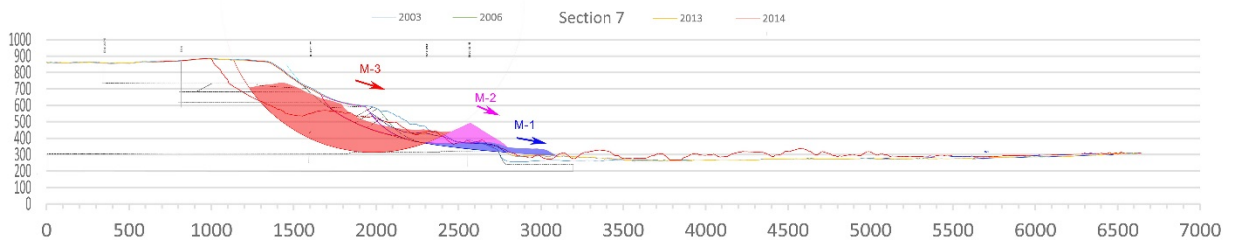
M-3 Movement Shortly After Initiation Along Section 7 (Yellow Line on Map).

APPENDIX G

Tree Displacement Mapping

Tree Evidence

GEER conducted an analysis of the post-slide distribution and orientation of tree trunks and larger tree trunk fragments in the SR-530 Landslide footprint. In general, the orientation of some of the larger concentrations of trees appears aligned with the inferred movement direction during the slide, with some notable exceptions in the central portion of the slide covering the former Steelhead Haven neighborhood.

In an effort to triangulate the post-failure location of different portions of the SR 530 Landslide source area, we evaluated tree species (whether conifer or deciduous), the completeness of the trees in the deposit (whole trunk from root ball to top, partial trunk only, broken-out tops) and length of these segments. In addition, coniferous trees located in the interior of a stand tend to have green branches only near the crowns, whereas those trees located along the margins of a stand tend to have green branches from nearly ground level to the top of the tree.

Tree Locations & Lengths

Identification of tree locations prior to and following the landslide was used as a technique to ascertain material movements associated with the SR 530 Landslide. The 2013 "All Return" (tile q48121c73hh) and "Bare Earth" (tile q48121c73be) Aerial LiDAR data sets were used to generate a map showing spatial distribution of tree height classes. Tree heights were calculated by subtracting (via QGIS) the "Bare Earth" LiDAR raster (Figure G-1) from the "All Return" LiDAR raster (Figure G-2). The tree heights were then classified and color coded into height ranges (Figure G-3, Figure G-4, Figure G-5).
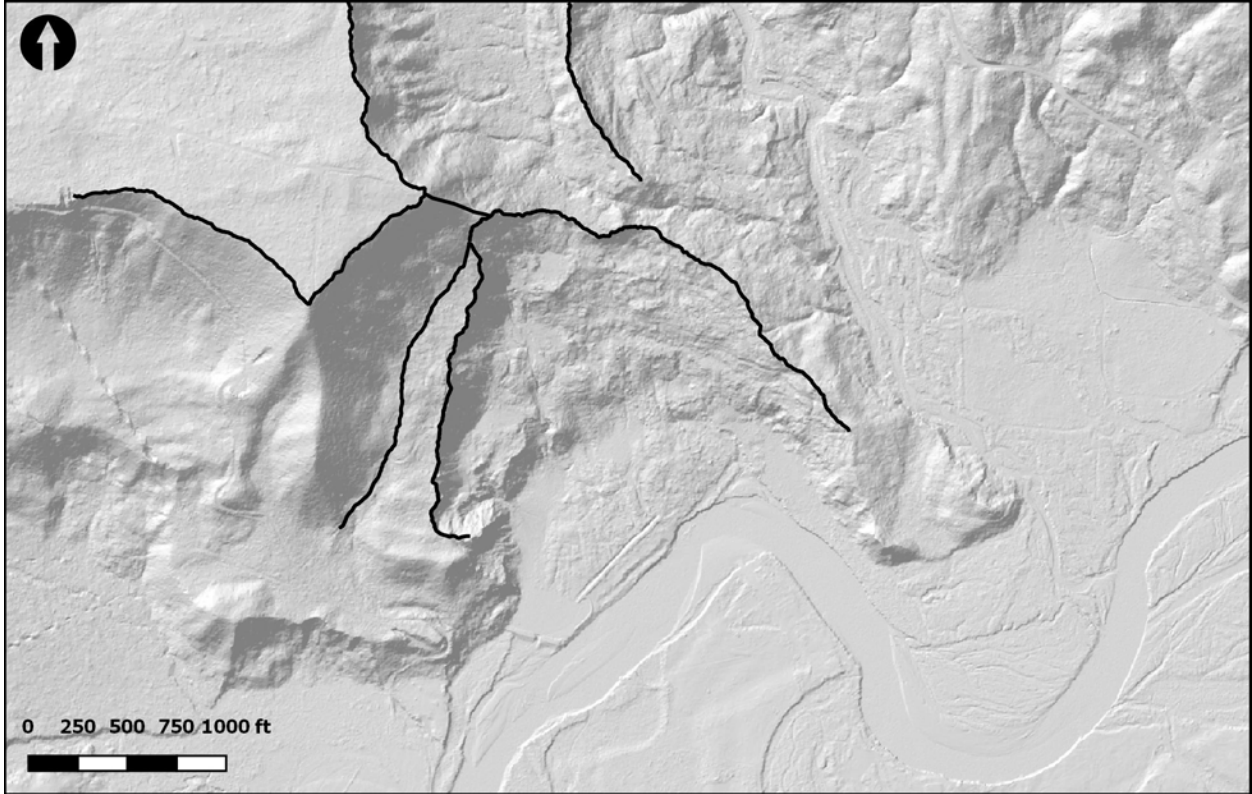
Figure G-1: Bare earth surface derived from filtered 2013 Aerial LiDAR.
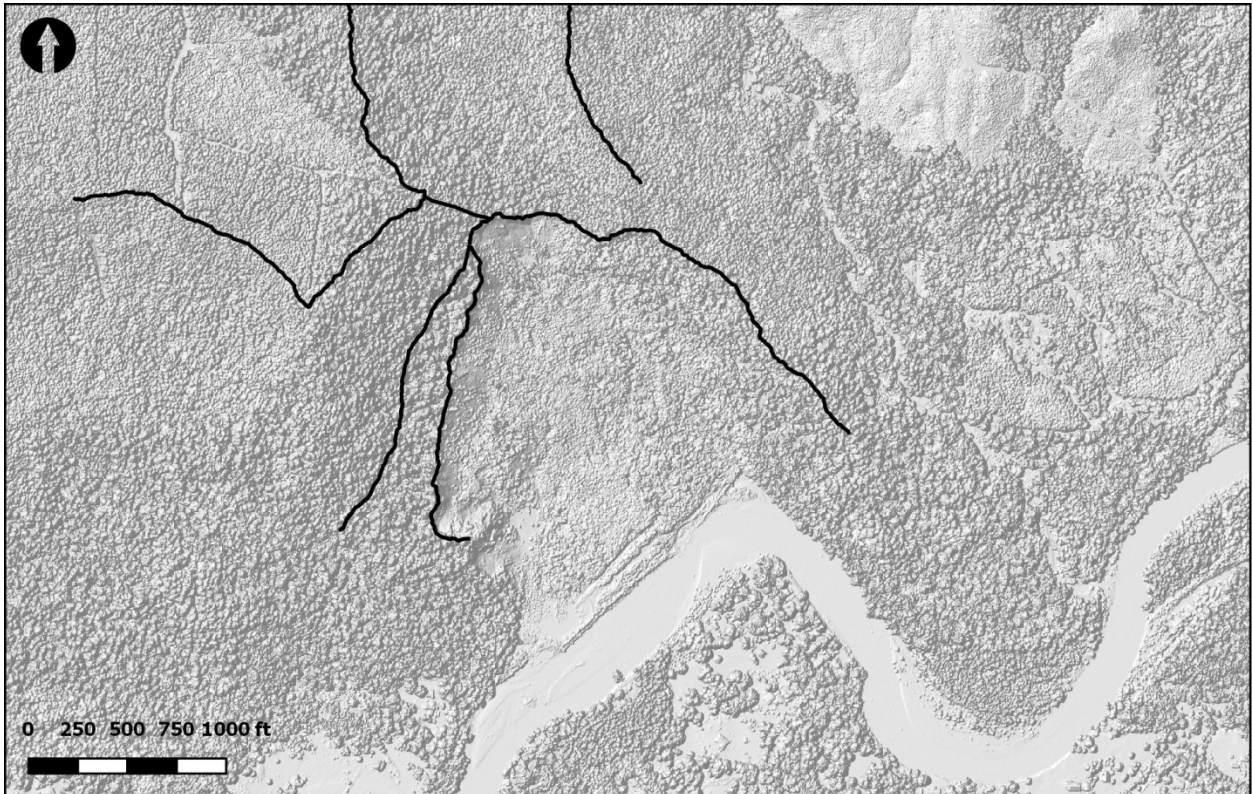
Figure G-2: 2013 Aerial LiDAR showing "All Returns" that map the top of trees at the time of the survey.
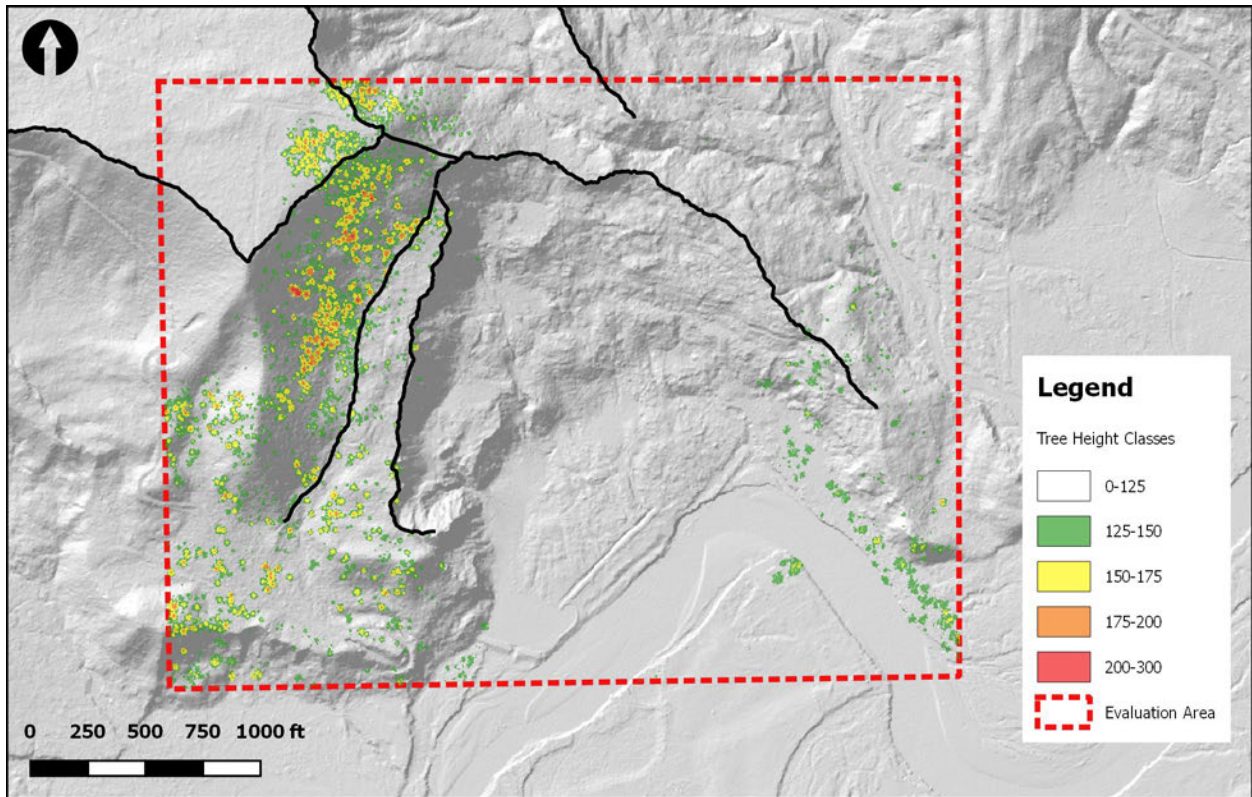
Figure G-3: Spatial distribution of trees (2013) in the evaluation area and associated height classes.
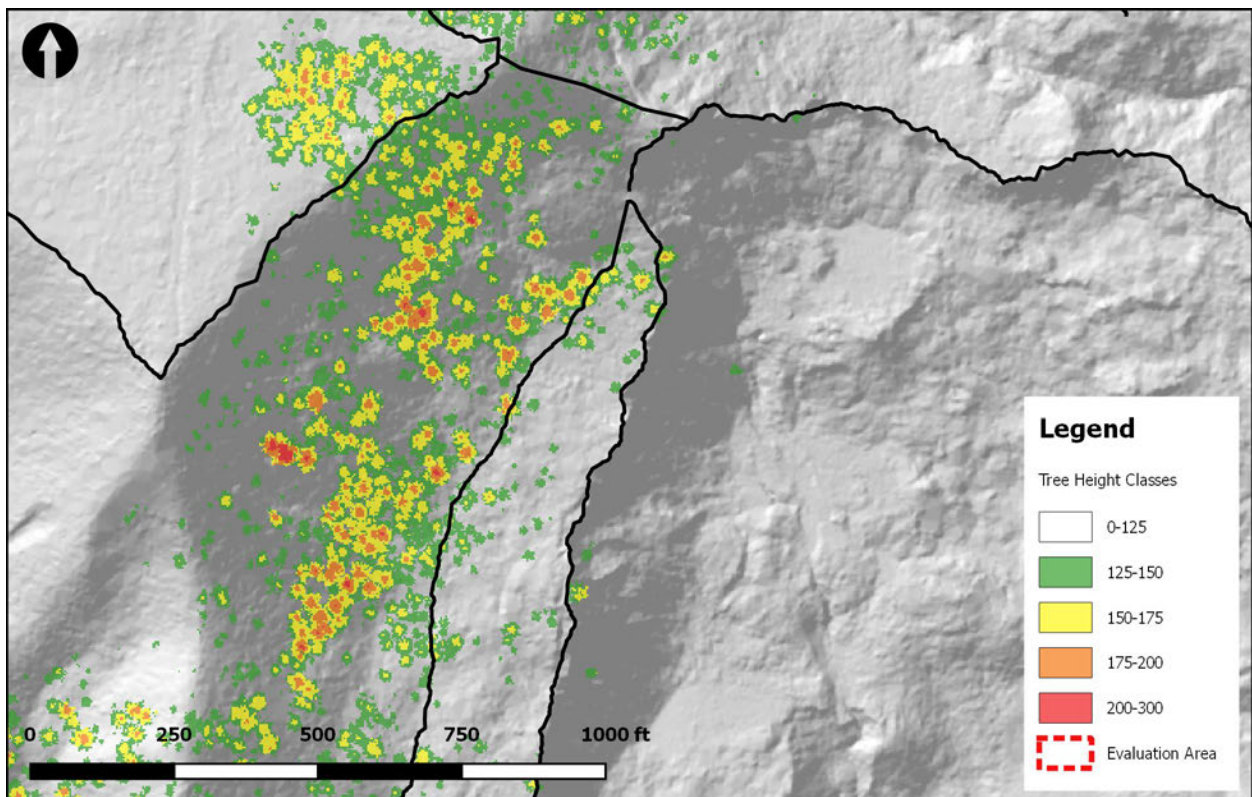
Figure G-4: Zoomed in view of the 2013 tree heights on the Whitman Bench Southeast slope.
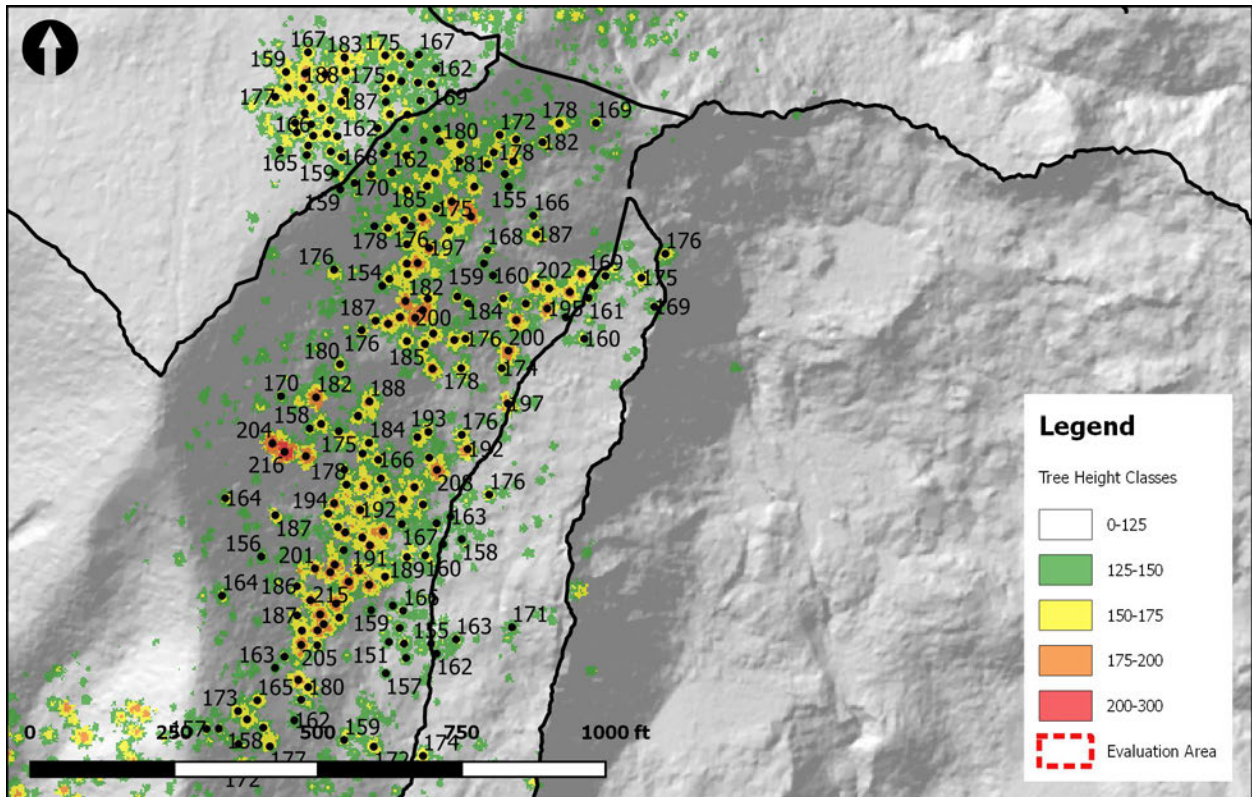
Figure G-5: Height values (feet) of the 2013 tree stand.
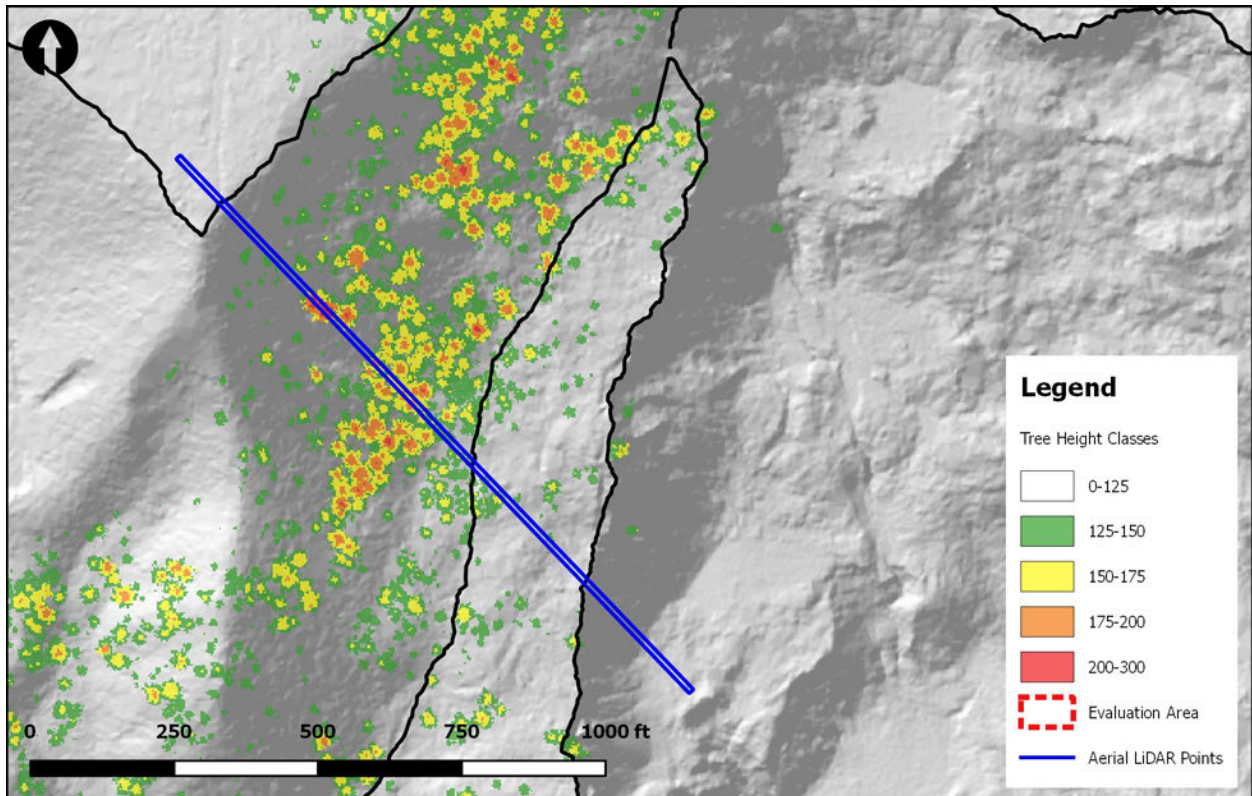
Figure G-6: Blue box indicates location of unfiltered LiDAR points shown in Figure G-7.
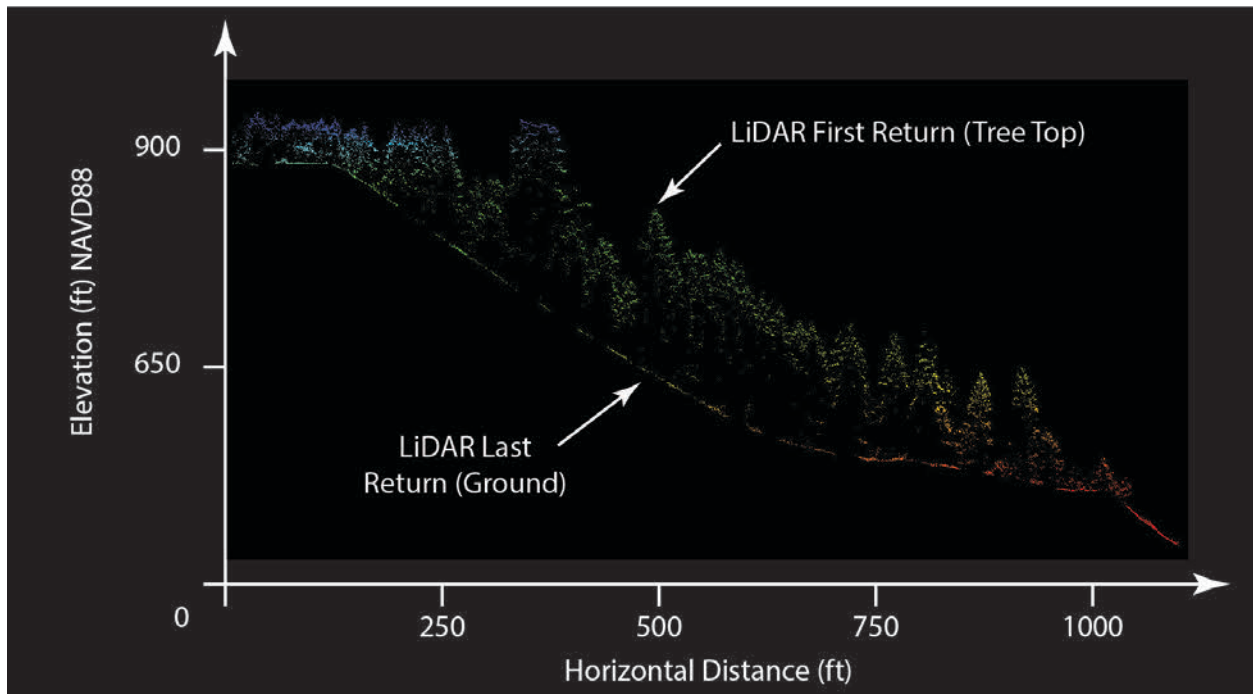
Figure G-7: Cross-sectional view of unfiltered Aerial LiDAR points within blue box show in Figure G-6.

To illustrate the data available via the Aerial LiDAR point cloud, a region of points was selected across the southeast slope of Whitman Bench (blue box, Figure G-6). A cross sectional view of these is shown in Figure G-7. The laser beam from the Aerial LiDAR generates multiple returns as portions of the laser beam bounce off segments of physical features below the laser emitter. The 'first' returns capture the tops of the trees and the 'last' returns. By subtracting the elevation of the top of the tree with the ground surface elevation, the overall height of the tree can be calculated.

Both Aerial LiDAR and ground-based LiDAR were used to map the post-slide locations of trees). Our team was not afforded access to the slide debris within the Steelhead Haven neighborhood, so we the Aerial LiDAR data was especially helpful in mapping locations and lengths of trees deposited in this area (Figure G-8).
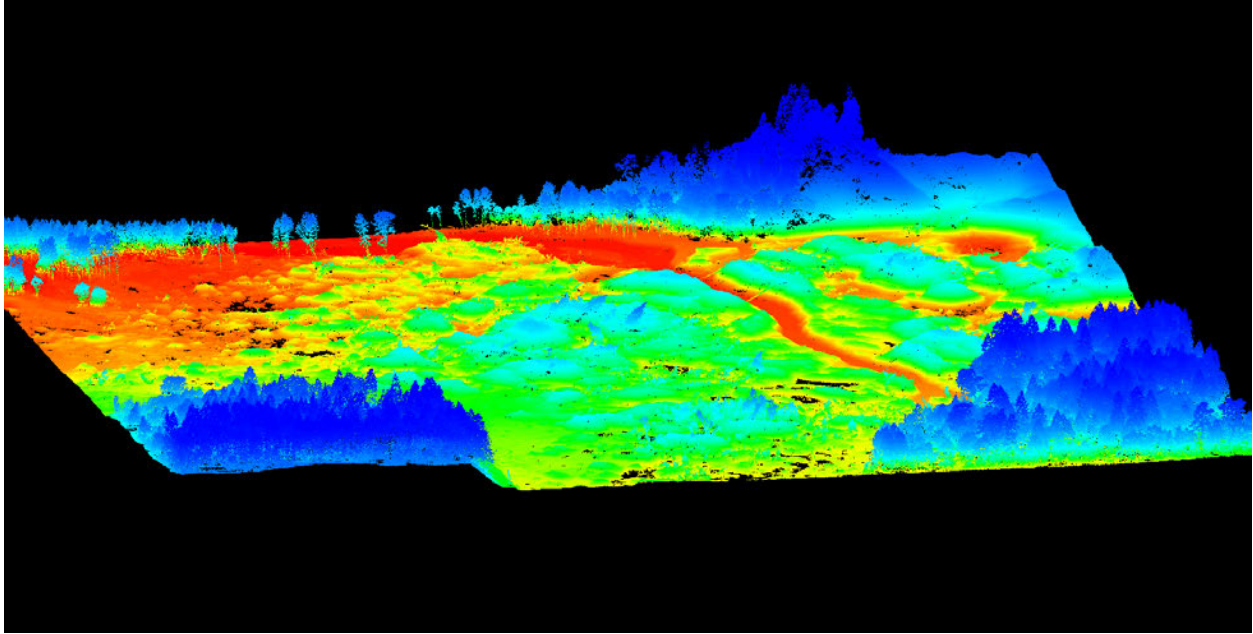
Figure G-8: Aerial oblique view of March 2014 Aerial LiDAR point cloud in Steelhead Haven neighborhood.

Utilization of LiDAR points were advantageous over aerial imagery due to the inclination of the trees, which makes it difficult to measure the 3D length of the tree on a 2D image. Figure G-9 shows a perspective view of the ground-based LiDAR. Because the point cloud is 3D, it enables lines to be drawn along the tree trunk, while obtaining the full representative 3D tree length.
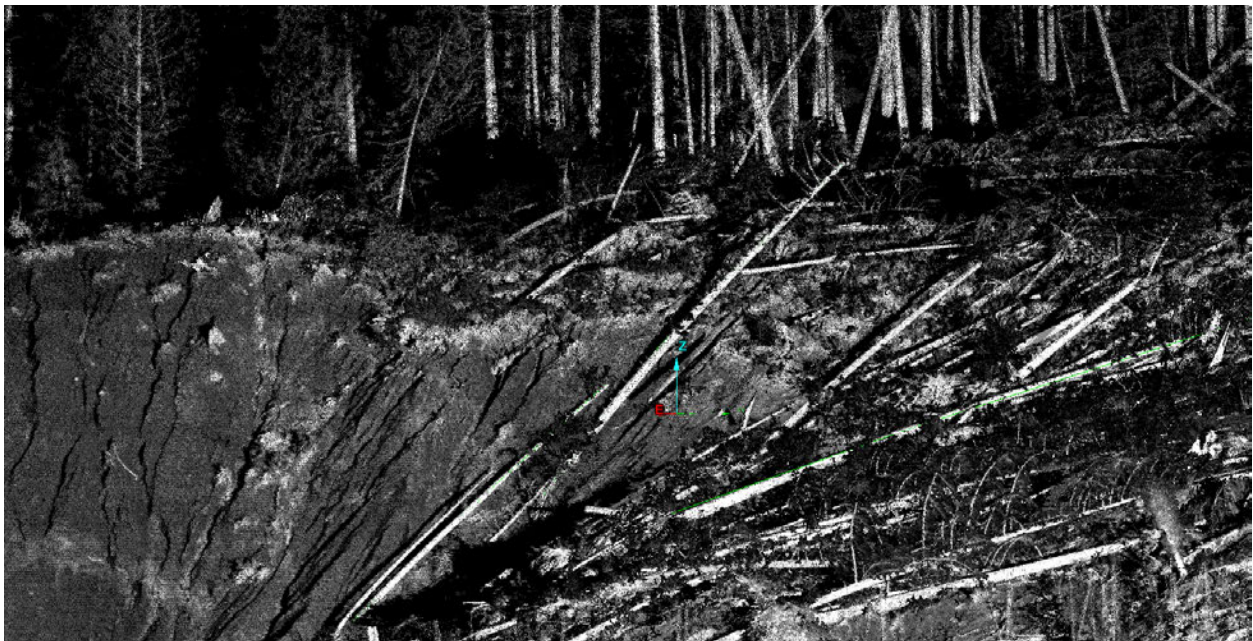
Figure G-9: Grayscale image of high-resolution ground-based LiDAR allowing for spatial mapping of tree locations and 3D lengths.
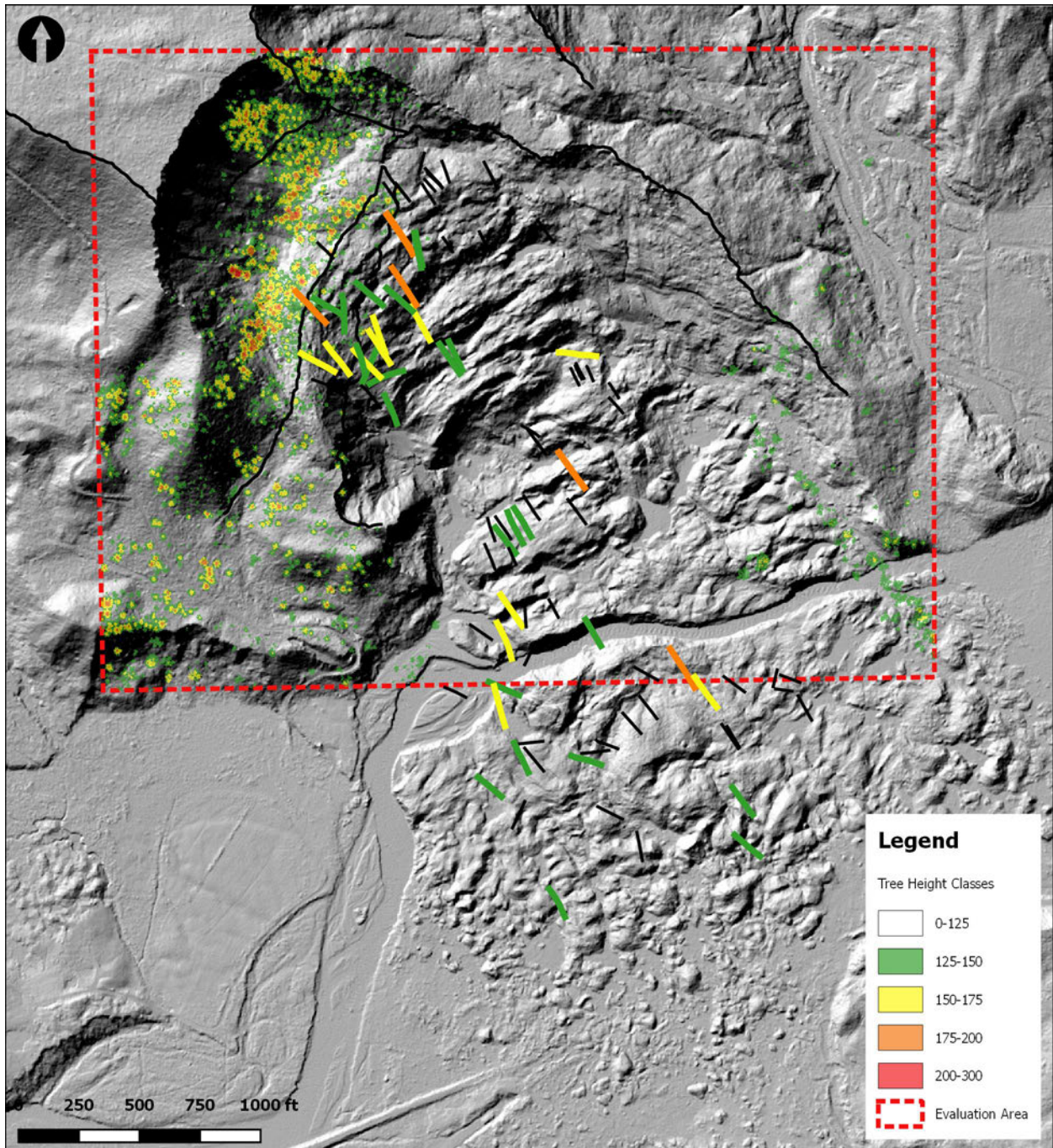
Figure G-10: Example distribution of mapped tree lengths, color coded by tree height/length as observed post-slide by reviewing the available LiDAR data.

Not all trees were mapped. Effort was focused on the longer length trees (>150 feet in length) as there were only a few locations where these tall trees existed just prior to the SR 530 Landslide. Some trees had obscured bases and/or tops. Some trees were broken.

Alder Mapping

Also mapped on an ortho-rectified photo from 2012 (provided by Snohomish County) were mature alders in the portion of Whitman Bench affected by the March 22, 2014 SR 530 Landslide. Alders were distinguished on the photo from conifers by their different branch distribution and foliage. The alder brush which had grown up on the 2006 Hazel Landslide footprint was not mapped in the pre-failure photos. No evidence of this brush was noted anywhere on the post-SR 530 Landslide high-resolution aerial photos.

The trees found on post-slide high-resolution aerial photos were classified and color-coded in QGIS according to the following criteria:

- Fully limbed (green) conifers   (57 found)
- Whole conifers (with bare trunks below green crowns)   (236 found)
- Conifer Trunks (with or without root-balls, but lacking tops)   (1,094 found)
- Conifer Tops (lacking root balls)   (159 found)
- Alders (deciduous trees)   (61 found)

Smaller, fully limbed conifers were found exclusively along the outer edge of scattered remnants of intact forest floor on the material with coloration of recessional outwash occupying the southwest, south-central, and eastern portions of the former Steelhead Haven neighborhood.

On the former mid-slope bench, a total of 13 alders, including at least one very large tree or two or even three individual trees were found on the pre-failure 2012 aerial photo. Post-failure, 15 alder trunk segments were mapped in the area south of the post-failure river channel.

Numerous large conifers are found between the area containing the fully limbed trees and the gray deposit immediately south of the post-failure river alignment which apparently overriding the block covered with less extended forest floor. The overwhelming majority of large trees south of the gray deposit consists of conifer trunks with broken-out tops. Especially in the western portion of this concentration of larger fir trees, the trunks are arranged more or less parallel or sub-parallel to the lobate margin of the gray deposit. Several large-diameter trunks were observed that had been completely shattered and broken into several shorter segments.

A similar concentration of broken-top trees is found along the lower edge of the collapsed till section of the main scarp which covers the northeastern portion of the new mid-slope bench block. Downslope from there, many of the trees covering the outer slope of the mid-slope bench block are either whole conifers, or, along the bottom portion of this block, very long sections of large trees without apparent root-balls. It is possible that some of these trees do indeed have their root balls still attached, but that these are buried in debris from secondary failures along the downslope edge of the block. Effective tree mapping off air photos is essentially impossible in the westernmost part of the mid-slope bench block mainly because the trees are so crowded in this area that they overlap, sometimes several tree trunks deep, with the lower tiers covered by the upper layer of firs.

Another concentration of broken-top conifers is present in the deposits along the toe of the western side scarp in the lower half of the failure area north of the current river location.

Also of interest in the distribution of trees and associated former forest floor sections is the fact that there are very few trees in the area surrounding and directly downslope from EB-07SI-15, EB-09SI-15, and H-12SI-15. Scattered trees and forest floor patches are more prevalent again in the more gently sloping (general topography) sections of the 2014 deposit located within approximately 800 feet of the north bank of the river as shown on the 3/24/2014 air photo.

An attempt was made using the LiDAR point clouds from 2013 (pre-SR 530 Landslide) and 2014 (post-failure, both airborne and terrestrial LiDAR) to correlate some of the tallest trees (200+ feet) formerly located above the mid-slope bench to long tree trunks in the post-failure distribution of trees. However, no trees longer than 200 feet could be located in the slide debris, presumably because these trees were broken during the movement. As a result, using only the height/length of trees as a means of determining where portions of the pre-failure slope ended up post-SR 530 Landslide was deemed not representative.

Interpretation of Tree Evidence

The evaluation of available tree evidence provide insight into the movement of the SR 530 Landslide:

1. All 57 identified fully limbed green conifers found in the slope movement deposit are located in a wide band along the outer edge of the extremely extended forest floor on the material now located south of the river. Whereas according to Tart photo IMG_0315 there are a few such trees (possibly 15 to 20) in two groups on failure blocks at the base of the former mid-slope bench, the overall number of such trees in the deposit requires that the trees along the outer upper edge of the former mid-slope have been moved to the area south of the river, with the shortest transport distance around 1,230 feet and the longest approximately 3,360 feet to the south side of the highway in the western portion of the run-out.

2. The number of mature conifers or significant conifer segments identified on the SR 530 Landslide deposits south of the post-failure river alignment is 693. This consists of 75 whole mature conifers, 497 large trunk/root-ball combinations, 64 fir tops without root-balls and 57 fully limbed green trees. Because significant numbers of mature conifers were not located within the confines of the Hazel Landslide movement of 2006, the large number of mature fir trees deposited requires that the deposits on the Steelhead Haven community consist to a large degree of the top of the former mid-slope bench and a portion of the side slope of Whitman Bench above the former mid-slope bench.

3. Large numbers of broken conifer trunks are concentrated in concentric bands around the grey deposit located partially on the treed slope movement blocks immediately south of the river. This infers that the grey material likely "rode up" on the treed blocks a significant distance (up to 350 feet or more), sweeping trees up and ahead of it. In turn, this implies some velocity differential between the two soil masses, with the grey material moving significantly faster than the treed blocks.

4. The number of large alder trunk segments found in the area south of the river (15) corresponds relatively well with the number of mature alder trees mapped on the former mid-slope bench on pre-SR 530 Landslide aerial photos (13). This is another indication that the entire portion of the former mid-slope bench which was involved in the SR 530 Landslide came to rest on the

south side of the post-failure river. Significant portions of this block crossed the highway in the western portion of the run-out (see #1, above).

5. The fact that the dense alder brush present over the entire footprint of the 2006 Hazel Landslide deposit by 2012 is nowhere to be found on aerial photos after the March 22, 2014 event implies that the brush may been over-ridden by slide blocks from above the Hazel slide deposit.

Legend
— Alders [61]
— Whole Conifers [237]
— Fir Tops [159]
— Conifer Trunks [1096]
— Fully Green Conifers [57]

0   750   1500   2250 ft
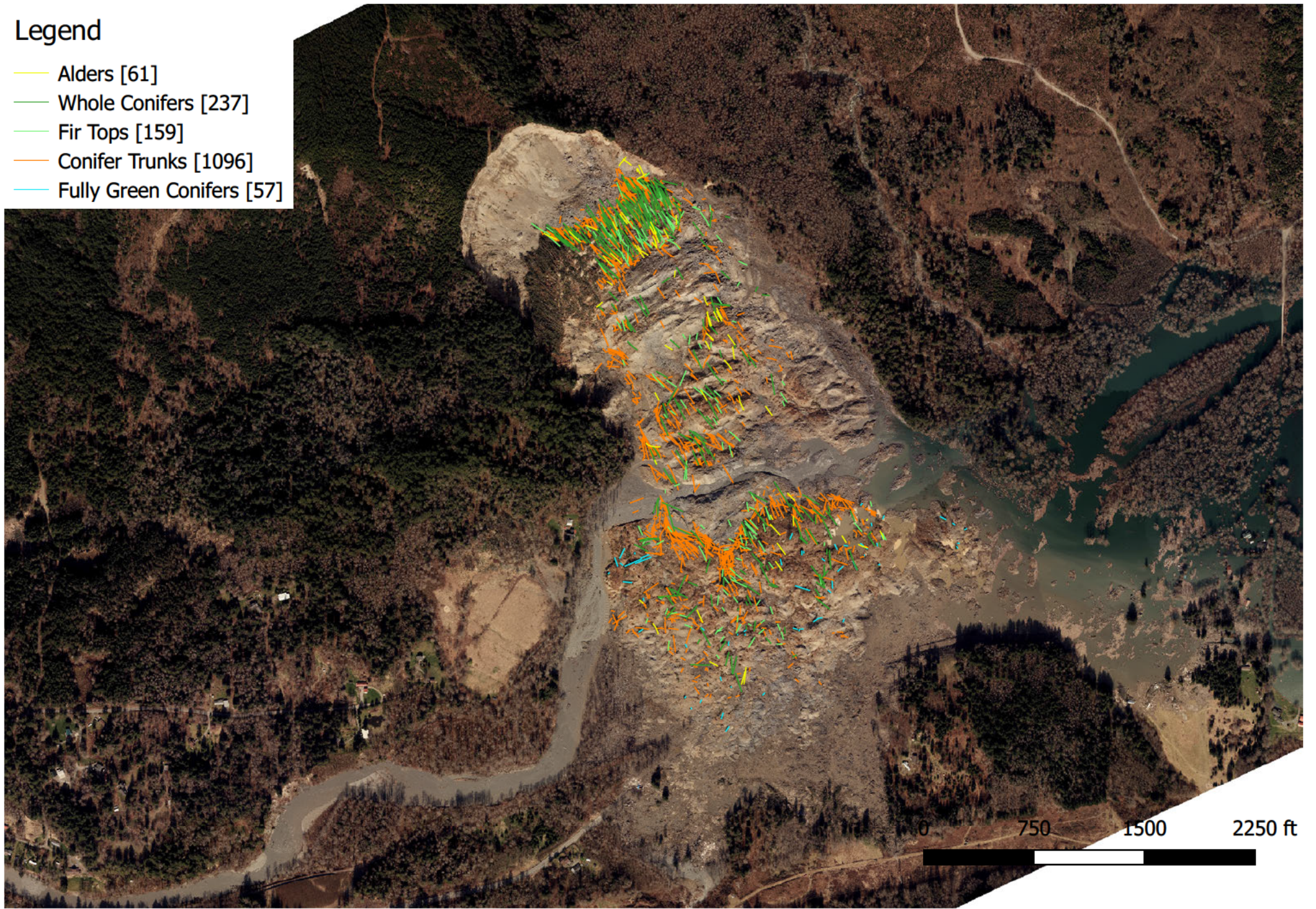
APPENDIX H

Avulsion Analyses

River Avulsion/Erosion Rates for Slide Debris

We employed two different methods to determine rates of river erosion. The first method involved using historic aerial photos (including the aerial photos provided as evidence by Mr. McShane), and, in Adobe Photoshop scaling all the air photos the same by overlaying subsequent air photo years digitally, with the younger of the pair partially transparent. The north bank of the river was then marked in the older of a pair of air photos, along with the alignment of both SR-530 and the BNSF/Whitehorse Trail route. The three lines were then transferred to the younger of the air photos and the maximum distance of channel migration was measured, along with the length of the channel segment affected by erosion of the north bank and the approximate location relative to the Hazel/SR-530 slide. The results are shown in the following table (negative numbers indicate deposition, positive numbers erosion along the north bank):

Interval	Max Dista	Length	Location	Years	Avg Annu	Material		
1933-1947	241	660	Center	14	17	In-place?		
1947-1955	162	840	NE	8	20	In-place?		
1955-1956	-94	925	NW-Cente	1	-94	Debris		
1956-1965	361	1519	NW Cente	9	40	Debris/In-place		
1965-1969	-784	1625	All	1	-784	Debris		
1969-1971	14	594	Center	2	7	Debris		
1971-1974	90	623	Center	3	30	Debris		
1974-1976	222	1209	All	2	111	Debris		
1976-1978	64	1498	All	2	32	Debris		
1978-1980	91	1813	All	2	45	Debris		
1980-1983	157	1538	All	3	52	Debris		
1983-1984	22	853	NW-Cente	1	22	Debris		
1984-1987	102	1864	All	3	34	Debris		
1987-1989	70	478	NE	2	35	Debris		
1989-1991	143	806	NE-Cente	2	71	Debris		
1991-1993	127	1325	All	2	63	Debris		
1993-1996	138	1393	NW-Cente	3	46	In-place?		
1996-1998	154	790	NW	2	77	In-place?		
1998-2002	215	1066	NW	4	53	In-place?		
2002-2005	-180	1128	NW	3	-60	Debris		
2005-2006	-685	2201	All	1	-685	Debris		
					44.41	Average of Net Removal Years		
2006-2007	234	1875	NW-Cente	1	234	In-place?		

As shown, for those years during which net erosion occurred anywhere along the right (north or east) bank of the river (looking downstream), the average maximum (!) rate of relocation of the bank was 44 feet per year.

However, given that this involves distances only, and does not necessarily reflect the area of slide debris remaining near river level after the slide events, another, more accurate method was employed:

Aerial photos provided by Mr. McShane were geo-rectified in QGIS. The younger of each set of air photo years was then made partially transparent, and the areas of either deposition or erosion (or both, when appropriate) along the north (right) bank between two air photos were mapped as polygons. The s area of each polygon is then calculated.

The table on the following page shows areas of deposition, as a result of either Hazel Landslide activity or river aggradation, or erosion. Shape files for all the polygons measured are included with the QGIS project which also contains all the air photos.

Begin Inte	End Interv	Depositio	Removal	Net Value	Avg Net R	% Remove	% Remaining
1947	1953	493101		493101			100
1953	1954		241071	-241071	241071	48.89	51.11
1954	1955		84053	-84053	84053	17.05	34.07
1955	1965		102489	-102489	10249	20.78	13.28
1965	1968	912424		912424			100
1968	1970		75955	-75955	37978	8.32	91.68
1970	1974	40016	24157	15859	-3965	-1.74	93.41
1974	1976	83638	181186	-97548	48774	10.69	82.72
1976	1985		344001	-344001	38222	37.70	45.02
1985	1989		88952	-88952	22238	9.75	35.27
1989	1991	86506	30144	56362	-28181	-6.18	41.45
1991	1995	9231	264100	-254869	63717	27.93	13.52
1995	2003		86282	-86282	10785	9.46	4.06
2003	2006	736441		736441			100

As is apparent from the table, after the 1951/52 Hazel Landslide activity, 13.28 of the debris deposited then remained in place in 1965, or at least 13 years following the slide event. The 1967 slide debris was almost completely removed in 2003, or 36 years following the event. Several smaller episodes of sliding had placed more material into the river, with the largest such event between 1989 and 1991. Even nine

years after the 1967 event (1976), 82.72% of the area covered by slide debris from 1967 remained in place.
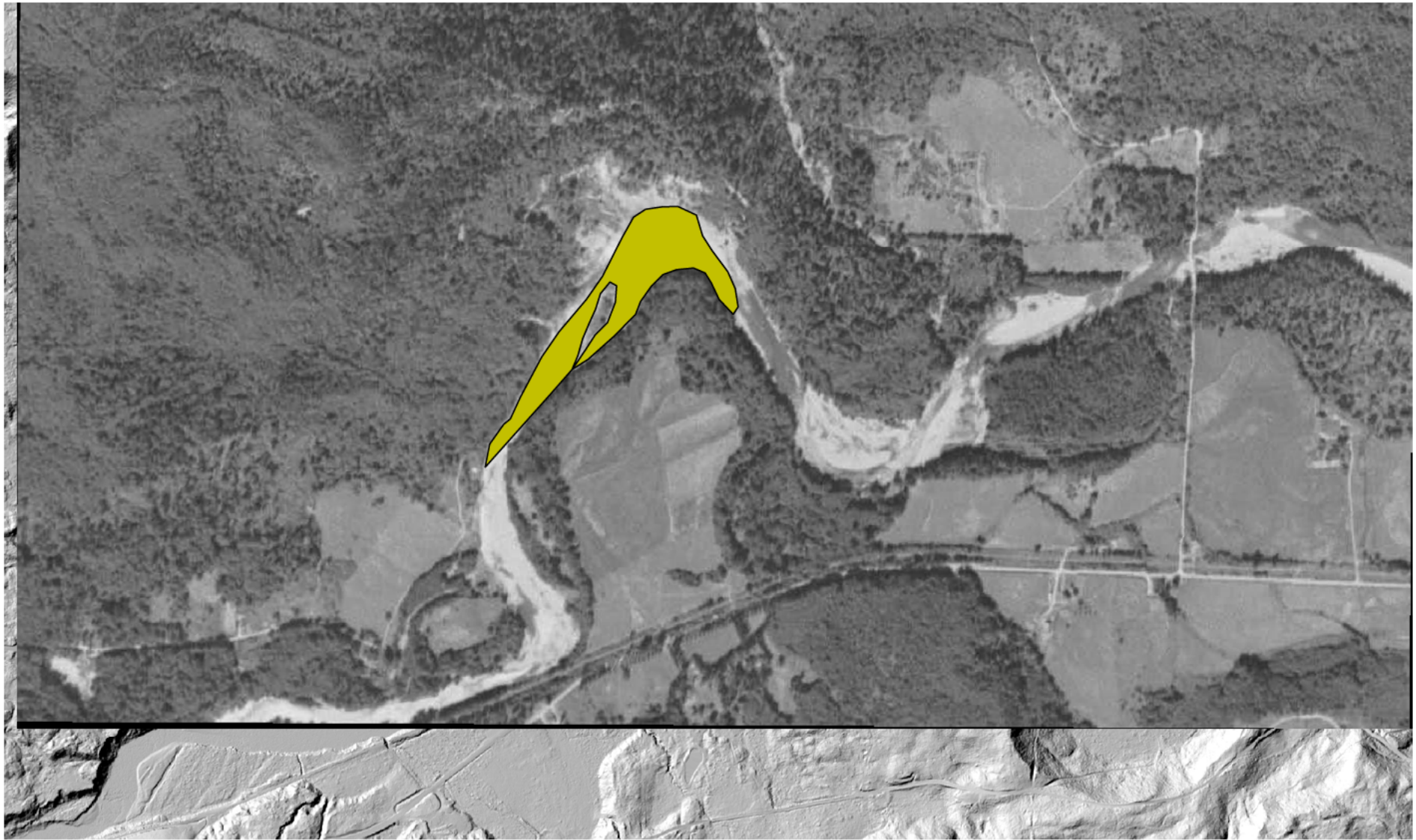
1947 to 1953 Deposition
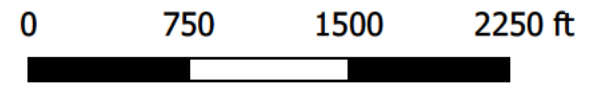
0   750   1500   2250 ft

1954 to 1955 Erosion

| 0 | 750 | 1500 | 2250 ft |
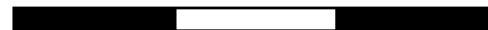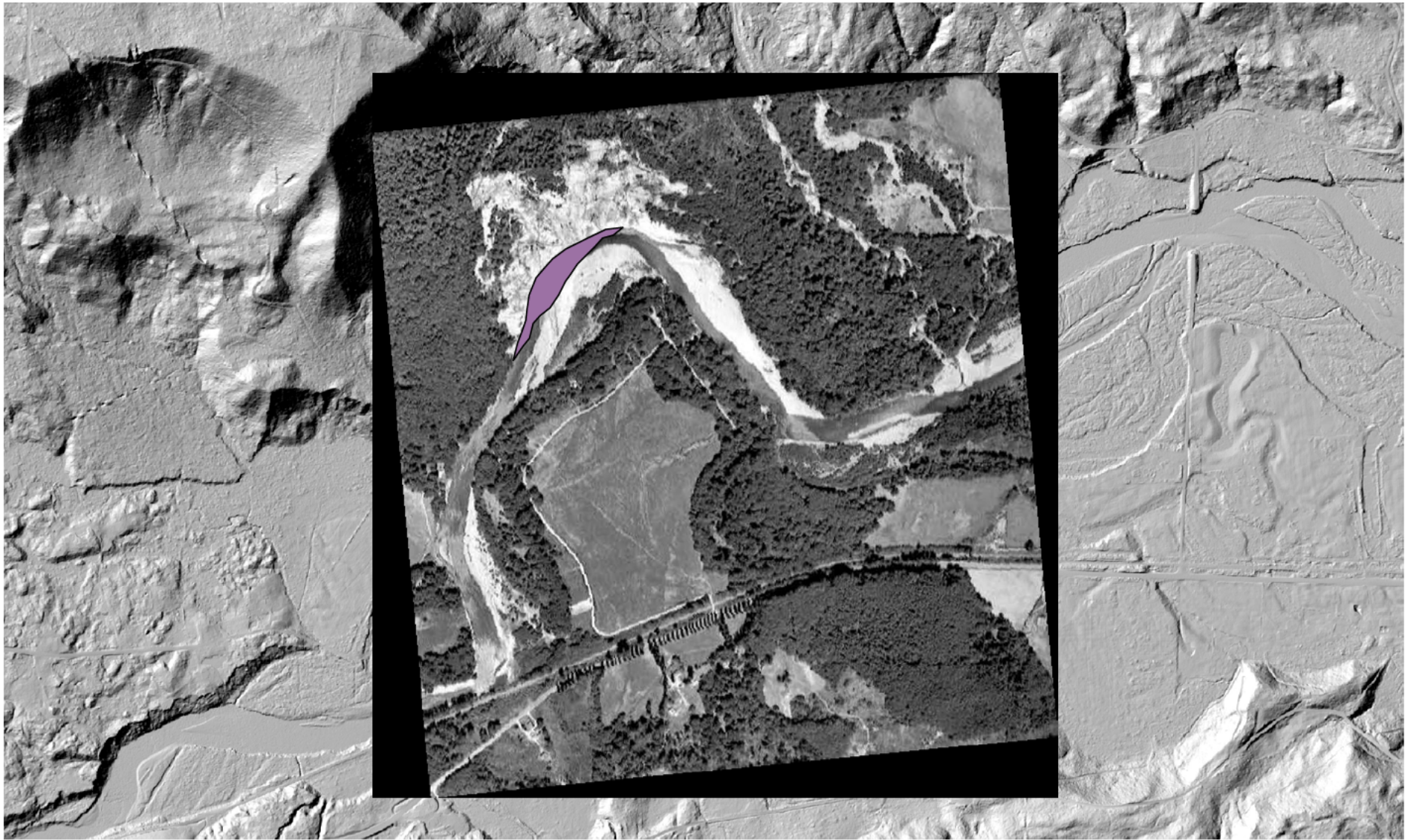
1955 to 1965 Erosion
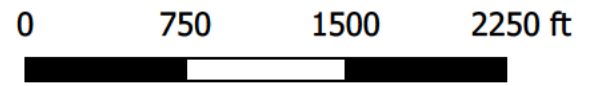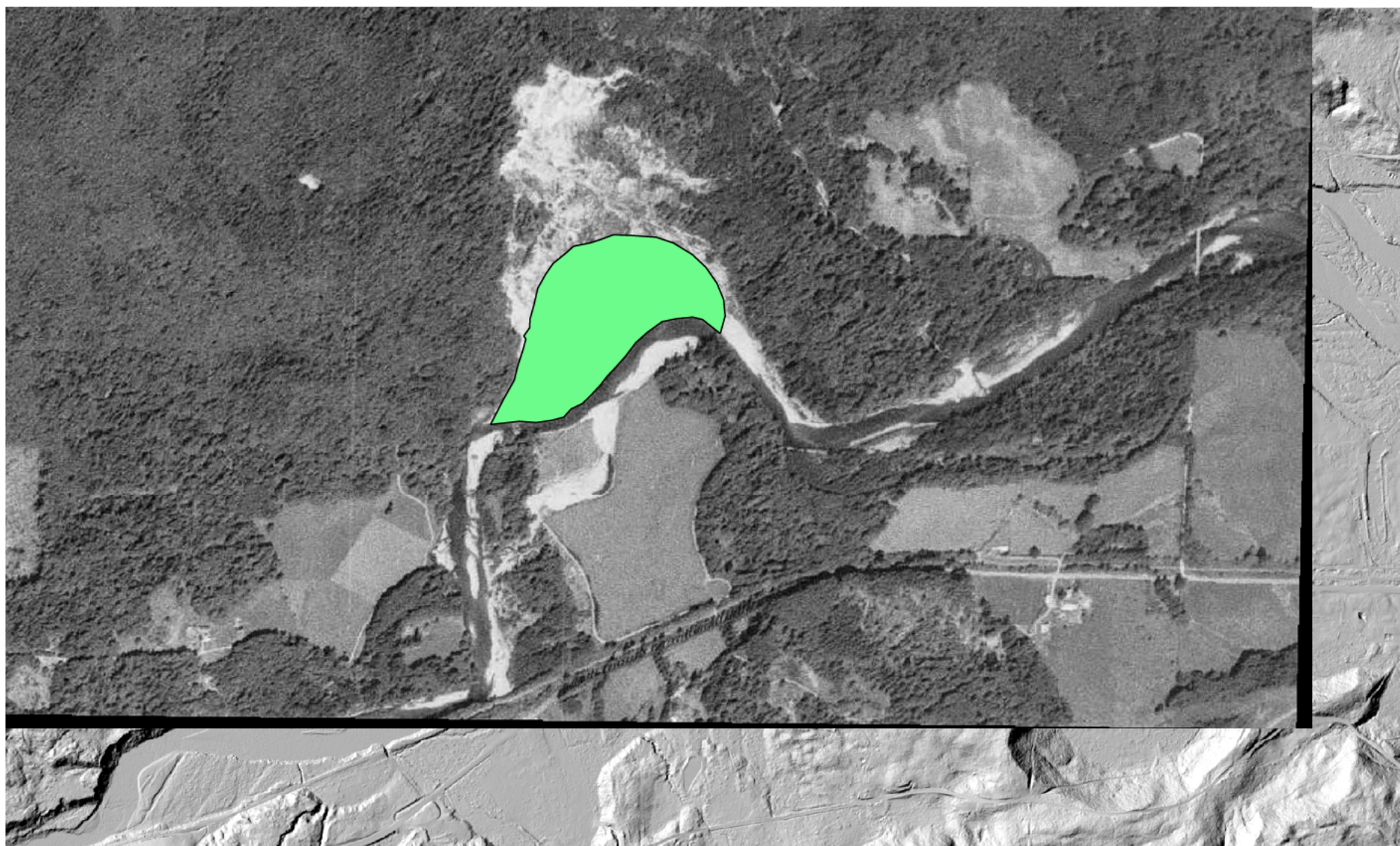
0   750   1500   2250 ft

1965 to 1968 Deposition
(1967 Slide)
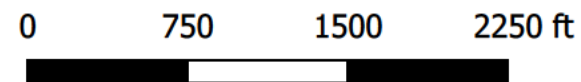
| 0 | 750 | 1500 | 2250 ft |

1968 to 1970 Erosion
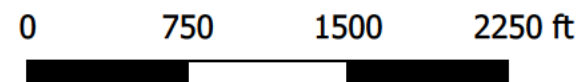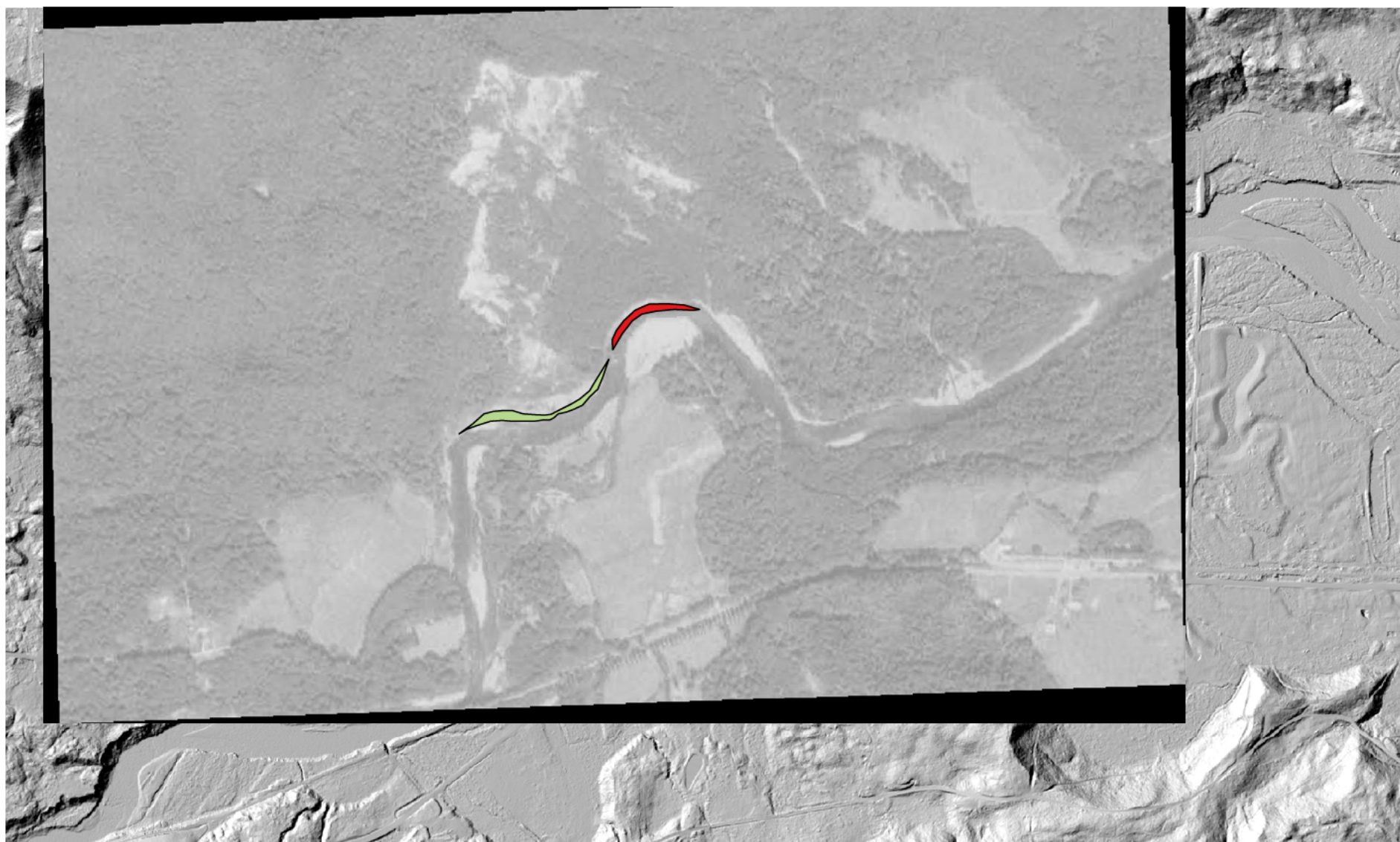
| 0 | 750 | 1500 | 2250 ft |

1970 to 1974 Erosion (Red) and Deposition (Green)
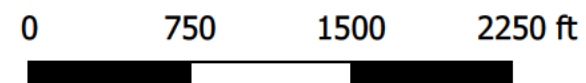
0   750   1500   2250 ft

1974 to 1976 Erosion (Red) and Deposition (Green)
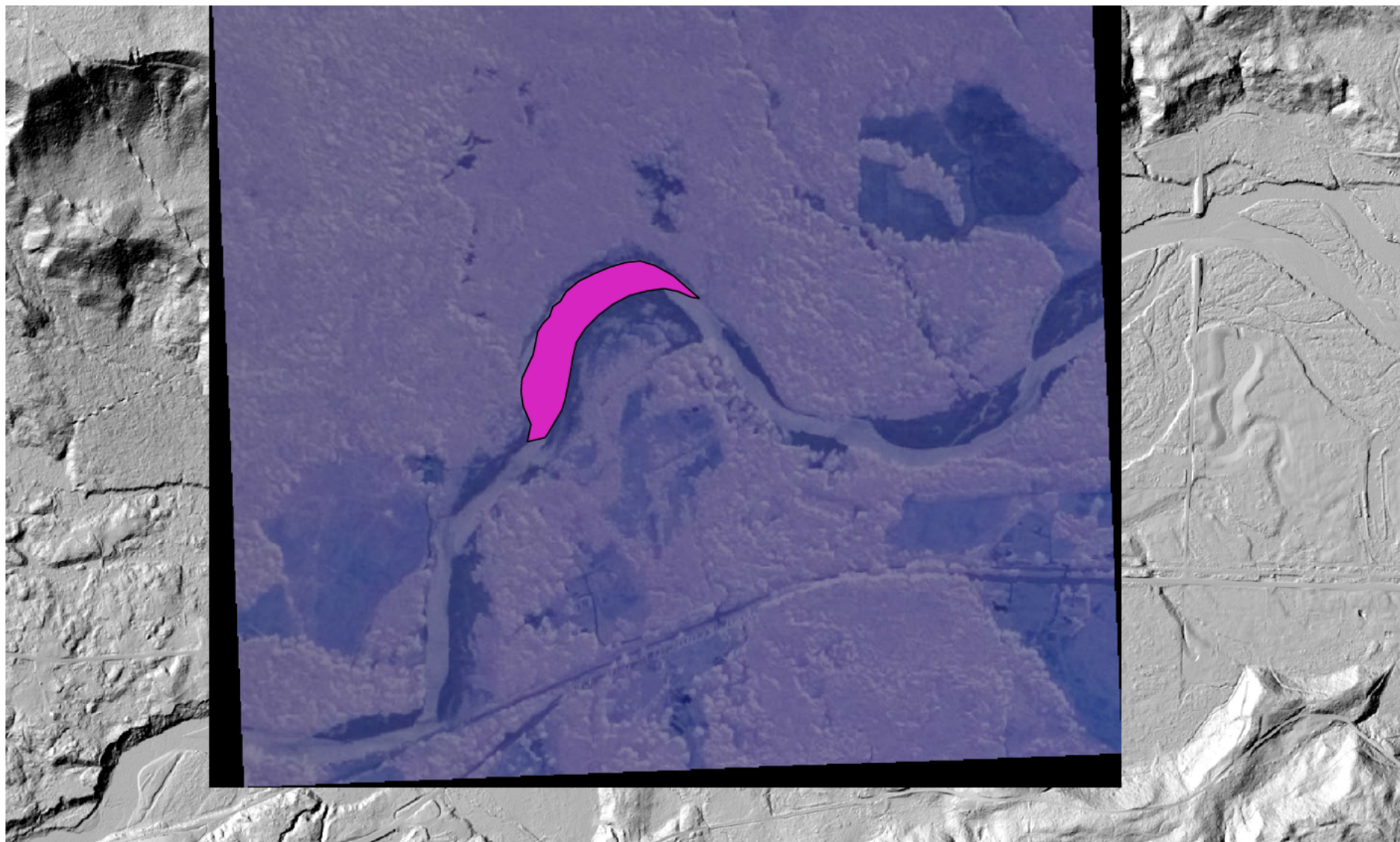
0   750   1500   2250 ft

1976 to 1985 Erosion

| 0 | 750 | 1500 | 2250 ft |
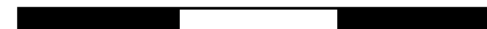
1985 to 1989 Erosion

| 0 | 750 | 1500 | 2250 ft |
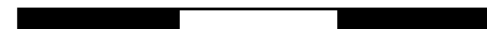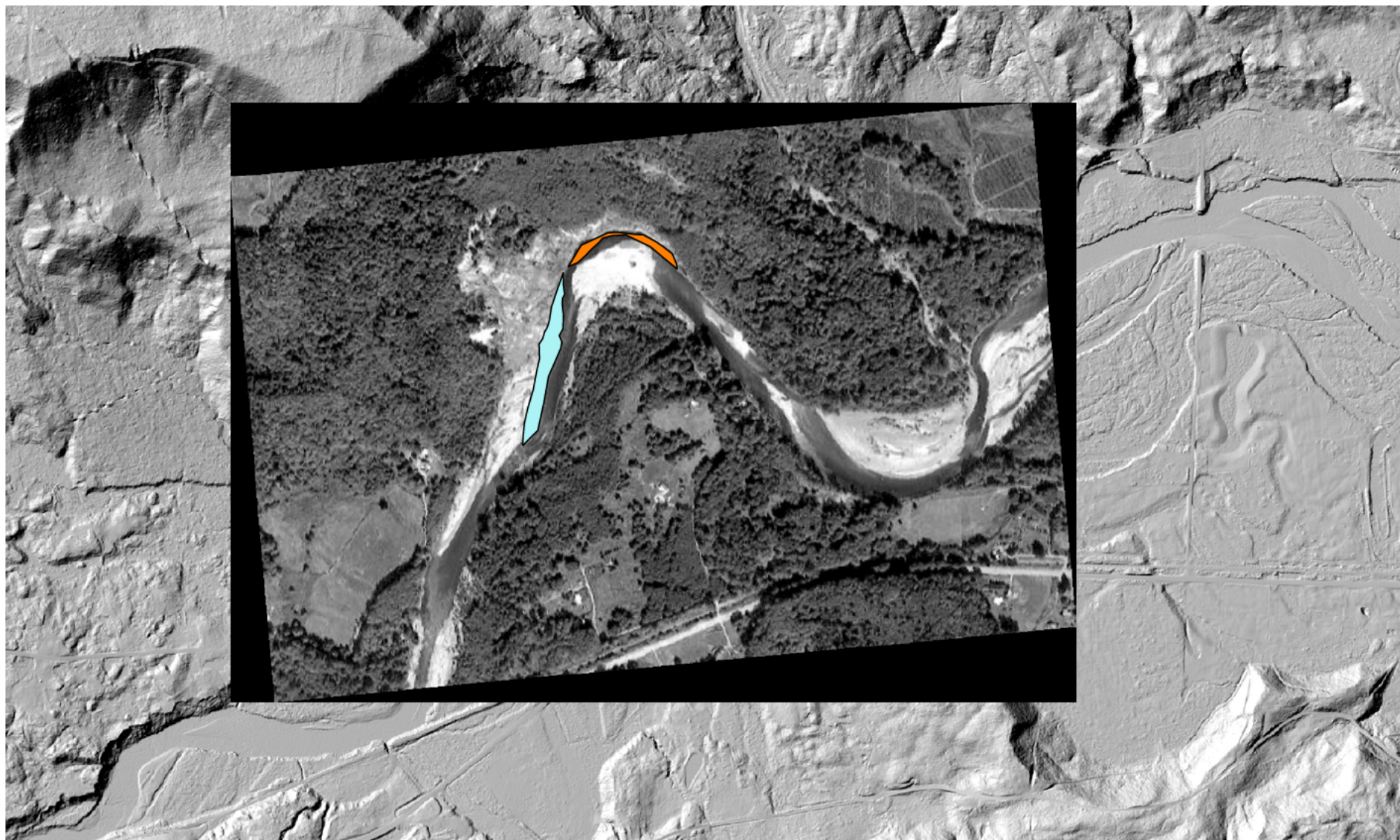
1989 to 1991 Erosion (Orange) and Deposition (Aqua)

0   750   1500   2250 ft
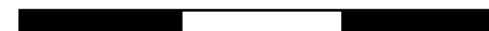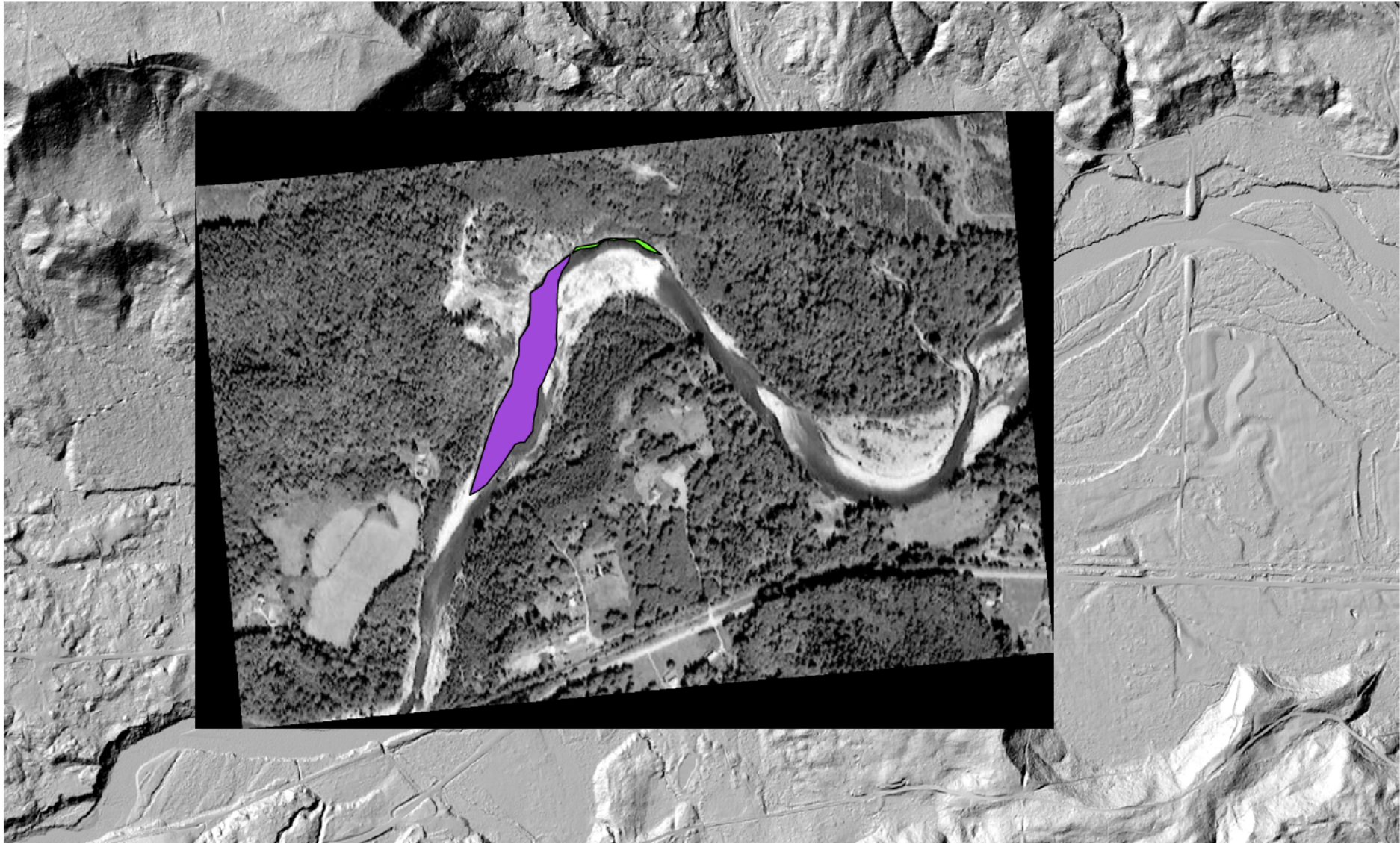
1991 to 1995 Erosion (Purple) and Deposition (Green)

| 0 | 750 | 1500 | 2250 ft |
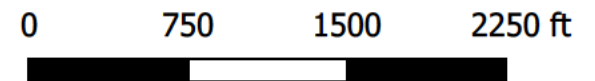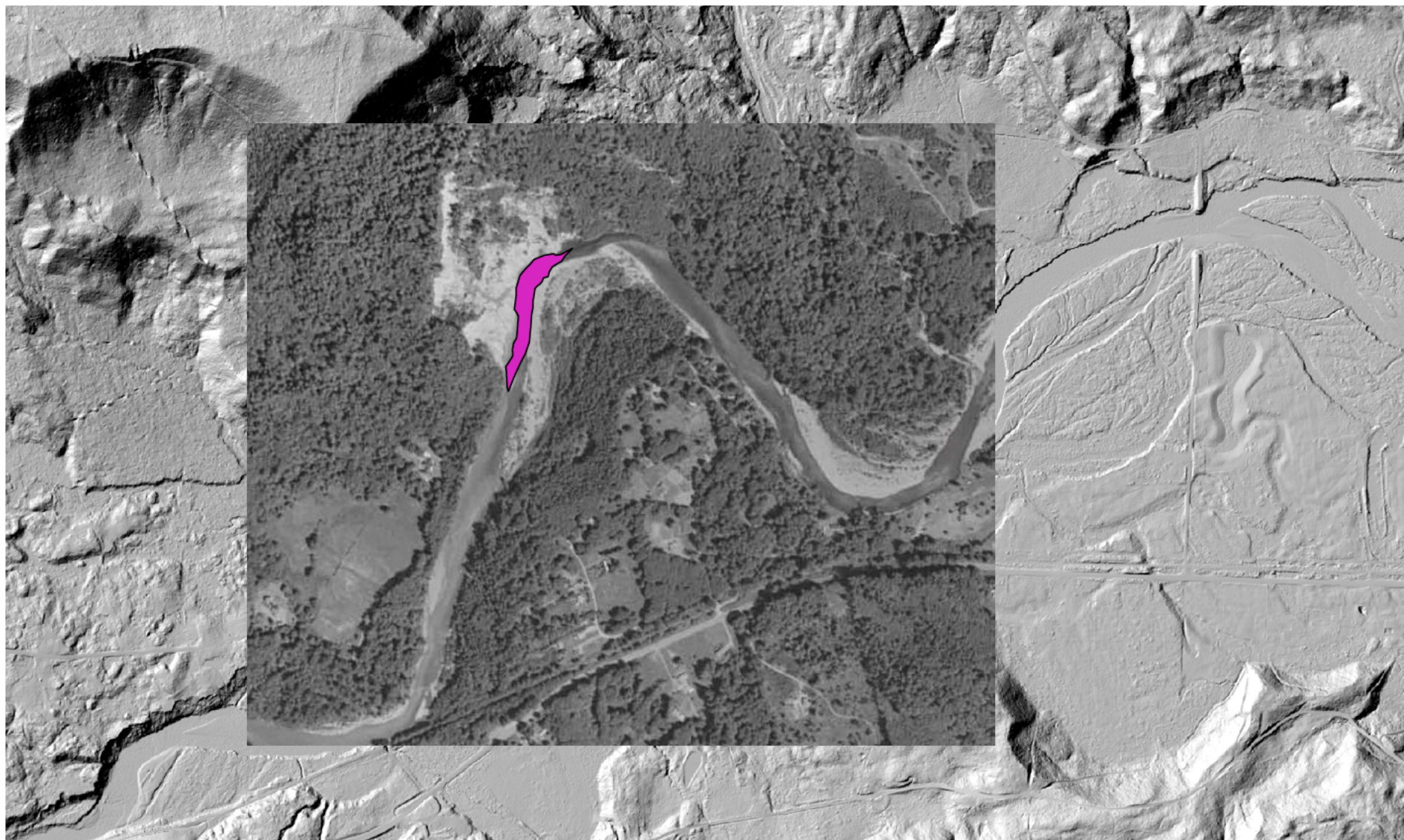
1995 to 2003 Erosion

| 0 | 750 | 1500 | 2250 ft |
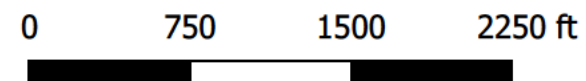
2003 to 2006 Deposition
(2006 Slide)

| 0 | 750 | 1500 | 2250 ft |
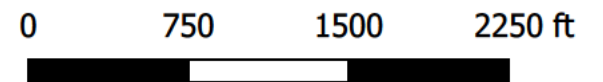
APPENDIX I

Groundwater Evaluations

This appendix provides detail background for the elements of the opinions presented in the report that rely on interpretation of groundwater levels and groundwater flow. This includes interpretation of the piezometer record, and estimates of groundwater levels and pore water pressures that may be used in slope stability analysis.

Piezometer Record

Analysis and Quality Assurance

41 piezometers were installed between the initial exploration program undertaken by WSDOT in the fall of 2014 and the exploration program undertaken for this study in the summer and fall of 2015. Initial readings from the WSDOT borings [H-1vwp-14 and H-2vwp-14] suggested that there might be reliability issues with the readings. Reliability can have three different components, (1) accuracy of the reading at some level of precision, (2) the true level of precision, and (3) the coincidence in time between the actual piezometric level in the soil surrounding the bore hole and the piezometer reading sensed by the piezometer.

The WSDOT report which is included in Appendix B includes manufacturer's specifications for the piezometers used at the site. For all practical purposes, beyond the basic calibration function, no adjustments to the piezometer readings are necessary. Any adjustments associated with barometric pressure which is not part of the basic calibration function are small enough that they are not significant from a geomechanics perspective. None-the-less, response to barometric pressure changes over time can be a helpful indicator of the reliability of the readings from a particular piezometer. Early in the subsurface exploration program, it was recognized that the piezometer readings were being influenced by normal changes in barometric pressure. This prompted a change in the piezometer installation plan such that we could verify from paired piezometer readings both in the same bore hole and between adjacent bore holes what the true reliability of the piezometers was at the SR 530 landslide site. A summary table of the installed piezometers was provide in Appendix D of the January 22, 2016 interim report. In particular, the piezometers in bore hole EB-06 at depths of 124 ft, 128 ft, and 132 ft, provided an opportunity to understand the accuracy between piezometers since these were all expected to be below the groundwater table in the unconfined aquifer located above the silt/glacial till aquitard below the Whitman Bench. Further, piezometers in this same aquifer in borings EB-02 [depth, 112 ft] and SP-

01 [piezometer suspended at depth, 99 ft] which are side by side, allowed the absolute accuracy between piezometer types and installation methods to be determined. The piezometer in Boring SP-01 is an open standpipe type with a vibrating wire piezometer suspended at the indicated depth. The open standpipe allows the true water level to be verified at any time after installation of the piezometer. This verification is not possible for the fully grouted installations used in all other cases.

Observations of response to Barometric pressure changes

Early observations of piezometer readings suggested that interpretation would not necessarily be straightforward. First, the piezometer readings from the WSDOT borings [H-1vwp-14 and H-2vwp-14] suggested that the piezometric conditions beneath Whitman bench were not hydrostatic, and that negative pore pressures existed at some levels in the profile. The lack of apparent hydrostatic or near-hydrostatic conditions meant that it was not possible to confirm the readings from one piezometer by comparing them to another piezometer either higher or lower in the profile. Second, the barometric pressure that was evident in some of the readings, but not in others called into question the validity of some readings. Further investigation, following installation of a barometric pressure sensor at the site, bore this out. The criteria points below capture the basis for acceptance of a given piezometer reading as valid, in order of certainty. Two or more examples are provided for each criteria. In only a few cases, is there support for the accuracy of one piezometer based on another piezometer reading – these are the strongest cases. In other cases, inferences must be made with more limited certainty.

1. **Agreement Between Two Piezometers**. When two piezometers that can be reasonably expected to have correlated readings have correlated readings, they both can be considered to be operating correctly and the absolute value of the reading can be considered accurate.
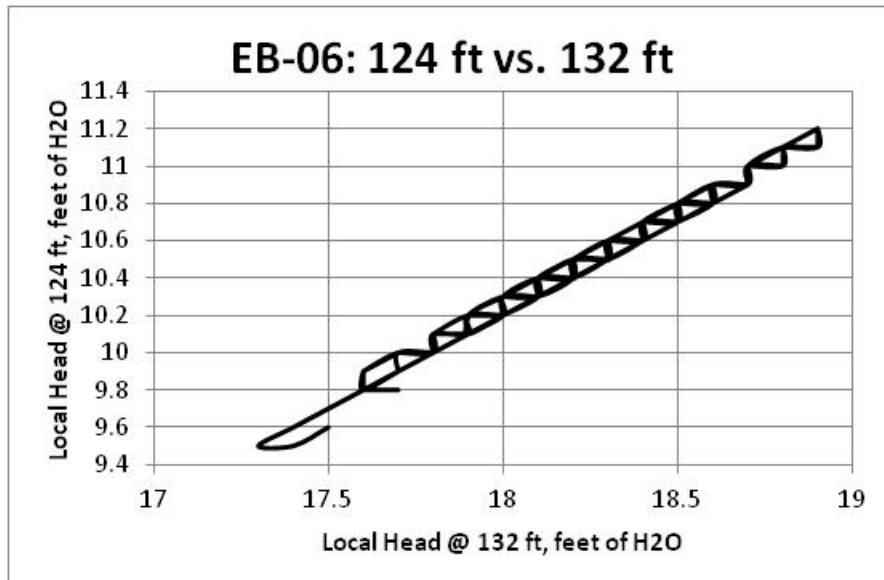
Figure I-1. Piezometer readings from boring EB-06 at 124 ft versus 132 ft from 21 December 2015 through 22 February 2016. The departures from a perfect linear relationship are the result of the reading resolution employed in the data logger connected to the piezometers. Note that a change in local head of 1.0 ft at 132 ft corresponds to exactly the same 1.0 ft change at 124 ft. Further, the difference in head between the two piezometers is very close to the 8 foot difference in the elevation of the piezometer tips, indicating identical, and in this case hydrostatic readings.
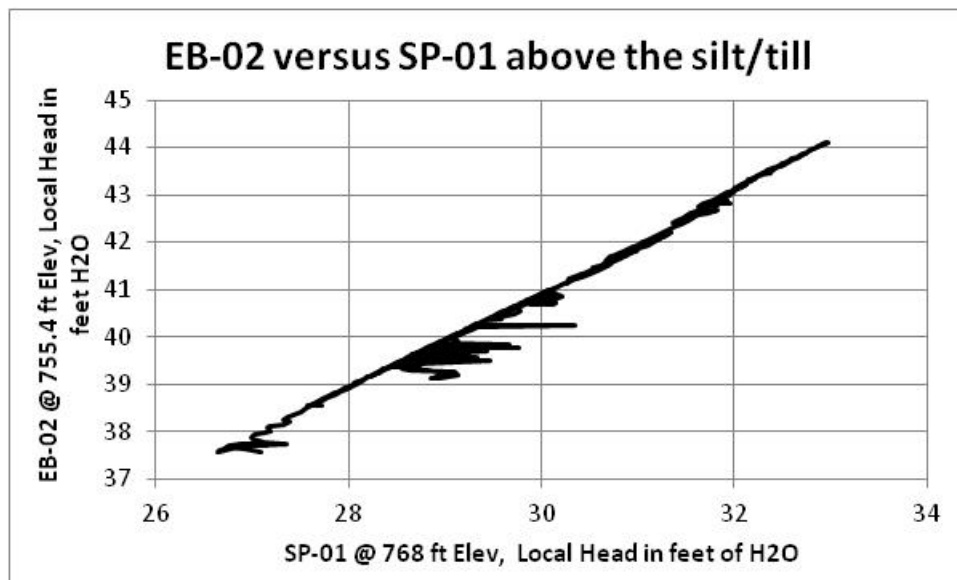
Figure I-2. Borings EB-02 and SP-01 are within feet of each other, hence they should produce corresponding readings. The linear relationship indicates that head changes between the two

piezometers are nearly identical, and the difference in the local head [11 feet] nearly matches the elevation difference between the two piezometers [768 ft − 755.4 ft = 12.6 ft]. The departures from the linear relationship appear to occur only with the piezometer in SP-01, which can be expected with an open standpipe piezometer. Obtaining a seal on an open standpipe piezometer is difficult and is often imperfect.

2. **Positive and Linear Response to Barometric Pressure**. A positive and linear response to positive barometric pressure change over a short interval such as a few days when actual changes in piezometric level are likely to be small indicates that the piezometer is operating correctly and the absolute value of the reading can be considered accurate if the reading is positive. Negative readings were interpreted to mean that the piezometric pressure was either negative with saturation in the case of fine grained soil, or the soil was not saturated in the case of sand at that level in the profile.
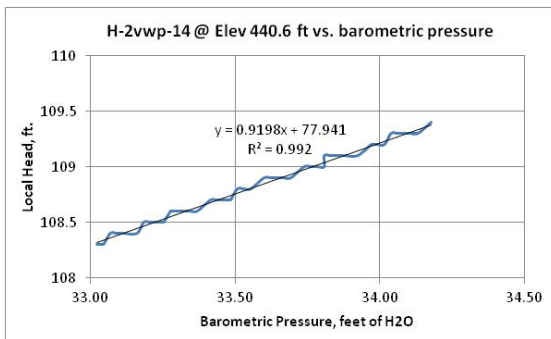
[31 Dec 2015 @ 12:00 to 5 Jan 2016 @ 8:00] @20:00]   [31 Dec 2015@ 12:00 to 4 Jan 2016
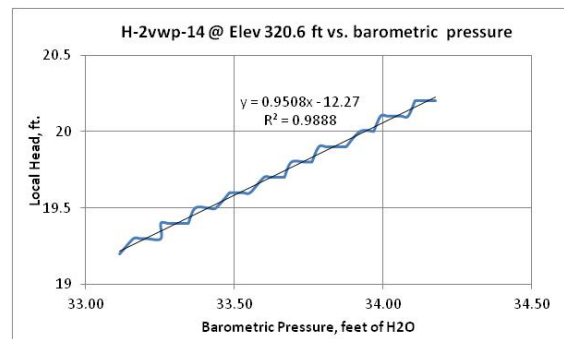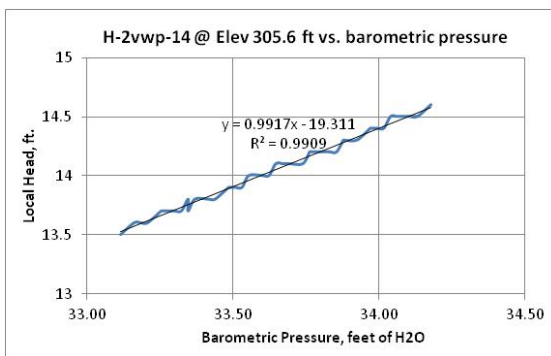
[31 Dec 2015 @ 12:00 to 4 Jan 2016 @ 20:00]   [23 Dec 2015 @ 22:00 to 26 Dec 2015 @ 4:00]

H-15 @Elev 387.59 ft vs. barometric pressure

$y = 1.0902x - 6.2195$
$R^2 = 0.9849$

EB-07 @ Elev 337.25 ft vs. barometric pressure

$y = 0.986x - 3.733$
$R^2 = 0.9956$
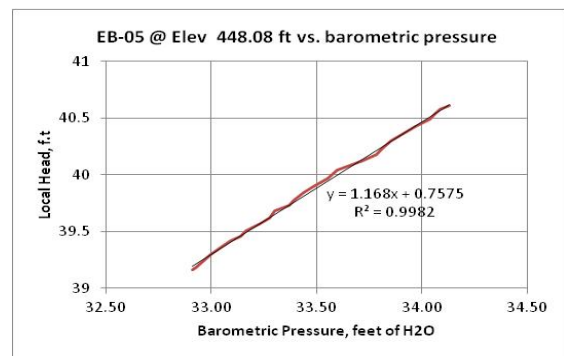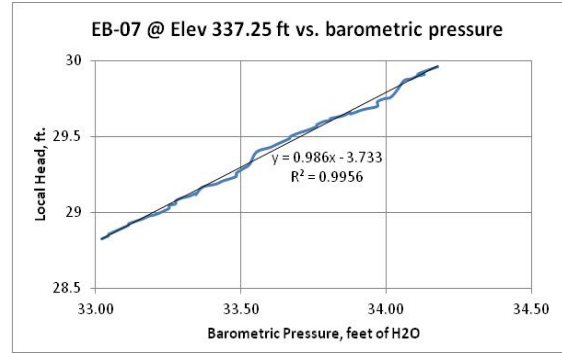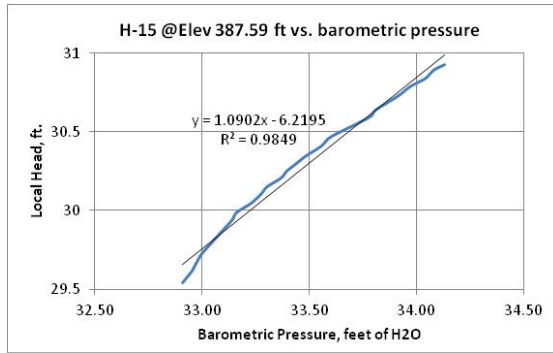
[23 Dec 2015 @ 22:00 to 26 Dec 2015 @ 4:00]   [31 Dec 2015 @ 12:00 to 5 Jan 2016 @ 8:00]

Figure I-3. Selected piezometer records that show a positive response to barometric pressure, indicating that they are operating correctly. Nearly one to one relationships with barometric pressure in these cases also indicate that there was little actual change in piezometric pressure occurring during the few days represented in each plot. A simultaneous change in actual pressure would result in other than a one to one slope of the line – numerous cases like this exist.

3. **Matched Pattern of Piezometric and Barometric Pressure Changes**. A pattern of increases and decreases in piezometric pressure that reasonably matches the pattern of barometric pressure changes, albeit delayed in time, indicates that the piezometer is operating correctly and the absolute value of the reading can be considered accurate if the reading is positive. Negative readings were interpreted to mean that the piezometric pressure was either negative with saturation in the case of fine grained soil, or the soil was not saturated in the case of sand at that level in the profile.
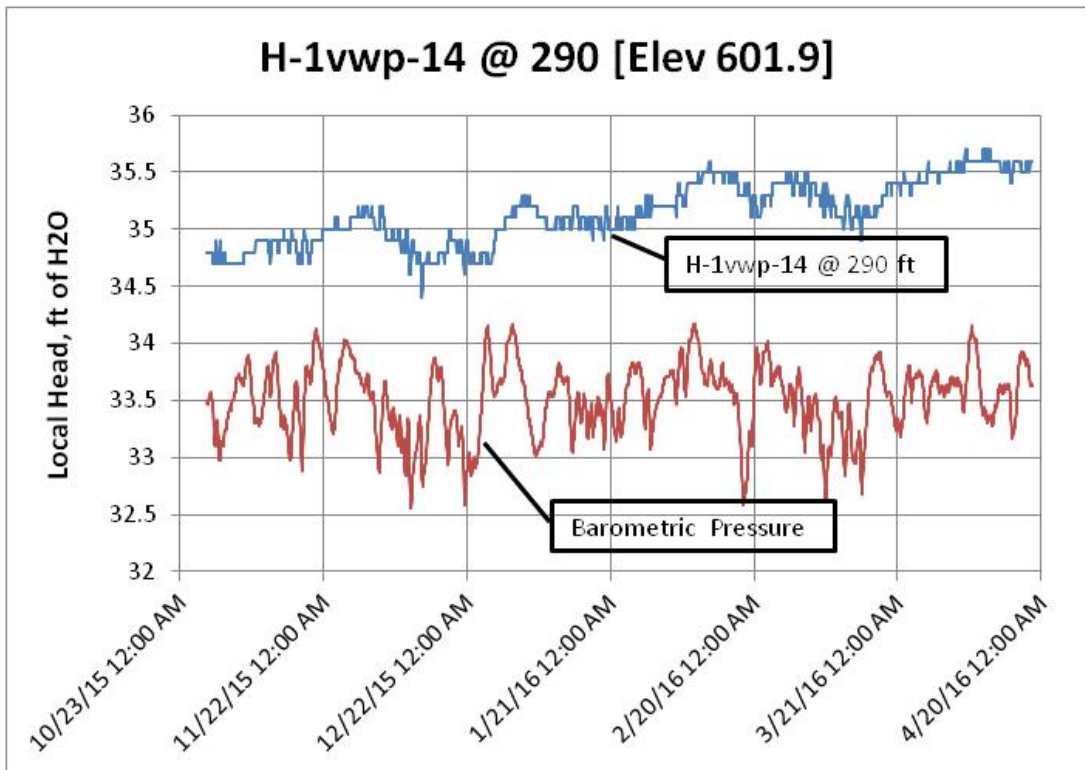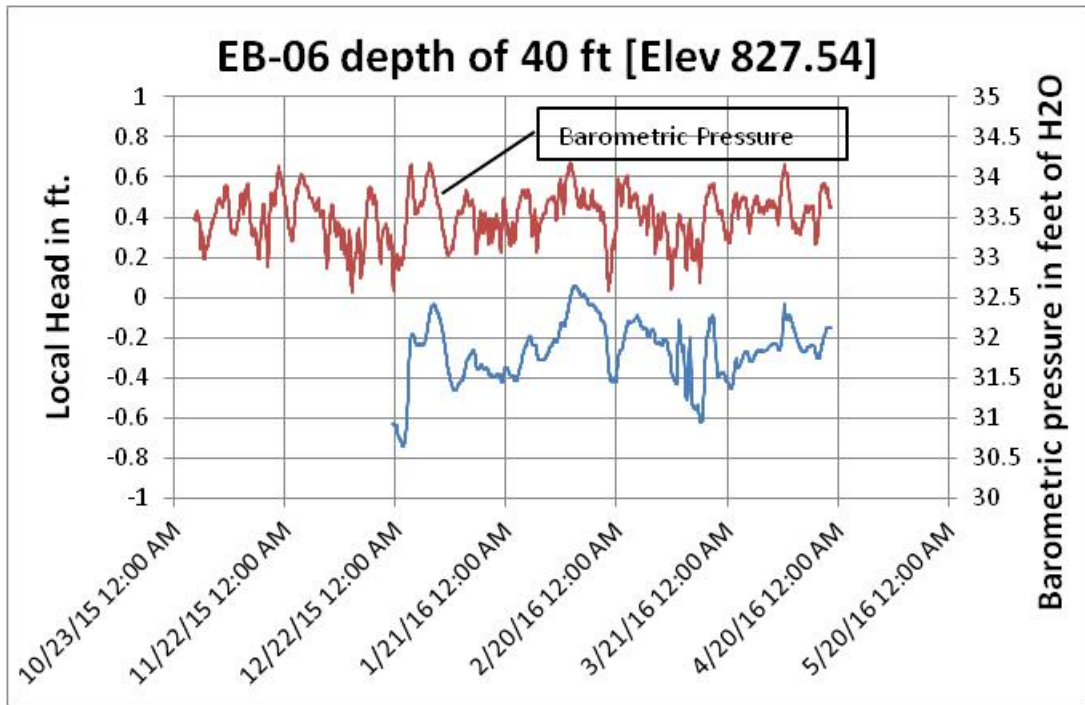
Figure I-4. Examples of piezometers where the pattern of change in piezometric reading indicates a delayed and subdued response to changes in barometric pressure.

The Tables below indicate which piezometers have been accepted as accurate based on the particular acceptance criteria and their stratigraphic position.

Table I-1. Accepted Piezometer Readings

Acceptance Criteria	Piezometer list
1. Paired Comparison	EB-06 @ 124 ft
	EB-06 @ 128 ft
	EB-06 @ 132 ft
	EB-02 @ 112 ft
	SP-01 @ 99 ft
2. Response to Barometric pressure	H-1vwp-14 @ 128 ft
	H-2vwp-14 @ 450 ft
	H-2vwp-14 @ 570 ft
	H-2vwp-14 @ 585 ft
	EB-01 @ 127 ft
	EB-02 @ 112 ft
	EB-03 @ 124 ft
	EB-05 @ 49 ft
	EB-05 @ 76 ft
	EB-06 @ 20 ft
	EB-06 @ 60 ft
	EB-06 @ 80 ft
	EB-06 @ 124 ft
	EB-06 @ 132 ft
	EB-07 @ 75 ft
	EB-07 @ 90 ft
	EB-08 @ 72.5 ft
	EB-10 @ 98.8 ft
	EB-11 @ 64 ft
	EB-14 @ 137 ft
	H-13 @ 38.5 ft
	H-13 @ 48 ft [piezometer failed on Feb 18, 2016]

	H-15 @ 50 ft
	H-15 @ 65 ft
	H-18 @ 40 ft
	H-18 @ 60 ft
	SP-01 @ 99 ft
3. Pattern of response to barometric pressure with time lag.	H-1vwp-14 @ 230 ft
	H-1vwp-14 @ 290 ft
	EB-06 @ 40 ft
	EB-07 @ 150 ft
	EB-14 @ 237.5 ft
	EB-14 @ 276.5 ft
	H-12 @ 125 ft
	H-12 @ 175 ft
	H-13 @ 118 ft [piezometer failed on Feb 18, 2016]

Table I-2. Accepted piezometers with respect to the stratigraphic position of the piezometer tip.

Stratigraphic position	Piezometer
Recessional Outwash	H-1vwp-14 @ 128 ft
	EB-01 @ 127 ft
	EB-02 @ 112 ft
	EB-03 @ 124 ft
	EB-06 @ 20 ft
	EB-06 @ 40 ft
	EB-06 @ 60 ft
	EB-06 @ 80 ft
	EB-06 @ 124 ft
	EB-06 @ 128 ft
	EB-06 @ 132 ft
	EB-08 @ 72.5 ft
	EB-10 @ 98.8 ft
	EB-11 @ 64 ft
	SP-01 @ 99 ft

Glacial Till	
Advance Outwash	H-1vwp-14 @ 230 ft
	H-1vwp-14 @ 290 ft
Lacustrine Silt/clay	H-2vwp-14 @ 450 ft
	H-2vwp-14 @ 570 ft
	EB-05 @ 76 ft
	EB-07 @ 75 ft
	EB-14 @ 137 ft
	H-13 @ 48 ft [piezometer failed on Feb 18, 2016]
	H-15 @ 65 ft
Bear Lake Sands	H-2vwp-14 @ 585 ft
	EB-07 @ 90 ft
	EB-07 @ 150 ft
	EB-14 @ 237.5 ft
	EB-14 @ 276.5 ft
	H-12 @ 125 ft
	H-12 @ 175 ft
	H-13 @ 118 ft [piezometer failed on Feb 18, 2016]
2014 SR 530 Landslide Debris	EB-05 @ 49 ft
	H-13 @ 38.5 ft
	H-15 @ 50 ft
	H-18 @ 40 ft
	H-18 @ 60 ft

Observations on Piezometric Pressures

There are a number of observations from the piezometer records that pertain to the groundwater regime at the SR 530 landslide site and have the potential to influence the stability of the slope from the Whitman Bench to the Stillaguamish River. These will be listed below along with discussion of the importance of each observation.

- Groundwater is perched on the recessional silt and glacial till that directly underlies the recessional sand and gravel deposits that make up the surface strata on Whitman Bench.

- The near surface recessional outwash material on the Whitman Bench is predominantly sand with occasional silt and gravel lenses. This material has a very high hydraulic conductivity and is not saturated down to the level of an unconfined water table that is perched on the silt/till member at the base of the recessional outwash strata. Evidence of the perching can be seen in
    - The water caused erosional gullying of the Headache Creek escarpment to the east of Whitman Bench. This gullying indicates that groundwater perched on the silt/till strata surfaces in springs at the level of the top of the glacial till and flows eastward into Headache Creek
    - Groundwater table surface above the silt/till strata in borings H-1vwp-14, EB-01, EB-02, EB-03, EB-06, EB-08, EB-10, EB-11, and SP-01, coupled with piezometer readings from H-1vwp-14 from below the till that show a discontinuity in the piezometric pressures.
    - Minor seasonal seepage from the top of the silt that overlies the glacial till visible in the SR 530 landslide scarp. This seepage can be considered minor because it is seasonal, and visibly does not flow as surface water very far below the silt/till interface.
- Perched groundwater flow above the silt/till strata is predominantly to the east into the Headache Creek basin.
    - The erosional gullying indicated above, and a corresponding absence of similar gullying in the SR 530 scarp and south facing slopes to the west of the SR 530 slide indicate that groundwater perched on the silt/till strata flows predominantly to the east, and not toward the SR 530 slide.
    - The seasonal changed in groundwater levels in the borings on the Whitman Bench is consistent with perched groundwater and groundwater flow to the east.
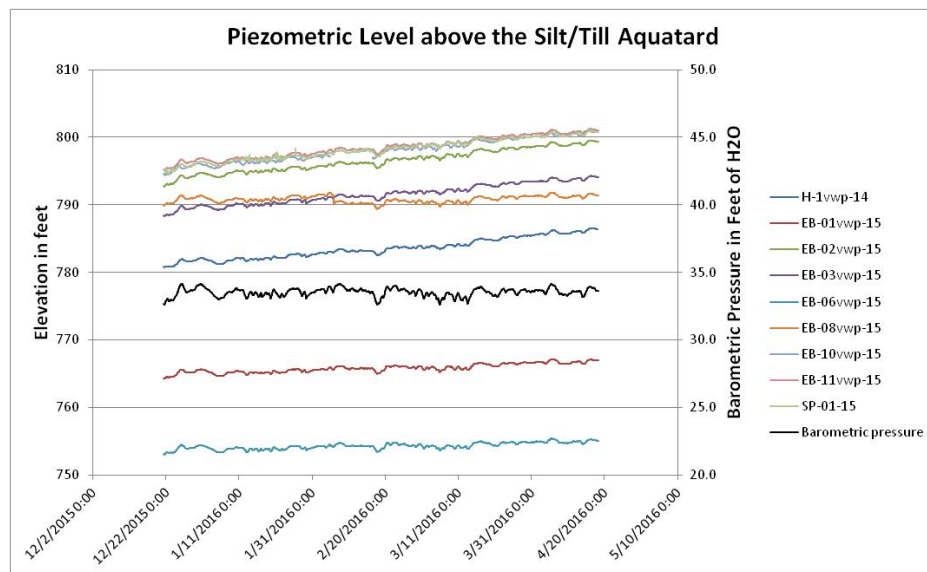
Figure I-5. Piezometric levels in the piezometers above the till interface beneath Whitman Bench.

- Two distinct groups of piezometric level traces plotted against time can be seen in the above figure. The piezometers in EB-01, EB-06, and EB-08, all have slopes with respect to time that are less than half of the slopes of the other piezometers above the till. These three piezometers are near the Headache Creek escarpment. A lesser slope with respect to time indicates that seasonal changes in groundwater level are less effected near the Headache Creek escarpment than at some distance away from the escarpment. This observation is consistent with lateral groundwater flow toward headache creek – in effect, the escarpment face is a boundary condition to the groundwater flow regime with little change in groundwater level as seasonal increases and decreases in seepage occur.

- It should be noted, that the piezometic level in EB-03 which is near the escarpment to the south into the Stillaquamish valley has a similar response with time to the piezometers further from the two escarpments, indicating that there is not a seepage boundary condition in that direction – in other words, significant seepage does not occur in a southerly direction.

- A schematic diagram of the piezometric surface from the vicinity of EB-02 and EB-10 toward EB-01 and the Headache Escarpment is shown below. As can be seen in this schematic, the change in piezometric level near the point of drainage at the right of the section from early winter to later in the water year is less than the change at the left edge of the section – this is exactly the behavior exhibited in the piezometers.
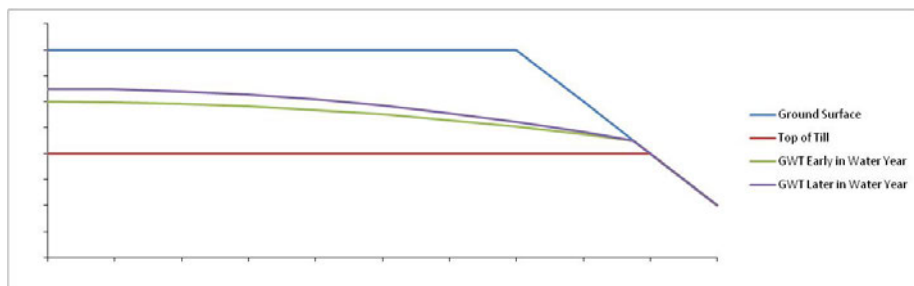
Figure I-6. This schematic illustrates the groundwater profile in a West to East direction with drainage of the recessional outwash deposits above the till draining toward the Headache Creek escarpment.

- Further, in our dataset, the maximum groundwater levels in the recessional outwash occur in the spring. They do not occur in the winter during the regional wet mantle storms when the highest daily, weekly, and monthly precipitation occurs. The piezometer record from boring H-2vwp-14, just above the glacial till surface, illustrates this behavior (Figure I-7). An explanation for this behavior becomes apparent when the 80 to 100 feet of unsaturated sandy soil that extends from the ground surface to the glacial till is considered. Assume that the sandy soil above the glacial till has a dry density of 1.7 gms/cm^3 (106 lbs/ft^3)

and the specific gravity of the soil solids is 2.73. The result is that the porosity of the sandy soil is 38 percent. Further, assume a value for the volumetric water content of the sandy soil at field capacity of six percent (Φ_{vol} = 6 %). Thus, 32 percent of the volume of the soil is pore space when the soil is at field capacity. To take this soil from field capacity to saturation would require 3.84 inches of rainfall per foot of soil. For a 100 foot depth of the recessional outwash, it would require 384 inches of rainfall. This, of course, never happens. The piezometric data shows that the groundwater table varies by about five feet. To saturate five feet of the sandy soil that is at field capacity would require about 20 inches of rainfall. This requires additional rainfall to raise the water content of the sandy soil to the point where it will transmit the needed 20 inches of rainfall to depth. Assume that to transmit rainfall to depth the sandy soil needs to be at a soil tension of 0.1 atm, which translates in a sandy soil to a volumetric moisture content of 12 percent (Φ_{vol} = 12 %). If the value for field capacity, Φ_{vol} = 6 %, is subtracted from the value at 0.1 atm, Φ_{vol} = 12 %, then a volumetric moisture content of 6 percent is needed to bring the soil up to a moisture content that will allow it to easily transmit rainfall down into and through the soil. The 6 % volumetric moisture content translates into a rainfall value of 0.72 inches per foot of soil. Thus, to raise the moisture content of 95 feet of the sandy soil from field capacity (Φ_{vol} = 6 %) to a moisture content that would allow rainfall to be transmitted to depth (Φ_{vol} = 12 %) would require about 68 inches of rainfall. Add to that value the 20 inches required to saturate the bottom five feet of the soil and the result is about 88 inches of rainfall. This is similar from the average annual precipitation for the Whitman Bench. This simple exercise helps explain the behavior of the water table above the glacial till on Whitman Bench. Of course, drainage from the recessional outwash to the east to Headache Creek will occur at some level during the whole year. Because this is not a closed system and these losses will be ongoing it means that amount of precipitation or even more is required to explain the behavior of the groundwater table above the glacial till on Whitman Bench.
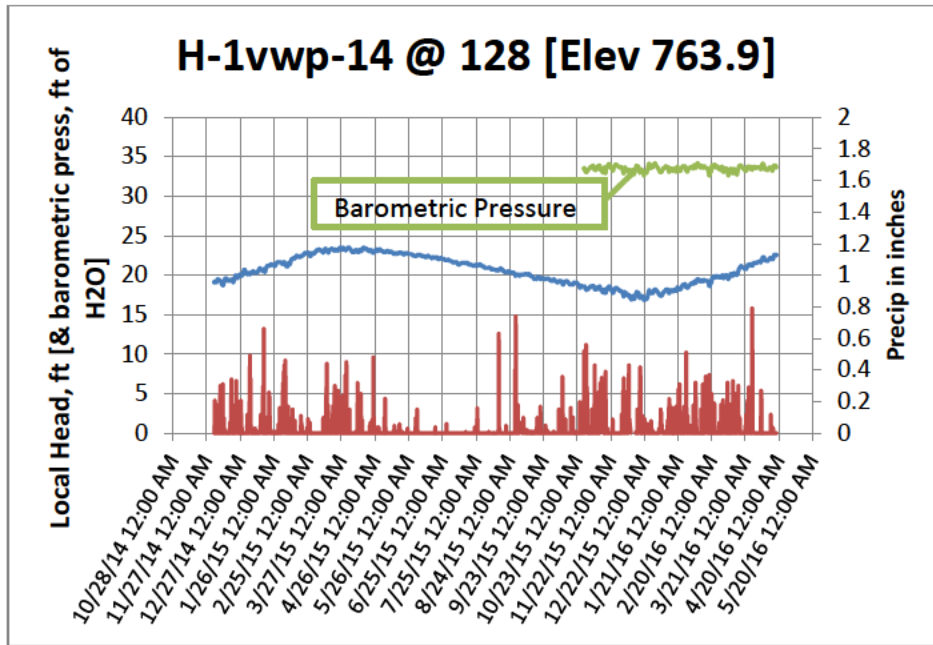
Figure I-7. Piezometric record from above the till in H-1vwp-14.

- The Bear Lake Sands which underlie the entire landslide area and beyond, from the toe of the surface of rupture through to at least the location of boring EB-02 on the Whitman Bench are either not saturated or not significantly pressurized at the base of the Glacial Lacustrine silts and clays the directly overlie the Bear Lake Sands.
  - o Evidence of a lack of saturation can be inferred from the samples that were obtained in split spoon samplers from the Bear Lake Sands in Boring EB-09. The photo below shows such a sample. Saturated sand is unlikely to be retained in a sample tube, and if it is retained, will not retain its texture when tub is split open.

Figure I-8. Split spoon sample from the Bear Lake Sands.

- o The piezometers in the Bear Lake Sands that are below, but near the overlying glacial
     lacustrine silts and clays, register very low pressure head that does not broadly reflect
     continuous hydrostatic conditions from (a) the lacustrine silt and clay above, (b) one
     bore hole to the next at this level, nor (c) with deeper piezometers.

Table I-3. Bear Lake Sands piezometer readings.

Piezometer	Pressure head, ft [April 18 2016] {implied piezometric surface elev. ft}	Elev. of Bear Lake Sands interface, ft	Implied Hydrostatic pressure head at the Bear Lake Sands interface, ft
H-2vwp-14 @ 585 ft [Elev. 305.6 ft]	14.6 {320.2}	312	8.2
EB-07 @ 322.25 ft [Elev. 322.25 ft]	6.5 {328.75}	323	5.75
H-12 @ 313.6 ft [Elev. 313.06 ft]	0.5 {313.56}	319	-5.44
EB-14 @ 301.95 ft [Elev. 300.43 ft]	0.7 {301.13}	313.5	-12.37

- Piezometer readings from deeper in the Bear Lake Sands suggest a consistent piezometric
  surface over a broad area with drainage toward the Stillaguamish River to the south. The water
  surface elevation in the Stillaguamish River varies with flow, but at wet season base level
  elevation is approximately 268 ft at the center of the slide debris field. The table below shows
  the deep piezometer readings from the Bear Lake Sands in conjunction with the approximate
  distance from the piezometer to the current river position.

Table I-4. Bear Lake Sands piezometers that reflect continuity with river levels.

Piezometer	Pressure head, ft [April 18 2016] {implied piezometric surface elev. ft}	Approximate distance to the River, ft [as of late 2015]	Implied hydraulic gradient
EB-07 @ 150 ft	10.8 {273.05 ft}	1400	0.0036

EB-14 @ 276.5 ft	10.5 {271.93 ft}	2000	0.002
H-13 @ 118 ft [piezometer failed on Feb 18, 2016]	11.6 {273.13 ft}	1100	0.0047

- The significance of a lack of saturation and/or very low pore pressures in the Bear Lakes Sand is that shear failure through this sand is virtually impossible any time there is significant overburden over the sand. The reason for this is that sand is a frictional material that behaves in cases like this according to the Coulomb friction law wherein the shearing resistance of the sand is directly related to the amount of overburden soil above any potential surface of rupture. Shallow planar slides wherein the overburden soil is rather thin are possible, but deep seated slides like the SR 530 slide without some source of elevated pore pressures are not.

- Piezometer readings in H-1vwp-14 and H-2vwp-14 from below the glacial till down to the Bear Lake Sands indicate four modes of behavior.
    - First, the near zero piezometer reading at elevation 662 indicates that the till above is in fact an aquitard.
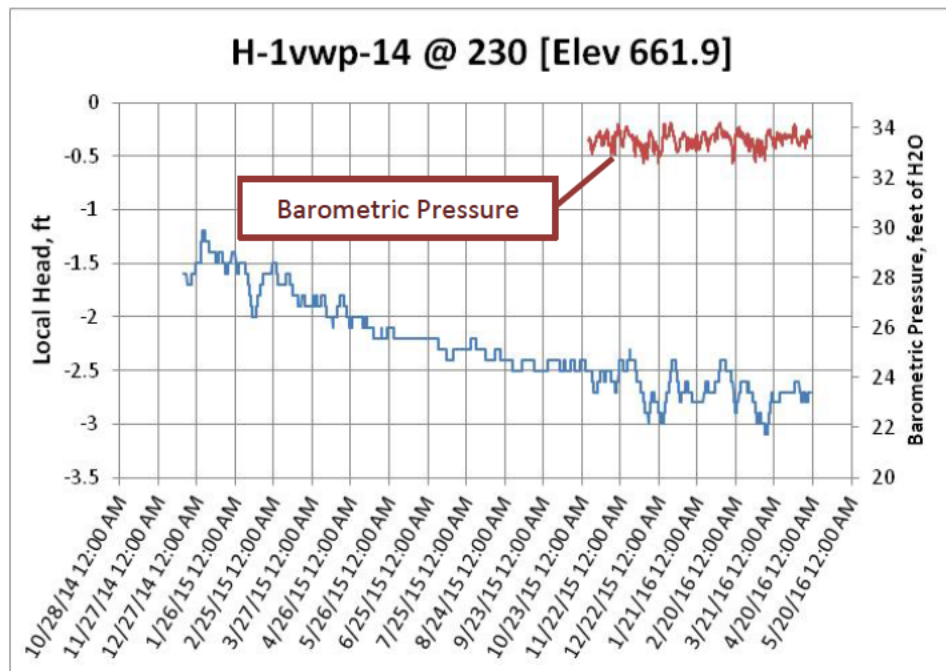
Figure I-9. Piezometer reading from advance outwash strata beneath the glacial till

    - Second, the significant decline in pressure head at elevation 441 from the beginning of the piezometer readings in early December of 2014 through late summer of 2015

indicates that there was a significant period of adjustment of internal seepage patterns below the Whitman Bench following the SR 530 landslide.
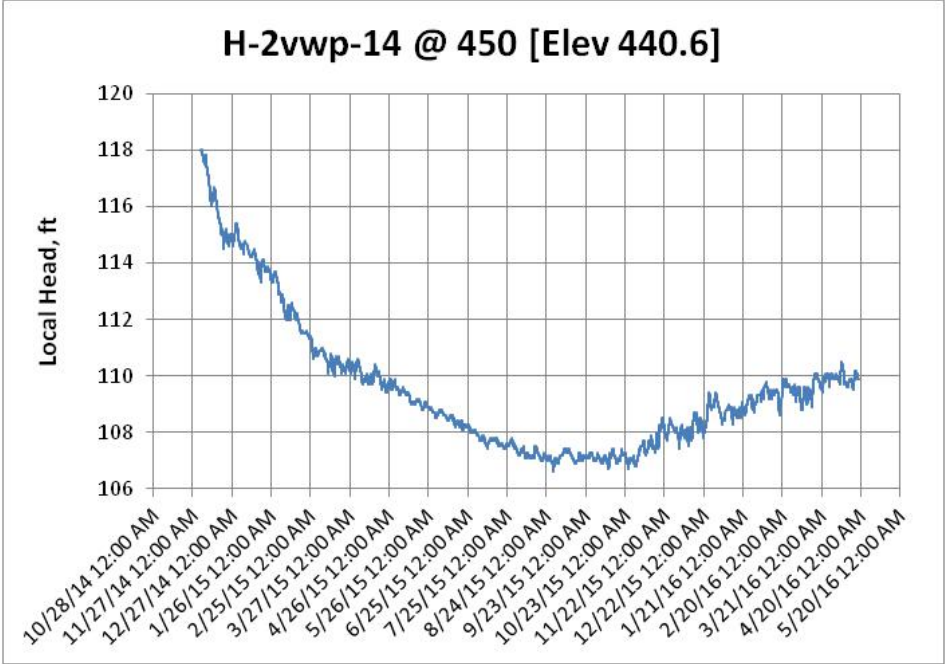
Figure I-10.   Adjustment of the piezometric level in one piezometer attributed to changes following the SR 530 landslide.

- Third, a modest increase in pressure head indicated at elevation 602 which is near the base of the advance outwash deposit indicates that there is likely localized leakage of groundwater through the silt/till strata. This observation is consistent with the presence of a sizable body of outwash sand and gravel visible in the scarp face that appears to

coincide with a locally much thinner and broken section of the silt/till aquitard layer.
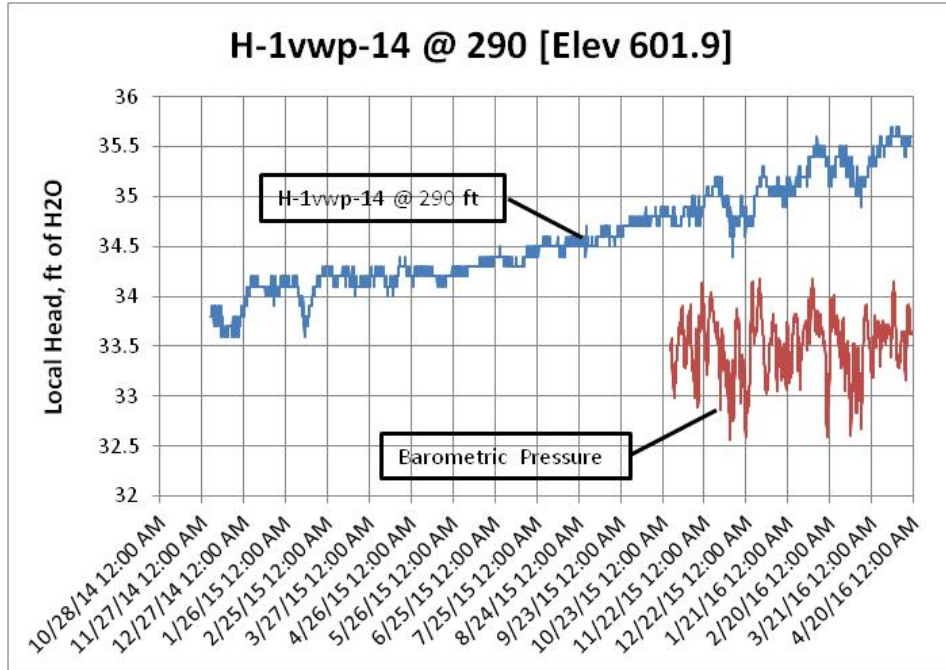
Figure I-11. Piezometer reading indicate slight leakage through the silt/till aquitard.

- Fourth, the piezometer at elevation 321 shows a less significant declining seepage adjustment than at elevation 441, a near zero pressure head indicating drainage into the Bear Lake Sands at Elevation 312, and an annual cycle which can be reasonably assumed to be in response to annual precipitation. A time delay in response seems apparent given that precipitation started in September, but a rise in the piezometer reading did not occur until early November.
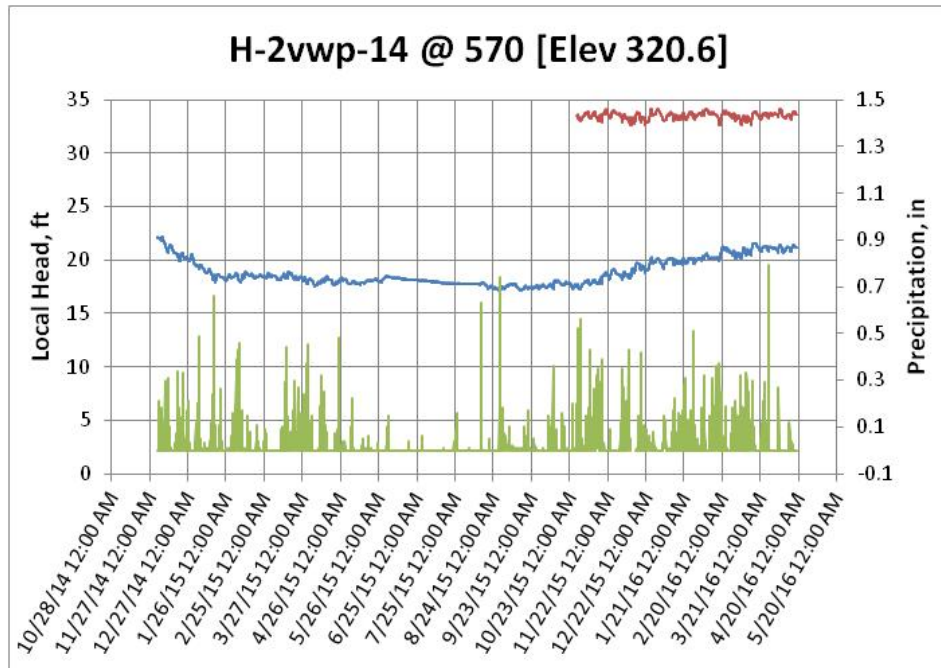
Figure I-12. Bear Lake Sands piezometer in H-2vwp-14 showing a seasonal response.

- Piezometers located within the SR530 slide mass demonstrate varied behavior that appears to be a function of the local connectivity of the piezometer tip to stratigraphy including the basal surface of rupture. Piezometers located in the slide debris above the surface of rupture, and some distance from the SR 530 landslide scarp exhibit relatively quick response to precipitation, whereas piezometers in the "free field" installed in bore holes on the Whitman Bench, exhibit only an annual cycle of response to wet season precipitation with a time delay of months.
    - Quick response to wet season precipitation is illustrated in the figure below.
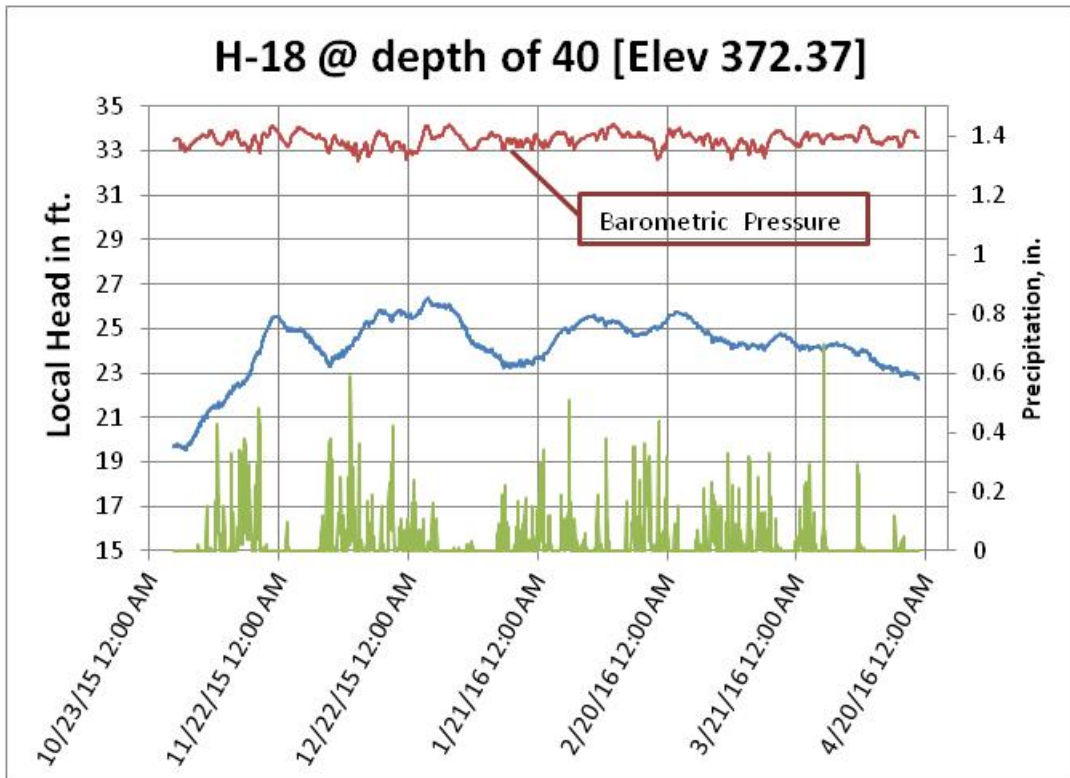
Figure I-13. Piezometer response to precipitation within the slide debris.

- The piezometer in EB-05 that is within the slide debris reacts differently than the other piezometers in the slide debris. This piezometer record is shown in the figure below for comparison with the piezometer in EB-05 that is below the surface of rupture and a similar piezometer in EB-14 that is below the surface of rupture. There is only the most subtle signature of precipitation in the piezometer records – a slight increase or decrease in the rate of general increase in the readings. The fact that both piezometers in EB-05 are responding similarly to the piezometer in EB-14 just below the surface of rupture indicates connectivity between the slide debris and the lacustrine silt/clay strata below the surface of rupture at the location of EB-05.
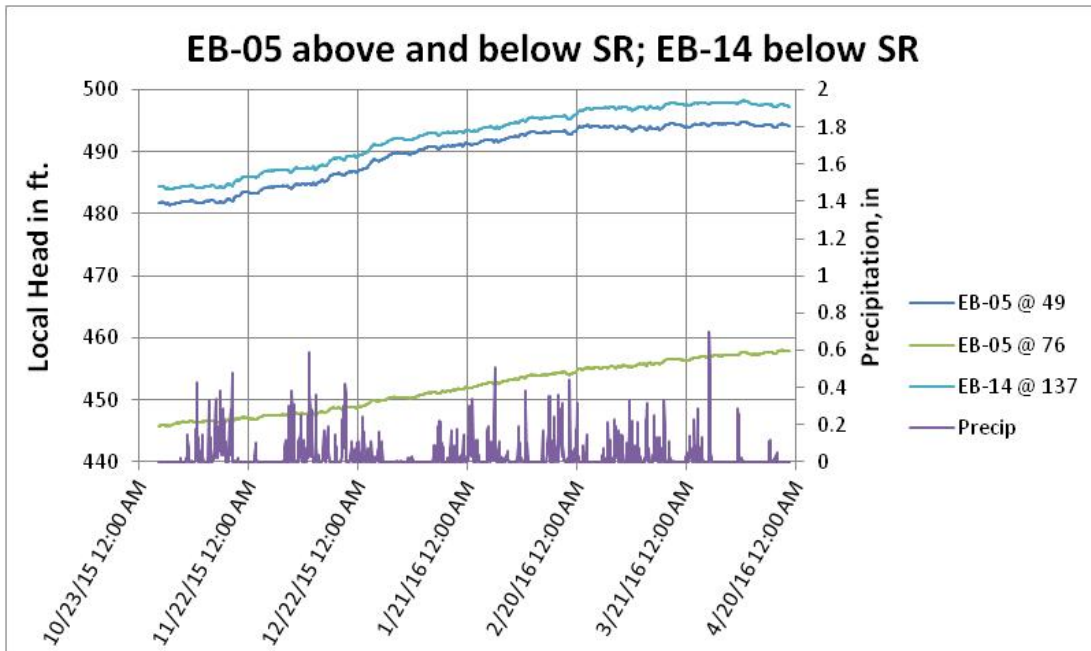
Figure I-14. Pieometers indicating connectivity between the slide debris and the lacustrine silt/clay below the surface of rupture.

- With the exception of the piezometer in EB-05 that is located within the slide mass, the piezometers in the slide mass all show a decline in piezometric levels through the late winter and early spring at a time when the general response in the other piezometers – those in the recessional outwash above the till, and those below the till – appears to be an increase in piezometric level. This common behavior in the piezometers within the slide mass is illustrated in the figure below
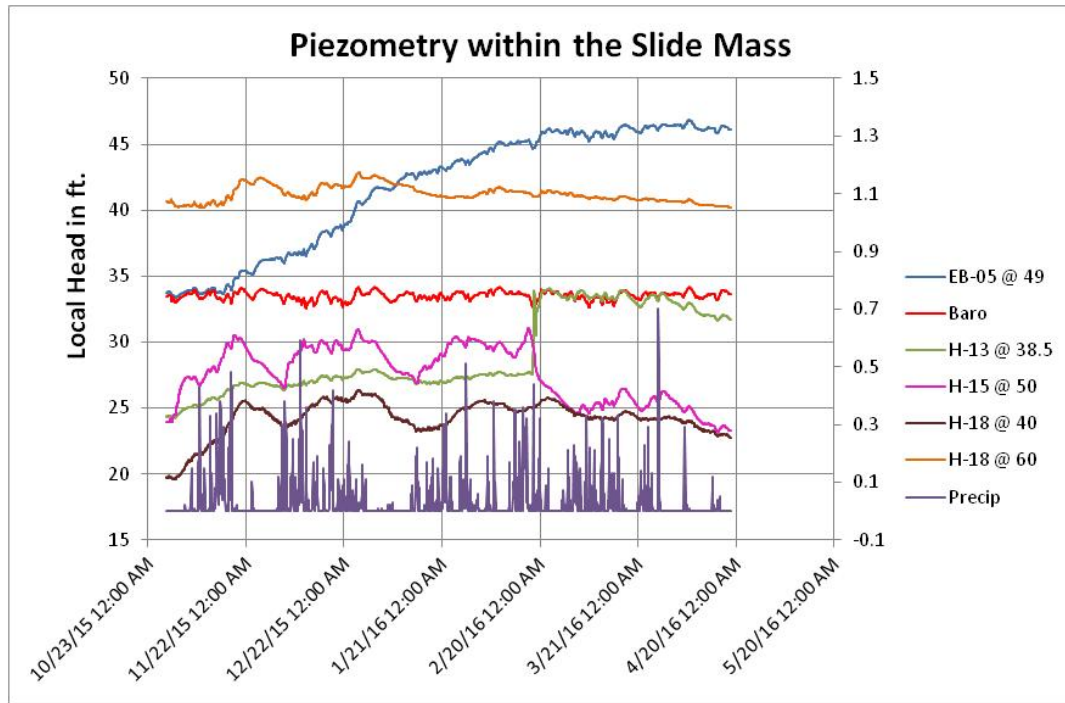
Figure I-15. Response of piezometers in the slide debris.

- If we infer that the previously failed portions of the SR 530 slide mass [the prehistoric failures and the Hazel slide in 2006] had groundwater behavior prior to the slide that is similar to that which we now see in the failed portions of the SR 530 slide mass after the slide, we can state that the piezometric levels within the slide mass from the north edge of the midslope bench south to the toe of the initial slide mass on the Bear Lake Sands respond to direct rainfall, while piezometric levels deep below the Whitman Bench do not.
- The net result of this response is that a near ground surface piezometric surface should be expected in the mid-slope bench and in the Hazel slide debris. This observation is illustrated in Figure I-16 below.
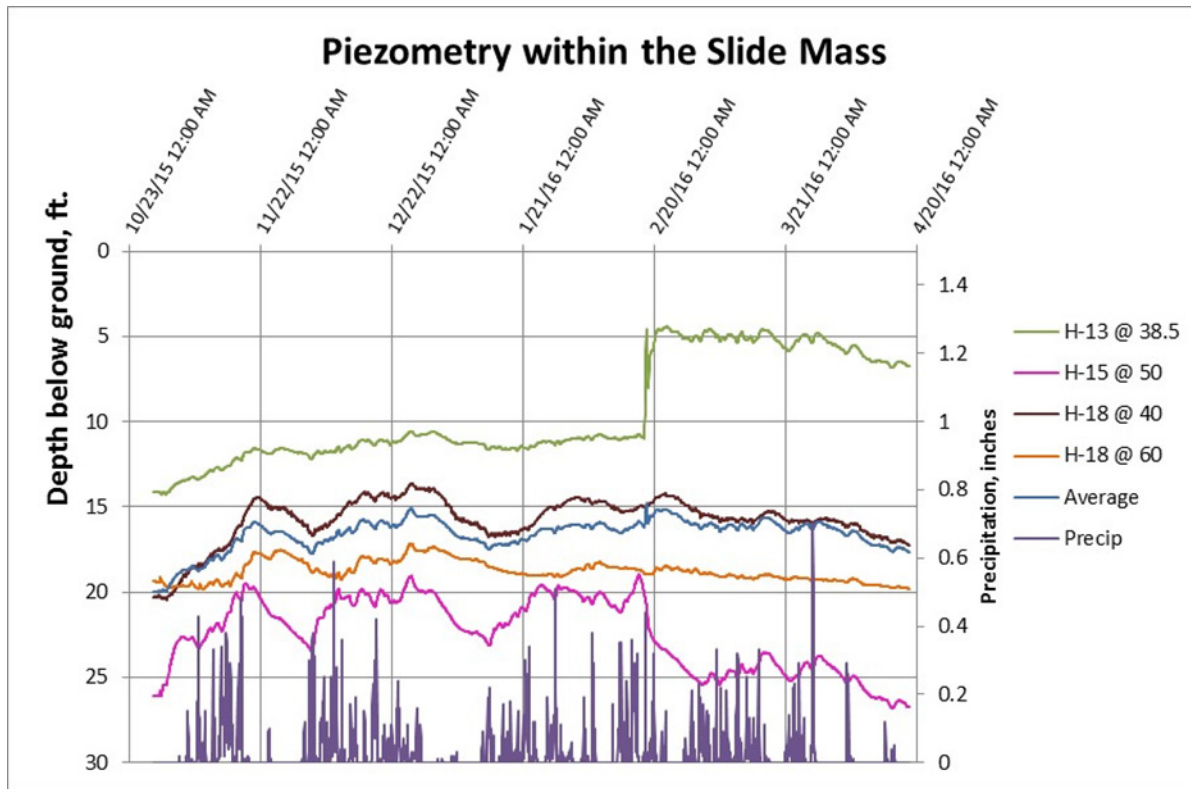
Figure I-16. Depth below ground of the Groundwater Table in the slide debris.

Two Dimensional Finite Element Seepage Modeling

As the pattern of seepage and pore pressures obtained from the piezometer network became apparent, and after an initial estimate of groundwater conditions between piezometers was made, it was decided that Finite Element modeling would allow confirmation of the estimated seepage pattern, and produce systematically interpolated pore pressure values that were necessary for slope stability analysis.

Finite Element Seepage Analysis

Introduction

Seepage analyses were performed using SeepW (GEO-SLOPE International Ltd. 2010. *Seepage Modeling with SEEP/W 2007 Version, An Engineering Methodology*, 4th Ed.) in order to calculate pore pressures within Whitman Bench and in the debris sections for 2006, 2014, and 2016 and confirm the pore water pressure patterns inferred from the piezometer network. Correspondence with the piezometer network patterns was considered necessary for the seepage analyses results to be used in stability analysis.

Seepage Boundary Conditions

The boundary conditions used in seepage analyses for the 2006, 2014, and 2016 Whitman Bench stratigraphy are shown in Figures I-17a-c. The names of each layer are shown in Figure I-17d. Note that the debris in Figure I-17c is considered to be homogeneous M2 debris. An initial steady state analysis was run for each analysis in order to establish baseline pore pressures, and then stable pore pressure conditions were achieved by running transient seepage analyses for 2 years to allow the water in the debris sections to lower to a constant minimum level. The stable conditions were achieved using a rainfall flux of 0.015 ft/day along the ground surface. This flux represents the annual average rainfall in the regions surrounding Whitman Bench. In order to replicate the conditions of heavy rainfall prior to the 2014 SR 530 landslide, a 22-day transient analysis was run with a 0.06 ft/day rainfall flux. The 0.06 ft/day rainfall flux represents the average rainfall in the regions surrounding Whitman Bench during the 22-days prior to the 2014 failure. Note that in Figure I-17a the M1 debris is assumed to be made up of a combination of Whitman Bench materials. This was done to facilitate a higher water table within the debris that would be more consistent with field observations of surficial ponding, but due to time constraints further seepage analyses focusing on the debris were not completed.
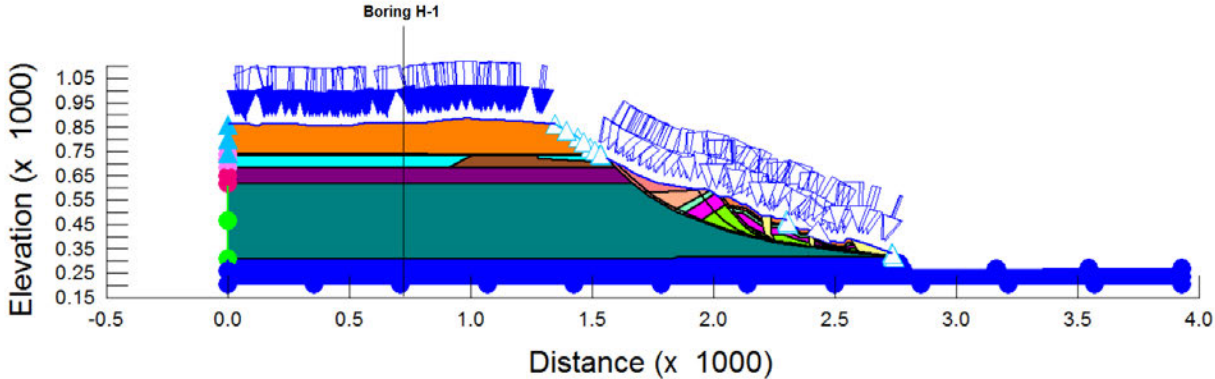
Figure I-17a: Boundary conditions for 2006 seepage analyses.
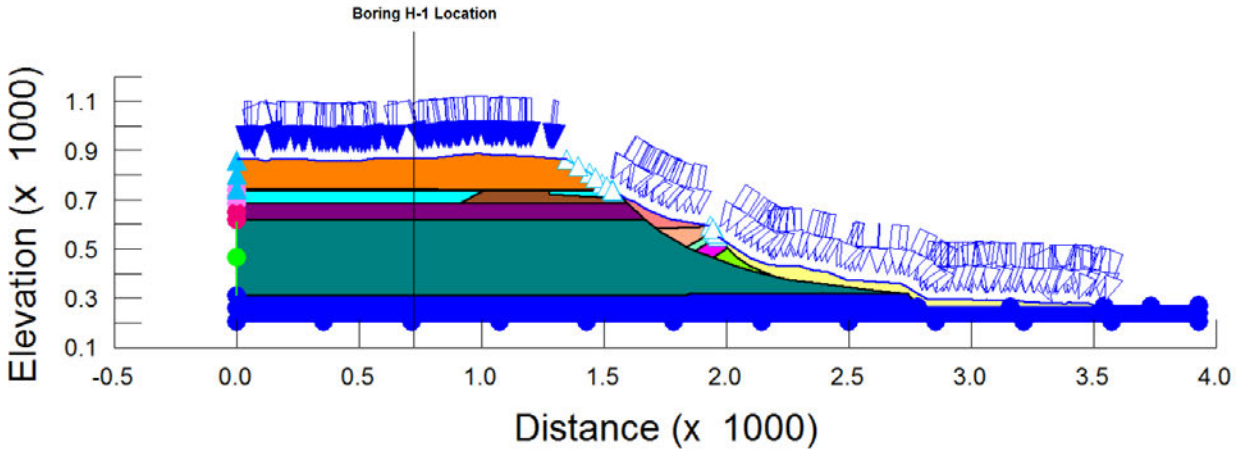
Figure I-17b: Boundary conditions for 2014 seepage analyses.
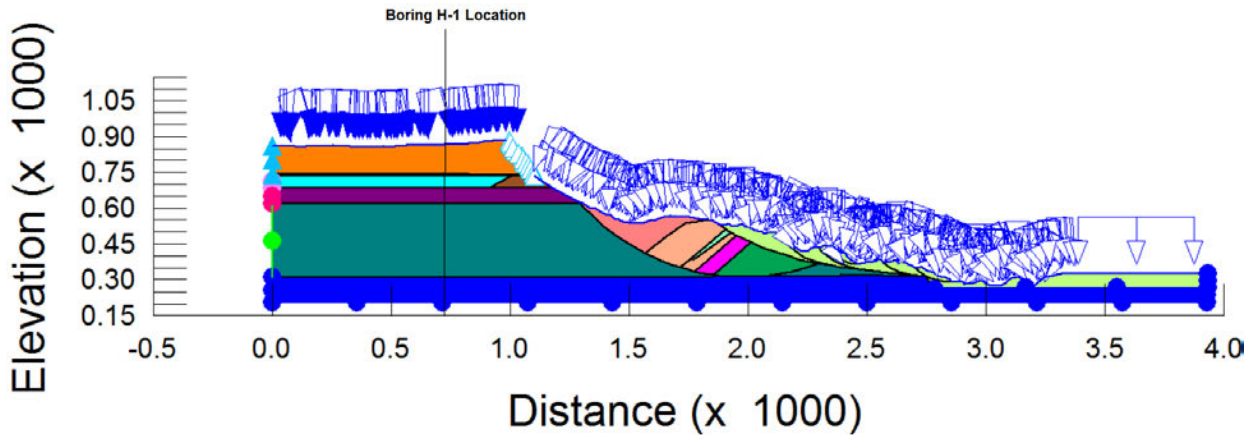
Figure I-17c: Boundary conditions for 2016 seepage analyses. The green debris is considered homogeneous M2 debris.
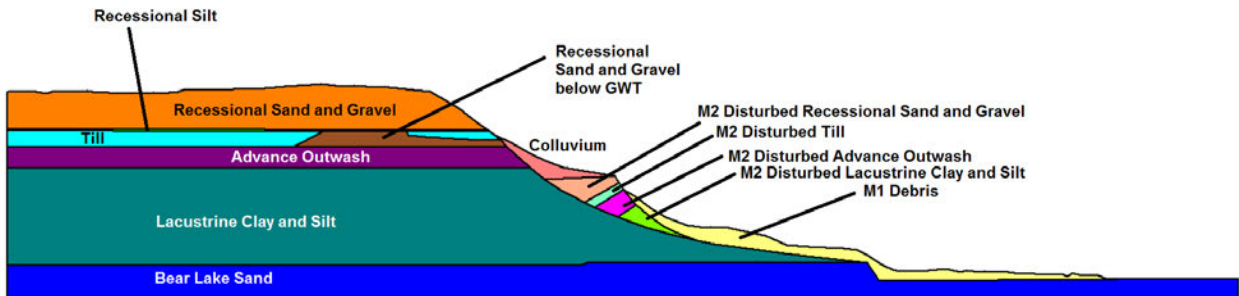
Figure I-17d: Whitman Bench layer names.

The rainfall flux boundary conditions are also set as potential seepage faces in SeepW below the recessional sand layer. A total head boundary condition of elevation 268 feet is applied to the bear lake sand boundary, except along its interface with the lacustrine clay. The lacustrine layer and advance outwash layer total heads are set to 600 feet along the northwestern boundary, corresponding to the elevation of Rollins Creek. The till total head is set to 740 feet along the northwestern boundary, corresponding to the top of the till layer. A no-seepage boundary condition is applied to the northwest boundary of the recessional silt and recessional sand layers.

The rainfall flux is applied perpendicular to each line on which it is applied. SeepW does not have an option to apply this flux only in the y-direction. No rainfall is applied to very steep slopes, and instead a potential seepage face boundary condition is applied to these sections.

Seepage Parameters

Unsaturated/saturated hydraulic conductivity functions were estimated using the Van Genuchten method in SeepW, which takes residual water content, saturated horizontal conductivity, and a volumetric water content function as inputs. If not known, the residual water content was set to zero. Volumetric water content functions can be estimated from grain size distribution data using D10, D60, and liquid limit as inputs. If grain size distribution data was not available, a sample function built into SeepW was used with an assumption on the saturated water content. SeepW documentation recommends using a sample function when data is not available because results would still be more accurate than assuming an unsaturated soil is completely saturated.

Recessional sand conductivity was estimated using the vertical conductivity data in Table I-5. The volumetric water content function was estimated from grain size distribution data in Table I-6. The liquid limit was assumed to be zero. The recessional silt layer was assumed completely saturated with a horizontal conductivity of 0.02 ft/day and a Ky/Kx ratio of 0.1. This is based on the vertical conductivity obtained from laboratory data from the sample obtained from a depth of 106 feet below the surface of boring EB-01.

Table I-5: Data used to estimate hydraulic conductivity function for recessional sand and silt

Depth within EB-01 (ft)	Soil Description	Test Type	Final Saturation (%)	Saturated Kv (cm/s)	In-Situ Water Content (%)
15-17	Yellowish Brown GRAVEL w/ silt and sand	Constant	99.5	0.6	8.9
22-24	Yellowish Brown GRAVEL w/ silt and sand	Constant	99.8	0.5	9.8
38.5-39	Grayish Brown Silty SAND	Falling	95.9	3.00E-04	18.2
41-41.5	Grayish Brown Silty SAND (cemented)	Falling	95.1	7.00E-04	36.1
45-47	Yellowish Brown GRAVEL w/ silt and sand	Constant	99.6	0.03	6.6
60-61.5	Olive Gray Silty SAND	Constant	99.2	0.03	15.8
75.5-76	Olive Silty SAND	Falling	95.5	1.00E-05	36.3
80.5-81	Grayish Brown Silty SAND (cemented)	Falling	97.8	9.00E-05	36.5
99-99.5	Olive Silty SAND (slightly cemented)	Falling	95	3.00E-04	40.6
106-106.5	Bluish gray SAND w/ Silt grading to SILT (slightly plastic) (Silt end tested)	Falling	97.5	8.00E-07	35.2

Table I-6: Data used to estimate volumetric water content function for recessional sand

Source	Depth	Description	%Gravel	%Sand	%Silt	%Clay	D10 (mm)	D50 (mm)	D60 (mm)
EB-01	38-40	Greenish Gray Silty SAND	0	72.1	25.5	2.4	0.0438	0.0988	0.109
EB-01	40-42	Greenish Gray Silty SAND	0	58	39.3	2.7	0.0338	0.0843	0.0961
SP-01	75-76.5	Dark Greenish Gray Silty SAND	0	60.4	36.9	2.7	0.0392	0.0859	0.097
EB-01	80-81.5	Dark Greenish Gray Silty SAND	0	82.6	14.9	2.5	0.053	0.122	0.139
EB-01	98-99.5	Dark Greenish Gray Sandy SILT	0	44.5	52.7	2.8	0.0232	0.0695	0.08
SP-01 (excluded from average)	105-106.5	Gray Silty SAND w/ Gravel	24.3	57.3	14.2	4.2	0.0134	0.907	1.71
						Average	0.0386		0.104

The volumetric water content function for the lacustrine layer was estimated from the grain size distribution data in Table I-7. The vertical conductivity was estimated to be 2×10^{-5} ft/day based on CRS laboratory tests.

Table I-7: Data used to estimate volumetric water content function for lacustrine layer

Source	Depth	Description	%Gravel	%Sand	%Silt	%Clay	D10 (mm)	D50 (mm)	D60 (mm)
EB-14vwp_15	219.5-220	Gray Lean CLAY	0	0.2	58.2	41.6	0	0.0074	0.0124
EB-14vwp-15	154.6	Gray Fat CLAY	0	0	16.4	83.6	0	0	0
EB-14vwp-15	145.8	Light Gray CLAY	0	0.4	72.2	27.4	0	0.0069	0.0097
EB-14vwp-15	147.5	Light Gray CLAY	0	0.1	54.8	45.1	0	0.0025	0.0037
EB-14vwp-15	213	Gray Lean Fat CLAY	0	3	88.1	8.9	0.0023	0.0273	0.0332
EB-14vwp-15	219.5-220	Gray Lean CLAY	0	0.5	79.8	19.7	0	0.013	0.0179
EB-14vwp-15	N/A	Light Gray CLAY	0	0	60.3	39.7	0	0.0027	0.0036
EB-14vwp-15	216.7	Light Gray CLAY	0	0	44.3	55.7	0	0.0016	0.0023
EB-14vwp-15	216.9	Light Gray CLAY	0	0	33.2	66.8	0	0.0012	0.0016
EB-14vwp-15	N/A	Light Gray CLAY	0	0	46.4	53.6	0	0.0017	0.0025
EB-14vwp-15	N/A	Light Gray CLAY	0	0.5	46.5	53	0	0.0017	0.0027
EB-14vwp-15	N/A	Gray Fat CLAY	0	0	51.4	48.6	0	0.0022	0.0034
EB-14vwp-15	N/A	Gray Fat CLAY	0	0.2	52.5	47.3	0	0.0023	0.0035
EB-14vwp-15	N/A	Light Gray CLAY	0	0	56.8	43.2	0	0.0028	0.004
EB-14vwp-15	N/A	Light Gray CLAY	0	0	58.8	41.2	0	0.0029	0.0043
EB-14vwp-15	N/A	Light Gray CLAY	0	0.3	74.1	25.6	0	0.007	0.0101
						Average	0.00014	0.0052	0.00718

Built-in sample volumetric water content functions were used for materials with no accompanying laboratory data. A sample volumetric water content function for silty sand was used for the advance outwash. A sample volumetric water content function for a silty clay was used for the till. A sample volumetric water content function for sand was used for the bear lake sand. Any other unspecified parameters were obtained through calibrations with H-1 piezometer data.

Recessional Sand Calibration

The recessional sand conductivity and conductivity ratio was estimated through calibration with groundwater data on January 1, 2016. This data in relation to the till surface and ground surface in shown in Figure I-18. The calibration analysis was done for a section oriented west to east through borings EB-10 and EB-02 on the west and EB-01 on the east.
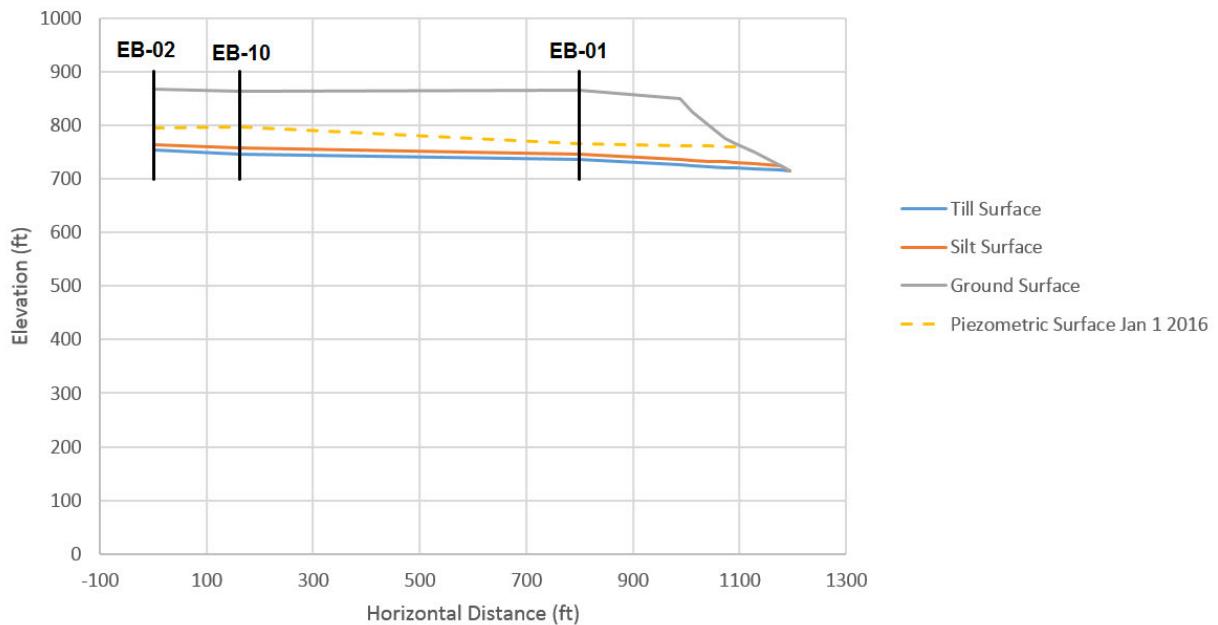
Figure I-18: Piezometric data from January 1, 2016, in relation to the recessional sand topography.

No seepage was assumed for the western boundary and the bottom of the recessional silt layer. A rainfall flux of 0.015 ft/day was applied to the surface of the recessional sand. A potential seepage face boundary condition was applied to the eastern boundary. The boundary conditions are shown below in Figure I-19.
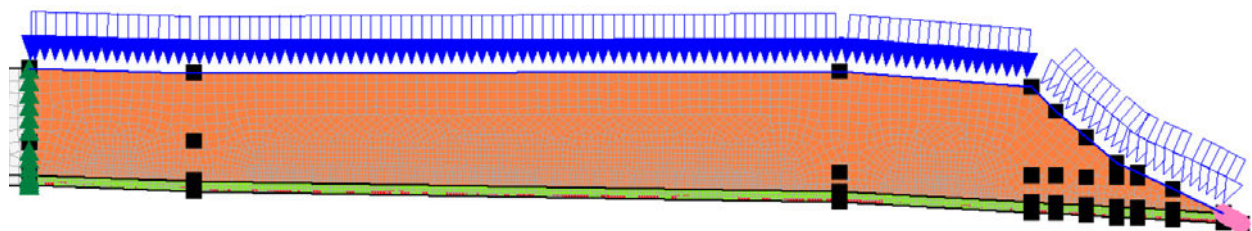
Figure I-19: Recessional sand calibration boundary conditions.

Steady state analyses were run in order to approximately match the piezometer data in Figure I-18. Transient analyses from September 2014 to March 2016 were run in order to capture seasonal fluctuations in the ground water table. The 21-day and 42-day rainfall rates compared with the calculated monthly average rainfall rates are shown in Figure I-20 below. These monthly rainfall fluxes were used for the top boundary condition in transient SeepW analyses.
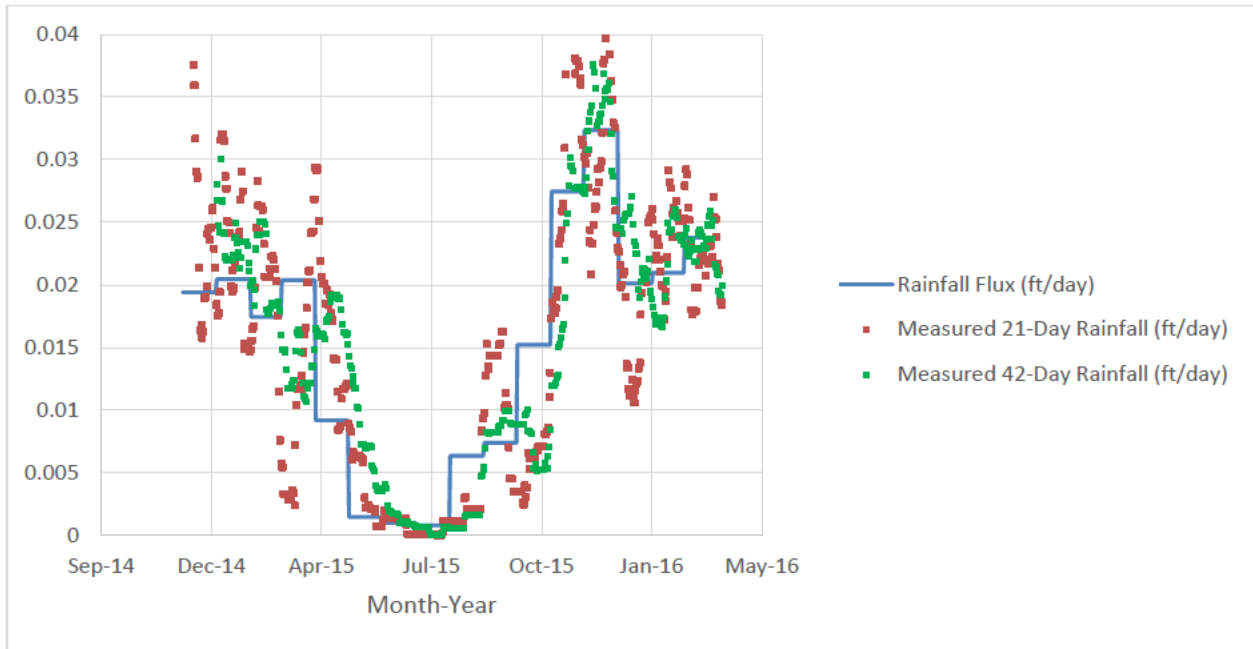
Figure I-20: Rainfall fluxes used in transient SeepW analyses compared with measured 21-day and 42-day rainfall rates.

The results that best match the January 1, 2016, piezometer data were obtained with a horizontal conductivity of 10 ft/day and a conductivity ratio (Horizontal Conductivity:Vertical Conductivity) of 1:1 in the recessional sand. Figure I-21 shows the calculated water surface and distribution of pore pressures at the conclusion of transient analyses using the monthly rainfall fluxes in Figure I-20. The points in the interior of the recessional sand region indicate measured water table elevations from January 1, 2016.
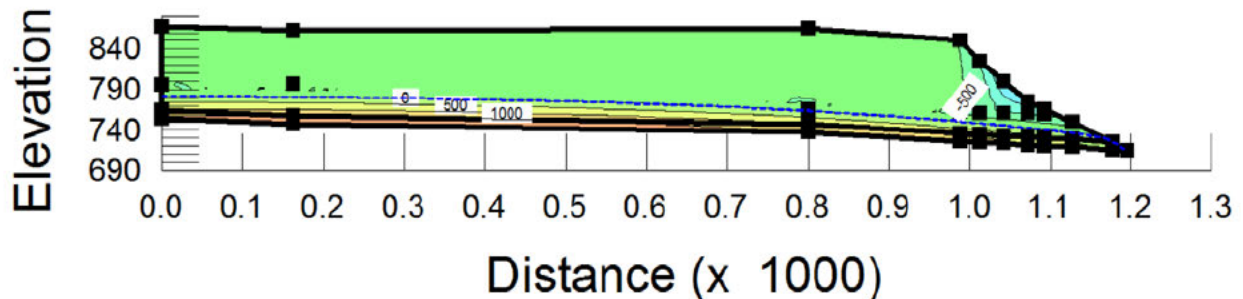
Figure I-21: Recessional sand and gravel pore pressures at the conclusion of transient analyses (contours shown in psf).

Figure I-22 shows the seasonal fluctuations in the recessional sand ground water table calculated with SeepW for a horizontal conductivity of 10 ft/day and a conductivity ratio of 1:1. Results indicate a seasonal fluctuation amplitude of about 5 feet and about a 5-month delay in the response of the groundwater table.
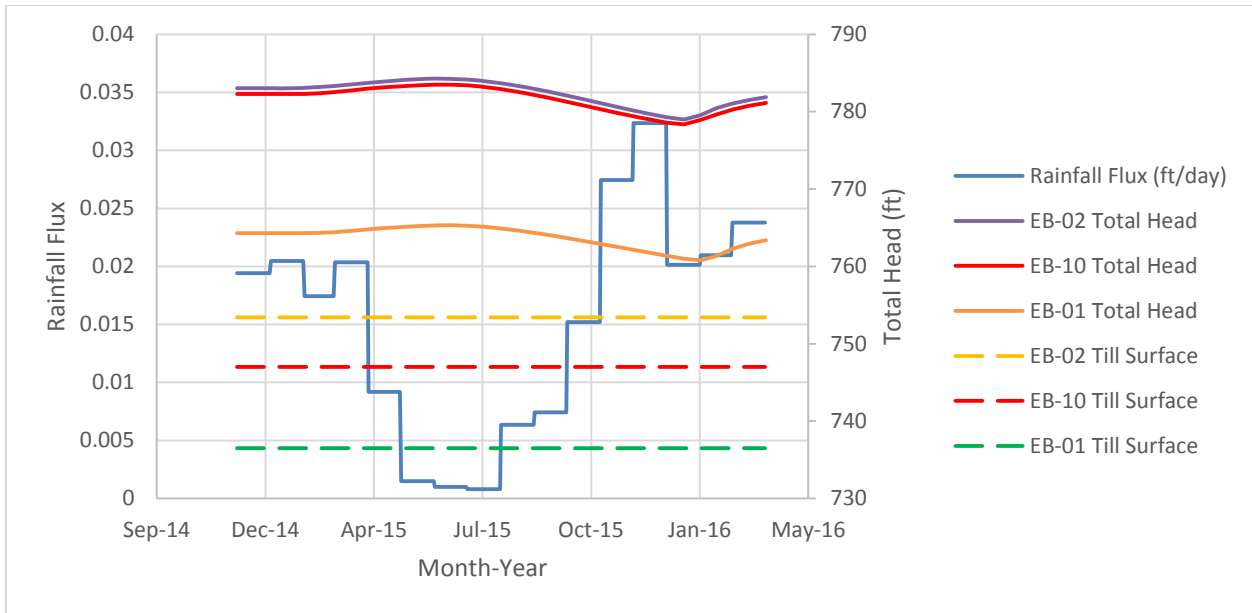
Figure I-22: Seasonal fluctuations in recessional sand calculated by SeepW.

A flux out of the slope face of about 82 gallons/min is estimated from these analyses assuming an out-of-plane length of about 1200 feet.

Calibration of Undisturbed Materials

Calibrations for the undisturbed materials within Whitman Bench were performed based on the H-1 piezometer data. H-1 is located approximately 275 feet back from the 2016 headscarp of the SR 530 landslide. Results at the location of H-1 are unaffected by the conductivity properties of the M-1 debris, so calibrations for the undisturbed materials could be performed separately from calibrations of the debris conductivities. The calibrated conductivity parameters are provided in Table I-8. Note that the orientations of the conductivity directions are inclined or declined through debris materials that have slid down the slope of Whitman Bench.

Table I-8: Calibrated Conductivity Parameters

Material	Fully Saturated?	Kx (ft/day)	Ky/Kx	Saturated Water Content	Residual Water Content
Recessional Outwash	No	10	1	0.37 (from lab data)	0.066
Recessional Silt	Yes	0.02	0.1	0.35 (from lab data)	0
Till	No	0.02	0.05	0.5 (estimated)	0
Advance Outwash	No	1	0.1	0.4 (estimated)	0
Lacustrine	No	0.0025	0.008	0.5 (from lab data)	0
Bear Lake Sand	No	1	0.5	0.3 (estimated)	0

The pore pressure results for the 2006, 2014, and 2016 geometries are shown in Figure I-23. Results for 2006 and 2014 geometries are nearly equivalent since the material bordering the southeast end of the undisturbed materials is the same. Results for the 2016 geometries are different from the 2006 and 2014 geometries because the advance outwash and till have a free seepage face instead of being bounded by disturbed recessional sand and colluvium. The calculated pore pressures are reasonably close to the measured piezometer data. The SeepW results succeed in capturing the confined nature of the lacustrine aquifer by showing local minimum pore pressures near the bottom of the till layer and near the top of the lacustrine layer. The spike in pore water pressure at about elevation 625 feet for the transient analyses is a result of the boundary between the advance outwash sand and the lacustrine silt/clay. The lacustrine soil acts as an aquitard in relation to the more conductive advance outwash sands.
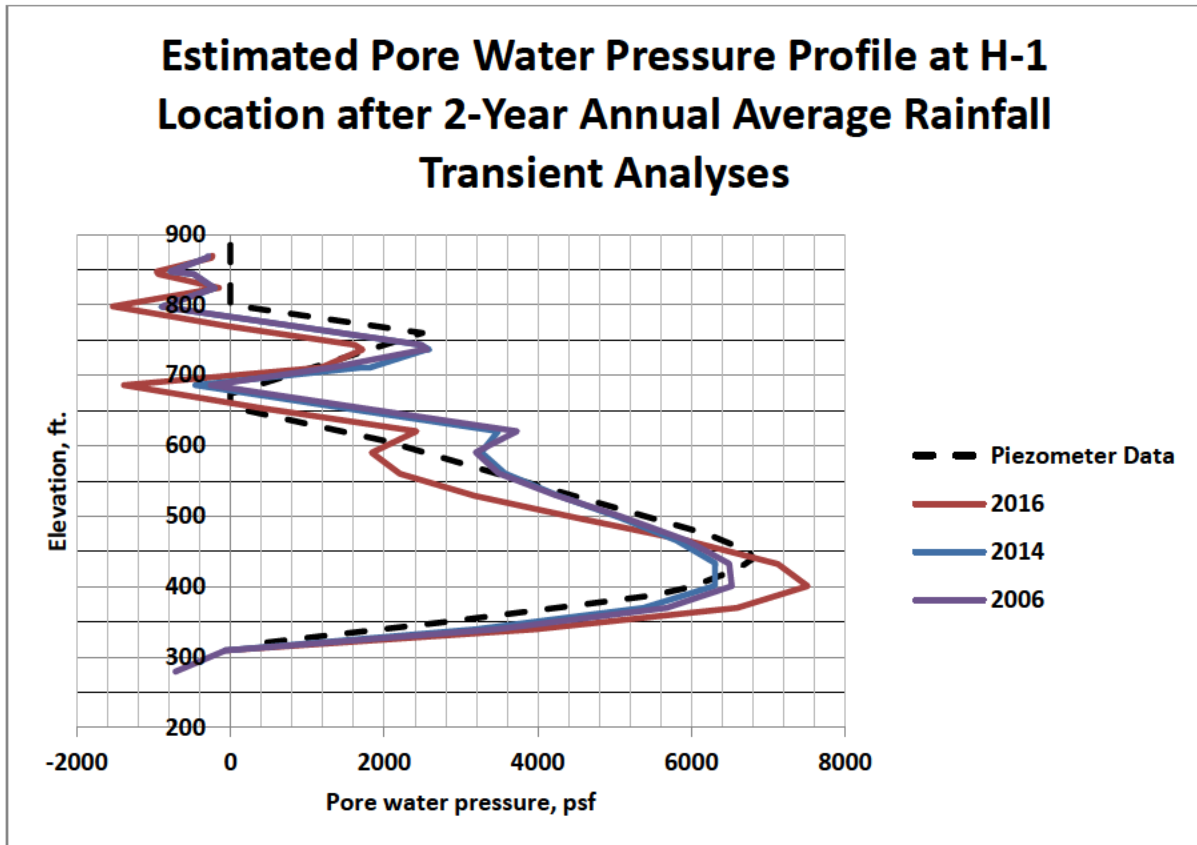
Figure I-23: Porewater pressures at the location of H-1 as measured in the field and as calculated using SeepW.

Pore Pressure Results

Seepage calculations were performed in the following steps:

Step 1: Perform steady state analysis with annual average rainfall of 0.015 ft/day to establish baseline pore pressures.

Step 2: Run transient analysis for 2 years with annual average rainfall to allow water levels to reduce to a minimum level.

Step 3: Run transient analysis for 22 days with a rainfall flux of 0.06 ft/day to represent the 22 days of intense rainfall in the regions surrounding Whitman Bench prior to the SR-530 landslide. This step was only done for the 2014 analyses.

The results following Step 2 are shown in Figures I-24 through I-26 below. As was seen in Figure I-23 above, the pore pressure distributions within the interior of Whitman Bench at the location of H-1were very similar. Note than in Figures I-24a and 24b only, the M1 debris was modeled as a heterogeneous soil with different conductivity layers in order to facilitate ponding and a higher groundwater level. The modeling choice for the M1 debris does not affect pore

pressures in the interior section of Whitman Bench. Due to time constraints, further seepage analyses to refine the piezometric surface within the M1 debris were not performed. The M1 debris in the 2014 analyses and the M2 debris in the 2016 analyses remain homogeneous.
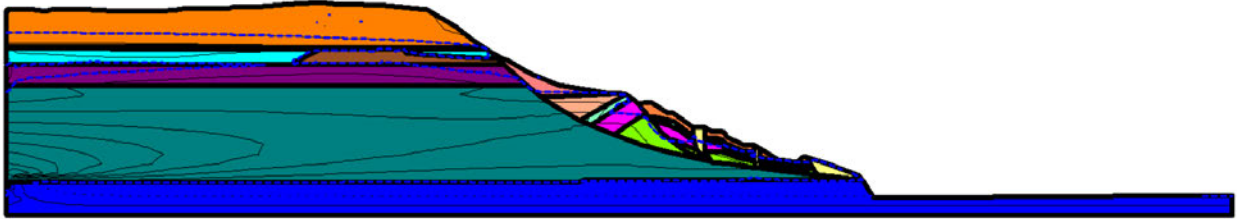
Figure I-24a: 2006 piezometric surface after 2 years of annual average rainfall with an unsimplified M1 debris.
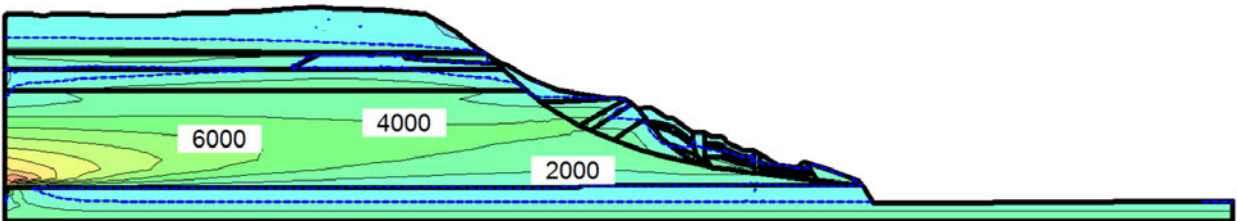
Figure I-24b: 2006 pore pressure distribution after 2 years of annual average rainfall with an unsimplified M1 debris (contour labels shown in psf).
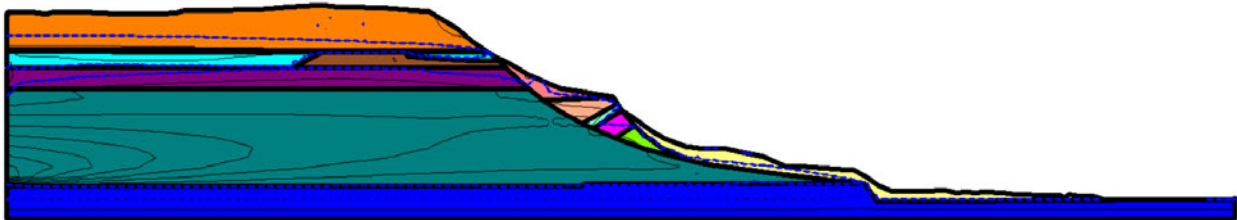
Figure I-25a: 2014 piezometric surface after 2 years of annual average rainfall with homogeneous M1 debris.
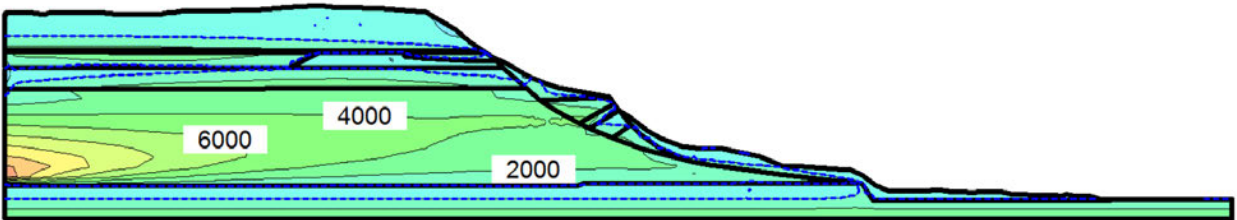
Figure I-25b: 2014 pore pressure distribution after 2 years of annual average rainfall (contour labels shown in psf).
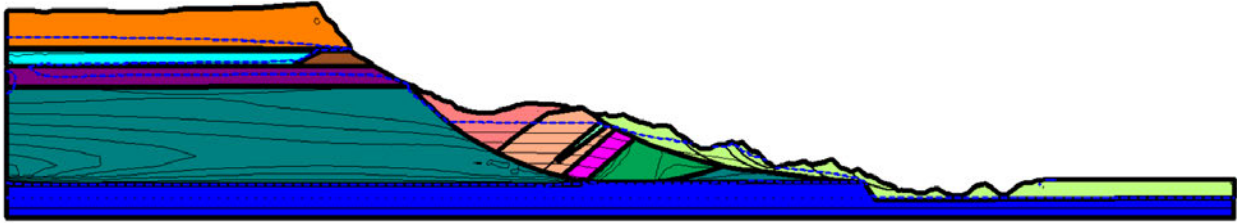
Figure I-26a: 2016 piezometric surface after 2 years of annual average rainfall with homogeneous M2 debris.
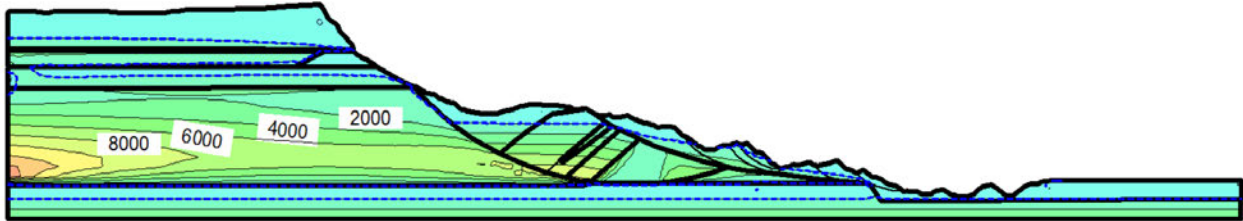
Figure I-26b: 2016 pore pressure distribution after 2 years of annual average rainfall (contour labels shown in psf).

Concluding Remarks

It is not possible to know the piezometric conditions at the time of the SR 530 landslide. Yet the piezometric conditions are key to understanding causation of the slide. Analysis of the piezometric records obtained following the slide have allowed a number of initial speculations advanced by the plaintiffs in this case without benefit of site specific factual information to be ruled out as important causative element. This said, ruling out a particular allegation is not the same as reaching a sound conclusion regarding causation. The use of Finite Element seepage analysis result may allow a bounding of the problem from the slope stability perspective, and suggest causation.

APPENDIX J

Slope Stability Analyses

APPENDIX J – SLOPE STABILITY STUDIES

J.1 - 2006 Landslide Slope Stability Analyses

Introduction

The January 2006 Hazel landslide was back-analyzed to evaluate the capability of static slope stability analysis to capture some of the salient features of this landslide feature with reasonable estimates of soil strength and unit weight parameters, groundwater conditions, and landslide geometry. Preliminary analyses were required to calibrate the values of the soil strength parameters and the likely landslide geometry and groundwater conditions to obtain reasonable results. There is considerable uncertainty of the input to the slope stability analyses, and reasonable back-analyses were only obtained after several iterations. The final set of analyses employed reasonable input parameters and geometry, and therefore provide realistic insights into the conditions of the slope at the time of the 2006 Hazel landslide and some of the mechanisms that likely contributed to its initiation.

Soil Model Stratigraphy

The generalized stratigraphy of Whitman Bench and the Hazel slide at the conclusion of 2005 is shown in Figure J.1-1. The Hazel slide debris had displaced previously multiple times. It is assumed to be disaggregated and modeled as one material type using the strength properties defined in the Interpreted Strength Parameters table in Appendix E. The mid-slope bench is modeled as a heterogeneous zone consisting of different constituent materials from the same table of strength parameters. The materials in the mid-slope bench are somewhat disturbed due to previous episodes of movement. Their strength properties are reduced initially to 90% of their values listed in the Interpreted Strength Parameters table (i.e., 90% of c and tan ϕ). The remaining materials within the Whitman Bench were considered to be undisturbed materials with strength parameters corresponding to the values given in the Interpreted Strength Parameters table in Appendix E.

Figure J.1-1: Generalized stratigraphy of Whitman Bench and the Hazel slide as of 2005 (see legend in Table J.1-1 for the identification of specific soil units).

The Hazel slide is also referred to as the M1 slide material of the 2014 SR-530 landslide. In these analyses, it corresponds to eastern M1 slide debris. The M1 slide material consists of three zones: M1 body material, lower M1 interface immediately adjacent to the lacustrine layer of

Whitman Bench along the bottom of M1, and upper M1 interface immediately adjacent to the mid-slope bench materials (see Figure J.1-1 and Table J.1-1).

The M1 body material was assigned a friction angle of 22 degrees, which is slightly greater than the fully softened friction angle for eastern M1 slide debris. After several iterations wherein the calculated factor of safety was too low, it was realized that the strength of the body of M1 was too low. We hypothesized that the body of M1 was not completely disturbed at the time of the 2006 landslide, so a slightly higher friction angle is reasonable. The upper and lower M1 interfaces are expected to have some strength reduction due to sliding, and were assigned a friction angle of 20 degrees, which corresponds to the fully softened friction angle of the eastern M1 slide debris.

The mid-slope bench, which is also referred to as the M2 slide material of the 2014 SR-530 landslide, consists of five materials: 1) disturbed recessional sand and gravel that is treated as cohesionless colluvium, 2) disturbed recessional sand and gravel, 3) disturbed till, 4) disturbed advance outwash silt and sand, and 5) disturbed lacustrine clay and silt (See Figure J.1-1 and Table J.1-1). The strength parameters of these units are reduced to 90% of their undisturbed strengths. The colluvium is given a friction angle of 26 degrees because it is assumed to be at the angle of repose for a loose cohesionless material. The lacustrine friction angle is representative of its softened strength, which is expected to be the representative strength at the initiation of mass movement failure in this material.

An apparent cohesion value of 200 psf was assigned to the undisturbed lacustrine layer and any disturbed materials that might have a significant percentage of fines with apparent cohesion. The disturbed till is excluded from this additional cohesion because it already had a high cohesion value. The added cohesion provides reasonable factors of safety that indicate marginal stability of the M1 slide debris. This added cohesion is considered to arise from a combination of the presence of cohesive fines in some materials, some ageing/cementation effect, and an apparent cohesion due to capillary suction within unsaturated materials.

An apparent cohesion value of 100 psf was assigned to the undisturbed recessional sand and gravel, as well as the M2 disturbed recessional sand and gravel, because these materials were observed to be steeply inclined at an angle higher than their estimated friction angle. This implies some apparent cohesion, possibly due to capillary suction, but without having a significant percentage of cohesive fines. An apparent cohesion of 100 psf was also assigned to the undisturbed advance outwash layer because this material is expected to contain significant cohesive fines, but since this material is likely saturated, it was not expected to exhibit additional cohesion due to capillary suction.

In these slope stability analyses, a slope failure is assumed to be coincident with an increase in pore water pressures and soil saturation, due to increased rainfall during the winter rainy season. There are other mechanisms that are not captured by these analyses such as erosion of soil due to water flow from springs within the slide mass, which steepens the slope in places as soil is transported downslope. The increased saturation in the debris could also reduce the capillary suction within the M1 and M2 slide debris, so a cohesion of 100 psf is used to represent the failure conditions in late January 2006. The unit weight of the M1 slide debris was also increased

from 115 pcf to 120 pcf to represent the increased weight of water within the recent slide debris material. The cohesion value of the recessional sand layers was reduced to zero for failure conditions, because this cohesion was assumed to emanate solely from capillary suction. The cohesion of the lacustrine layer was also reduced to 100 psf because the surface of rupture of the M1 slide debris might intersect with the undisturbed lacustrine layer, and provide water to this zone. Material properties used in the slope stability analyses are summarized in Table J.1-1.

Table J.1-1: Material Properties (see Figure J.1-1 for generalized stratigraphy)

Materials

Name	Color
Recessional Sand and Gravel above GWT	
Recessional Sand and Gravel below GWT	
Recessional Silt	
Till	
Advance Outwash Silt and Sand	
Lacustrine Clay and Silt	
Bear Lake Sand	
M1 Slide Debris	
M1 Slide Debris Lower Interface	
M1 Slide Debris Upper Interface	
M2 Disturbed Recessional Sand and Gravel	
M2 Disturbed Till	
M2 Disturbed Advance Outwash Silt and Sand	
M2 Disturbed Lacustrine Clay and Silt	
Colluvium	

Material	Unit Weight (pcf)	Model	Cohesion (psf)	Phi (°)
Recessional Sand and Gravel above GWT	120	Mohr-Coulomb	0*, 100	43
Recessional Sand and Gravel below GWT	130	Mohr-Coulomb	0	43
Recessional Silt	125	Mohr-Coulomb	0	38
Till	140	Mohr-Coulomb	2000	40
Advance Outwash Silt and Sand	125	Mohr-Coulomb	100	38
Lacustrine Clay and Silt	125	Mohr-Coulomb	100*, 200	20
Bear Lake Sand	130	Mohr-Coulomb	0	40
M2 Disturbed Recessional Sand and Gravel	120	Mohr-Coulomb	0*, 100	40
M2 Disturbed Till	140	Mohr-Coulomb	1800	37
M2 Disturbed Advance Outwash Silt and Sand	125	Mohr-Coulomb	100*, 200	35
M2 Disturbed Lacustrine Clay and Silt	125	Mohr-Coulomb	100*, 200	18
M1 Slide Debris above Toe of Slide	115, 120*	Mohr-Coulomb	100*, 200	22
M1 Slide Debris Lower Interface	115, 120*	Mohr-Coulomb	100*, 200	20
M1 Slide Debris Upper Interface	115, 120*	Mohr-Coulomb	100*, 200	20
Colluvium	115	Mohr-Coulomb	0	26

*Indicates the value used to represent failure conditions.

Back-Analyses Stages

The 2006 landslide slope stability analyses were performed in two stages. Stage 1 is shown in Figure J.1-2a. In this first stage, the critical surface of rupture was expected to be located within the M1 interfaces, and possibly, somewhat within the M1 body material, or lower lacustrine clay and silt unit (Table J.1-1).

Stage 2 is shown in Figure J.1-2b. The lower part of the M1 debris below the toe of the slide in Stage 2 represents the geometry mapped in 2013. The surface of the upper part of the M1 was dropped approximately 100 feet from its Stage 1 elevation. The topography of the M1 debris was adjusted so that the total volume of the M1 debris in Stage 1 and in Stage 2 would be within 0.1% of each other. No interface zones were used for the M1 debris in Stage 2, because it is assumed to be fully disturbed. In Stage 2, the critical surface of rupture was expected to be shallow, based on our observations, and the mid-slope deep surface of rupture is expected to be marginally stable at this time.
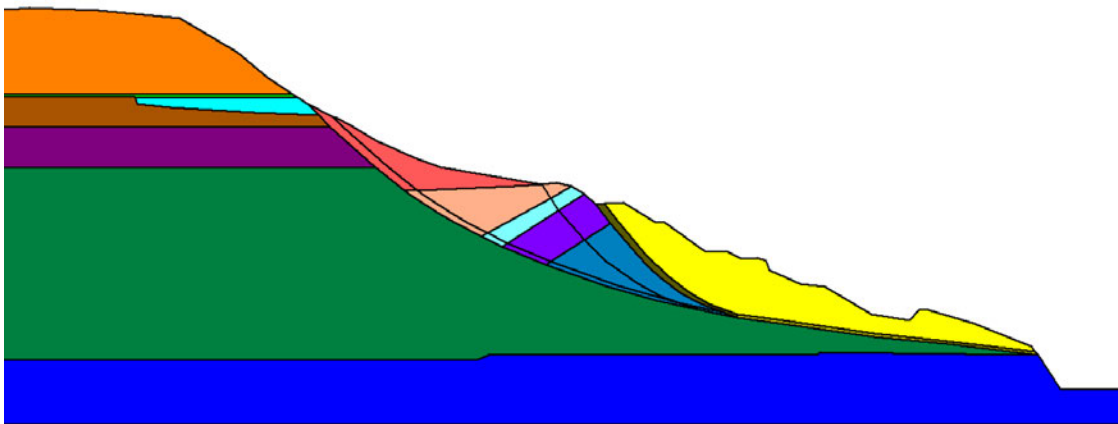
Figure J.1-2a: View of the slide debris material zones in the Stage 1 back-analyses of the 2006 Hazel slide (see legend in Table J.1-1).
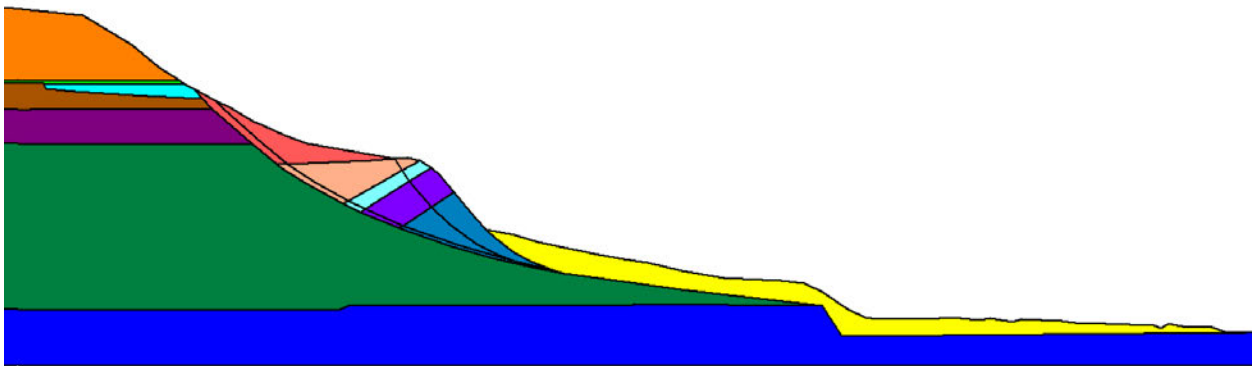
Figure J.1-2b: View of the slide debris material zones in the Stage 2 back-analyses of the 2006 Hazel slide (see legend in Table J.1-1).

Groundwater

The high groundwater level for the 2006 Hazel landslide was estimated based on our interpretation of the piezometer measurements and reasonable interpretations of likely groundwater conditions that existed before the 2014 SR-530 landslide. The height of the assumed groundwater level was varied by 10 feet in the suite of analyses to evaluate the effects of the groundwater level on the stability of the landslide debris. As mentioned previously, there are other mechanisms that are not captured by these analyses such as erosion of soil due to water flow from springs within the slide mass, which steepens the slope in places as soil is transported downslope.

The groundwater levels analyzed in Stage 1 are shown in Figure J.1-3a. The lower three groundwater levels are separated by 10, 20, and 30 feet below the estimated high water level. Slight changes were made to the shape of the groundwater level near the toe of the slide to impart a groundwater level above the low permeability lacustrine layer and to model the groundwater level with a smoothed sloping surface within the M1 debris. The groundwater levels analyzed in Stage 2 are shown in Figure J.1-3b. In the M2 debris sections, the analyzed groundwater levels are again separated by 10 feet. However, they converge to the same path through the M1 debris just above the undisturbed lacustrine clay and silty unit.
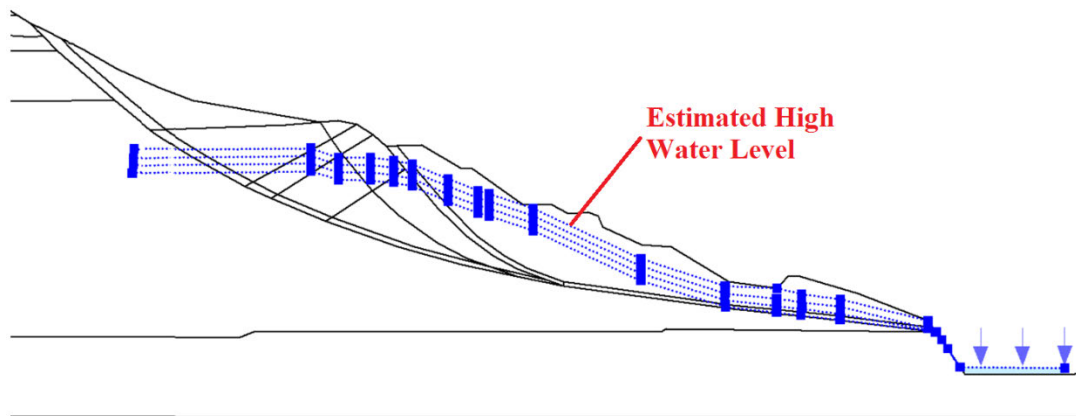
Figure J.1-3a: Groundwater levels used in the slide debris for Stage 1.
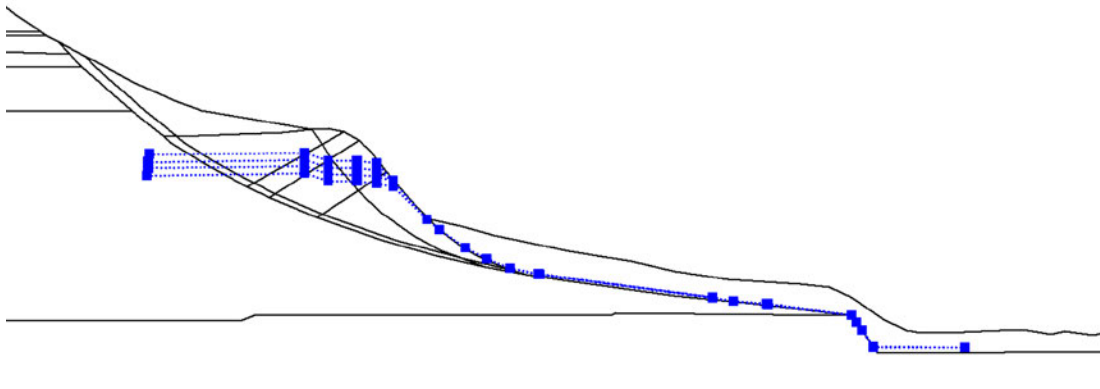
Figure J.1-3b: Groundwater levels used in the slide debris for Stage 2.

Calculation Methods

The Morgenstern-Price and Spencer limit equilibrium methods as implemented in the program SlopeW (GEO-SLOPE International Ltd. 2010. *Stability Modeling with SLOPE/W 2007 Version, An Engineering Methodology*, 4th Ed.) were employed in the slope stability analyses performed for this study. These two methods provided consistent results, so results are only shown for analyses using the Morgenstern-Price method.

Circular surfaces of rupture using the grid and radius method in SlopeW were used to calculate a global minimum factor of safety as shown in Figure J.1-4a. Non-circular surfaces of rupture using the fully specified method in SlopeW were used to calculate the factors of safety for specific surfaces of rupture estimated from field investigations. Fully specified, non-circular surfaces of rupture are shown in Figure J.1-4b. Non-circular surface of rupture 1 corresponds to slip through the two M1 interface materials. Non-circular surface of rupture 2 corresponds to shallow slip through the mid-slope bench as observed for the 2006 Hazel landslide. Non-circular surface of rupture 3 corresponds to the deeper mid-slope surface (also referred to as P2). These fully specified, non-circular surfaces of rupture were also optimized in SlopeW to search for any surface of rupture with a lower factor of safety within the vicinity of the estimated surfaces of rupture. Optimization was performed by randomly adjusting the points of the most critical fully specified surface of rupture for 2000 iterations to calculate a lower factor of safety in the vicinity of the most critical fully specified, non-circular surface of rupture.
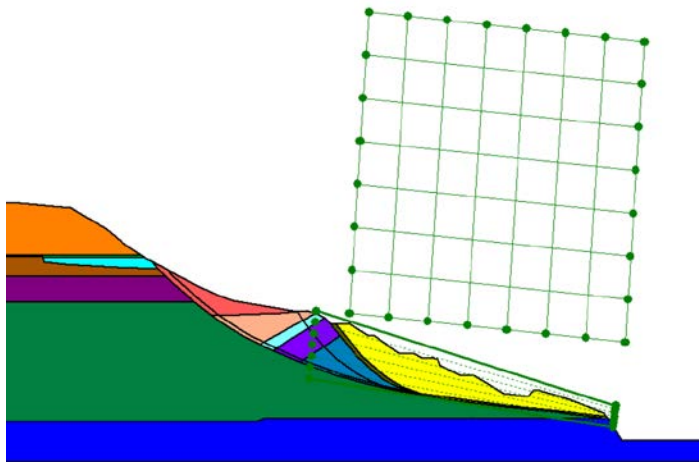
Figure J.1-4a: Circular surface of rupture search using the grid and radius method.
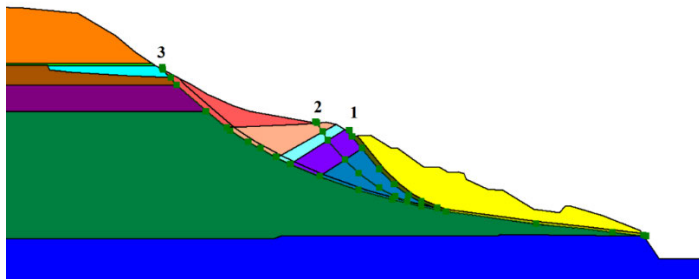
Figure J.1-4b: Fully specified, non-circular surfaces of rupture.

Calibration of Selected Strength Parameters for Initial Stability

Given the uncertainty involved in the slope stability analyses (due to uncertainties in landslide geometry, groundwater levels, and soil parameters), marginal stability is assumed for cases wherein $0.9 \leq FS \leq 1.1$, failure is assumed when $FS < 0.9$, and stability is assumed when $FS > 1.1$. Thus, we judge that a calculated $FS < 0.9$ indicates that a slope failure should have occurred. A calculated $FS > 1.1$ indicates clearly that the slope should be stable for the conditions analyzed. However, for cases wherein $0.9 \leq FS \leq 1.1$, the slope could have failed or could have been marginally stable.

With the pre-failure strength parameters shown in Table J.1-1, the calculated factors of safety (FS) indicate marginal stability (i.e., $FS > 0.9$) when the groundwater level is 30 feet below the estimated high water level. Without the adjustments in the strength parameters (e.g., added cohesion values), the calculated factors of safety for the initial (stable) conditions were below 0.9, which indicates failure. Additionally, use of the residual friction angle for the M1 slide debris (i.e., $\phi = 12^{\circ}$; see Appendix E) resulted in FS values well below 0.9; thus, a higher friction angle was used to characterize this material.

Figures J.1-5a-c show the surfaces of rupture for the groundwater level 30 feet below the estimated high water level. The circular surface of rupture in Figure J.1-5a includes a small amount of M2 material and has a marginally stable factor of safety close to 1. The non-circular surfaces of rupture shown in Figures J.1-5b-c have higher factors of safety than the circular surface of rupture, so the circular surface of rupture involving mostly M1 material is most likely to represent the initial failure geometry. The factor of safety of the circular surface of rupture drops to 0.9 if the groundwater level is raised to 20 feet below the estimated high groundwater level, as shown in Figure J.1-6a. The optimized non-circular surface of rupture is also low, but still above 0.9, and the fully specified surface of rupture actually remains above 1. This further suggests that a circular surface of rupture involving mostly M1 material and only a small amount of M2 material would fail when the water level is raised from 30 feet below the estimated high water level to 20 feet below the estimated high water level.

Table J.1-2 summarizes the factors of safety for different estimated water levels when the pre-failure strength parameters are used. Factors of safety are indicated where the surface of rupture intersects an acceptably small amount of M2 debris that is less than the amount in non-circular surface of rupture 2 (e.g., see Figures J.1-5a and 6a) and where the surface of rupture intersects a large amount of M2 material that approximately corresponds to non-circular surface of rupture 2 (e.g., see Figures J.1-5b and 6b). The factors of safety for the two lowest groundwater levels are consistent with field observations, because the most critical surfaces of rupture with the lowest factors of safety are the surfaces of rupture that involve a relatively small amount of M2 material.
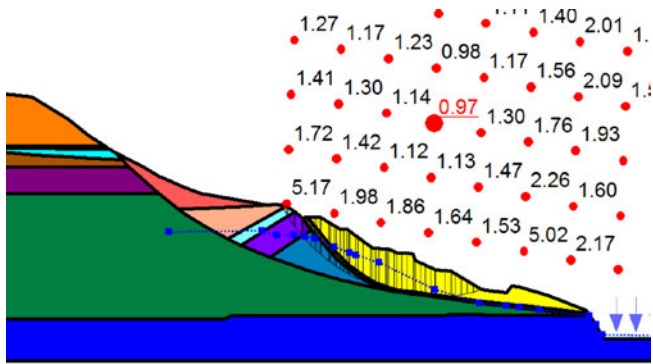
Figure J.1-5a: Critical circular surface of rupture using pre-failure strengths with the groundwater level located 30 feet below its estimated high level.
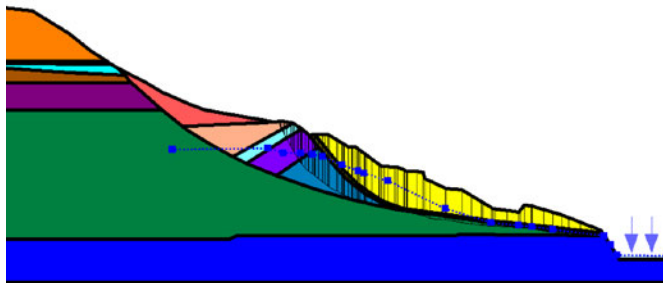
Figure J.1-5b: Optimized non-circular surface of rupture using pre-failure strengths with the groundwater level located 30 feet below its estimated high level.
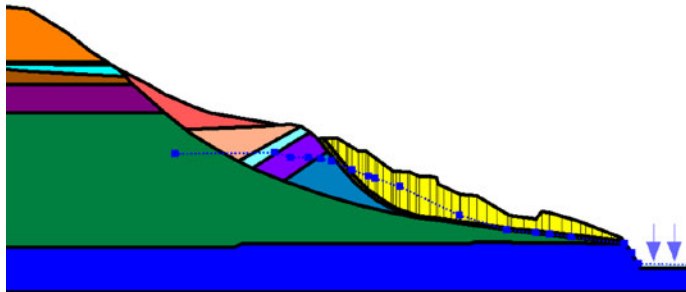
Figure J.1-5c: Fully specified surface of rupture 1 using pre-failure strengths with the groundwater level located 30 feet below its estimated high level.
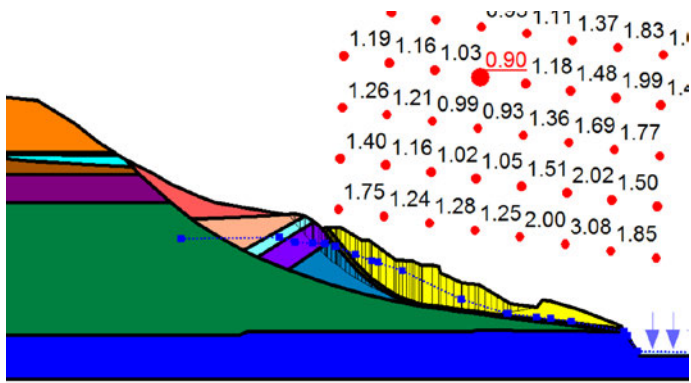
Figure J.1-6a: Critical circular surface of rupture using pre-failure strengths with the groundwater level located 20 feet below its estimated high level.
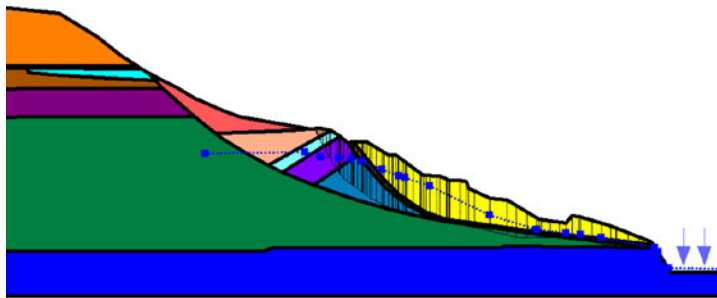
Figure J.1-6b: Optimized non-circular surface of rupture using pre-failure strengths with the groundwater level located 20 feet below its estimated high level.
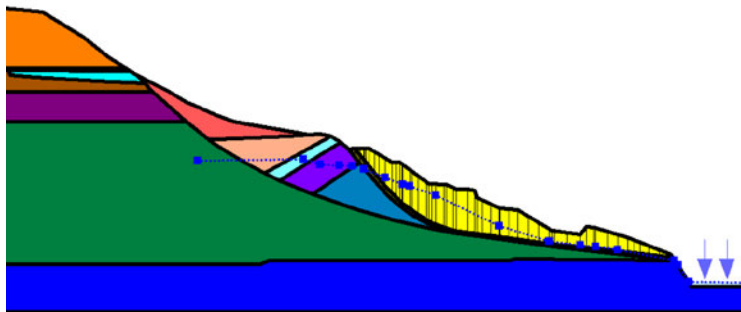
Figure J.1-6c: Fully specified surface of rupture 1 using pre-failure strengths with the groundwater level located 20 feet below its estimated high level.

Table J.1-2: Factors of Safety Obtained Using Pre-Failure Strength Parameters

Position of Groundwater Level Below Estimated High Water Level (feet)	Factor of Safety		
	Non-Circular Surface of Rupture 1	Optimized Non-Circular Surface of Rupture	Circular Surface of Rupture
0	0.81	0.76*	0.76**
10	0.92	0.85*	0.87*
20	1.01	0.92*	0.90**
30	1.09	0.98*	0.97**

*Indicates a surface of rupture that intersects a large amount of M2 debris that approximately corresponds to non-circular surface of rupture 2.
**Indicates a surface of rupture that intersects some M2 debris but less than the amount for non-circular surface of rupture 2.

Assessment of Ponding within M1 Debris

If there is a perched water level within the M1 debris with its surface at the same elevation of the estimated high water level, the pore water pressures along the surface of rupture would be lower. This condition would increase the calculated factor of safety, because the effective stresses along the M1 surface of rupture would be higher. This case was one of the cases analyzed in a larger sensitivity study. It is included herein to illustrate the sensitivity of the analytical results to reasonable variations in the input parameters to the slope stability analyses.

A ponded region with its surface elevation at the high groundwater level is shown in Figure J.1-7a. Figures J.1-7b-d show shallow, medium, and deep ponding cases with the ponded regions shown in purple. The unit weight of the ponded M1 debris was increased to 120 pcf to account for the added weight of water, and the cohesion of the ponded M1 debris was reduced to 100 psf to account for the reduction in capillary suction for a saturated material. Note that the water level outside of the ponded region also corresponds to the high groundwater level but adds no pore water pressures to the M1 interfaces. The effective stresses are equal to the normal stresses within the M1 interfaces and in the M1 body material that has no ponding. The effective stresses within the ponded regions are affected by increased pore water pressures.

Figures J.1-8a-c present the results of a subset of the analyses with shallow, medium, and deep ponding within the M1 debris that does not create any pore pressures along the M1 interfaces. If there is shallow ponding within the M1 debris and no pore water pressures along the M1 interfaces, the M1 debris is more stable with a factor of safety above 1. For medium ponding with no pore pressures along the M1 interfaces, a shallow circular surface of rupture through the ponded region is most critical with a factor of safety slightly below 0.9. The factor of safety for the deep ponded region is below 0.9 for the circular surface of rupture. The shallow ponding case is considered to be most reasonable for the pre-failure case, because it provides a calculated factor of safety that is above 1, so it is marginally stable which is consistent with the pre-failure

state of the slope. Table J.1-3 summarizes the factors of safety for analyses that include ponding in the M1 debris with no pore water pressures along the M1 interfaces.
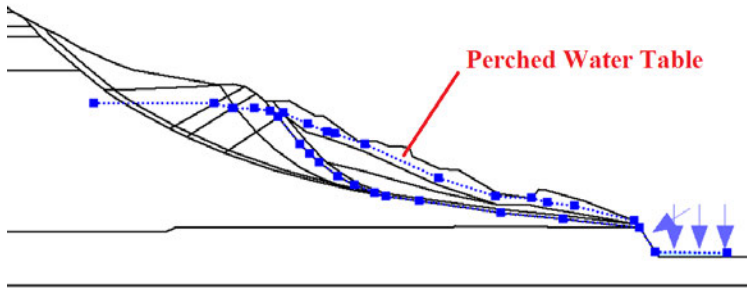
Figure J.1-7a: Perched water level used for ponded region of M1 body material and a groundwater level outside the ponded region. None of these water tables increase pore water pressures within the M1 interfaces.
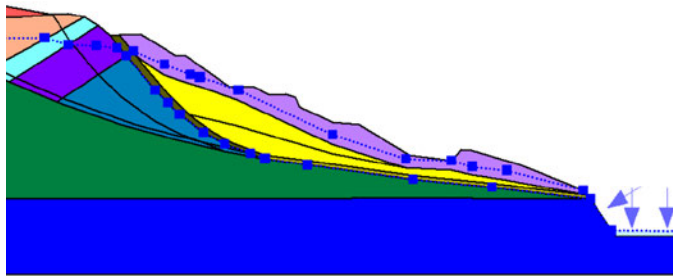
Figure J.1-7b: Shallow ponding schematic with no pore water pressures along M1 interfaces. The ponded region is shown in purple.
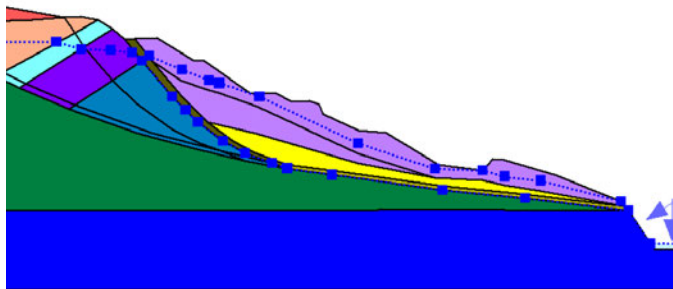
Figure J.1-7c: Medium ponding schematic with no pore water pressures along M1 interfaces. The ponded region is shown in purple.
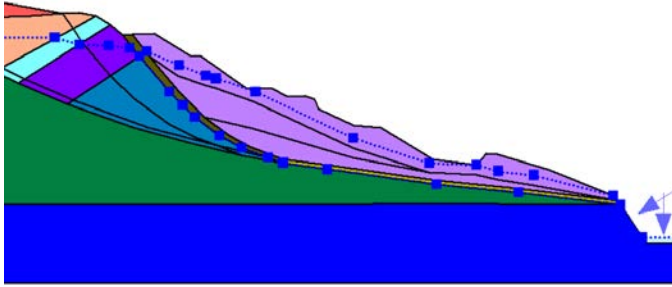
Figure J.1-7d: Deep ponding schematic with no pore water pressures along M1 interfaces. The ponded region is shown in purple.
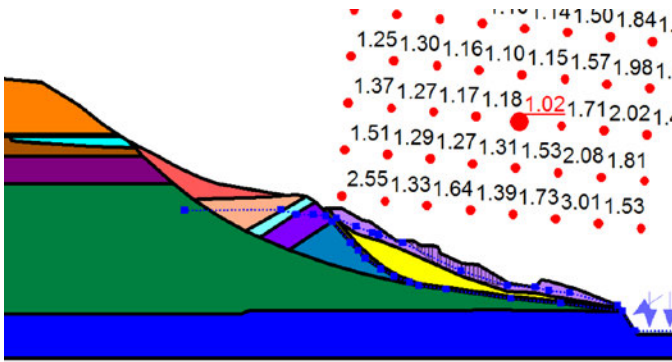
Figure J.1-8a: Circular surface of rupture for shallow ponding with no pore water pressures developed along the M1 interfaces.
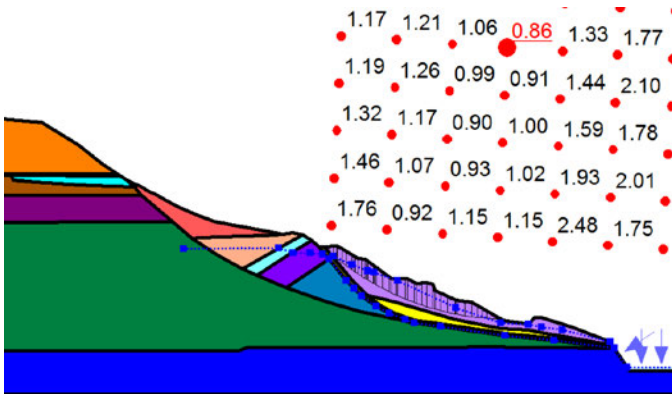
Figure J.1-8b: Circular surface of rupture for medium ponding with no pore water pressures developed along the M1 interfaces.
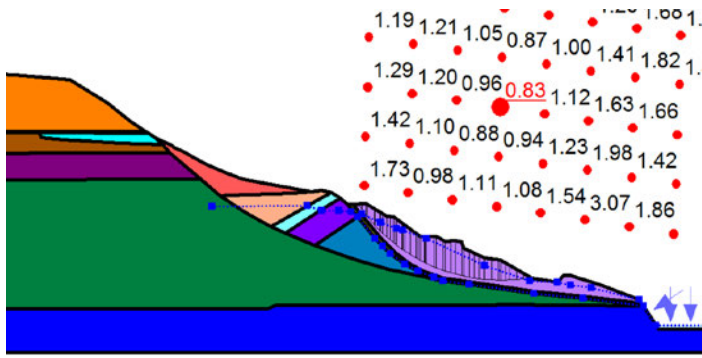
Figure J.1-8c: Circular surface of rupture for deep ponding with no pore water pressures developed along the M1 interfaces.

Table J.1-3: Factors of Safety with Ponding Included in M1 Debris and No Pore Water Pressures Developed along M1 Interfaces

Ponding Type	Factor of Safety		
	Non-Circular Surface of Rupture 1	Optimized Non-Circular Surface of Rupture	Circular Surface of Rupture
Shallow	1.27	1.10*	1.02
Medium	1.27	1.10*	0.86
Deep	1.27	0.99*	0.83

*Indicates a surface of rupture that intersects a large amount of M2 debris that approximately corresponds to non-circular surface of rupture 2.

Some pore water pressures were likely present along the interfaces of the M1 debris. Analyses were also performed with different estimates of the water levels that were applied to the M1 interfaces along with a perched water level within the M1 body. When no pore water pressures were developed along the M1 interface for the shallow ponding case, the factor of safety was above 1 for circular and non-circular surfaces of rupture. When pore water pressures were developed from a groundwater level directly below the ponded region, the factor of safety drops dramatically to about 0.85. This is due to the fact that the shallow ponding case considered has high pore pressures, because the groundwater level that creates the M1 interface pore pressures in these cases is approximately 15 feet below the high groundwater level. In the analyses that do not consider ponding (Table J.1-2), the calculated factors of safety were below 0.9 for circular surfaces of rupture when the groundwater level was less than 20 feet below the estimated high water level. The Hazel landslide is marginally stable if shallow ponding is present within the M1 debris level and pore pressures along the M1 interface are developed from a groundwater level no higher than the bottom of the medium ponded region as shown in Figure J.1-8d. The results of this set of analyses are summarized in Table J.1-4.
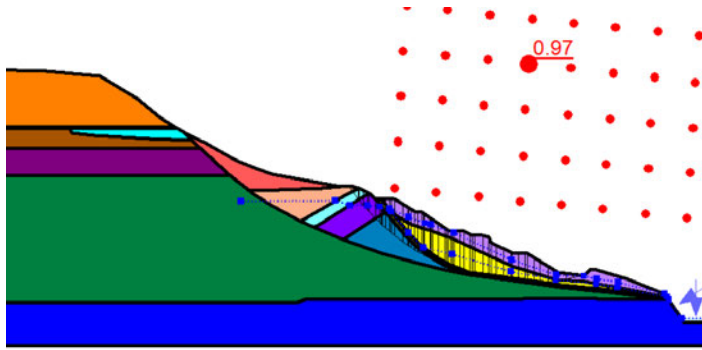
Figure J.1-8d: Circular surface of rupture for shallow ponding with M1 interface pore water pressures developed from the medium ponding case.

Table J.1-4: Factors of Safety with Ponding Included in M1 Debris and Pore Water Pressures Developed along M1 Interfaces

| Ponding Type | Factor of Safety | | |
	Non-Circular Surface of Rupture 1	Optimized Non-Circular Surface of Rupture	Circular Surface of Rupture
Shallow	0.96	0.87*	0.85**
Medium	1.08	0.96*	0.86
Deep	1.21	1.05*	0.83
Shallow with Interface Pore Pressures of Medium Ponding	1.09	0.96*	0.97**

*Indicates a surface of rupture that intersects a large amount of M2 debris that approximately corresponds to non-circular surface of rupture 2.
**Indicates a surface of rupture that intersects some M2 debris but less than the amount for non-circular surface of rupture 2.

Stage 1 - 2006 Hazel Landslide Analysis

The engineering soil properties listed in Table J.1-1 for the failure scenario are used in the Stage 1 – 2006 Hazel landslide analyses. When the groundwater level is 30 feet below its estimated high level, the calculated factors of safety indicate marginal stability with $0.95 \leq FS \leq 1.04$ (Figures J.1-9a-b). When the groundwater level is raised to 20 feet below the estimated high water level, the calculated FS falls below 0.9 (Figures J.1-9c-d). When the pre-failure strengths were used, all factors of safety remained above or equal to 0.9 when the water level was 20 feet below the estimated high water level. The factors of safety for these analyses are summarized in Table J.1-5.
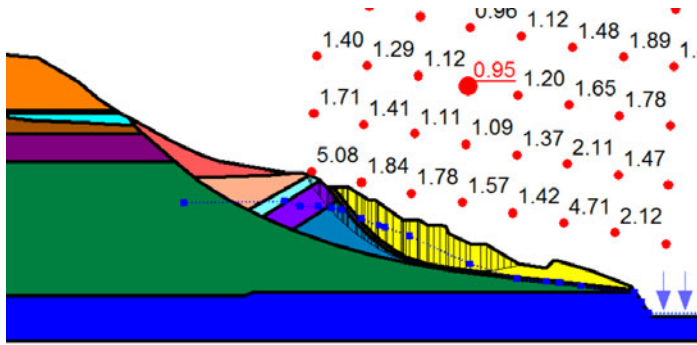
Figure J.1-9a: Critical circular surface of rupture using at-failure strength parameters with the groundwater level located 30 feet below its estimated high level.
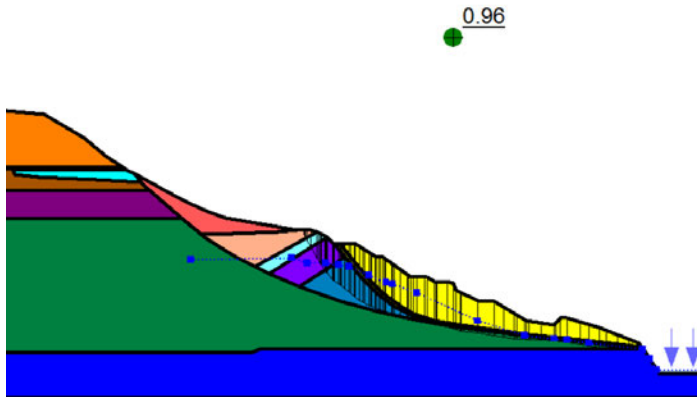
Figure J.1-9b: Optimized non-circular surface of rupture using at-failure strength parameters with the groundwater level located 30 feet below its estimated high level.
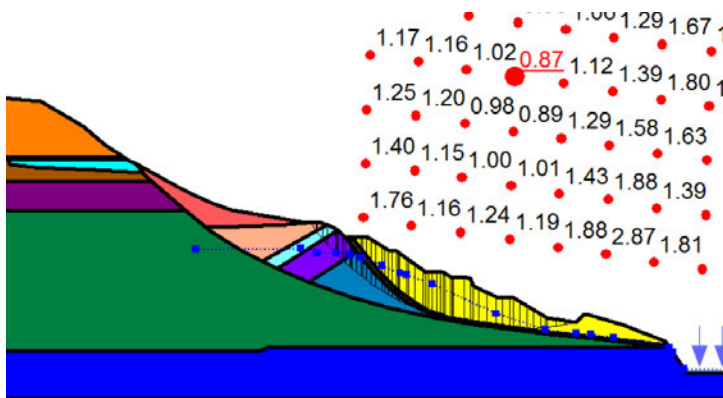
Figure J.1-9c: Critical circular surface of rupture using at-failure strength parameters with the groundwater level located 20 feet below its estimated high level.
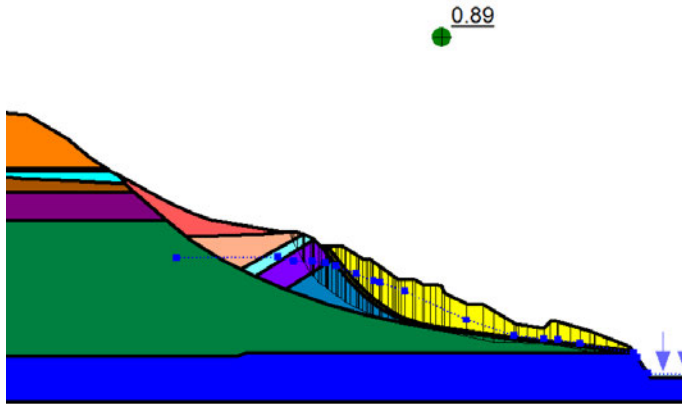
Figure J.1-9d: Optimized non-circular surface of rupture using at-failure strength parameters with the groundwater level located 20 feet below its estimated high level.

Table J.1-5: Factors of Safety Obtained Using Strength Parameters at Failure

Position of Groundwater level Below Estimated High Water Level (feet)	Factor of Safety		
	Non-Circular Surface of Rupture 1	Optimized Non-Circular Surface of Rupture	Circular Surface of Rupture
0	0.78	0.74*	0.73**
10	0.88	0.82*	0.85**
20	0.97	0.89*	0.87**
30	1.04	0.96*	0.95**

*Indicates a surface of rupture that intersects a large amount of M2 debris that approximately corresponds to non-circular surface of rupture 2.
**Indicates a surface of rupture that intersects some M2 debris but less than the amount for non-circular surface of rupture 2.

The analyses indicate that the critical surface of rupture includes a small part of the M2 debris. If a tension crack forms along the upper M1 interface, then the surface of rupture would follow this low-resistance path instead of intersecting M2 debris. To analyze the effects of a tension crack, the strength parameters for the upper M1 interface were reduced to zero. The tension crack was assumed to be filled with water by analyzing cases that include shallow, medium, and deep ponding with pore water pressures along the lower M1 interface resulting from a water level that coincides with the bottom of the ponded region. The results of these analyses are shown in Figures J.1-10a-d for shallow and medium ponding. The factors of safety are summarized in Table J.1-6. All of the calculated factors of safety are below 0.9, which indicate that the M1 debris would fail for these conditions.

The Stage 1 – 2006 Hazel landslide slope stability analyses suggest that the 2006 Hazel landslide was likely to occur when the groundwater level rises within the M1 slide debris. Surfaces of rupture will not intersect M2 debris if a tension crack with zero strength forms along the upper M1 interface.
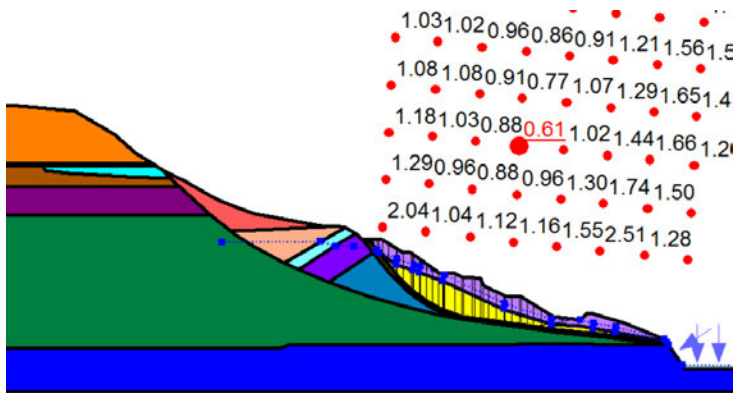
Figure J.1-10a: Circular surface of rupture for shallow ponding with a tension crack formed along the upper M1 interface.
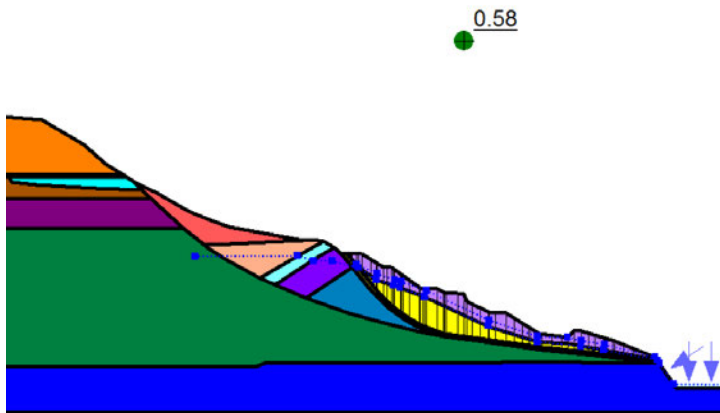
Figure J.1-10b: Optimized non-circular surface of rupture for shallow ponding with a tension crack formed along the upper M1 interface.
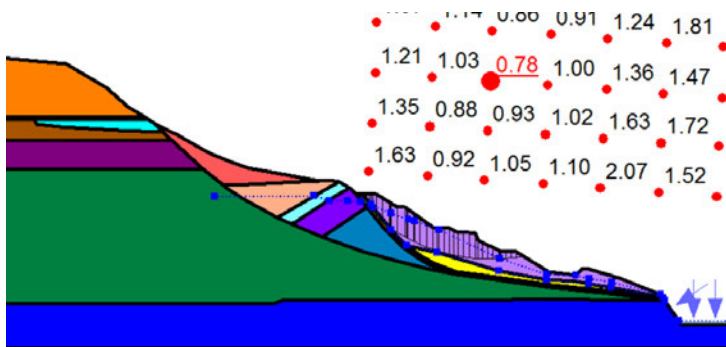
Figure J.1-10c: Circular surface of rupture for medium ponding with a tension crack formed along the upper M1 interface.
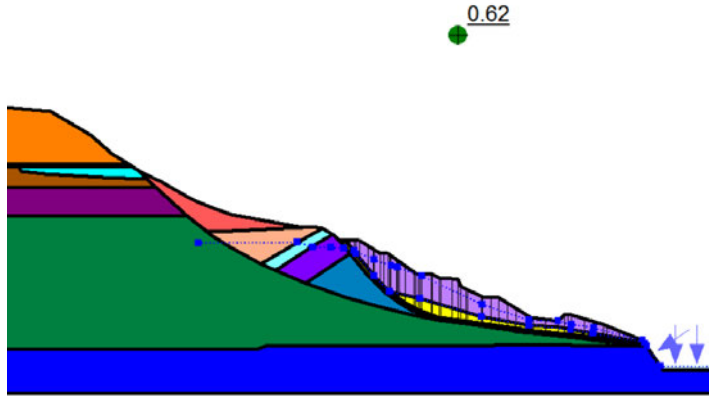
Figure J.1-10d: Optimized non-circular surface of rupture for medium ponding with a tension crack formed along the upper M1 interface.

Table J.1-6: Factors of Safety with Tension Crack Formed along Upper M1 Interface and Ponding

Ponding Type	Factor of Safety		
	Non-Circular Surface of Rupture 1	Optimized Non-Circular Surface of Rupture	Circular Surface of Rupture
Shallow	0.61	0.58	0.61
Medium	0.64	0.62	0.78
Deep	0.72	0.69	0.67

Stage 2 - 2006 Hazel Landslide Analyses

The Stage 2 – 2006 Hazel landslide failure is expected to be a partial failure of the mid-slope bench following failure of the M1 debris. The M1 debris was lowered 100 feet in the Stage 2 failure analyses, and the total volume of M1 debris was kept equal to the volume it had in Stage 1. A residual friction angle of 12 degrees was used for the M1 debris, because it is in the midst of sliding in this stage. Figures J.1-11a-f show selected results of the Stage 2 slope stability analyses. The circular surfaces of rupture shown in Figures J.1-11a and 11e indicate shallow failures within the M2 disturbed lacustrine and advance layers. All optimized non-circular surfaces of rupture found that a failure through the mid-slope bench that corresponds to non-circular surface of rupture 2 with an exit above the M1 debris to be most critical. The factors of safety for non-circular surface of rupture 3 were close to or above 1. This factor of safety is not expected to reduce significantly following the Stage 2 failure, because the failed M2 material would likely still provide a buttressing force for the rest of the mid-slope bench. The results of Stage 2 analyses are summarized in Table J.1-7.

These slope stability analyses suggest that failure of part of the mid-slope bench likely occurred soon after the M1 slide material failed. This is consistent with the observations following the 2006 landslide. After the 2006 Hazel landslide, the mid-slope bench was marginally stable.
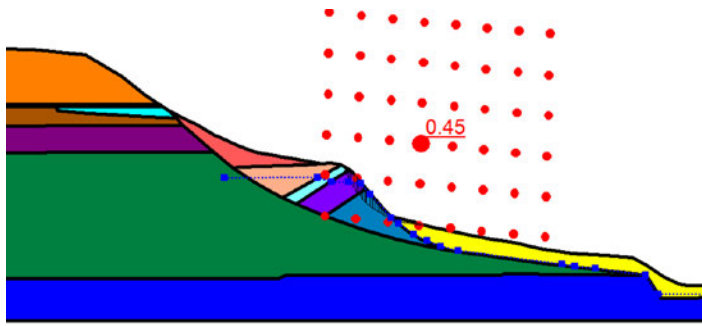
Figure J.1-11a: Critical circular surface of rupture with the groundwater level at the estimated high water level.
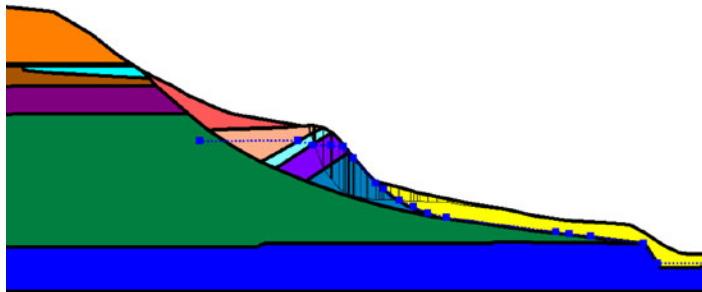
Figure J.1-11b: Optimized non-circular surface of rupture with the groundwater level at the estimated high water level.
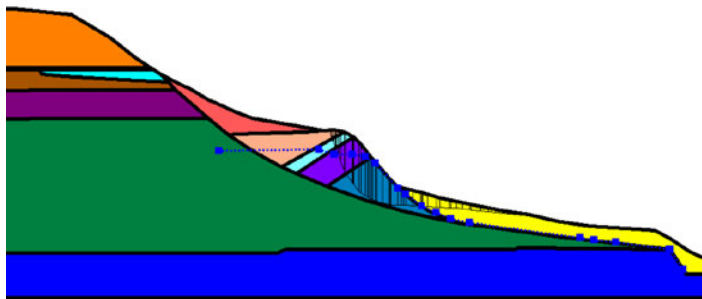
Figure J.1-11c: Optimized non-circular surface of rupture with the groundwater level 10 feet below the estimated high water level.
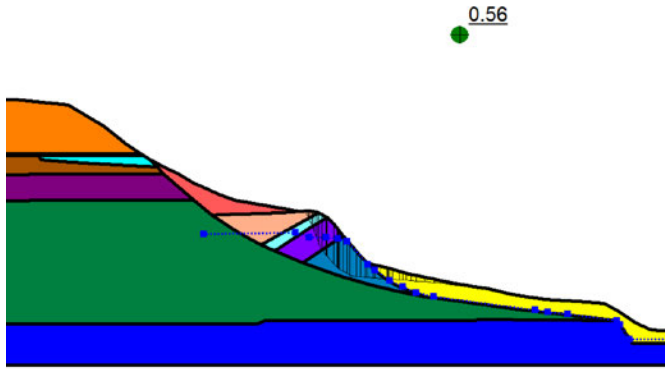
Figure J.1-11d: Optimized non-circular surface of rupture with the groundwater level 20 feet below the estimated high water level.
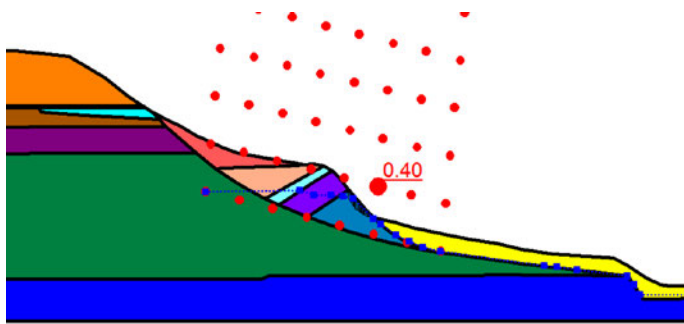
Figure J.1-11e: Critical circular surface of rupture with the groundwater level 30 feet below the estimated high water level.
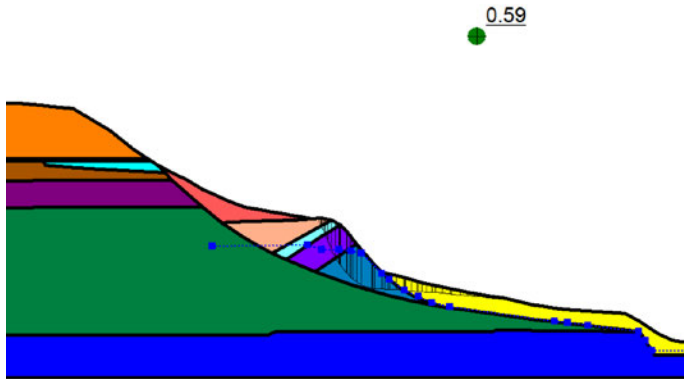
Figure J.1-11f: Optimized non-circular surface of rupture with the groundwater level 30 feet below the estimated high water level.

Table J.1-7: Stage 2 Failure Factors of Safety

Position of Groundwater level Below Estimated High Water Level (feet)	Non-Circular Surface of Rupture 2	Non-Circular Surface of Rupture 3	Optimized Non-Circular Surface of Rupture	Circular Surface of Rupture
0	0.84	1.05	0.55	0.45
10	0.85	1.09	0.56	0.54
20	0.86	1.12	0.56	0.52
30	0.88	1.15	0.59	0.40

Findings

The findings of the back-analyses of the 2006 Hazel landslide are:

- Marginally stable factors of safety (i.e., above 0.9) are calculated for the 2005 conditions with a low groundwater level. Thus, the slope stability analyses support the 2005 slide geometry being marginally stable before the January 2006 Hazel landslide with the calibrated soil parameters and estimated landslide geometry for a low groundwater and pore water pressure condition.

- Calculated factors of safety are higher for the pre-failure condition if negligible pore water pressures are assumed along the M1 interfaces and shallow ponding is assumed within the M1 debris material. Shallow ponding with the assumed low pore water pressures produces calculated factors of safety above 0.9 for circular and non-circular surfaces of rupture. Thus, it is possible that the groundwater conditions were not in equilibrium before failure and that the pore water pressures along the surface of rupture at the pre-failure stage are lower than those assumed with a high groundwater level in the analyses without ponding. For example, the Hazel landslide is marginally stable if shallow ponding is present within the M1 debris level, and the groundwater level for the surface of rupture is assumed to be at least 20 feet below the estimated high water level.

- When the groundwater level is increased to 20 feet below the estimated high groundwater level, the calculated factor of safety drops to or below 0.9, which indicates failure as observed for the January 2006 Hazel landslide. Thus, the slope stability analyses support the initiation of the January 2006 Hazel landslide with the calibrated soil parameters and landslide geometry for an increased groundwater and pore water pressure condition. The slope stability analyses indicate that landslide stability depends significantly on the groundwater conditions in the slope.

- Circular surfaces of rupture are generally more critical than non-circular surfaces of rupture, and these circular surfaces of rupture utilize a smaller portion of the M1 interfaces than the non-circular surface of ruptures. The circular surfaces of rupture also include a small part of the M2 material. The Stage 1 surfaces of rupture do not intersect M2 debris if a tension crack forms along the upper M1 interface.

- The Stage 2 analyses indicate that a partial failure of the mid-slope bench is possible, which corresponds to non-circular surface of rupture 2 with an exit above the failed M1 debris. The non-circular surface of rupture 3 is moderately stable during Stage 2 analyses and likely remained moderately stable if the failed M2 material continued to act as a buttressing force for the remaining part of the mid-slope bench.

- There are other mechanisms that are not captured by these analyses, such as erosion of soil due to water flow from springs within the slide mass, which steepens the slope in places as soil is transported downslope. Therefore, these findings are only appropriate for gaining insight for the conditions analyzed, which focused on the effects of groundwater.

APPENDIX J – SLOPE STABILITY STUDIES

J.2 - 2014 Landslide Slope Stability Analyses

Introduction

The March 22, 2014 SR-530 landslide was analyzed using static slope stability procedures to capture some of the salient features of this landslide and to evaluate some of the potential triggering mechanisms using reasonable estimates of soil strength and unit weight parameters, groundwater conditions, and landslide geometry. The soil parameters are based on the results of field and laboratory tests and calibration analyses of the 2006 Hazel landslide (see Appendices D and I.1). Additionally, the post-2006 landslide geometry, which is based on the 2013 LiDAR survey, was used as the pre-failure geometry of the 2014 landslide for further calibration analyses. The final set of analyses employed reasonable input parameters and geometry, and therefore provide realistic insights into the conditions of the slope at the time of the 2014 SR-530 landslide and some of the mechanisms that likely contributed to its initiation.

Soil Model Stratigraphy

The generalized stratigraphy of the Whitman Bench and the Hazel slide as of the conclusion of 2013 is shown in Figure J.2-1. This cross section is approximately in the center of the slide area, and represents an average condition. To the east and west of this central section, both the un-failed strata and the post-2006 Hazel slide debris have varying cross sections and material makeup. The post-2006 Hazel slide debris is assumed to be disaggregated significantly and is modeled as one material type, initially using the strength properties defined in the Interpreted Strength Parameters table in Appendix E. The mid-slope bench is modeled as a heterogeneous zone consisting of different constituent materials from the same table of strength parameters. The materials in the mid-slope bench are somewhat disturbed due to previous episodes of movement. Their strength properties are reduced initially to 90% of their values listed in the Interpreted Strength Parameters table (i.e., 90% of c and tan ϕ). The remaining materials within the Whitman Bench were considered to be undisturbed materials with strength parameters corresponding to the values given in the Interpreted Strength Parameters table in Appendix E.

Figure J.2-1: Generalized stratigraphy of Whitman Bench and the Hazel slide as of 2013 (see legend in Table J.2-1 for the identification of specific soil units).

The Hazel slide debris is also referred to as the M1 slide material of the 2014 SR-530 landslide. In these analyses, it corresponds to the eastern M1 slide debris. The M1 material was assigned a friction angle of 18 degrees, which corresponds to 90% of the fully softened frictional strength

(i.e., tan ϕ) of the eastern M1 slide debris material (see Figure J.2-1 and Table J.2-1). The reduction represents the effects of partial remolding and disruption. It is assumed that a residual strength characterization is not appropriate, because the pre-failure geometry is not stable if residual strength for this material are used. It is likely that the 2006 Hazel slide dug into the lacustrine clay and silt unit in some areas, and reconsolidation of the debris and slide materials with ageing effects increased the strength of the M1 material and its interface with materials below it.

The mid-slope bench, which is also referred to as the M2 slide material of the 2014 SR-530 landslide, consists of five materials: 1) disturbed recessional sand and gravel that is treated as cohesionless colluvium, 2) disturbed recessional sand and gravel, 3) disturbed till, 4) disturbed advance outwash silt and sand, and 5) disturbed lacustrine clay and silt (see Table J.2-1). The strength parameters of these units were reduced to 90% of their undisturbed strengths. The colluvium was given a friction angle of 26 degrees, because it is assumed to be at the angle of repose for a loose cohesionless material. The lacustrine friction angle is representative of its fully softened strength (i.e., $\phi = 20^o$), which is expected to be representative of its condition at the initiation of mass movement failure in this material.

An apparent cohesion value of 200 psf was assigned to M2 debris materials that might have a significant amount of fines with apparent cohesion (Table J.2-1). The disturbed till is excluded from this additional cohesion, because it already had a high cohesion value. The added cohesion gives reasonable factors of safety that indicate marginal stability of the M2 slide debris. This added cohesion is considered to arise from a combination of the presence of cohesive fines in some materials, some ageing/cementation effects, and an apparent cohesion due to capillary suction within unsaturated materials. An apparent cohesion value of 200 psf was assigned to the undisturbed lacustrine clay and silt unit for similar effects. The cohesion value of the M1 debris in the year 2013 was maintained at the value used in the 2006 Hazel landslide failure analyses (i.e., c = 100 psf) to account for the disturbance of the debris following the 2006 slide.
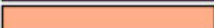
An apparent cohesion value of 100 psf was assigned to the undisturbed recessional sand and gravel as well as the M2 disturbed recessional sand and gravel because these materials were observed to be steeply inclined at a slope greater than their friction angle. This implies some apparent cohesion, possibly due to capillary suction, but without having significant cohesive fines. An apparent cohesion of 100 psf was also given to the undisturbed advance outwash layer, because this material was expected to have significant cohesive fines, but as this material is likely saturated, it was not expected to possess any additional cohesion due to capillary suction.

In these slope stability analyses, a slope failure is assumed to be coincident with an increase in pore water pressures and soil saturation, due to increased rainfall during the winter rainy season. There are other mechanisms that are not captured by these analyses such as erosion of soil due to water flow from springs within the slide mass, which steepens the slope in places as soil is transported downslope. The increased saturation of the debris would also reduce the capillary suction within the M1 and M2 slide debris, so a cohesion of 100 psf and 50 psf for the M2 and M1 debris, respectively, was used to represent the failure conditions on March 22, 2014. The cohesion value of the recessional sand layers was reduced to zero for the failure conditions, because this cohesion was assumed to emanate solely from capillary suction. Along with the

reduction in cohesion, the unit weight of the M1 slide debris was increased from 115 pcf to 120 pcf to replicate the increased weight of water within the debris material. The cohesion of the lacustrine clay and silt unit was also reduced to 100 psf, because the failure surface of the M1 slide debris might intersect with the undisturbed lacustrine unit and provide water to this zone.

Material properties used in the slope stability analyses are summarized in Table J.2-1. Analyses were also performed with alternative strength parameters (e.g., c'=400 psf and ϕ' = 27° for the lacustrine unit) to evaluate the sensitivity of the results. The input and output files of these analyses are included in the electronic files. In summary, the results presented herein are not highly sensitive to reasonable variations in the strength parameters used in the analyses.

Table J.2-1: Material Properties (see Figure J.2-1 for generalized stratigraphy)

Materials

Name	Color
M1 Debris	
Lacustrine	
Bear Lake Sand	
Advance	
Till	
Recessional	
Silt	
Saturated Recessional	
M2 Disturbed Lacustrine	
M2 Disturbed Advance	
M2 Disturbed Recessional	
Colluvium	
M2 Disturbed Till	

Material	Unit Weight (pcf)	Model	Cohesion (psf)	Phi (°)
Recessional Sand and Gravel above GWT	120	Mohr-Coulomb	0*, 100	43
Recessional Sand and Gravel below GWT	130	Mohr-Coulomb	0	43
Recessional Silt	125	Mohr-Coulomb	0	38
Till	140	Mohr-Coulomb	2000	40
Advance Outwash Silt and Sand	125	Mohr-Coulomb	100	38
Lacustrine Clay and Silt	125	Mohr-Coulomb	100*, 200	20
Bear Lake Sands	130	Mohr-Coulomb	0	40
M2 Disturbed Recessional Sand and Gravel	120	Mohr-Coulomb	0*, 100	40
M2 Disturbed Till	140	Mohr-Coulomb	1800	37
M2 Disturbed Advance Outwash Silt and Sand	125	Mohr-Coulomb	100*, 200	35
M2 Disturbed Lacustrine Clay and Silt	125	Mohr-Coulomb	100*, 200	18
M1 Slide Debris above Toe of Slide	115, 120*	Mohr-Coulomb	50*, 100	18
Colluvium	115	Mohr-Coulomb	0	26

*Indicates the value used to represent failure conditions.

Back-Analyses Stages

The 2014 SR-530 landslide slope stability analyses were carried out in three distinct stages. A hypothesized fourth stage, which includes blocks of Whitman bench falling down after the removal of the large third stage of the slide, was not important for understanding the initiation of the most damaging effects of the landslide, so it was not analyzed.

Stage 1 is shown in Figure J.2-2a. In this initial stage, failure was re-initiated in the 2006 Hazel landslide debris (effectively treated as M1 debris). The critical surface of rupture was expected to be located through the M1 debris, or through both the M1 and M2 debris. Shallow surfaces of rupture within the mid-slope bench were not considered in the Stage 1 failure analyses, because these shallow failures were assumed to be continuously occurring after the 2006 Hazel landslide. Although a shallow failure could cause a cascading effect that might trigger failure in a marginally stable slope, sufficient information is not available to confidently analyze this case.
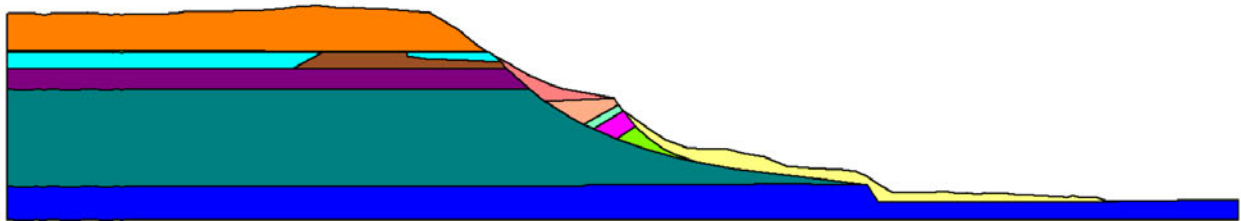
Figure J.2-2a View of the slide debris material zones in Stage 1 (see legend in Table J.2-1).

In the second stage of the analyses, the M1 debris was removed from the analyses so that the buttressing force it provided previously to the mid-slope bench would no longer be applied, as shown in Figure J.2-2b. This stage of analyses focuses on the stability of the M2 debris that makes up the mid-slope bench.
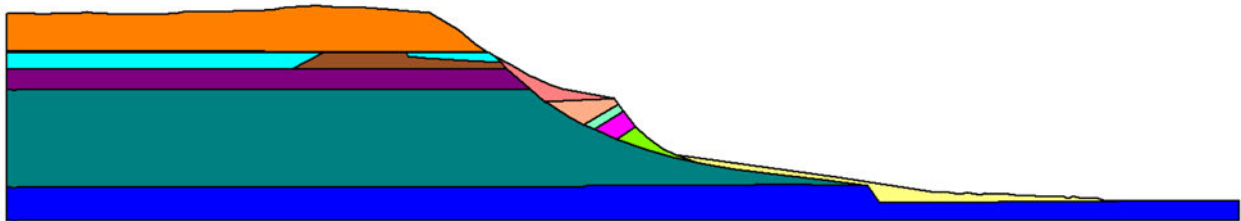
Figure J.2-2b: View of the slide debris material zones in Stage 2 (see legend in Table J.2-1).

In the third stage of analysis, the M2 debris sections were moved downslope to the initial location of the M1 debris, as shown in Figure J.2-2c, and potential deep slope failures through Whitman Bench were analyzed. Drained and undrained lacustrine layer strengths were used in this stage of analysis.
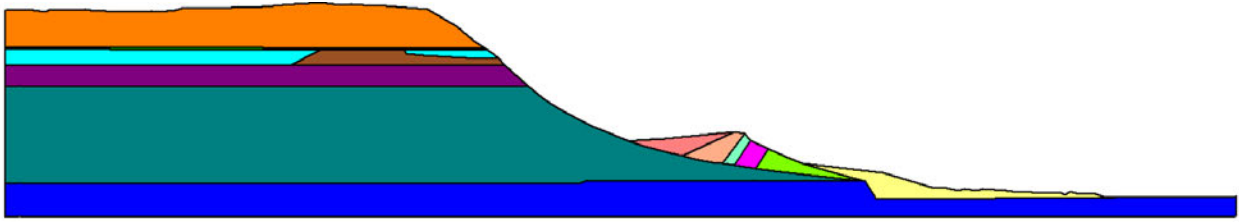
Figure J.2-2c: View of the slide debris material zones in Stage 3 (see legend in Table J.2-1).

Groundwater

The high water level for the initial 2014 slide is based on our interpretation of the piezometer measurements and reasonable interpretations of groundwater conditions that likely existed immediately before the 2014 SR-530 landslide. The estimated water level is shown in Figure J.2-3a. A low water level that runs along the boundary of the undisturbed lacustrine layer was used as an estimated low water level, as shown in Figure J.2-3b. As mentioned previously, there are other mechanisms that are not captured by these analyses such as erosion of soil due to water flow from springs within the slide mass, which steepens the slope in places as soil is transported downslope.
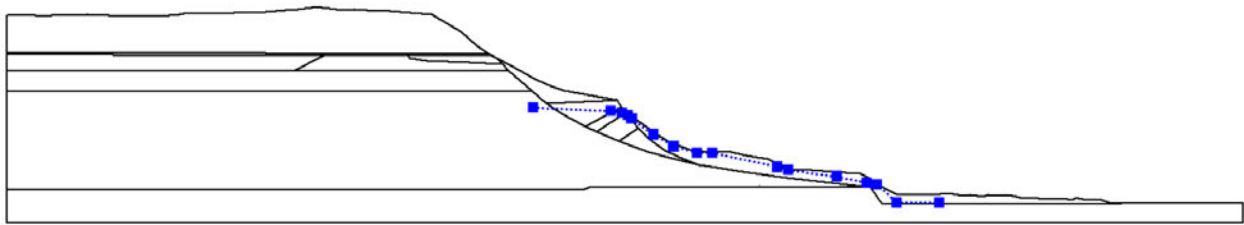
Figure J.2-3a: Estimated high water level used in Stage 1 analyses.
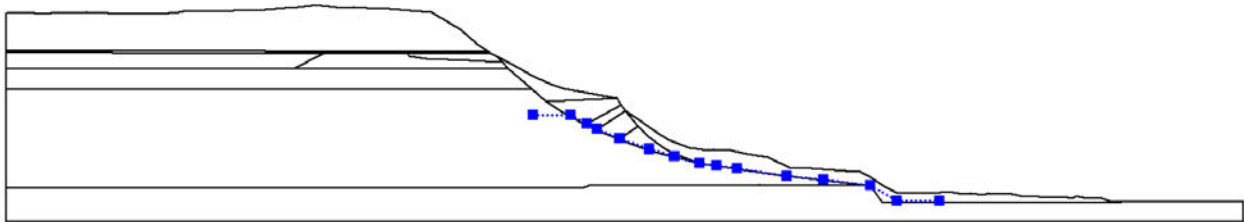
Figure J.2-3b: Estimated low water level used in Stage 1 analyses.

The estimated groundwater levels in Stage 2 analyses are lowered to the ground surface where the M1 debris was previously located, as shown in Figures J.2-4a-b.
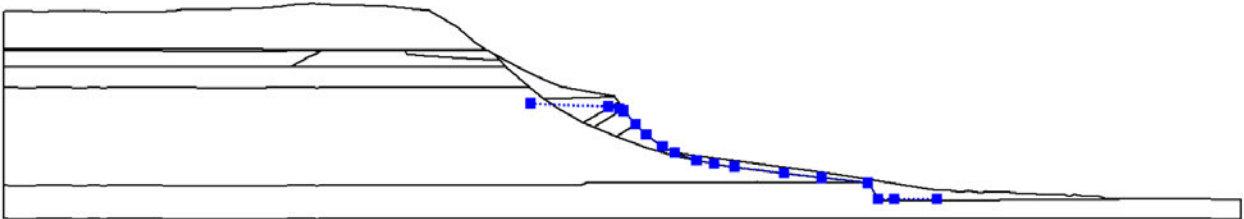
Figure J.2-4a: Estimated high groundwater level used in Stage 2 analyses.
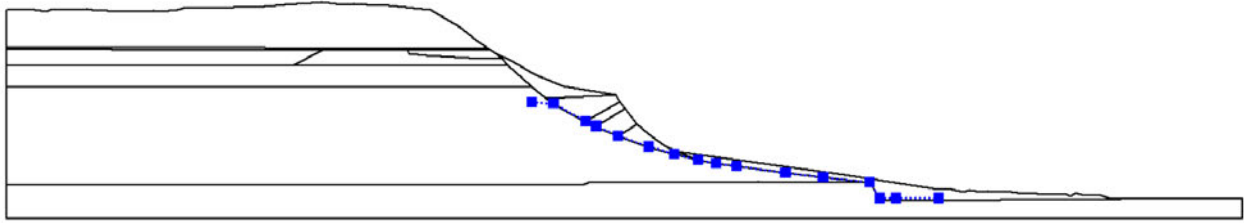
Figure J.2-4b: Estimated low groundwater level used in Stage 2 analyses.

The pore water pressures within Whitman Bench were calculated from a seepage analysis for the Stage 3 analyses. This seepage analysis calculates pore water pressures based on a 1-year transient analysis using the annual average rainfall in the region surrounding Whitman Bench (i.e., 0.2 inches/day) followed by 22 days of heavier rainfall equivalent to the measured rainfall in regions surrounding Whitman Bench in the 22 days prior to the SR-530 landslide (i.e., 0.7 inches/day). The groundwater level calculated from these analyses represents locations of zero pore pressure as shown in Figure J.2-5a. Figure J.2-5b shows contours of pore pressures within Whitman Bench.

Figure J.2-5a: Calculated water levels in Stage 3 analyses (blue dashed lines show 0 pressure contours).
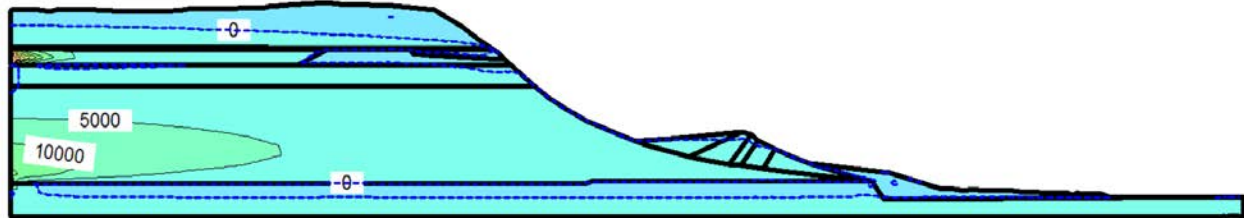
Figure J.2-5b: Pore water pressures in Whitman Bench (units of psf).

Calculation Methods

The Morgenstern-Price and Spencer limit equilibrium methods as implemented in the program SlopeW (GEO-SLOPE International Ltd. 2010. *Stability Modeling with SLOPE/W 2007 Version, An Engineering Methodology*, 4th Ed.) were employed in the slope stability analyses of this study. These two methods provided consistent results, so results are only shown for analyses using the Morgenstern-Price method.

Circular surfaces of rupture using the grid and radius method in SlopeW were used to calculate a global minimum factor of safety, as shown in Figure J.2-6a. Non-circular surfaces of rupture using the fully specified method in SlopeW were used to calculate the factors of safety for

specific surfaces of rupture derived from field investigations. Fully specified, non-circular surfaces of rupture are shown in Figure J.2-6b. Non-circular surface of rupture1 corresponds to slip through the M1 debris. Non-circular surface of rupture2 corresponds to full failure of the mid-slope bench with a surface of rupture exit through the upper portion of the M1 debris. Non-circular surface of rupture 3 corresponds to slip along the inner boundary of the M1 and M2 debris. The most critical non-circular surface of rupture was optimized in SlopeW to search for any surface of rupture with a lower factor of safety within the vicinity of the estimated surfaces. Optimization is performed by randomly adjusting the points of the most critical fully specified surfaces of rupture for 2000 iterations to locate a lower factor of safety in the vicinity of the most critical fully specified, non-circular surface of rupture.
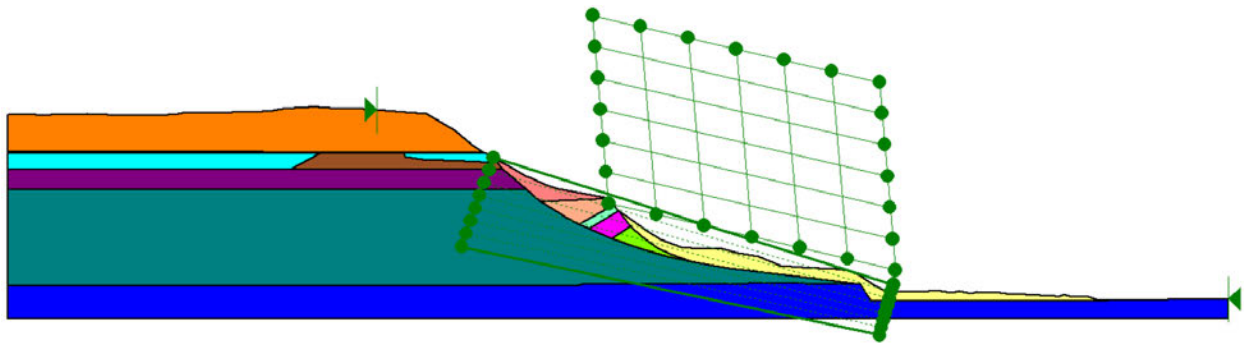
Figure J.2-6a: Circular surface of rupture search using the grid and radius method.
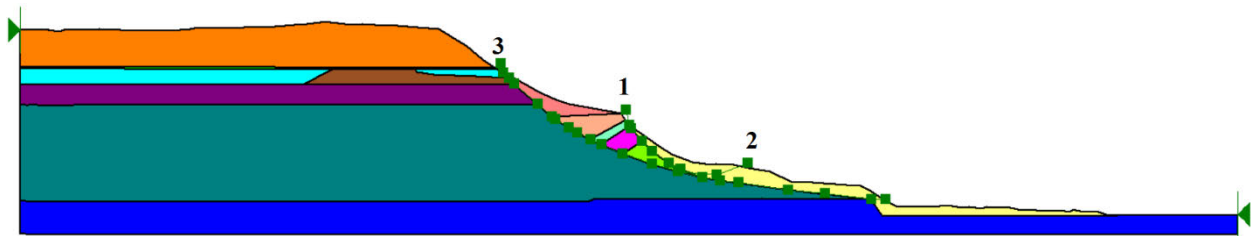
Figure J.2-6b: Fully specified, non-circular surfaces of rupture.

Calibration of Selected Strength Parameters for Initial Stability

Given the uncertainty involved in the slope stability analyses (due to uncertainties in landslide geometry, groundwater levels, and soil parameters), marginal stability is assumed for cases wherein $0.9 \leq FS \leq 1.1$, failure is assumed when $FS < 0.9$, and stability is assumed when $FS > 1.1$. Thus, we judge that a calculated $FS < 0.9$ indicates that a slope failure should have occurred. A calculated $FS > 1.1$ indicates clearly that the slope should be stable for the conditions analyzed. However, for cases wherein $0.9 \leq FS \leq 1.1$, the slope could have failed or could have been marginally stable.

The slope stability analyses in this study focused on deep-seated failures. Shallow raveling failures are possible on the steep face of the M2 debris, but these types of failures are assumed to be ongoing following the 2006 Hazel landslide. In these slope stability analyses, shallow raveling failures were not considered to be a primary trigger of the 2014 SR-530 landslide.

Moreover, there are other mechanisms that are not captured by these analyses such as the potentially destabilizing effects of soil erosion due to flowing surface water.

The potential surfaces of rupture shown in Figures J.2-7a-i were developed using the pre-failure strength and unit weight parameters (Table J.2-1). The deep circular surface of rupture for the estimated low groundwater level in Figure J.2-7a exhibited a marginally stable factor of safety. The optimized non-circular surface of rupture in Figure J.2-7b corresponds approximately to non-circular surface of rupture 2 and had a marginally stable factor of safety. The fully specified non-circular surfaces of rupture in Figures J.2-7c-e have factors of safety above 1.1, which indicate they are stable. Thus, for the low groundwater conditions, the slope is marginally stable or stable for the calibrated soil parameters and landslide geometry.

At the estimated high water level, a circular surface of rupture search indicated shallow failure of the mid-slope bench that is considered to be from continuous raveling of the steep slope face. The optimized non-circular surface of rupture in Figure J.2-7f has an unstable factor of safety and corresponds approximately to non-circular surface of rupture 1. Non-circular surface of rupture 1 before optimization is shown in Figure J.2-7g and exhibited a marginally stable factor of safety. The optimization procedure reduced the factor of safety for non-circular surface of rupture 1 by 0.18, which suggests that unstable non-circular surfaces of rupture may be near the assumed surfaces of rupture. Non-circular surfaces of rupture 2 and 3 in Figures J.2-7h and 7i have the same factor of safety, which suggests that including the M1 debris does not change the stability of the M2 slide significantly. Results are summarized in Table J.2-2.
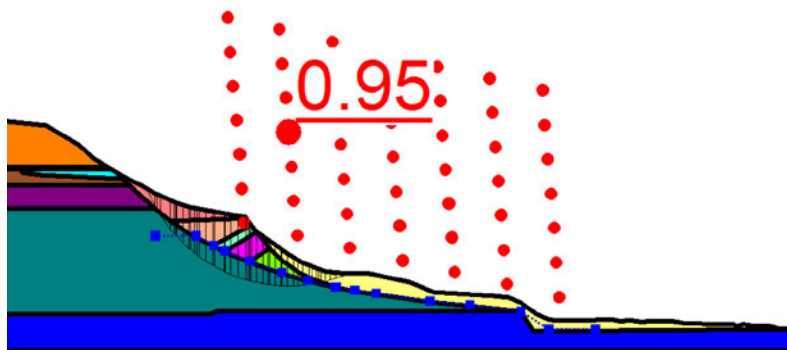
Figure J.2-7a: Critical circular surface of rupture with pre-failure strength parameters at the estimated low water level.
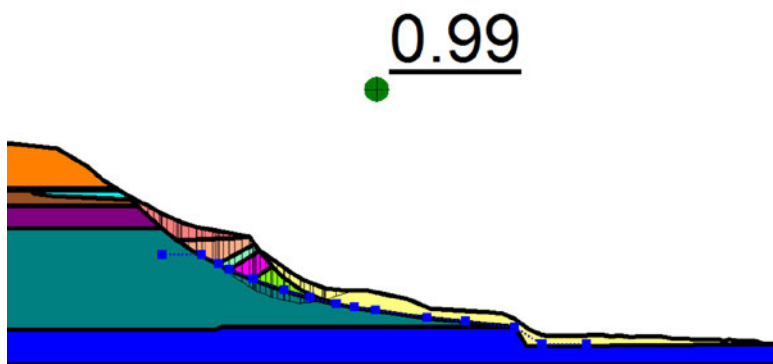
Figure J.2-7b: Optimized non-circular surface of rupture with pre-failure strength parameters at the estimated low water level.
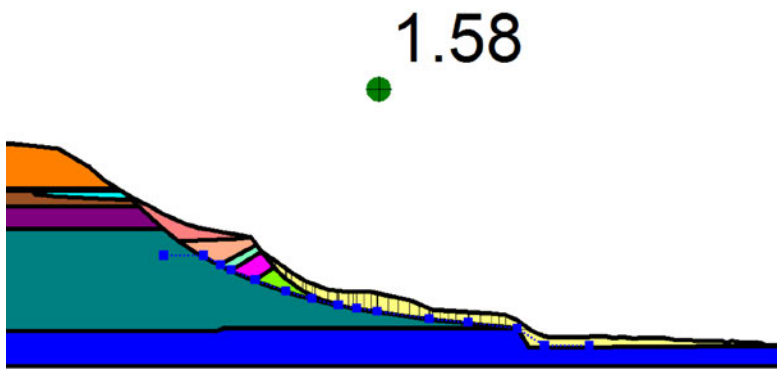
Figure J.2-7c: Non-circular surface of rupture 1, with pre-failure strength parameters at the estimated low water level.
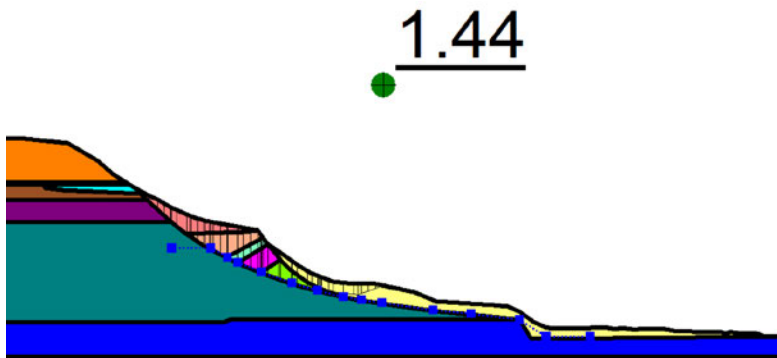
Figure J.2-7d: Non-circular surface of rupture 2, with pre-failure strength parameters at the estimated low water level.
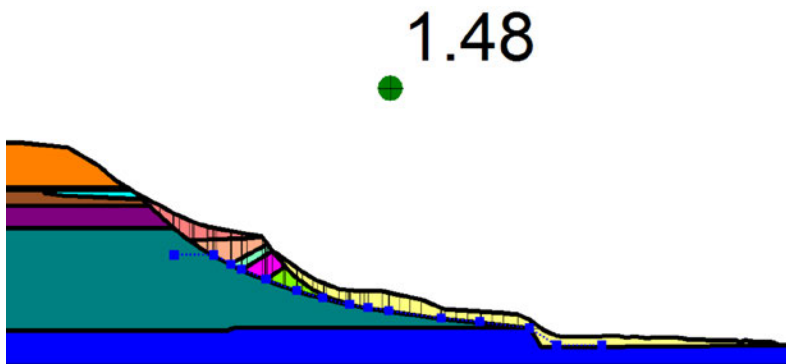
Figure J.2-7e: Non-circular surface of rupture 3, with pre-failure strength parameters at the estimated low water level.
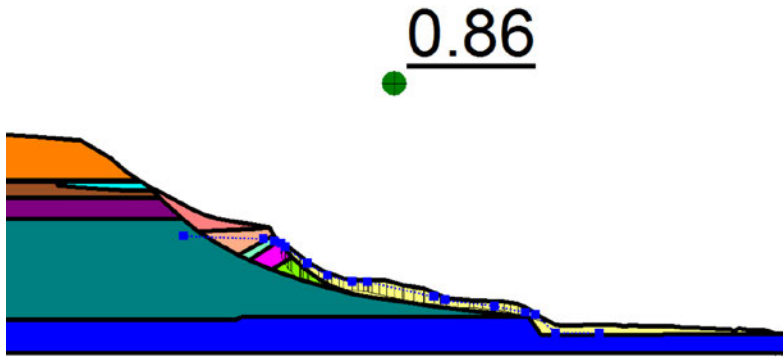
Figure J.2-7f: Optimized non-circular surface of rupture with pre-failure strength parameters at the estimated high water level.
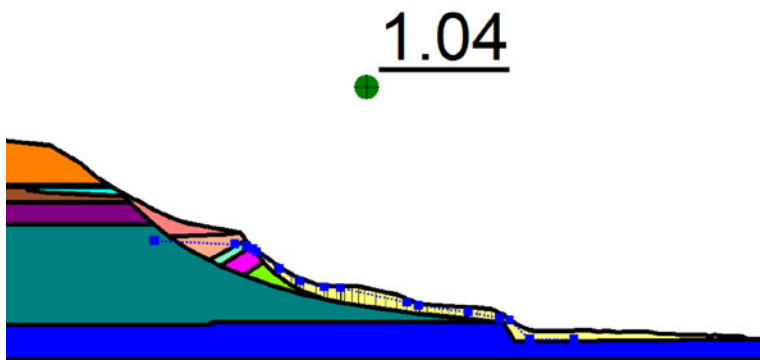
Figure J.2-7g: Non-circular surface of rupture 1 with pre-failure strength parameters at the estimated high water level.
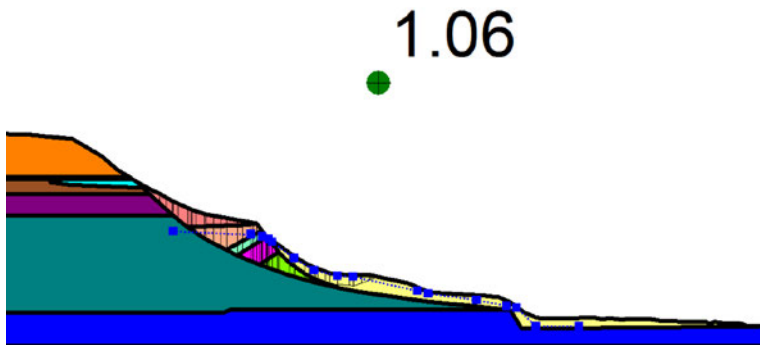
Figure J.2-7h: Non-circular surface of rupture 2 with pre-failure strength parameters at the estimated high water level.
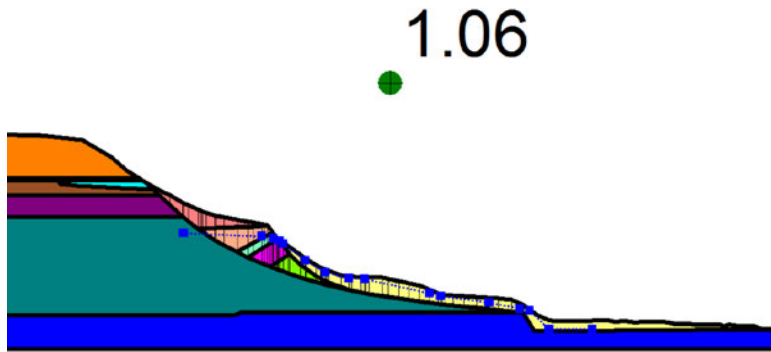
Figure J.2-7i: Non-circular surface of rupture 3 with pre-failure strength parameters at the estimated high water level.

Table J.2-2: Factors of Safety Obtained Using Pre-Failure Strength Parameters

Groundwater Level	Factor of Safety				
	Non-Circular Surface of Rupture 1	Non-Circular Surface of Rupture 2	Non-Circular Surface of Rupture 3	Optimized Non-Circular Surface of Rupture	Circular Surface of Rupture
High	1.04	1.06	1.06	0.86	0.62*
Low	1.58	1.44	1.48	0.99	0.95

*Indicates a shallow surface of rupture.

Stage 1 – 2014 SR-530 Landslide Analysis

The strength and unit weight parameters provided in Table J.2-1 for the failure scenario are used in the Stage 1 –2014 SR-530 landslide analyses. The circular surfaces of rupture at the estimated high groundwater level indicate shallow failures. The optimized non-circular surface of rupture at the estimated high groundwater level shown in Figure J.2-8a corresponds approximately to non-circular surface of rupture 1 and has an unstable factor of safety of 0.82. The non-circular surfaces of rupture in Figures J.2-8b through 8d exhibited factors of safety close to those obtained using pre-failure strength parameters for the case with the high groundwater level. At the estimated low groundwater level, the deep circular failure surface in Figure J.2-8e encompasses most of the mid-slope bench and suggests a marginally stable factor of safety. The optimized non-circular surface of rupture in Figure J.2-8f again corresponds approximately to non-circular surface of rupture 2 and had a marginally stable factor of safety. The fully specified surfaces of rupture in Figures J.2-8h to 8i have stable factors of safety. The fully specified surface of rupture results obtained using the strength parameters at failure show marginal stability at the estimated high groundwater level, while the optimized non-circular failure surface at the estimated high groundwater level indicates failure when the at-failure strengths are used. Results are summarized in Table J.2-3.
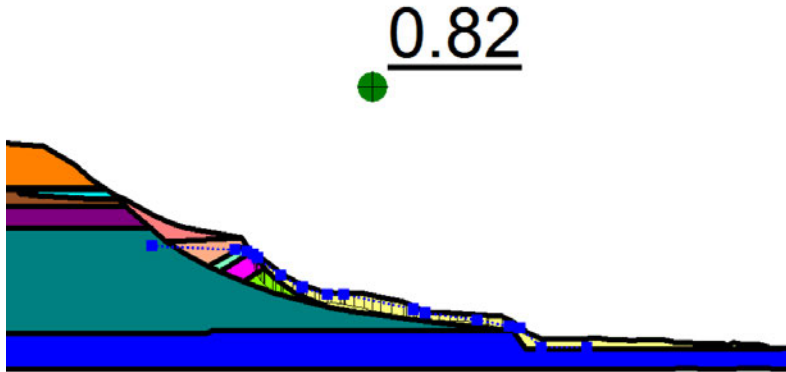
Figure J.2-8a: Optimized non-circular surface of rupture using strength parameters at failure with the estimated high water level.
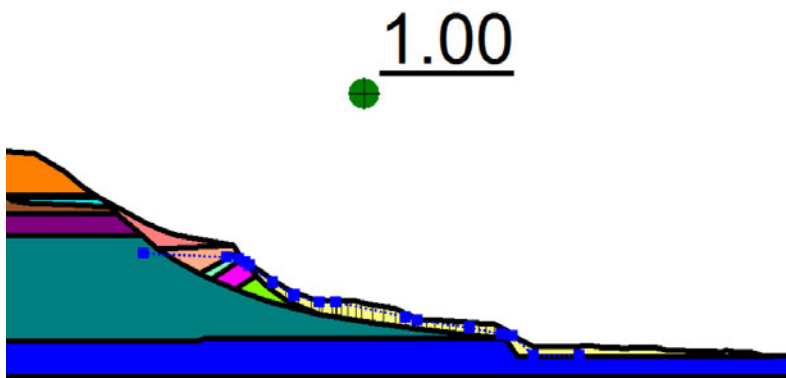
Figure J.2-8b: Non-circular surface of rupture 1 using strength parameters at failure with the estimated high water level.
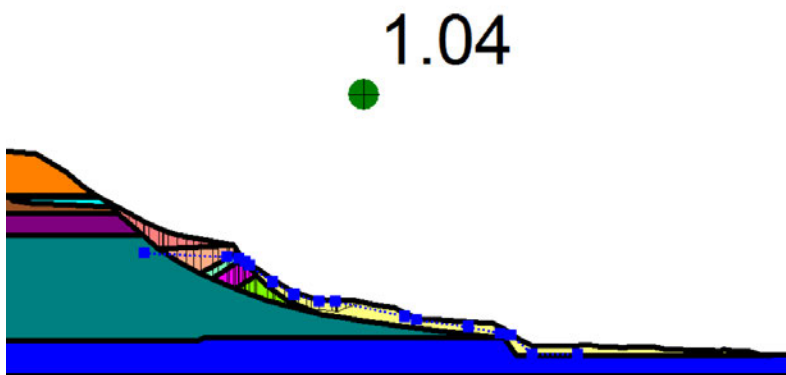
Figure J.2-8c: Non-circular surface of rupture 2 using strength parameters at failure with the estimated high water level.
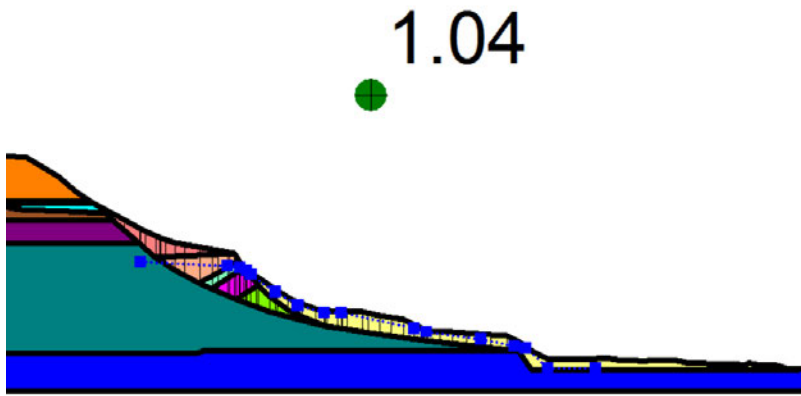
Figure J.2-8d: Non-circular surface of rupture 3 using strength parameters at failure with the estimated high water level.
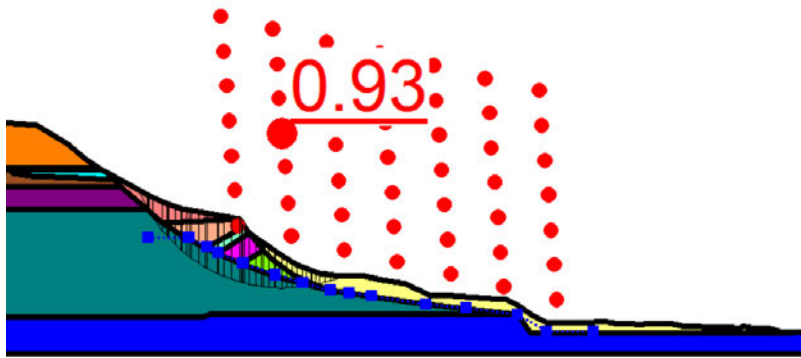
Figure J.2-8e: Critical circular surface of rupture using strength parameters at failure with the estimated low water level.
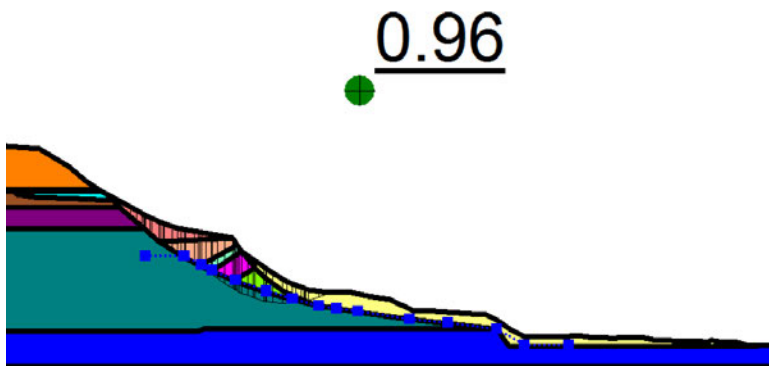
Figure J.2-8f: Optimized non-circular surface of rupture using strength parameters at failure with the estimated low water level.
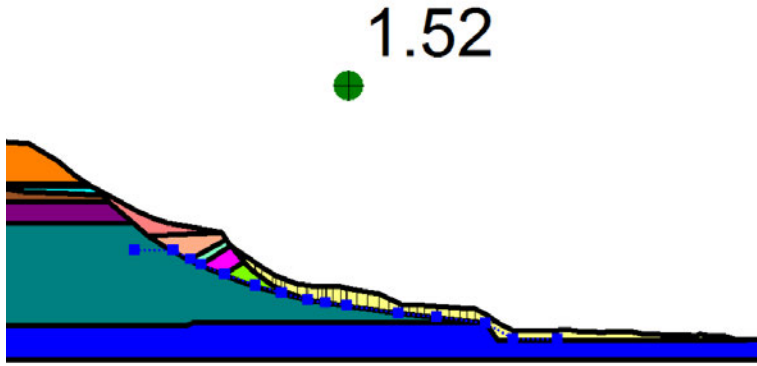
Figure J.2-8g: Non-circular surface of rupture 1 using strength parameters at failure with the estimated low water level.
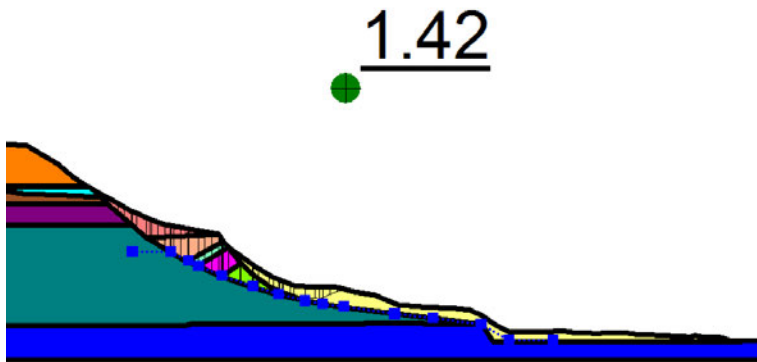
Figure J.2-8h: Non-circular surface of rupture 2 using strength parameters at failure with the estimated low water level.
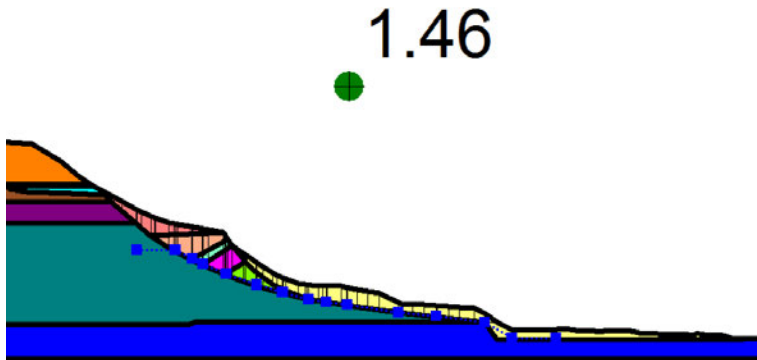
Figure J.2-8i: Non-circular surface of rupture 3 using strength parameters at failure with the estimated low water level.

Table J.2-3: Factors of Safety Obtained Using At-Failure Strength Parameters

Groundwater Level	Factor of Safety				
	Non-Circular Surface of Rupture 1	Non-Circular Surface of Rupture 2	Non-Circular Surface of Rupture 3	Optimized Non-Circular Surface of Rupture	Circular Surface of Rupture
High	1.00	1.04	1.04	0.82	0.59*
Low	1.52	1.42	1.46	0.96	0.93

*Indicates a shallow surface of rupture.

Stage 2 – 2014 SR-530 Landslide Analysis

The strength and unit weight parameters at failure listed in Table J.2-1 were used in the Stage 2 analyses after the M1 debris was lowered to simulate the effects of the Stage 1 landslide movement. At the estimated high groundwater level, the critical circular surface of rupture shown in Figure J.2-9a indicates a partial failure in the mid-slope bench. Non-circular surface of rupture 2 in Figure J.2-9b exhibited a marginally stable factor of safety. The curvature of the optimized surface of rupture changed direction dramatically for the high groundwater conditions and was judged to be unrealistic, so it is not reported.

At the estimated low groundwater level, the critical circular surface of rupture penetrates into the lacustrine clay and silt unit (Figure J.2-9c). The optimized surface of rupture (shown in Figure J.2-9d) produced a lower factor of safety than the non-circular surface of rupture 2 shown in Figure J.2-9e, but the optimized surface of rupture had an unrealistic, abrupt change in curvature, so it was judged to be unreliable. Figure J.2-9d is shown only to illustrate how the optimization scheme in SlopeW can sometimes produce surfaces of rupture with unrealistic shapes.

Overall, these results suggest that the critical surface of rupture in Stage 2 likely penetrates into the lacustrine clay and silt unit. These results are summarized in Table J.2-4.
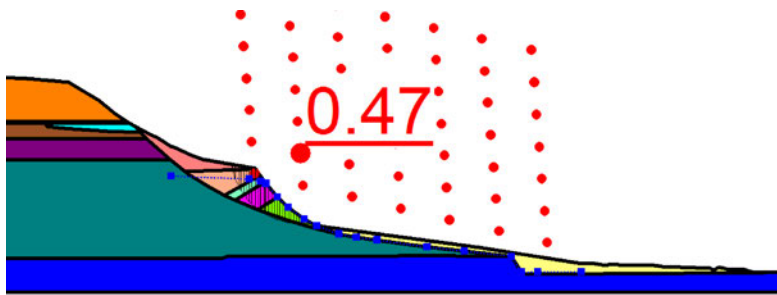
Figure J.2-9a: Critical circular surface of rupture at the estimated high groundwater level.
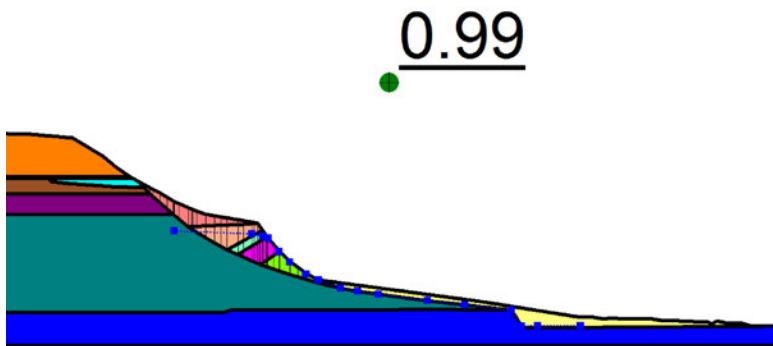
Figure J.2-9b: Non-circular surface of rupture 2 at the estimated high groundwater level.
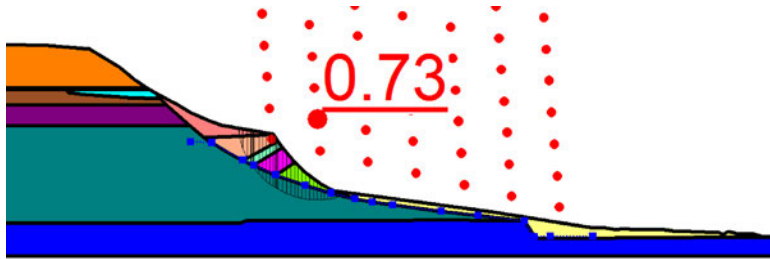
Figure J.2-9c: Critical circular surface of rupture at the estimated low groundwater level.
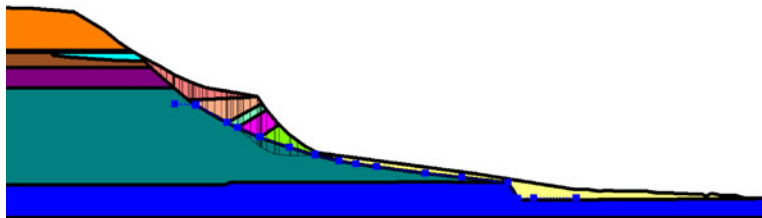
Figure J.2-9d: Optimized non-circular surface of rupture at the estimated low groundwater level.
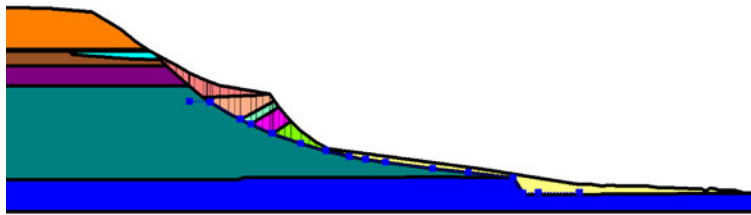
Figure J.2-9e: Non-circular surface of rupture 2 at the estimated low groundwater level.

Table J.2-4: Stage 2 Factors of Safety

Estimated Water Level	Factor of Safety		
	Non-Circular Surface of Rupture 2	Optimized Non-Circular Surface of Rupture	Circular Surface of Rupture
High	0.99	-**	0.47*
Low	1.32	0.88**	0.73

*Indicates a shallow surface of rupture.
**Judged to be unrealistic due to abrupt changes in the curvature of the surface of rupture.

Stage 3 – 2014 SR-530 Landslide Analysis

The Stage 3 analyses employed pore water pressures calculated with the program SeepW (GEO-SLOPE International Ltd. 2010. *Seepage Modeling with SEEP/W 2007 Version, An Engineering Methodology*, 4th Ed.) to capture their distribution within Whitman Bench (see Appendix I). The results presented in this section show critical circular surfaces of rupture, as well as the surfaces of rupture associated with calculated factors of safety closest to 1.0, which is indicative of how far back in the headward direction Whitman Bench might fail.

Slope stability analyses were initially performed using a fully softened friction angle for the lacustrine clay and silt unit, which is appropriate for an analysis of a first-time slide. Figures J.2-10a and 10b show the results obtained using the best estimate of the fully softened friction angle of 20° for the lacustrine clay and silt unit. A shallow circular surface of rupture is found to have the lowest calculated factor of safety. The shape and size of the circular surface of rupture that has a factor of safety of 1.0 is similar to the surface of rupture of the deep failure within Whitman Bench identified in the field.
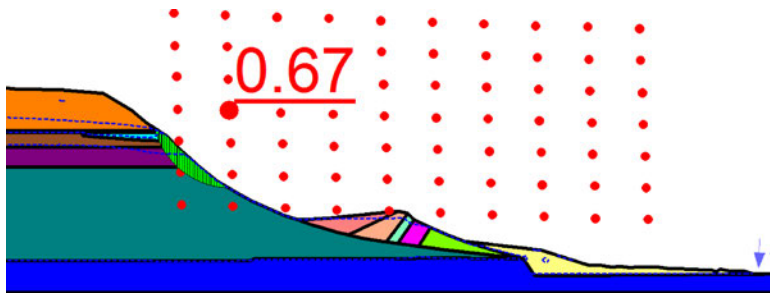
Figure J.2-10a: Critical circular surface of rupture within the lacustrine layer using a friction angle of 20 degrees.
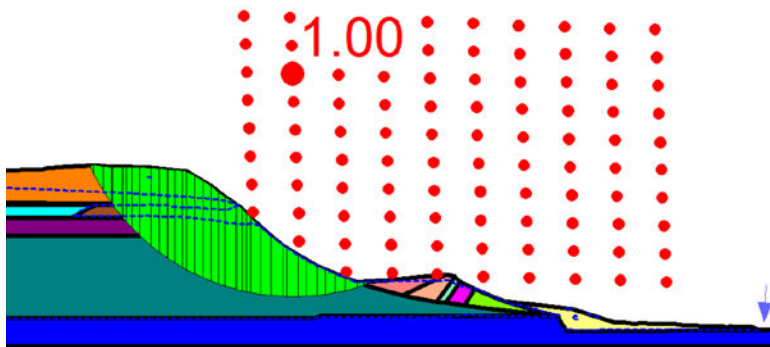
Figure J.2-10b: FS=1.0 circular surface of rupture within the lacustrine layer using a friction angle of 20 degrees.

Undrained (total stress) slope stability analyses were also performed using the estimated undrained shear strength ratios (c_u/σ_v') developed from the triaxial testing program (see Appendix E). This approach requires that the vertical effective stress (i.e., σ_v') be estimated in the lacustrine clay and silt unit so that the unit's undrained shear strength (i.e., c_u) can be calculated using the estimated value of c_u/σ_v'. The Stage 1 geometry was used to obtain the

vertical effective stresses for the Stage 3 analyses, because the vertical effective stresses in the lacustrine unit are in equilibrium with the conditions before the slope failure initiated. The Stage 3 vertical effective stresses calculated within the lacustrine clay and silt unit after the removal of the M2 material are not in equilibrium, as it is a rapid undrained response at this point. Unfortunately, the program SlopeW does not save the initial (pre-failure) undrained shear strength values that are based on the Stage 1 (pre-failure) vertical effective stresses for the Stage 3 analysis. Consequently, the initial vertical effective stresses were calculated based on the Stage 1 slope geometry using the pore water pressures calculated through the SeepW seepage analyses for this case (see Appendix I).

Assuming the lacustrine layer underlying the mid-slope bench in Stage 1 will fail under direct simple shear conditions in Stage 3, c_u values were estimated for different zones of the lacustrine clay and silt unit as shown in Figure J.2-11a. The remaining part of the lacustrine clay and silt unit was analyzed using SHANSEP parameters within the program SlopeW, because the vertical effective stresses do not change appreciably in the part of the lacustrine unit under Whitman Bench. The c_u values shown in Figure J.2-11a were verified by comparing the shear strengths along the 3 surfaces of rupture shown in Figure J.2-11b with the same surfaces in the Stage 1 geometry using the SHANSEP parameter $c_u/\sigma_v' = 0.35$ all throughout the lacustrine layer. Figure J.2-11c shows that the c_u values in Figure J.2-11a capture accurately the 2013 undrained shear strengths in a piecewise manner when the lacustrine layer is assumed to fail under direct simple shear conditions. The shear strength characterization in the zones shown in Figure J.2-11a overestimate the strength of the unit in these zones for the triaxial extension strength characterization and underestimate the strength of the unit in these zones for the triaxial compression strength characterization. However, the overall effect of these differences are negligible, because a large part of each surface of rupture for the FS = 1.0 case passes through the lacustrine clay and silt that is under Whitman Bench, where the vertical effective stress is unaffected by the mid-slope bench failure.
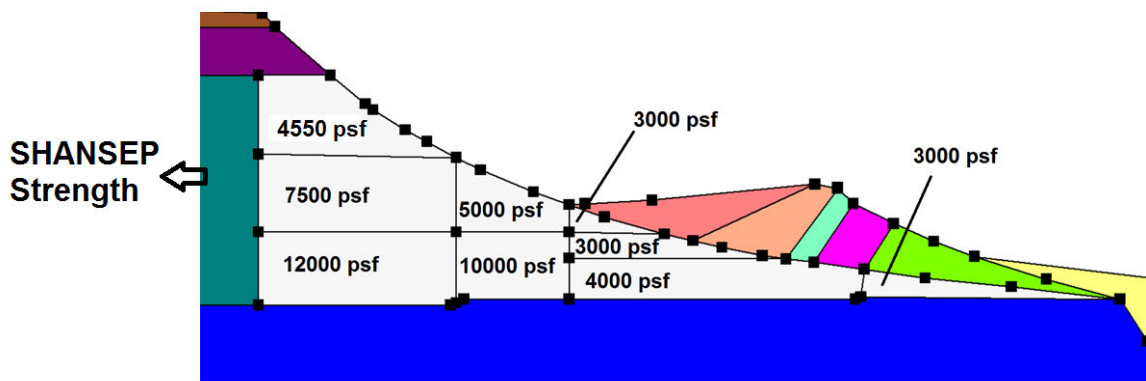
Figure J.2-11a: Estimated undrained shear strengths (c_u) for zones of the lacustrine clay and silt unit which are not under Whitman Bench. SHANSEP strength parameters are used in the lacustrine unit underneath Whitman Bench.
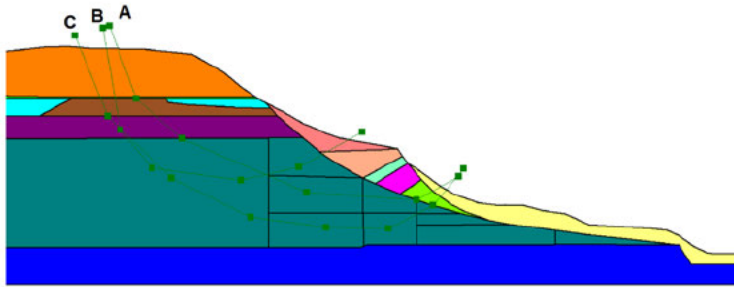
Figure J.2-11b: Fully specified slip surfaces used for validation of piecewise undrained shear strengths in Figure J.2-11a. Stage 1 geometry is shown.
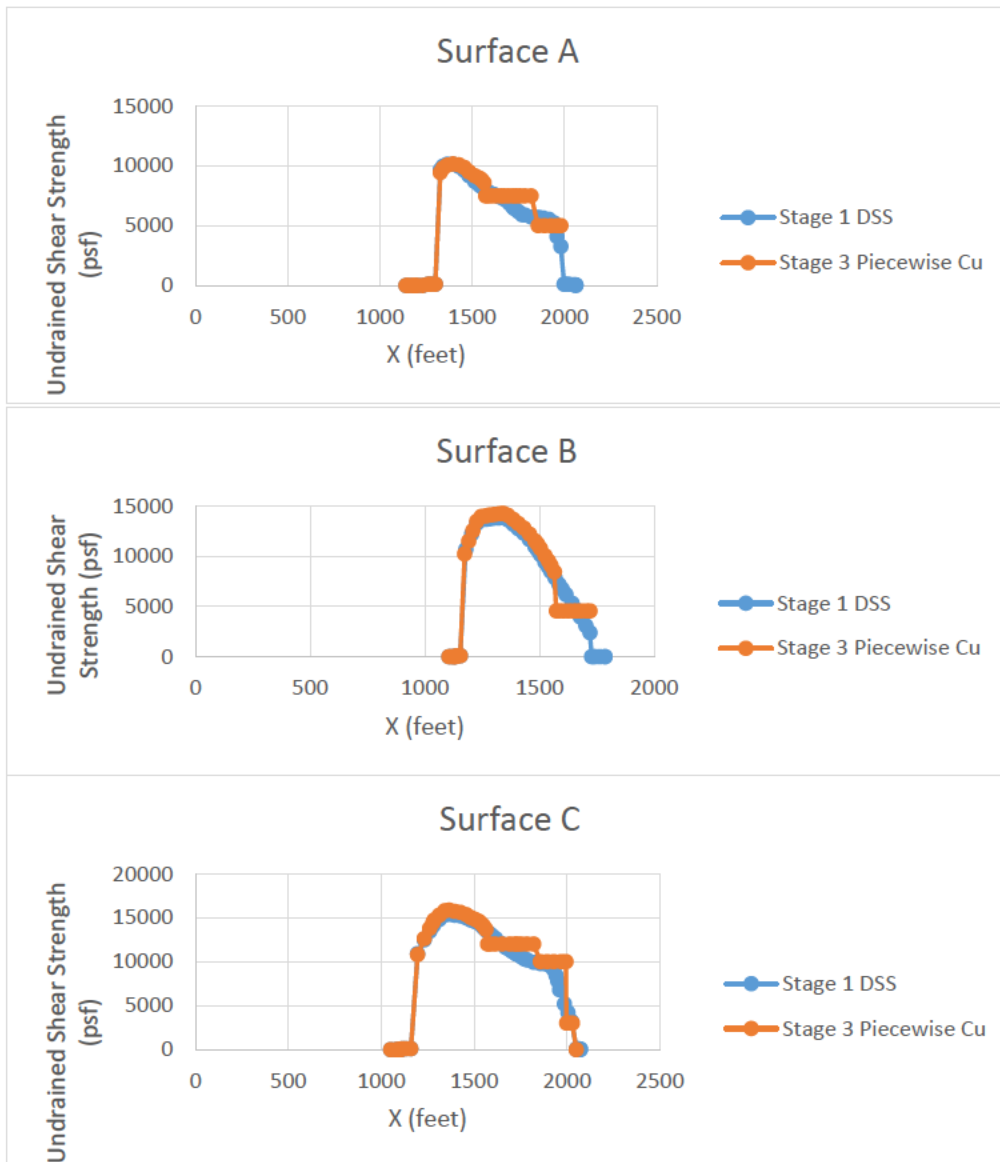
Figure J.2-11c: Comparison of slip surfaces A, B, and C (shown in Figure J.2-11b) for the Stage 1 geometry with $c_u/\sigma_v' = 0.35$ (direct simple shear strengths) in the lacustrine layer and the Stage 3 geometry using the zoned undrained shear strengths of Figure J.2-11a.

The results presented in Figures J.2-12a-f show critical circular and optimized non-circular surfaces of rupture for the Stage 3 slope stability analyses using the undrained shear strength characterization shown in Figure J.2-11a in that part of the lacustrine clay and silt unit under the slope and using the undrained shear strength parameters derived from the SHANSEP strength parameters for each shear mode in that part of the lacustrine unit under Whitman Bench. Figures J.2-12a and 12b show the results obtained with triaxial compression strength characterization under Whitman Bench. Figures J.2-12c and 12d show the results obtained with direct simple shear strength characterization under Whitman Bench. Figures J.2-12e and 12f show the results obtained with triaxial extension strength characterization under Whitman Bench.

All of the factors of safety are between 1.0 and 1.1, which indicates marginal stability for the Stage 3 slope assessment. The parts of the surfaces of rupture within the lacustrine unit constant undrained shear strength zones are nearly horizontal, which support the assumption that the surface of rupture fails under direct simple shear conditions underneath the original location of the mid-slope bench. The factors of safety for the critical circular and optimized non-circular surfaces of rupture are summarized in Table J.2-5. The deeper critical surfaces of rupture are similar to what was observed in the field.
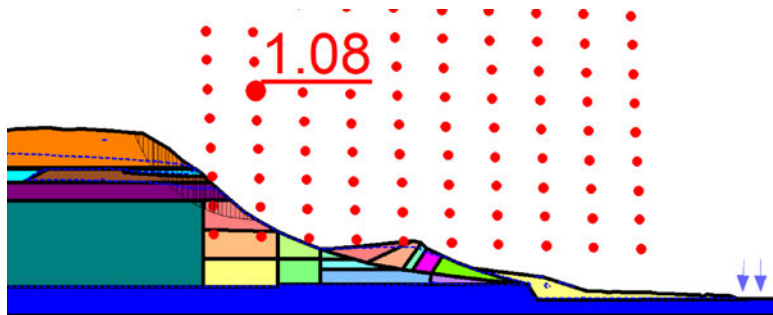
Figure J.2-12a: Critical circular surface of rupture using triaxial compression strength characterization (c_u/σ'_v of 0.41) in the lacustrine unit underneath Whitman Bench.
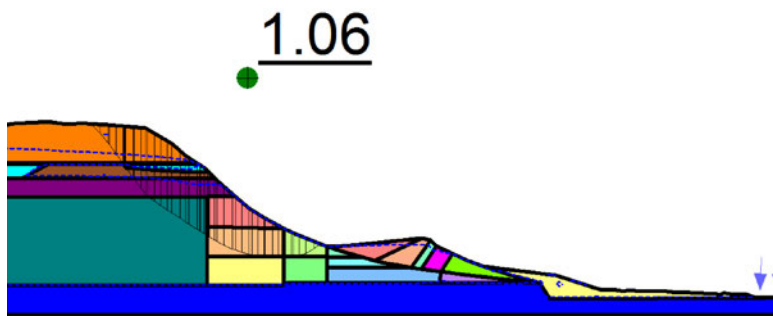
Figure J.2-12b: Optimized non-circular surface of rupture using triaxial compression strength characterization (c_u/σ'_v of 0.41) in the lacustrine unit underneath Whitman Bench.
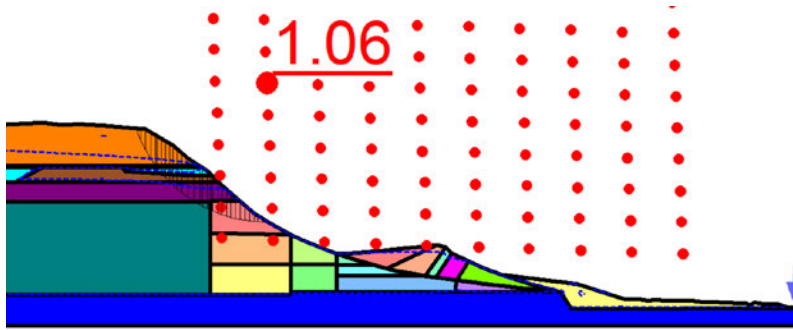
Figure J.2-12c: Critical circular surface of rupture using direct simple shear strength characterization (c_u/σ'_v of 0.35) in the lacustrine unit underneath Whitman Bench.
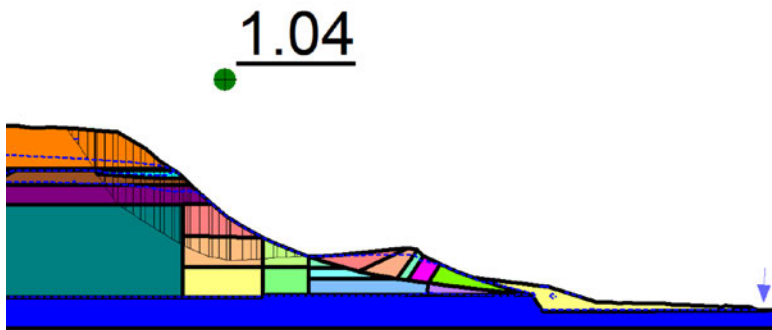
Figure J.2-12d: Optimized non-circular surface of rupture using direct simple shear strength characterization (c_u/σ'_v of 0.35) in the lacustrine unit underneath Whitman Bench.
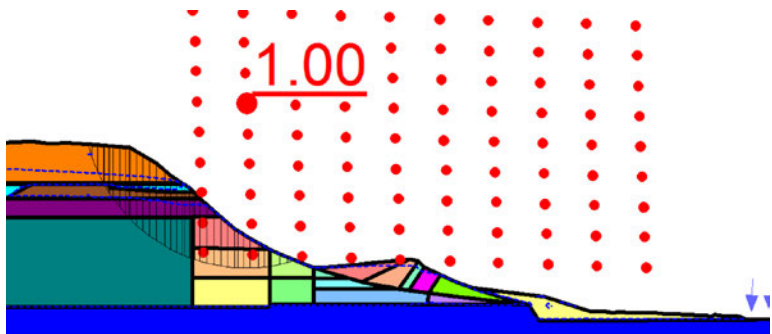
Figure J.2-12e: Critical circular surface of rupture using triaxial extension strength characterization (c_u/σ'_v of 0.31) in the lacustrine unit underneath Whitman Bench.
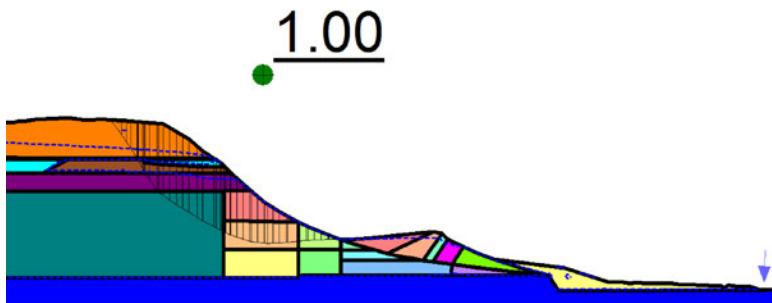
Figure J.2-12f: Optimized non-circular surface of rupture using triaxial extension strength characterization (c_u/σ'_v of 0.31) in the lacustrine unit underneath Whitman Bench.

Table J.2-5: Factors of Safety for Various Lacustrine Unit Shear Strength Characterizations underneath Whitman Bench

Analysis	Drained Analysis Factor of Safety	Undrained Analysis Factor of Safety		
Strength Characterization	$\phi' = 20°$	$c_u/\sigma'_v = 0.31$	$c_u/\sigma'_v = 0.35$	$c_u/\sigma'_v = 0.41$
Critical Circular Surface of Rupture	0.67	1.00	1.06	1.08
Optimized Non-Circular Surface of Rupture	-	1.00	1.04	1.06

2016 Stability Verification and Back-Analyses

The stability of the Whitman Bench after the 2014 SR-530 landslide was analyzed based on the 2016 geometry. The pre-failure strengths of Table J.2-1 were used for the materials underneath Whitman Bench. As shown in Figure J.2-13, the critical circular surface of rupture indicates a marginally stable shallow failure along the southeastern slope face of the recessional sand and gravel layer. These results are consistent with field observations of continuous raveling failures on the face of the slope following the 2014 landslide. As with the Stage 3 analysis of the 2014 landslide, SeepW was used to calculate the pore water pressures within Whitman Bench.
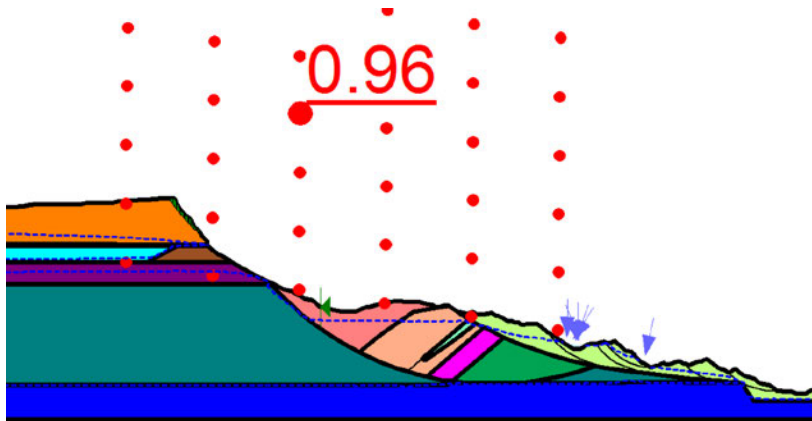
Figure J.2-13: Critical circular surface of rupture for the 2016 Whitman Bench geometry. A shallow surface of rupture can be seen on the slope face of the recessional sand layer.

Back-analyses of two known failures and three partial ground movements within the slide mass in 2016 were performed using the slide debris geometry shown in Figure J.2-14. Five fully specified non-circular surfaces of rupture that were known to slide partially or to fail are shown with the groundwater level estimated from observations of surficial ponding in the debris at that time. Surfaces 1 and 3 (which are shown in Figure J.2-14) failed in 2016, and surfaces 2, 4, and 5 only slipped partially. The stability of the highly disrupted M2 slide debris is back-analyzed assuming the slide debris is one material with a unit weight of 115 pcf, a friction angle of 26

degrees, and a cohesion of 100 psf. Marginally stable factors of safety between 0.9 and 1.0 are calculated for surfaces of rupture 1 and 3, which is consistent with the field observations (e.g., inclinometer data) of these slide masses failing completely in 2016. The factors of safety calculated for the other three surfaces are above 1.1, which suggests that these potential slide masses were significantly more stable than the failed surfaces of rupture 1 and 3. The calculated factors of safety for surfaces of ruptures 2, 4, and 5 are sufficiently high wherein the observed ground movements would have likely been due to creep movements or a result of shallow failures in the vicinity of these slopes that reduced their stability. These results are summarized in Table J.2-6.
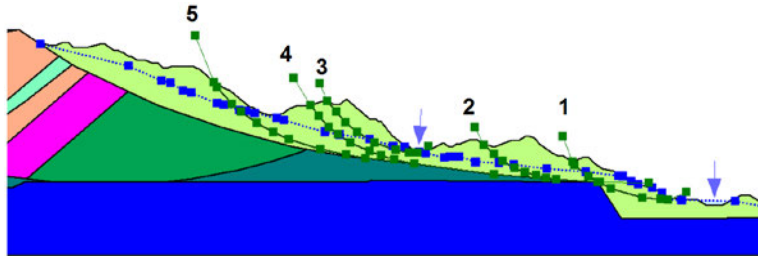
Figure J.2-14: Fully specified, non-circular slip surfaces analyzed in the 2016 slide debris.

Table J.2-6: 2016 Debris Failures Back-Analysis Factors of Safety

Factors of Safety				
Surface 1	Surface 2	Surface 3	Surface 4	Surface 5
0.91	1.98	0.96	1.89	2.15

Findings

The findings of the back-analyses performed on the 2014 SR-530 landslide are:

- The surfaces of rupture through the M1 debris possess stable factors of safety (i.e., above 1.1) at the estimated low groundwater level, but marginally stable to unstable factors of safety below 1.1 at the estimated high groundwater level.

- At the estimated low groundwater level, the mid-slope bench was found to be marginally stable before the failure of the M1 debris. At the estimated high groundwater level, the mid-slope bench was unstable if the M1 slide debris fails.

- The optimized non-circular surfaces of rupture evaluated in the Stage 1 analyses indicate that the initial failure of the 2014 SR-530 landslide was likely a failure of the M1 debris or a combined failure of the M1 and M2 debris.

- The surface of rupture in Stage 2 largely involved M2 debris material and likely penetrated slightly into the undisturbed lacustrine clay and silt unit.

- Critical surfaces of rupture obtained using fully softened strength or undrained strength characterizations of the lacustrine clay and silty unit in the Stage 3 analyses are similar to

the surface of rupture observed in this part of the 2014 SR-530 landslide. These surfaces of rupture are marginally stable with factors of safety between 0.9 and 1.1, which indicates that the M3 mass would likely fail after the M2 debris slid downslope.

- Slope stability analyses of the 2016 Whitman Bench and SR-530 landslide geometry indicate that the critical surfaces of rupture are marginally stable shallow surfaces along the southeast face of Whitman Bench. This is consistent with field observations of continuous shallow raveling on the face of this slope, following the 2014 landslide. Additionally, back-analyses of two slope failures that occurred in 2016 in the remaining slide debris failures are consistent with field observations.

- The slope stability analyses support the 2013 slide geometry being marginally stable before the March 22, 2014 SR-530 landslide with the calibrated soil parameters and estimated landslide geometry for a low groundwater and pore water pressure condition. When the groundwater level is increased to the estimated high groundwater level, the calculated factors of safety for the analyzed stages of landslide movement decrease to values that indicates failure as observed for the March 22, 2014 SR-530 landslide. Thus, the slope stability analyses support the initiation of the 2014 SR-530 landslide with the calibrated soil parameters and landslide geometry for an increased groundwater and pore water pressure condition. The slope stability analyses indicate that landslide stability depends significantly on the groundwater conditions in the slope.

- The slope stability analyses were performed on generalized, simplified two-dimensional cross sections that ran through the middle of the 2014 SR-530 landslide, which is inherently three-dimensional. The geologic study found the 2014 SR-530 landslide to be highly complex. The hydrogeology of the site is especially complex. Moreover, there are other mechanisms that are not captured by these analyses, such as erosion of soil due to water flow from springs within the slide mass, which steepens the slope in places as soil is transported downslope. Additionally, the effects of cascading shallow slope failures were not evaluated in this study. Therefore, these findings are only appropriate for gaining insight for the conditions analyzed, which focused on the effects of groundwater on the initiation of slope instability.

APPENDIX K

Runout Evaluations

APPENDIX K – RUNOUT EVALUATIONS

By Kenichi Soga, Alba Yerro, and Jonathan Bray

1. Introduction

The runouts of the 2006 Hazel landslide and the 2014 SR-530 landslide are back-analyzed using the material point method (MPM) to assess if the MPM models of these landslides can capture the key observed characteristics and distances traveled by the landslide debris during these two events. Once these two runout events are captured sufficiently well with the MPM models, the potential effects of the presence or absence of the 2006 debris field below the toe of the surface of rupture of the 2014 SR-530 landslide can be investigated. The model calibrated to capture the observed runout of the 2014 SR-530 landslide is rerun with all modeling aspects identical to the calibrated 2014 SR-530 landslide analyses with the exception that the debris field is completely removed and the North Fork of the Stillaguamish River reoccupies its former position before the January 2006 Hazel landslide. The primary objectives of the MPM analyses are to ascertain if the MPM models can capture and provide insight into the differing runout distances traveled by the 2006 Hazel landslide debris and the 2014 SR-530 landslide debris and to investigate if the presence of the debris field significantly affected the runout distance traveled by the 2014 SR-530 landslide debris.

The MPM formulation is fully dynamic to capture the kinematics of the landslides after their initiation. The MPM analyses of the runout of the 2006 Hazel and 2014 SR-530 landslides rely on the other work presented previously in this report. Data and information presented in Appendices B, C, D, E, F, I, and J are especially relevant as they provide the basis for the modeled stratigraphy and topography of the site before and after failure, including the surface of rupture geometry and characteristics, and the estimated engineering properties of materials involved in the landslides. Total stress undrained analyses are performed to capture the rapid response of the soil materials to loading and deformation. The calibration analyses provide the primary basis for the best estimate values of the strength parameters employed in the analyses. Reasonable undrained shear strength values that produce slope behavior similar to that observed in the actual runouts have been adopted for use in the analyses that investigate the potential effects of the presence or absence of the 2006 debris field below the toe of the surface of rupture of the 2014 SR-530 landslide.

2. The material point method (MPM)

The MPM was developed to simulate large deformations in history-dependent materials (e.g. Sulsky et al. 1994; 1995). It combines the advantages of Eulerian (i.e., fixed finite element grid) and Lagrangian (i.e., moving material points) approaches to discretize the continuum. Each material point represents a portion of the domain and the mass of such subdomain is assumed to be constant during the calculation to ensure mass conservation. Other quantities, such as velocities, strains, and stresses, are carried by the material points. Each material point moves attached with the solid skeleton, and these provide the Lagrangian description of the media. Governing equations (dynamic momentum balances) are solved at the nodes of the computational mesh which remains fixed during the calculation and covers the full domain of the problem. The variables required to solve the equations in the mesh at any step of the analysis are transferred from the material points

to the nodes of the mesh by using mapping functions. Boundary conditions can be imposed at the mesh nodes or at the material points and the governing equations are solved by using an explicit incremental scheme. Then, the quantities carried by the material points are updated through the interpolation of the mesh results, using the previously established mapping functions. The information associated with the mesh is not required for the next step of the analysis. Therefore, mesh distortion problems, which are typically a major shortcoming in the use of conventional finite element methods, are eliminated. Moreover, as the MPM is defined in a continuum framework, it enables incorporation of robust material constitutive models to capture realistic material behavior.

These features make MPM especially useful to solve problems involving large deformations and displacements in history-dependent materials. During the last decade, MPM has been applied to different fields, such as ice dynamics, gas advection, or fracture of wood. It has also recently received increasing attention toward the solution of geotechnical problems. For example, MPM has been used in the analysis of landslides and slopes (e.g., Andersen & Andersen, 2010; Zabala & Alonso, 2011; Abe, Soga and Bandara, 2014; Soga & Bandara, 2015; Soga, Alonso, Yerro, Kumar, & Bandara, 2015; Yerro, Alonso, & Pinyol, 2015; Yerro, Pinyol, & Alonso, 2015). It is also employed in studies of granular flows, modelling of anchors placed in soil, breaching of levees or dams, liquefaction, consolidation of soft soils, erosion and sedimentation, and displacement of earth retention structures.

3. MPM codes used in this study

Two MPM codes are used in this study. Three dimensional plane strain analysis are performed using the software *Anura3D*, whereas a depth-averaged quasi-3D analysis is performed using an in-house code *DA-MPM*, which was developed by T. Kobayashi and K. Soga at the University of Cambridge (Kobayashi et al., 2015).

The software *Anura3D* (http://www.anura3d.com) is a tool for MPM analyses developed by the MPM Research Community. This software is a 3D implementation of the MPM. It is used for simulating the physics involved in large deformation problems in geotechnics as well as for solid-fluid interaction problems. The performance of a numerical simulation with *Anura3D* requires the creation of input data (pre-processing) with *GiD* software and the visualization of results (post-processing) with *ParaView* software. The formulation implemented in *Anura3D* is fully dynamic and the principal governing equation is momentum balance.

In this study, a series of three dimensional plane strain analysis was conducted using *Anura3D*. The advantages of performing plane strain analysis is that the computational cost is much lower than in 3D simulations. In this way, parametric analysis can be performed efficiently to gain a better understanding of the behavior of the landslides. Moreover, a reasonable estimate of the magnitude of the runout can be obtained in most cases.

The Cambridge in-house 3D code *DA-MPM* adopts the depth-averaged technique, which is a common technique when simulating debris flows in three dimensional conditions for subaerial (e.g. Savage & Hutter, 1999; Denlinger & Iverson 2004; Hungr & McDougall 2009; Iverson and George 2014) and submarine conditions (e.g., Imran et al. 2001; Mazzanti & Bozzano 2009). It

assumes that the debris flow is uniform along its depth, which eliminates the dependency in the depth direction which in turn reduces the computational cost of running a truly three dimensional model. This assumption is often justified by the fact that a typical debris flow is extensively longer in the flow direction compared to its depth. The code outputs the temporal and spatial distribution of the debris on a horizontal plane and the depth at each point of the debris. Iverson and George (2016) use this assumption to simulate the 2014 SR-530 Landslide using their depth-averaged finite volume method code. The depth-averaged quasi-3D analysis provides reliable insights, although it should be noted that the variation in the material properties and behavior along the depth direction are not accounted for in the depth-averaged simulations.

The numerical scheme of the *DA-MPM* software is analogous to that of the regular MPM except for the treatment of constitutive models. In this analysis, the Bingham fluid model was used within the depth-integration framework, and its detail can be found in Pastor et al. (2006). As a result of the depth-integration, a landslide runout is represented by a collection of the material point "columns." Each material point "column" has a different height and travels on a 3D surface of the bathymetry while interacting with other material points. The simulation code was written in *C++* while the pre- and post-processes were performed by using *MATLAB®*.

4. Plane strain simulations of the 2006 Hazel landslide

4.1 Model

The computational mesh of the plane strain 2006 Hazel landslide is formed by linear tetrahedral elements. The thickness of model is one element and out-of-plane deformation is restricted to ensure plane strain conditions. The mesh is refined and made homogeneous in the region where the mobilized mass will move to optimize the computational time and to obtain more accurate results. The minimum edge of the elements is 3 m. A general view and a detailed view of the mesh are shown in Figure K-1. Note that elements indicated in red color are initially fully filled with material, while elements in blue are initially empty.

Initially, 4 material points are distributed within each element and are initially located at the corresponding integration points of a four-point Gaussian quadrature. Figure K-2 shows the initial location of the material points in the slope.

The model has 33,762 elements and 55,488 material points.

(a)

(b)
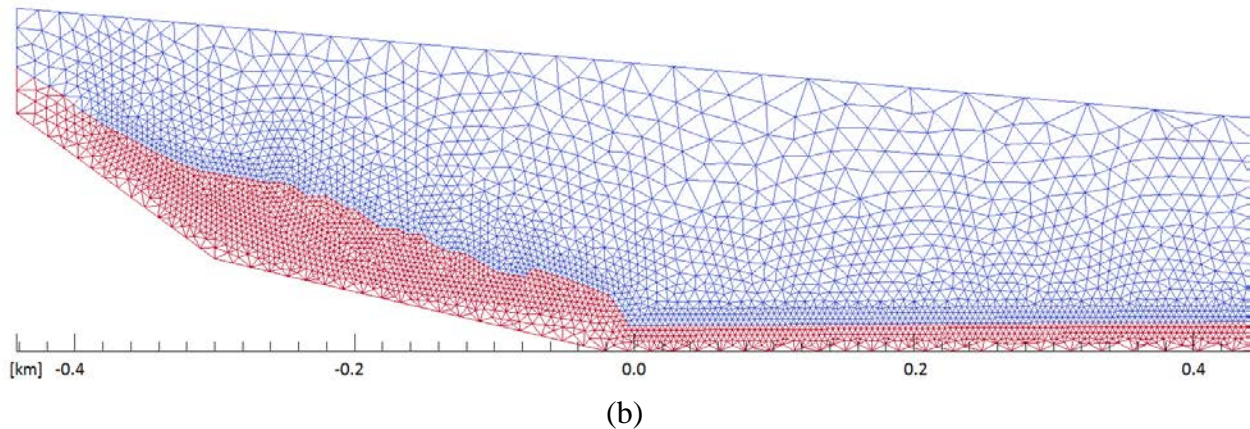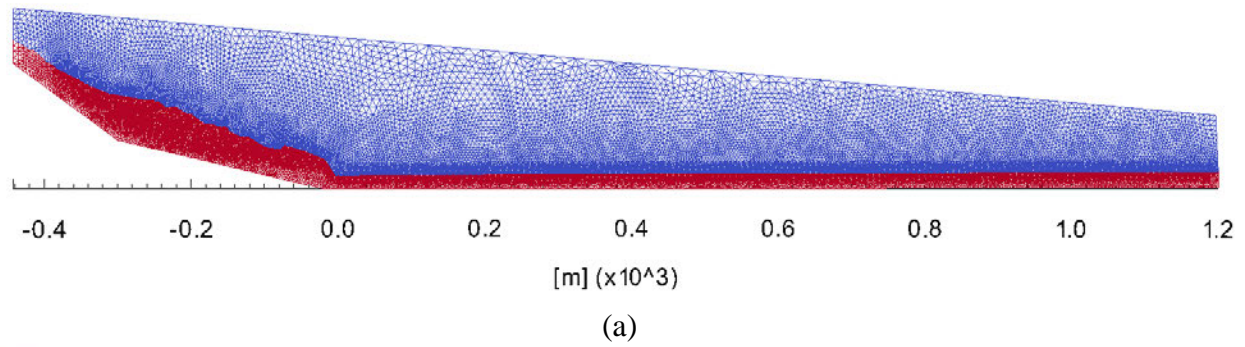
Figure K-1. Computational mesh. (a) General view. (b) Detailed view. Elements in red indicate that they initially are fully filled with material, while elements in blue are initially empty.
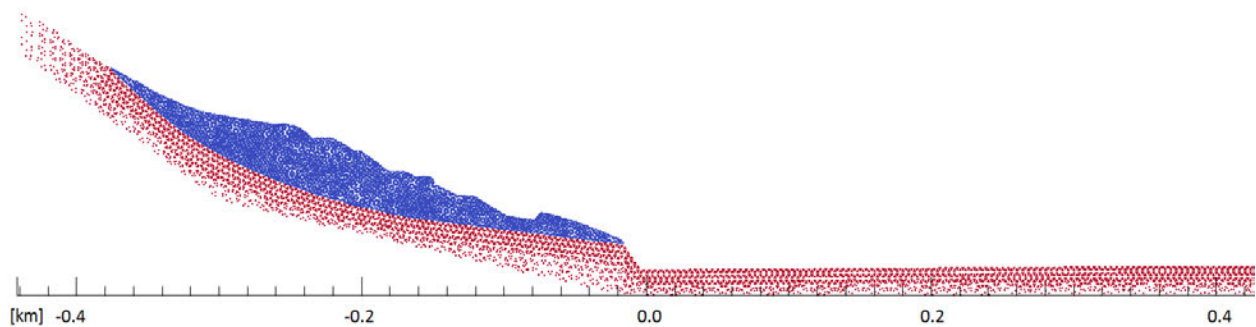
Figure K-2. Initial distribution of the material points. Materials located above the contact surface are indicated in blue, while material points below the contact surface are in red.

4.2 Model parameters

Undrained total stress analysis is performed, because the runout of the 2006 Hazel landslide occurred rapidly. The model is initialized under an elastic gravity loading. Then, the instability is triggered by decreasing the strength down to a specified value.

A geometry and stratigraphy adopted in the MPM runout analyses of the 2006 Hazel landslide is based on Figure J-1 of Appendix J.1 as shown in Figure K-3, which is in turn based on the available

pre-2006 landslide LiDAR and topographic data. The Hazel slide is also referred to as the M1 slide material of the 2014 SR-530 landslide. In these analyses (similar to the slope stability analyses of Appendix J), the disrupted M1 slide debris material is modeled as one material. A second material in the MPM model is the mid-slope bench, which is also referred to as the M2 slide material of the 2014 SR-530 landslide. The saturated unit weight of M1 and M2 materials is 18.05 kN/m^3, which is consistent with the unit weight values of these materials used in the slope stability analyses.

The constitutive model considered for all materials is the Tresca model, because an undrained total stress analysis is performed. The undrained shear strengths (c_u) of M1 and M2 during mobilization are estimated based on the parametric study reported in this section. For M1, the undrained shear strength reduces linearly when it reaches the river from its initial estimated value to 2 kPa once it reaches the opposite edge of the river. This is to model the fluidization process when the material mixes with the river water.

The sliding mass displaces over a predefined contact slip surface in these analyses. The surface of rupture contour is maintained fixed during the calculation, which means that the material below the contact surface cannot be eroded. In Figure K-2, material points located above the contact surface are indicated in blue, while material points below the contact surface are indicated in red.

The contact is divided into different sections to simulate changes in lithology and surface type. The location of each zone is indicated in Figure K-4. Different adhesion strengths (following the assumption of undrained total stress analysis) are assigned to each section as described below.

- **Contacts initially located below the sliding materials (CM1 and CM2)**
  Adhesion is assumed equal to the undrained shear strength of the material just above
- **River (CR)**
  50 m wide
  Adhesion = 0 kPa
- **Transition zone (CTZ)**
  100 m
  Adhesion = linear increase from 0 to 5 kPa
- **Areas with vegetation and others (CV)**
  Covers the contact surface from the end of the transition zone until the end of the model
  Adhesion = 5 kPa

An iterative parametric analysis of varying the undrained shear strengths (c_u) of M1 and M2 during slide mobilization was performed. Different scenarios are considered: (i) same c_u values for both M1 and M2, (ii) different c_u values for M1 and M2, and (iii) with or without fluidization of M1.

The effects of the M1 and M2 undrained shear strengths on the 2006 Hazel landslide runout behavior was examined considering that it was observed that: (i) the edge of the final runout was approximately 200 meters south of the toe of the surface of rupture in 2006, and (ii) the M2 slide mass did not mobilized fully in 2006.
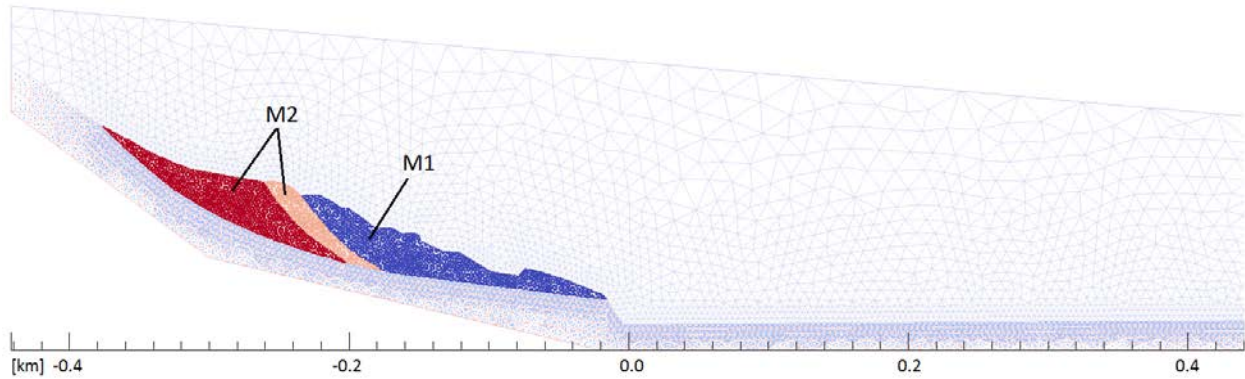
Figure K-3. Initial location of M1 and M2.
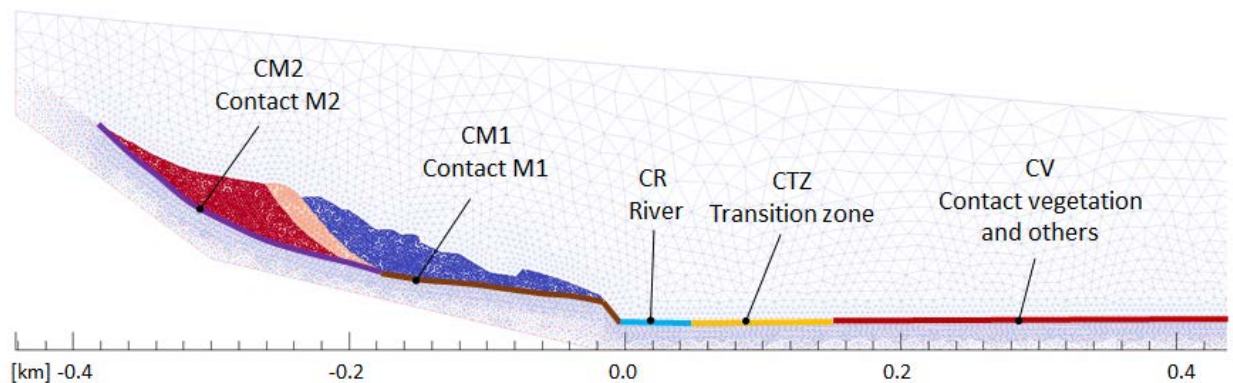
Figure K-4. Zones of the contact surface.

4.3 Results

The results of the parametric study show that the undrained shear strengths for M1 and M2 during slide mobilization are approximately 50 and 120 kPa, respectively. These values of undrained shear strength are consistent with the undrained shear strength of the M2 unit assuming that the pre-failure strength of this material is on average equivalent to that from the initiation slope stability analyses (Appendix J) and that the post-failure strength of the M1 unit is on average equivalent to a significantly reduced undrained shear strength of a material undergoing significant deformation and remolding during failure.

Figure K-5 (a) shows the initial distribution of the material points, whereas Figure K-5 (b) shows the final distribution of the material points at t = 53 seconds when the movement of the material points became small. The calculated debris field is higher than what was observed in the field, because these simulations are for plane strain conditions; whereas in the field, the debris displacement has a 3D aspect that enables material to move out of the cross section that was drawn down its middle. Additionally, a refined mesh would be necessary to capture the height of the debris field more accurately, but this would have led to excessive computational time.

The evolution of shear strain, which is shown in Figure K-6, indicates that different stages can be distinguished during the motion. Initially, the upper and center part of M1 is mobilized along a shear band. Then, this part pushes the toe of M1. Finally, the lower part of M2 also slides. However, the movement of M2 is limited, as observed in the field. The simulated extent of M1 movement matches with the field observation, which is shown by the dotted line in Figure K-5 (b).

The velocity field at three different times (t = 2, 10 and 53 seconds) is presented in Figure K-7. The maximum velocity is approximately 7 m/s.

The use of undrained shear strength values that differ only slightly from these calibrated undrained shear strength values of M1 and M2 should not have significant effects on the results. The use of significantly different undrained shear strength values than these calibrated undrained shear strength values of M1 and M2 do produce results that do not match field observations. Therefore, reasonable undrained shear strength values must be employed, but an unobtainable level of precision need not be achieved to produce reasonable results.
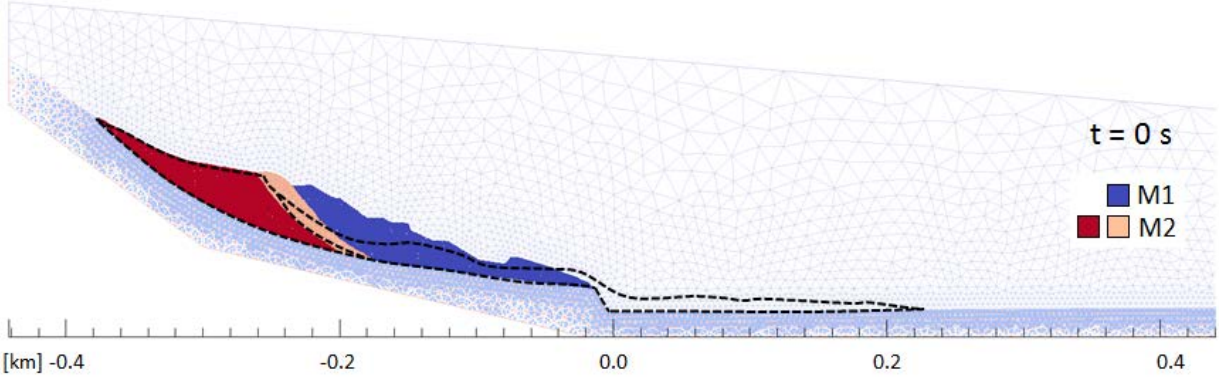
(a)
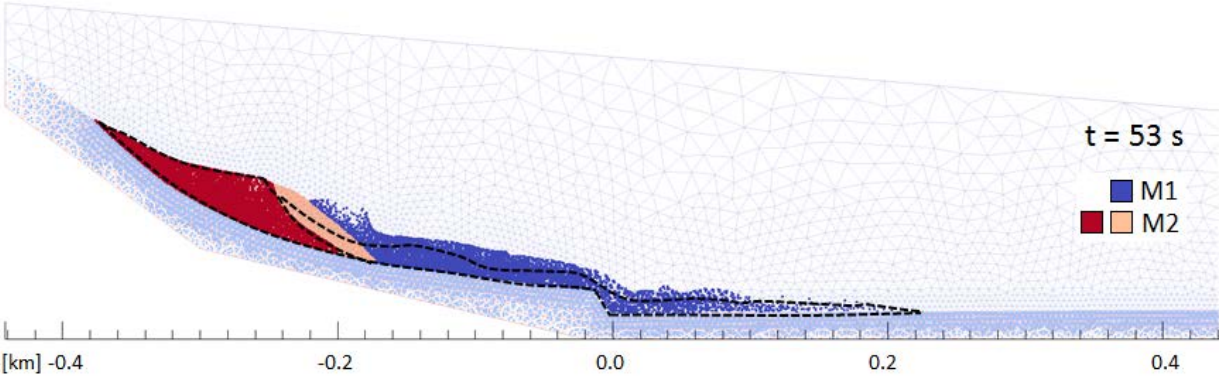
(b)

Figure K-5. (a) Initial distribution of the material points (t=0 s), and (b) final distribution of the material points (t=53 s) for the 2006 Hazel landslide runout. The observed final topography of the 2006 Hazel slide runout is indicated with a dashed line.
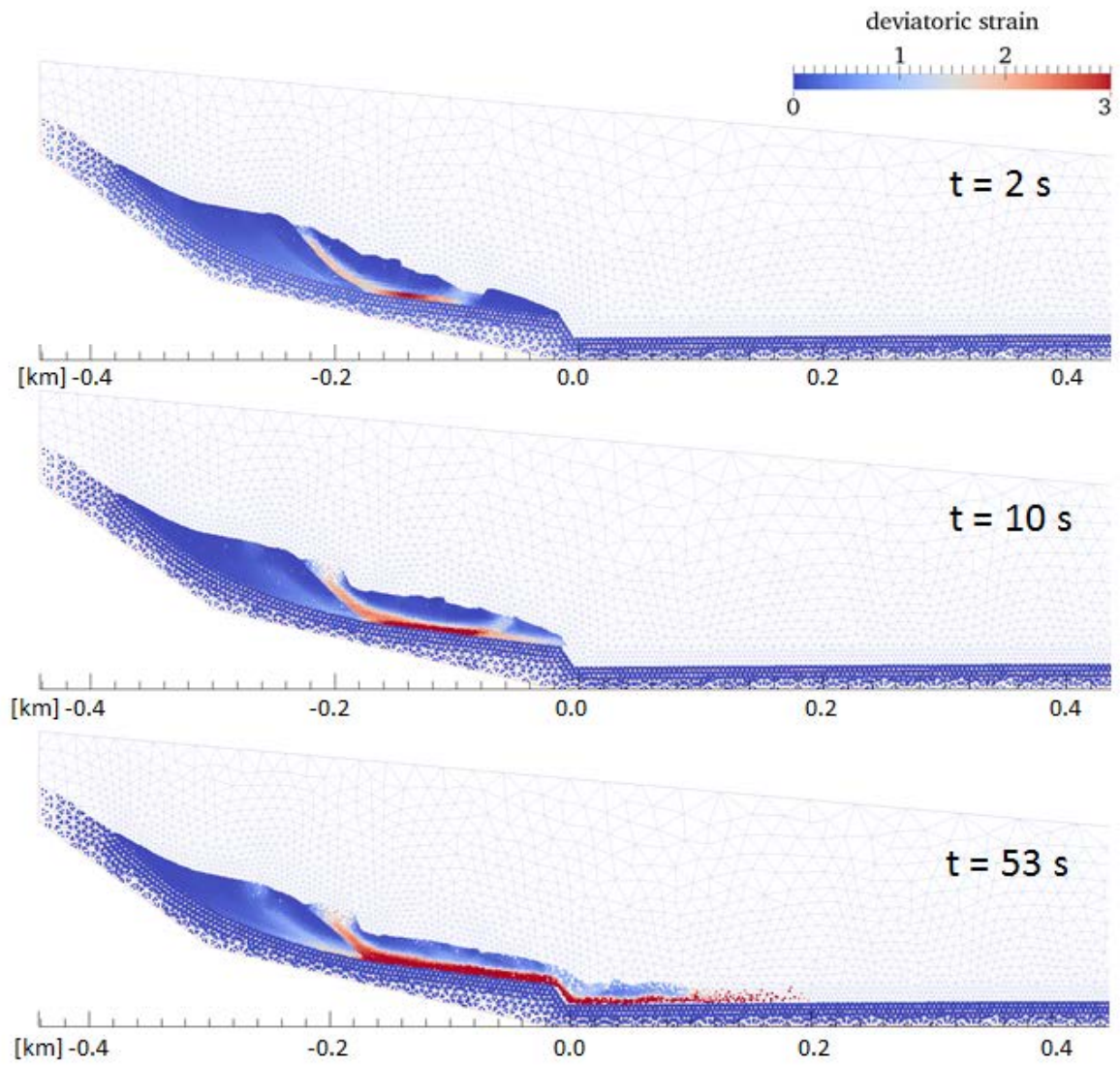
Figure K-6. Evolution of shear strain at 3 different moments during the 2006 Hazel landslide runout.
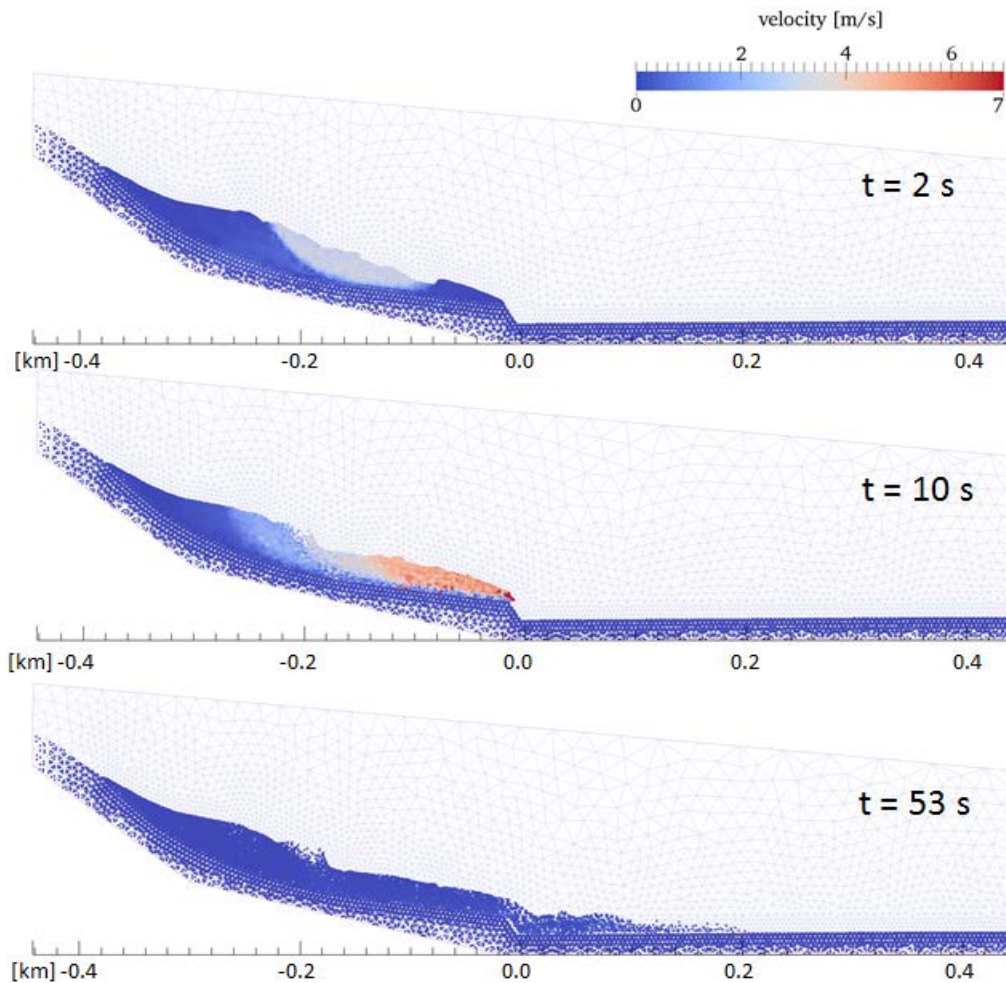
Figure K-7. Kinematics of the 2006 Hazel landslide runout. Velocity field at 3 different moments.

4.4 Findings

The adopted MPM model is able to capture the observed distance of the 2006 Hazel landslide runout. The results of the parametric MPM study of the 2006 Hazel landslide indicate that the observed runout is best captured when the undrained shear strengths and adhesions along the surface of rupture are 50 kPa for the M1 mass, which has been mobilized fully according to field observations and the slope stability analyses presented in Appendix J, and 120 kPa for the M2 mass, which has not been mobilized significantly in January 2006 according to field observations and the slope stability analyses presented in Appendix J.

Therefore, the undrained shear strength of the M1 material in future analyses is established to be 50 kPa. Similarly, the undrained shear strength of the M2 material in future analyses where it is mobilized fully is established to be 50 kPa. The undrained shear strength of similarly sized masses that do not displace significantly should be 120 kPa or higher.

5. Plane strain simulations of the 2014 SR-530 landslide

5.1 Model

The March 22, 2014 SR-530 landslide is now back-analyzed using the MPM using an approach similar to that employed in the previously discussed January 2006 Hazel landslide back-analyses. The undrained shear strength parameters used in the 2014 SR-530 runout analyses are consistent with those used in the calibration analysis of the 2006 Hazel landslide (which was presented in Section 4) when the material is in the same state (i.e., pre-failure or failure). The 2014 SR-530 landslide runout is analyzed considering the materials involved in the landslide and the end of the 2013 calendar year topography, geometry, and stratigraphy established and discussed in the previous appendices of this report.

As was done in the previous runout analysis, the computational mesh of the plane strain SR-530 landslide is formed by linear tetrahedral elements. The thickness of model is one element and out-of-plane deformation is restricted to ensure plane strain conditions. The mesh is refined and made homogeneous in the region where the mobilized mass will move to optimize the computational time and to obtain more accurate results. The minimum edge of the elements is 3 m. A general view of the mesh is shown in Figure K-8. Note that elements indicated in red color are initially fully filled with material, while elements in blue are initially empty.

Initially 4 material points are distributed within each element and are initially located at the corresponding integration points of a four-point Gaussian quadrature. Figure K-9 shows the initial location of the material points in the slope. This model has 49,674 elements and 98,448 material points.
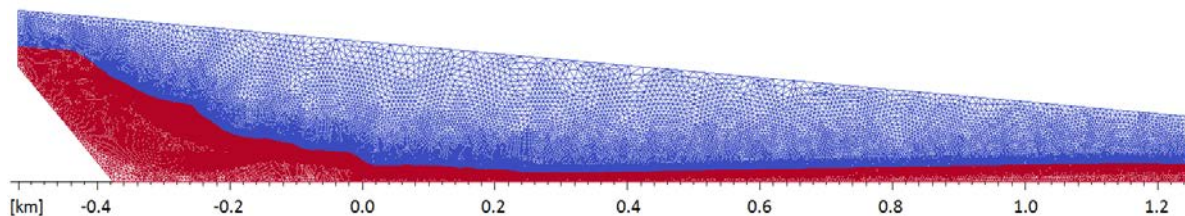
Figure K-8. General view of the computational mesh of the 2014 SR-530 landslide model with the 2006 debris field. Elements in red indicate that initially are fully filled with material, while elements in blue are initially empty.
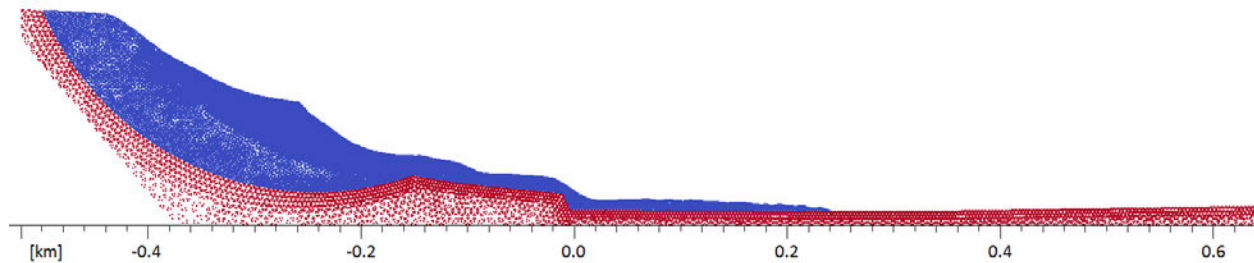
Figure K-9. Initial distribution of the material points in the 2014 SR-530 landslide model with the 2006 debris field. Materials located above the contact surface are indicated in blue, while material points below the contact surface are in red.

5.2 Model parameters

Undrained total stress analysis is performed again, because the runout of the 2014 SR-530 landslide occurred rapidly. The model is initialized under an elastic gravity loading. Then, the instability is triggered by decreasing the strength down to a specified value.

A geometry and stratigraphy adopted in the MPM runout analyses of the 2014 SR-530 landslide is based on Figure J-1 of Appendix J as shown in Figure K-10, which is in turn based on the available pre-2014 landslide LiDAR and topographic data. In addition to the M1 and M2 slide masses modeled in the 2006 Hazel landslide, the M3 slide mass is added because field observations indicated this mass displaced which is consistent with the slope failure initiation analyses presented in Appendix J. The 2006 debris field material that was deposited below the toe of the surface of rupture of the landslide during the 2006 Hazel landslide is modelled at the bottom of the slope between the toe of the surface of rupture and the north edge of the North Fork of the Stillaguamish River.

As shown in Table K-1, the saturated unit weight of M1/M2/debris materials is 18.05 kN/m^3, which is consistent with the 2006 landslide runout analyses discussed previously, whereas that of M3 is 19.62 kN/m^3, which is consistent with the average unit weight of this slide mass used in the slope stability analyses of Appendix J.

The constitutive model considered for all materials is the Tresca model, because an undrained total stress analysis is performed. The undrained shear strength of each material is assigned as shown in Table K-2. For the runout analysis of the 2006 Hazel landslide, the undrained shear strength (c_u) of M1 for the condition of full mobilization of the M1 slide mass was estimated to be 50 kPa. Similarly, the undrained shear strength of M2 was assigned as 50 kPa to simulate the 2014 SR-530 landslide, because it too achieved full mobilization during the 2014 SR-530 landslide (as evidenced by field observation and consistent with the results of the slope failure initiation analyses shown in Appendix J.2 in the Stage 2 analyses). The undrained shear strength of M3 during full mobilization is assigned to be 100 kPa based on an initial estimate of its pre-failure undrained shear strength which is consistent with the shear strength of the lacustrine clay and silt unit along the surface of rupture and a strength reduction similar in scale to that applied to M1 and M2. The undrained shear strength of the debris field material is assigned as 2 kPa based on the values developed for this material in Appendix E, which considers this material to be in a liquefied state or in a state close to the liquid state of soil.

As in the 2006 Hazel landslide runout analyses, the undrained shear strength of M1 reduces linearly when it reaches the river from its initial value of 50 kPa to 2 kPa once it reaches the opposite edge of the river. This is to model the fluidization process when the material mixes with the river water.

The runout analysis is performed in two stages to capture field observations and the seismic signal analysis inference that the 2014 SR-530 landslide movement occurred in two stages. Initially, M1 and M2 slide masses are triggered, while the M3 slide mass is initially maintained as a stable mass. After 25 seconds, the M3 slide mass is released by artificially decreasing its undrained shear strength from 9999 kPa to 100 kPa.

The seismic signal analysis of Dr. Douglas Dreger of the University of California, Berkeley was relied upon to assess the size and timing of the stages of the 2014 SR-530 landslide. Firstly, Dr. Dreger examined the available nearby seismic recordings at the time of the January 2006 Hazel landslide. No significant seismic long-period signal associated with the 2006 Hazel landslide (which was essentially just the M1 slide mass) was noticeable above the background noise in the signals. Likewise, it is hypothesized that the movement of a similar sized (or smaller) slide mass on March 22, 2014 would not produce a significant seismic signal. However, the mobilization of the larger M2 slide mass or a combined M1/M2 slide mass would likely generate a seismic signal that would be observable in the nearby recordings. This is considered the first part of the seismic signal recorded for the March 22, 2014 SR-530 landslide. A second subevent within the seismic signal was likely produced by a large slide movement such as the M3 slide mass. Dr. Dreger detected up and north-directed forces in his analysis of the seismic signals from the SR-530 landslide that indicate a mass movement down and to the south 25 seconds after the onset of the landslide. It is possible to interpret this inflection as a second subevent. While the resolution of the seismic signals recorded at the nearby stations does enable Dr. Dreger to identify unequivocally the start of the majority of this second stage of the slide movement, he does also see indications that it may have started 20 seconds after the onset of the slide in the force-rate plots. Thus, Dr. Dreger found evidence to support a two-stage landslide movement wherein the stages are separated by 20 to 25 seconds. Iverson et al. (2015) also identified two stages within the seismic signals of the 2014 SR-530 landslide movement, although their estimate was slightly longer than the separation time estimated by Dr. Dreger. Importantly, there is field evidence to support a two-stage landslide movement (Keaton et al. 2014). The upper estimate of the range provided by Dr. Dreger (i.e., 25 seconds) was used in these simulations of the runout of the 2014 SR-530 landslide.
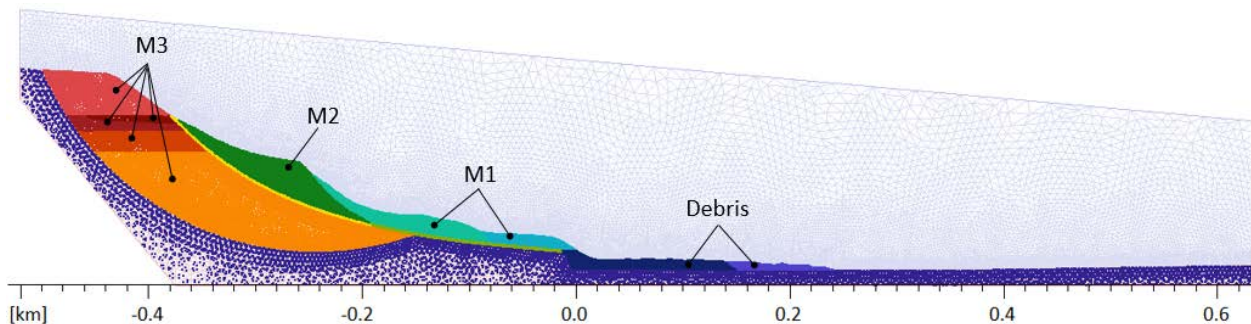
Figure K-10. Initial location of M1, M2, M3 and debris material in the 2014 SR-530 landslide model with the 2006 debris field.

Table K-1. Saturated unit weight of materials (and shear bands) [kN/m^3].

Saturated unit weight [kN/m3]			
M3	M2 / SBM2	M1 / SBM1	Debris
19.62	18.05	18.05	18.05

Table K-2. Undrained shear strength [kPa].

	Undrained shear strength [kPa]			
	M3	M2	M1	Debris
0 < t < 25 s	9999	50	50	2
t > 25 s	100	50	50	2

Similar to the 2006 Hazel landslide runout analysis, the 2014 SR-530 sliding masses displace over predefined contact slip surfaces in these analyses. The surface of rupture contour shown in Figure K-11 is maintained fixed during the calculation, which means that the material below the contact surface cannot be eroded. The contact is divided into different sections to simulate changes in lithology and surface type. In addition, to perform the two stages of the runout, the initial contact between M1/M2 and M3 has been simulated by means a shear band of two elements thick material (SBM1 and SBM2). This contact cannot be a fixed surface since M1, M2, and M3 all slide independently and move relative to each other. The saturated unit weight of the shear band material is 18.05 kN/m^3.

The adhesion values of the contact surfaces and the shear strengths of the shear bands are given in Table K-3. The values for the river section (CR), transition zone and areas with vegetation and others are the same as used for the 2006 Hazel landslide runout analyses. The debris section has 2 kPa, which is the same as the undrained shear strength of the debris material. The adhesion of the contacts below M3 (CDM3 and CSM3) is initially high (999 kPa) to ensure that M3 does not move. At t=25 seconds this value is decreased to initiate the motion of M3. The deep contact surface section of M3 (CDM3) has an adhesion strength of 50 kPa, whereas the shallow contact surface section of M3 (CSM3) has an adhesion strength of 0 kPa to represent a tension crack forming in the headscarp region.

The shear band strength under M2 (the purple section in Figure K-11, SBM2) and the contact and shear band strength under M1 (the brown section in Figure K-11, SBM1) are varied as either 50 kPa or 25 kPa. These values are considered to represent the possible degrees of strength softening along the sliding plane during the slide mobilization of M1 and M2.
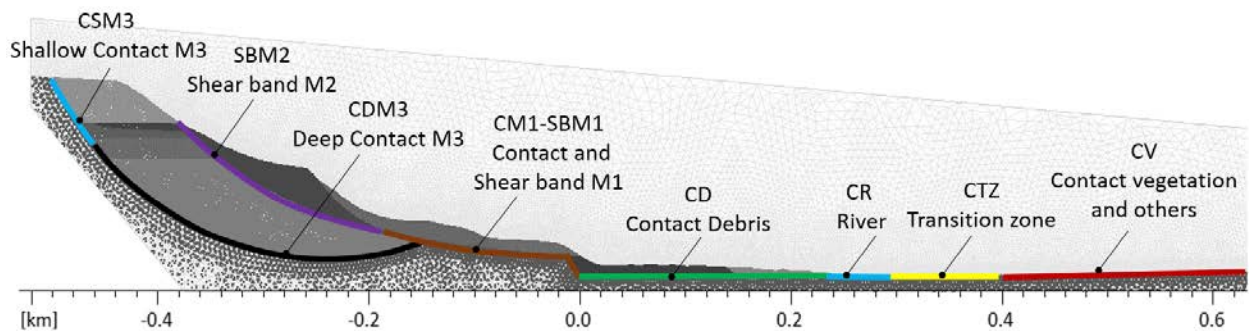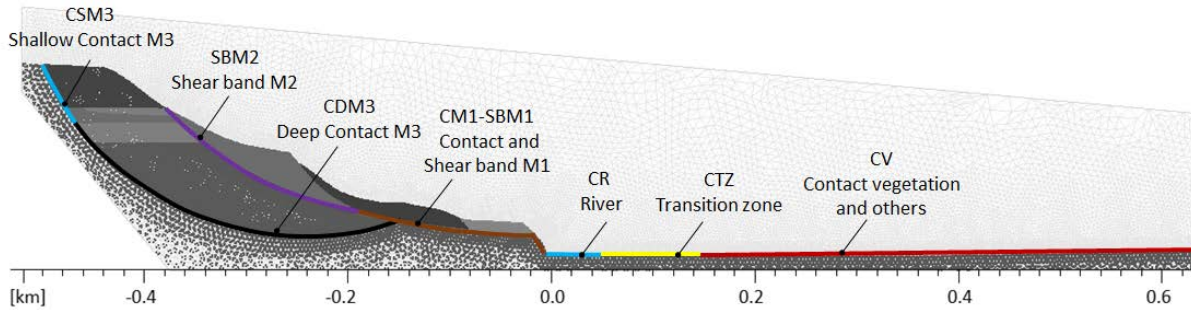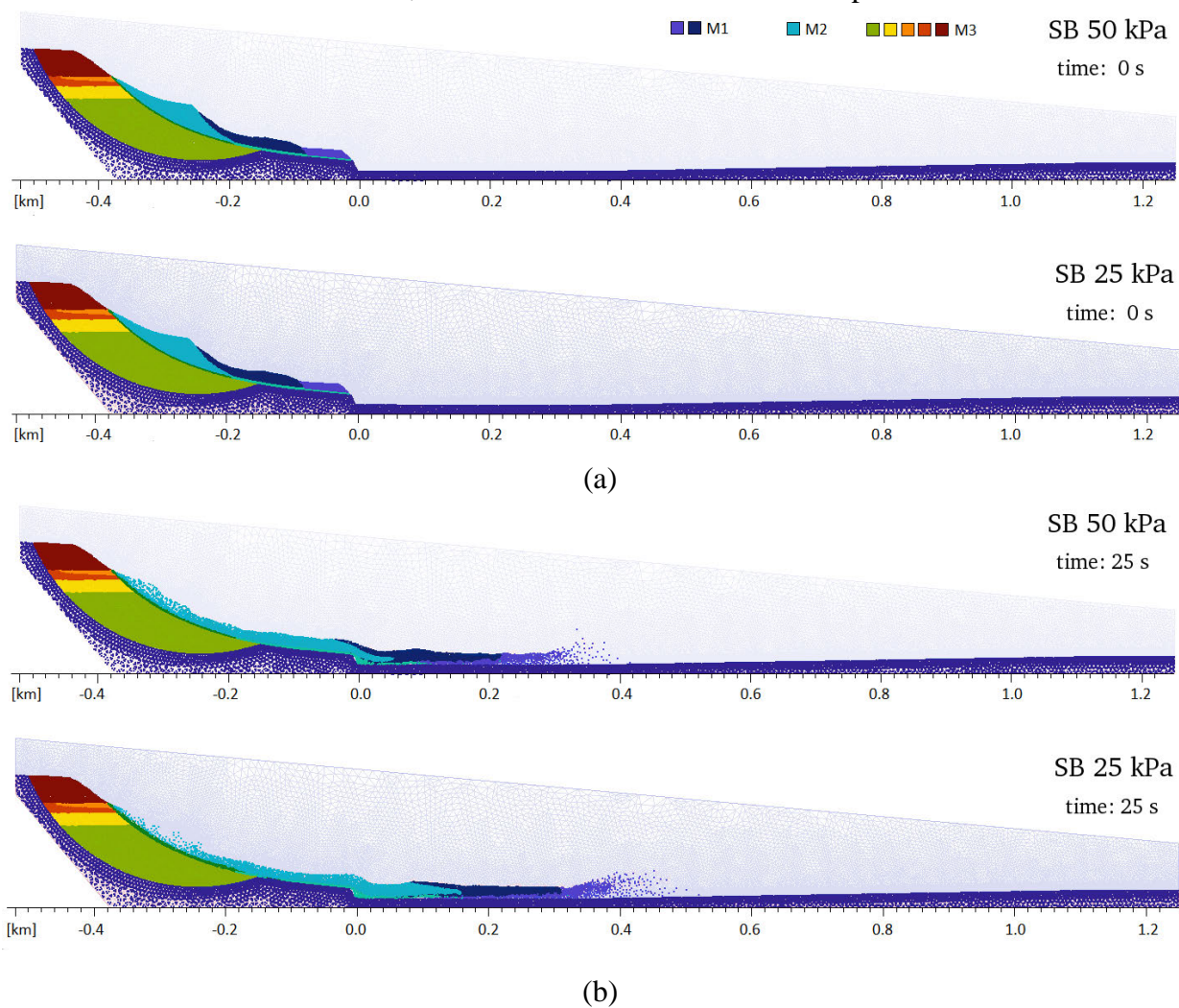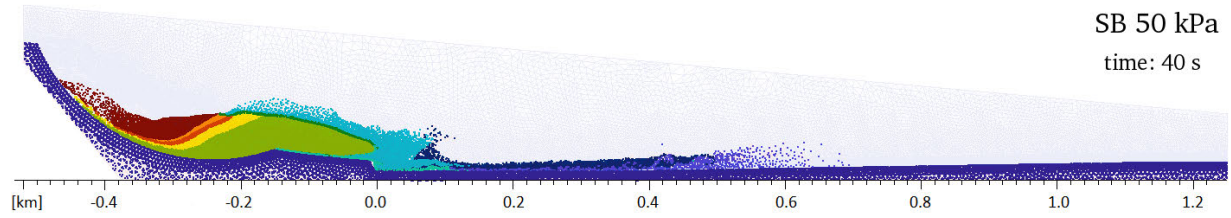

Figure K-11. Zones of the contact surface (C) and shear band (SB) in the 2014 SR-530 landslide model with the 2006 debris field.

Table K-3. Adhesion of contacts and shear bands [kPa].

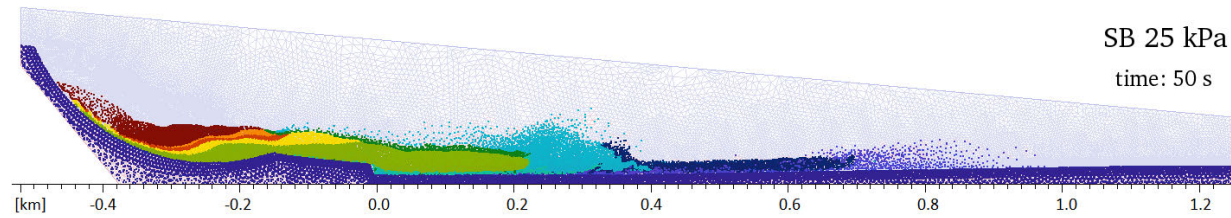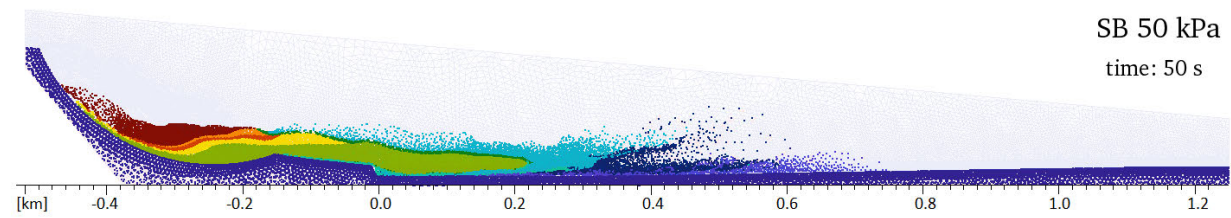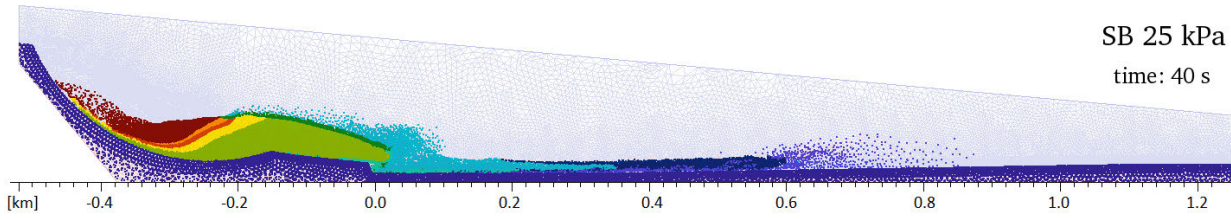|	Adhesion of Contact/Shear band [kPa]							
	CSM3	CDM3	SBM2	CM1-SBM1	CD	CR	CTZ	CV
0 < t < 25 s	999	999	*	*	2	0	0 to 5	5
t > 25 s	0	50	*	*	2	0	0 to 5	5

* depends on the analysis (25 kPa or 50 kPa)

5.3 Results

Figure K-12 shows the runout behavior at different times for the two cases of different adhesion and shear band strengths under M1 and M2 (i.e., 50 kPa and 25 kPa cases). From the results, the runout distances of the different units are evaluated and the evaluated values are compared to the field observation in Table K-4. The temporal behavior of each unit is different. For example, the movements of M1 and M2 prior to the initiation of M3 at t = 25 seconds are different and more movement of M1/M2 is observed when the adhesion and shear band strengths reduces from 50 kPa to 25 kPa. After M3 initiation, M1/M2 are pushed by M3 and the runout distances of M1/M2 increase. The positon of the leading edge of M3 varies between 150 m and 190 m from the origin (the river location in 2006). The computed positions are similar to those observed in the field.

(a)

(b)

SB 50 kPa
time: 40 s

SB 25 kPa
time: 40 s

(c)

SB 50 kPa
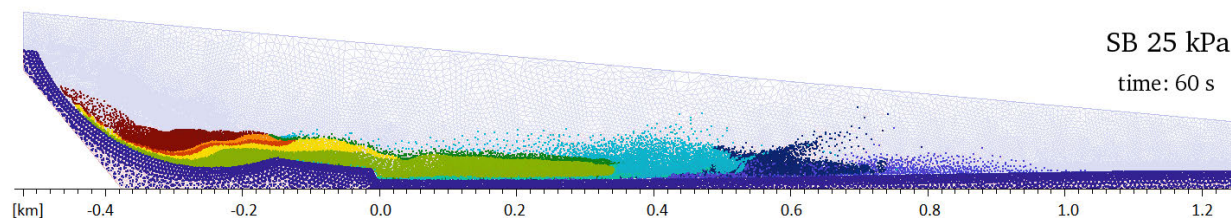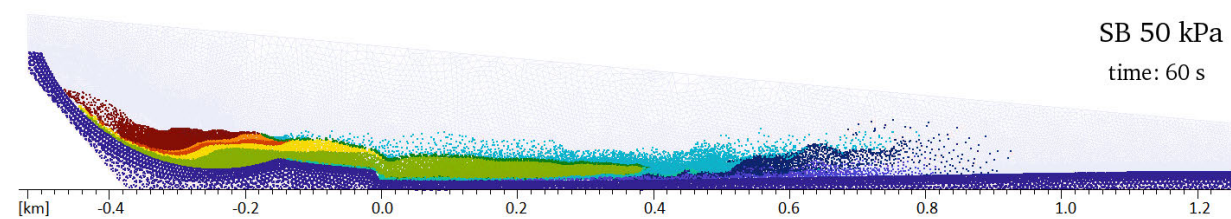time: 50 s

SB 25 kPa
time: 50 s

(d)

SB 50 kPa
time: 60 s

SB 25 kPa
time: 60 s

(e)

(f)
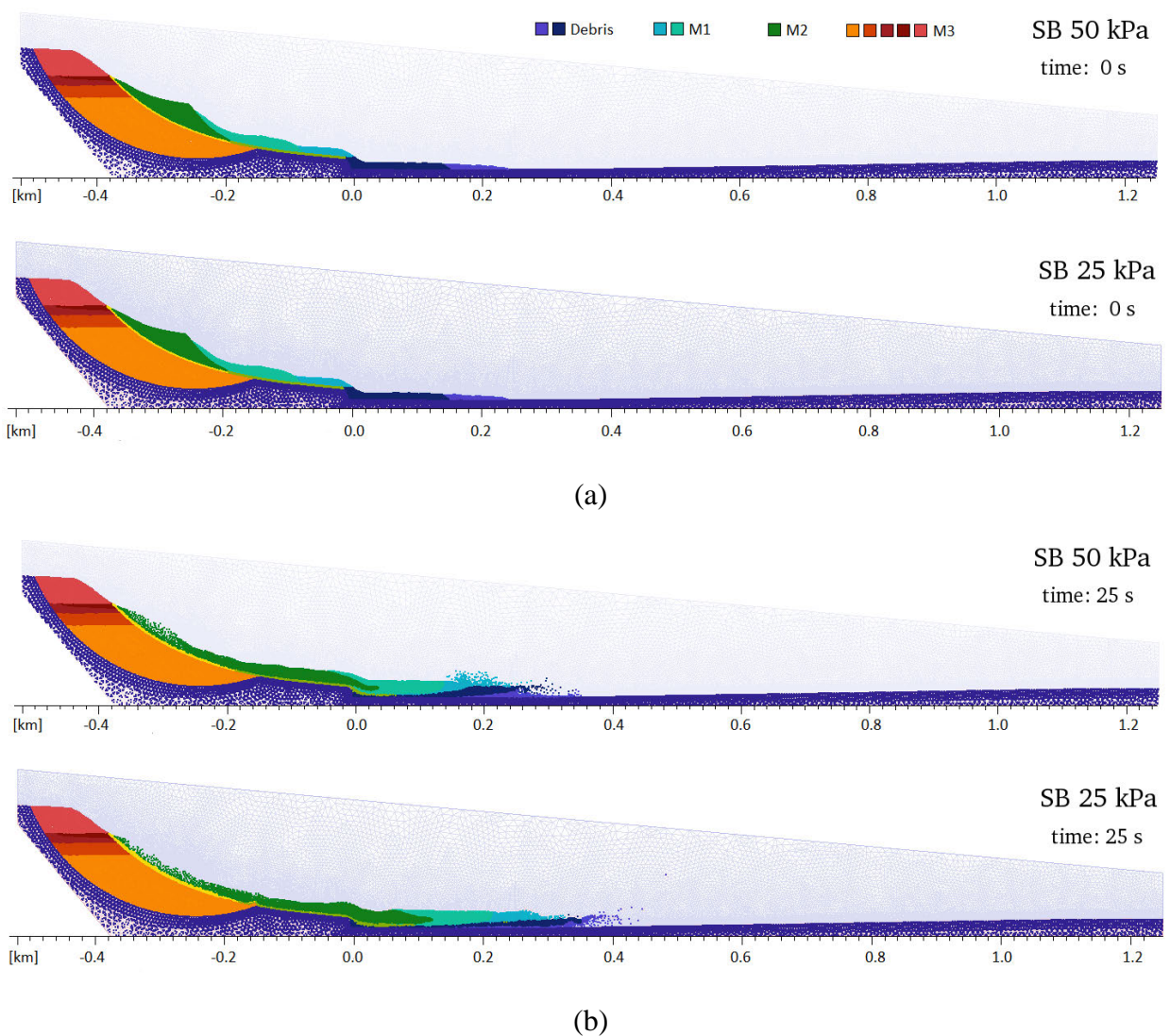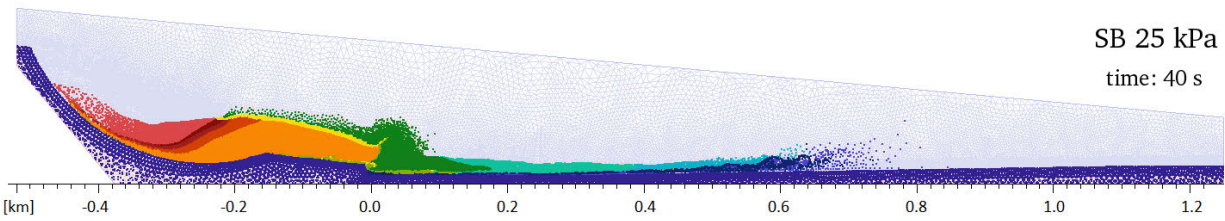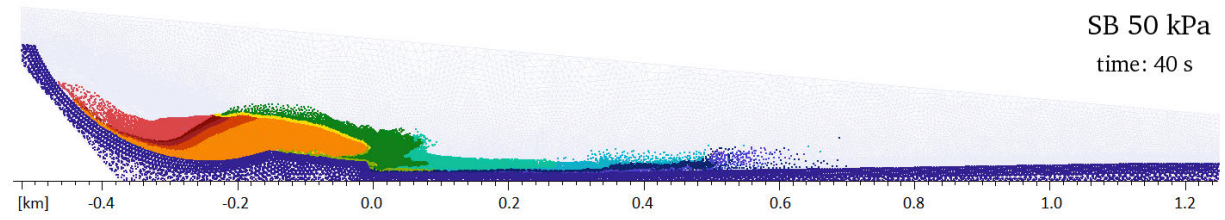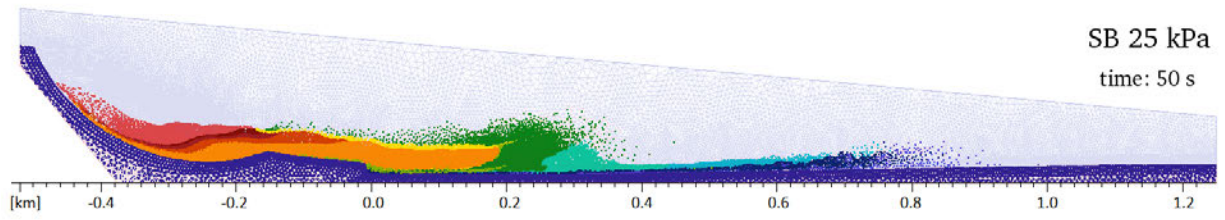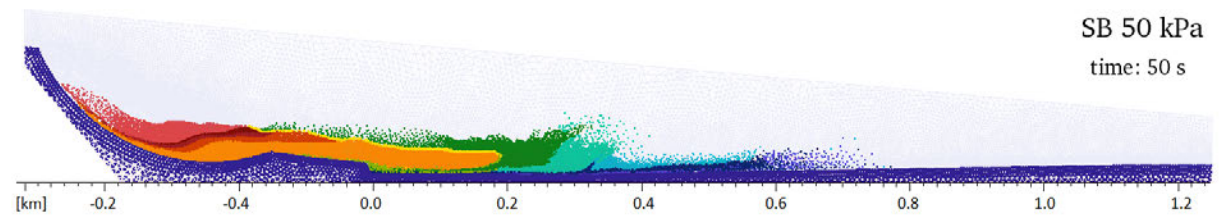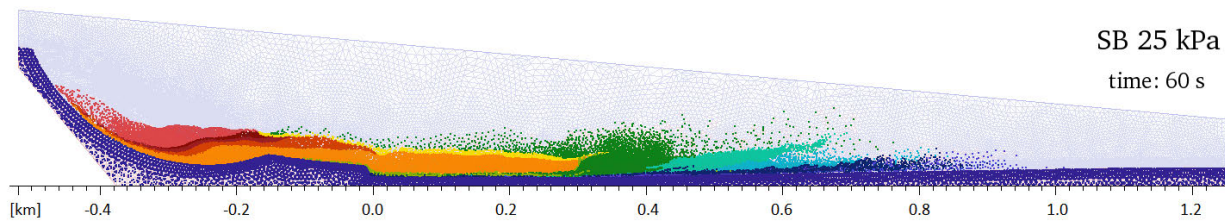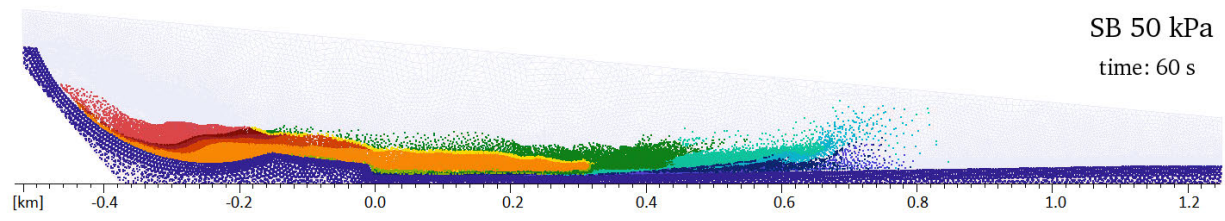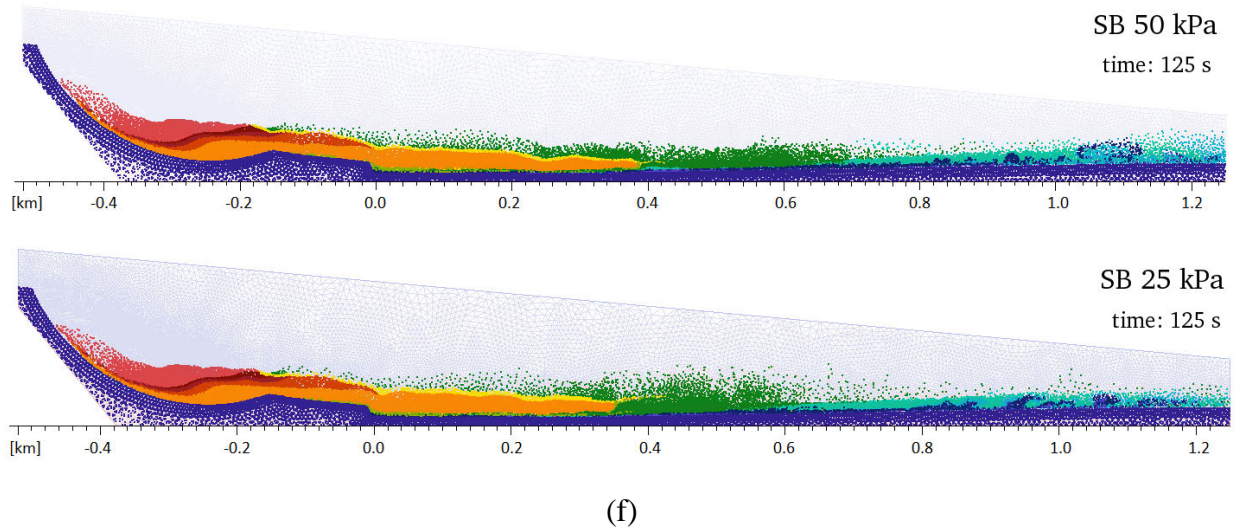
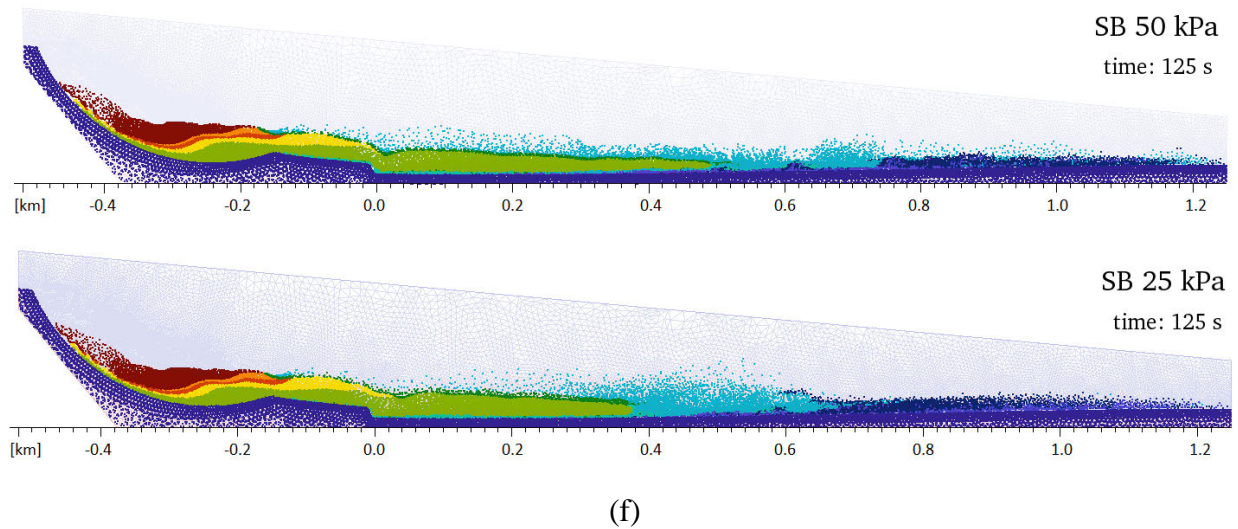Figure K-12. MPM results of the 2014 SR-530 landslide model with the 2006 debris field considering different adhesions in the shear band (SBM1 and SBM2): 50 and 25 kPa. (a) t = 0 s, (b) t = 25 s, (c) t = 40 s, (d) t = 50 s, (e) t = 60 s, (f) t = 125 s.

Table K-4. Distances from crib wall (in the model the crib wall is located at x-axis = 200 m).

Feature	Field observations	SB 50 kPa	SB 25 kPa
Leading edge M-3	+162m	+190m	+150m
Leading Edge of M-2 (lower portions of block)	+662m	+700-980m	+630-1000m
Leading Edge of Debris Flow (M-1)	+962m	+1050m	+1050m

5.4 Findings

The MPM model that was calibrated to capture the observed distance of the 2006 Hazel landslide runout was able to capture the general characteristics and runout distance of the 2014 SR-530 landslide. The results of the parametric MPM study of the 2006 Hazel landslide indicated that its observed runout is best captured when the undrained shear strength and adhesion along the surface of rupture are for slide masses of the size of M1 or M2 should be 50 kPa. Accordingly, this undrained shear strength value was used for M1 and M2 in the 2014 runout analyses. Likewise, the estimated undrained shear strength of the fully mobilized M3 slide mass was similarly reduced to a value of 100 kPa, which was judged to be appropriate for its larger size (and hence larger initial effective stresses, etc.). As suggested by the field evidence and seismic signal analysis, the M3 slide mass was released 25 seconds after the 2014 SR-530 landslide commenced. The calculated runout distance of the 2014 SR-530 landslide is captured well with these analyses, which are in turn consistent with the 2006 Hazel landslide analyses that captured its observed behavior well.

Results of a parametric study that varies the adhesion and shear band strengths under M1 and M2 to be either 50 or 25 kPa show that both cases exhibit similar final configurations of the materials that match with the field observations. The key difference between the runout distances of the 2006 Hazel landslide and the 2014 SR-530 landslide appears to be due to the larger and higher combined mass of the M1/M2 sliding mass and the push from the much larger and much higher M3 sliding mass. The larger mass of the combination of M1, M2, and M3 coupled with M2 and M3 initiating from a higher starting elevation produces the long runout of the 2014 SR-530 landslide.

Most importantly for this study, the calibrated MPM runout analyses of the 2014 SR-530 landslide captured the key attributes of the observed runout including its long runout distance. Consequently, the calibrated 2014 SR-530 MPM model can now be used to investigate the potential effects, if any, of changes in the landslide geometry such as the absence of the 2006 debris field at the bottom of the slide.

6. Plane strain simulations of a hypothetical case of the 2014 SR-530 landslide without the 2006 debris field material.

6.1 Model

The previously calibrated MPM model is redeveloped without the 2006 debris field material below the toe of the surface of rupture of the 2014 SR-530 landslide. The North Fork of the Stillaguamish River is repositioned at its position before the 2006 Hazel landslide. Figure K-13 shows the computer mesh, whereas Figure K-14 shows the initial distribution of material points. There are no material points at locations where the debris field material existed in the previous case, because it has been removed for these analyses.

The model has 49,674 elements and 98,448 material points.
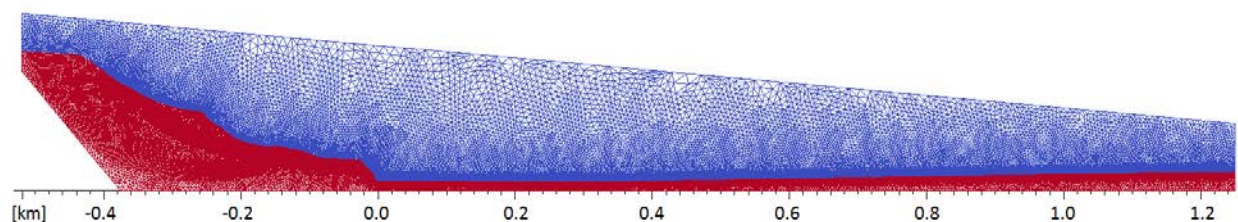
Figure K-13. General view of the computational mesh of the hypothetical 2014 SR-530 landslide model without the 2006 debris field. Elements in red indicate that initially are fully filled with material, while elements in blue are initially empty.
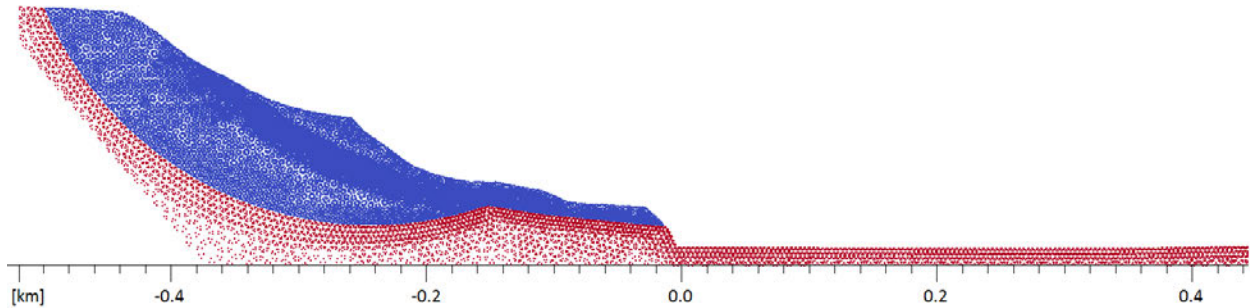
Figure K-14. Initial distribution of the material points in the hypothetical 2014 SR-530 landslide model without the 2006 debris field in place. Materials located above the contact surface are indicated in blue, while material points below the contact surface are in red.

6.2 Model parameters

Figure K-15 shows the initial locations of M1, M2, and M3. There is no debris field located below the toe of M1. The undrained shear strengths of M1, M2, and M3 as well as the adhesion and shear band strengths below M1, M2 and M3 are exactly the same as used in the previous runout analysis of the 2014 SR-530 landslide.

The contact surfaces and shear bands are shown in Figure K-16. The river position is placed to be the location where the river existed prior to the 2006 Hazel landslide. The adhesion values of the contact surfaces and the shear strength values of the shear bands are exactly the same as the 2014 SR-530 landslide case presented in Section 5. Again, the sensitivity of the adhesion and shear band strength values under M1 and M2 is examined by varying the values to be 50 kPa or 25 kPa.
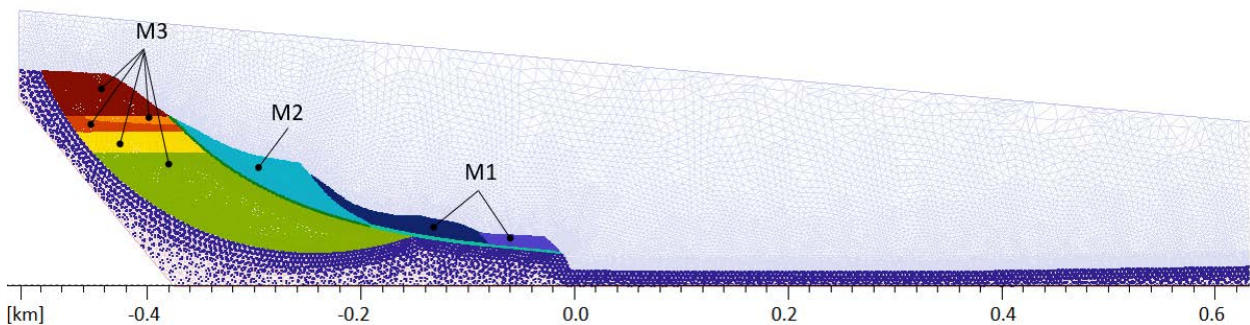
Figure K-15. Initial location of M1, M2, M3 in the hypothetical 2014 SR-530 landslide model without the 2006 debris field.

Figure K-16. Zones of the contact surface (C) and shear band (SB) in the hypothetical 2014 SR-530 landslide model without the 2006 debris field.

6.3 Results

Figure K-17 shows the runout behavior at different times for the two cases of different adhesion and shear band strengths under M1 and M2 (i.e., 50 and 25 kPa cases). The runout behavior of the two hypothetical cases where there is no 2006 debris field are similar to the cases which simulated the actual 2014 SR-530 landslide, which had the 2006 debris field in place.

(a)

(b)

SB 50 kPa
time: 40 s

SB 25 kPa
time: 40 s

(c)

SB 50 kPa
time: 50 s

SB 25 kPa
time: 50 s

(d)

SB 50 kPa
time: 60 s

SB 25 kPa
time: 60 s

(e)

(f)

Figure K-17. MPM results of the hypothetical 2014 SR-530 landslide model without the 2006 debris field considering different adhesions in the shear band (SBM1 and SBM2): 50 and 25kPa. (a) t = 0 s, (b) t = 25 s, (c) t = 40 s, (d) t = 50 s, (e) t = 60 s, (f) t = 125 s.

6.4 Findings

The MPM model that was calibrated to capture the observed distance of the 2006 Hazel landslide runout and the general characteristics and observed runout distance of the 2014 SR-530 landslide was rerun with only one change relative to the 2014 SR-530 landslide MPM model (i.e., the 2006 debris field located between the toe of the landslide and the river was removed) to investigate the potential effects of the absence of the 2006 debris field at the bottom of the slide. The simulated runout behavior of the hypothetical case where there is no debris field below the toe of the landslide is similar to the simulated runout behavior of the actual 2014 SR-530 landslide case.

The key difference between the runout distances of the 2006 Hazel landslide and the actual 2014 SR-530 landslide appears to be due to the larger and higher combined mass of the M1/M2 sliding mass and the push from the much larger and much higher M3 sliding mass. The larger mass of the combination of M1, M2, and M3 coupled with M2 and M3 initiating from a higher starting elevation produces the long runout of the 2014 SR-530 landslide. Removal of the 2006 debris field does not change the calculated results appreciably; that is, the presence or absence of the debris field is found to be relatively unimportant in these runout analyses.

7. Depth-averaged simulations of the 2014 SR-530 landslide

7.1 Model

Considering the 2D plane strain analysis of 2014 SR-530 landslide presented previously in sections 4 and 5, the same two different scenarios are simulated using *DA-MPM*: (Scenario 1) the 2006

debris field remained below the bottom of the toe of the surface of rupture; and (Scenario 2) the 2006 debris field has been removed and the position of the North Fork of the Stillaguamish River has been returned to its position before the 2006 Hazel landslide. Three dimensional bathymetries are generated based on the LiDAR data together with the estimated surface of rupture by 2D slope stability analyses. The results of the simulations were examined by comparing them with the runout extent observed after the 2014 SR-530 landslide. A reasonable agreement was shown when using the parameters calibrated in the plane strain runout analysis.

Figure K-18 is the bathymetry obtained by the LiDAR showing the area in 2013, before the 2014 SR-530 landslide. The areas shown by blue, red, and green lines indicate the estimated areas of M1, M2, and M3 slide masses, respectively. Based on the LiDAR data, the computational meshes are formed by quadrilateral elements whose size is 20 m × 20 m, as shown in Figure K-19. The total number of elements is 8,100.

The simulation consists of two stages. At the start of the analysis, 16 material points are distributed in each element that is contained in the source areas of M1 and M2. After releasing M1 and M2, the computation is conducted to 25 seconds. Then another collection of material points is allocated in the same manner for M3 landslide. Here, due to the depth-integration, a special scheme is needed to avoid an overlapping of the material points. The material points from the M1/M2 masses that remain above M3 are removed and added to the height of M3. As a result, some of the M1 and M2 material points are incorporated into the M3 material points. The initial numbers of material points are 1,495 for M1, 1,935 for M2, and 3,856 for M3 slide masses.
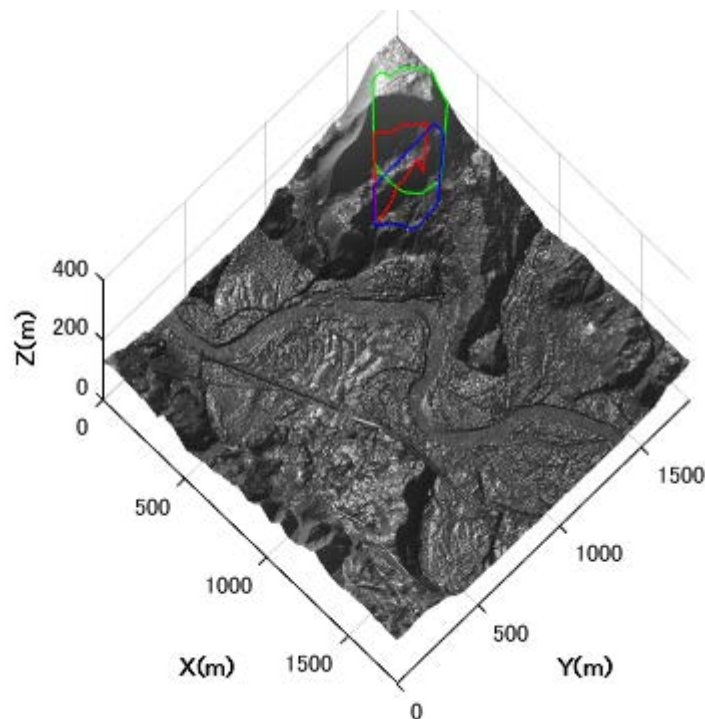
Figure K-18. Bathymetry based on 2013 LiDAR data (before the 2014 SR-530 landslide). The blue, red, and green lines indicate the estimated source areas of M1, M2 and M3 landslides, respectively.
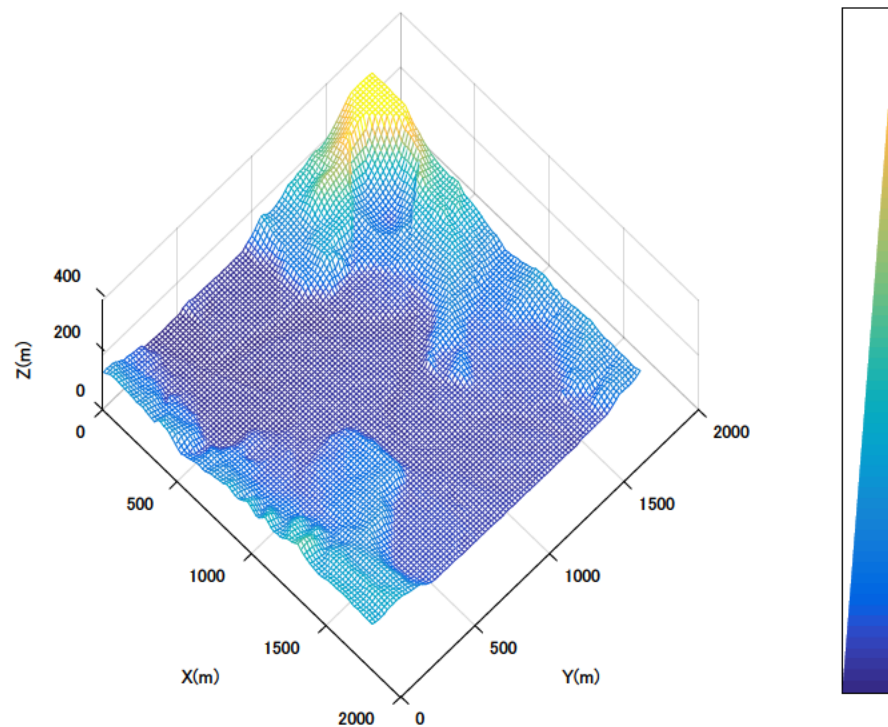
Figure K-19. Computational mesh with a 20 m resolution (90 x 90 = 8100 elements)

7.2 Model parameters

The Bingham fluid model has two parameters: yield strength τ_y and viscosity μ. These two parameters define the velocity profile in the depth direction, which is then integrated and averaged in the depth-averaged framework. In this depth-averaged analysis, the yield strength τ_y is assumed to correspond to the undrained shear strengths c_u evaluated in the plane strain analysis presented in the earlier sections. The initial yield strength is set at 25 kPa for M1 and M2 landslides and 50 kPa for M3 landslide. Meanwhile, the viscosity was fixed at 100 Pa-s for all simulations presented in this section. The runout behavior was similar when the viscosity was fixed at 1 Pa-s, indicating that the yield strengths (or undrained shear strengths) of the sliding masses governs the runout distance and front for this case.

After the initiation of each landslide, the yield strength varies depending on the positions reflecting the surface conditions of the bathymetry. In Scenario 1, the surface state of the location where the 2006 debris field material exists has a yield strength of 2 kPa. That is, when M1/M2/M3 material points move to this location, the yield strength of these material points becomes 2 kPa. Similarly, when the material points move on top of the river, the yield strength becomes a very small value of 1 Pa. As the material points then move on top of the area of vegetation, the yield strength becomes 5 kPa. In Scenario 2, there is no debris field condition and the North Fork of the Stillaguamish River is placed at the pre-2006 location.

Figures K-20 and K-21 show the two different runout scenarios considered in this study and summarize the yield strength for each boundary.
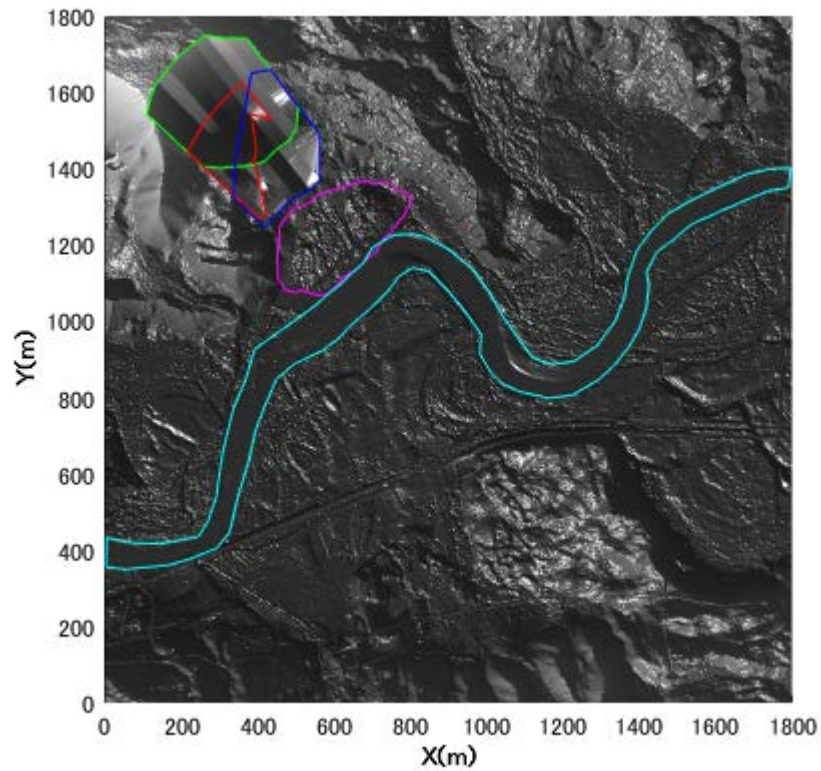
Figure K-20. Material parameters for Scenario 1: The debris from the 2006 Hazel landslide remain near the toe of the slope (corresponding to the actual scenario). M1 (Blue): Ty = 25 kPa, M2 (Red): Ty = 25 kPa, M3 (Green): Ty = 50 kPa, Debris from 2006 Hazel landslide (Magenta): Ty = 2 kPa, River (Cyan): Ty = 1 Pa, and South of river: Ty = 5 kPa
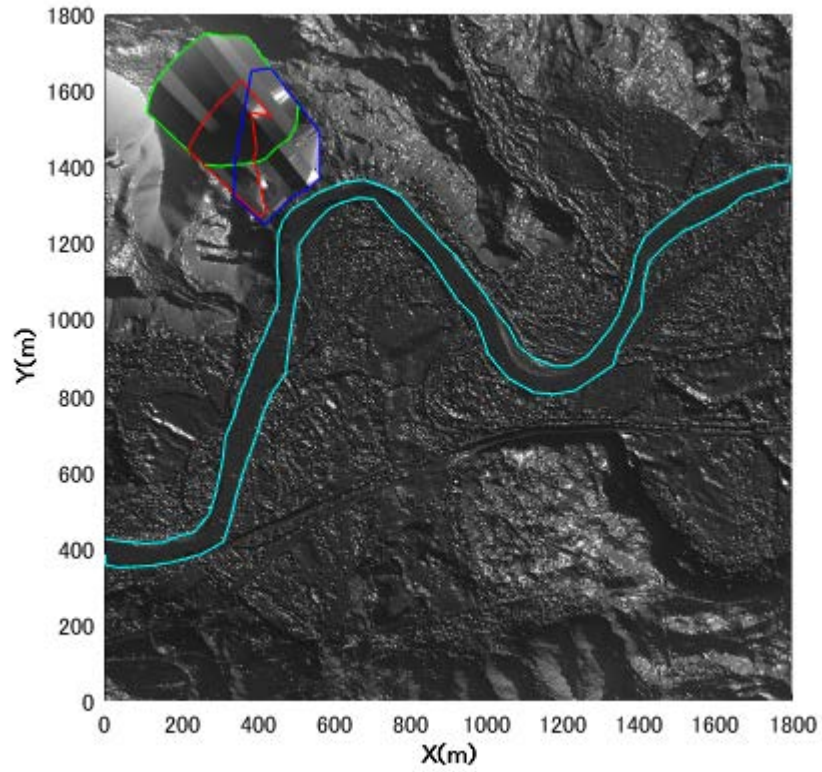
Figure K-21. Material parameters for Scenario 2: The 2006 debris field from the 2006 Hazel landslide has been removed and the river moved back to its original position. M1 (Blue): Ty = 25 kPa, M2 (Red): Ty = 25 kPa, M3 (Green): Ty = 50 kPa, River (Cyan): Ty = 1 Pa, and South of river: Ty = 5 kPa.

7.3 Results

Scenario 1 (Actual 2014 SR-530 landslide with the 2006 debris field in place)

The results of the 3D runout analyses of the actual 2014 SR-530 landslide with the 2006 debris field in place are shown in Figure K-22.

M1 and M2 landslides are represented by the blue and red material points. M3 landslide represented by the green material points is initiated at 25 seconds. Furthermore, the yellow solid line indicates the estimated flow extent of the 2014 SR-530 landslide event given in the GEER report (Keaton et al., 2014).
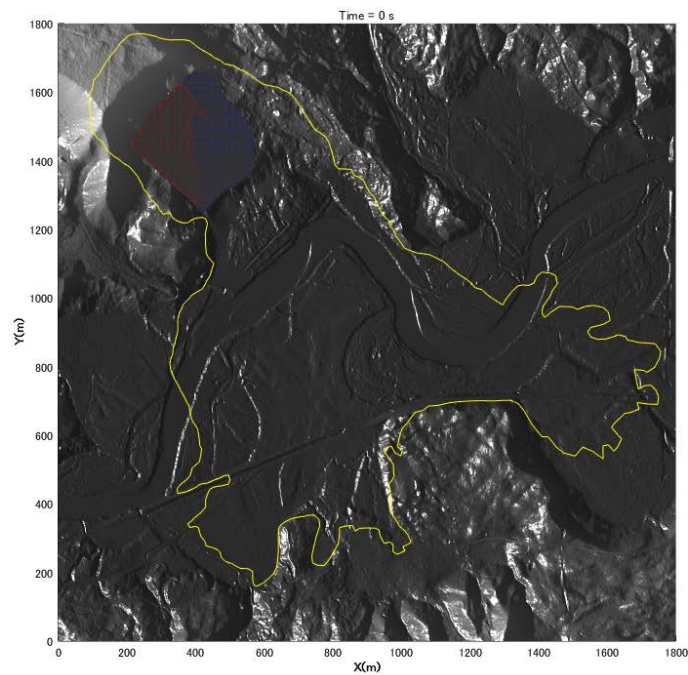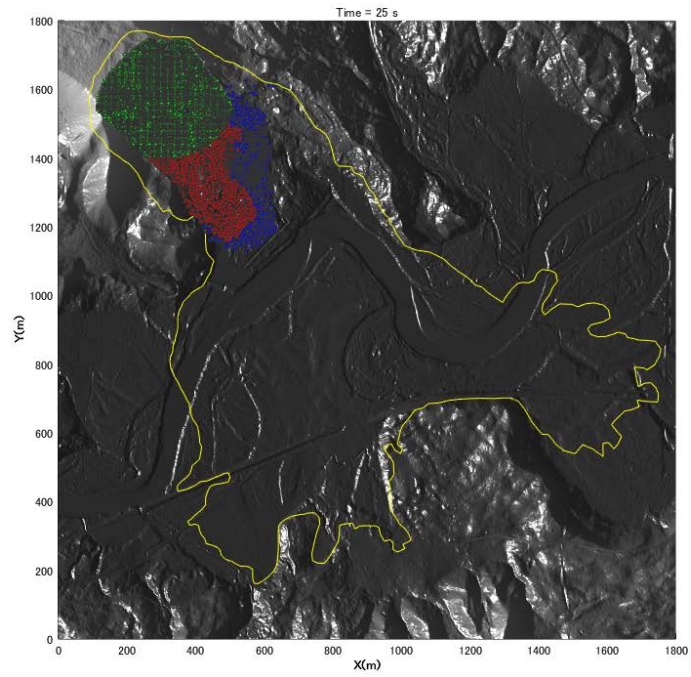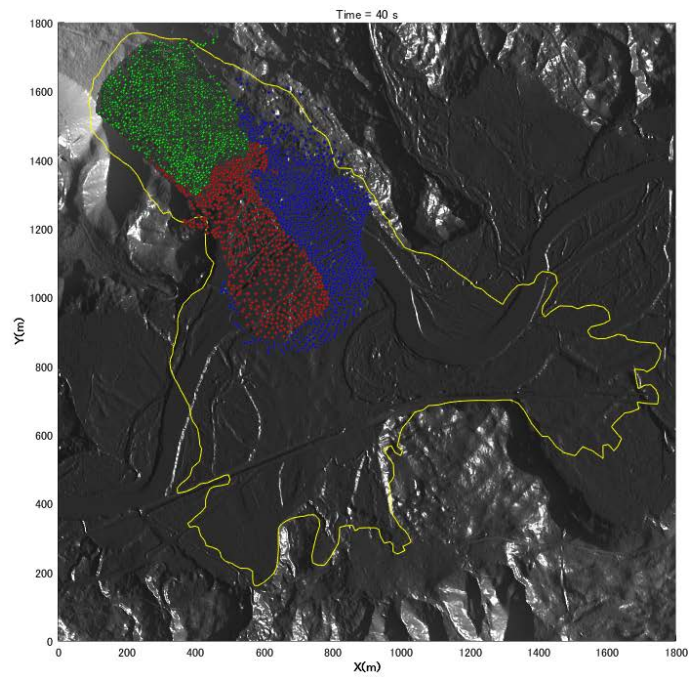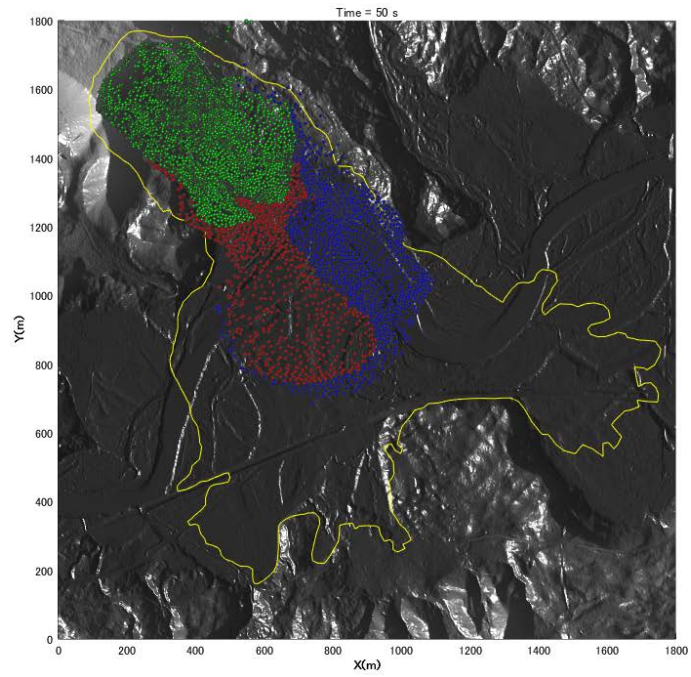
(a) t = 0 s
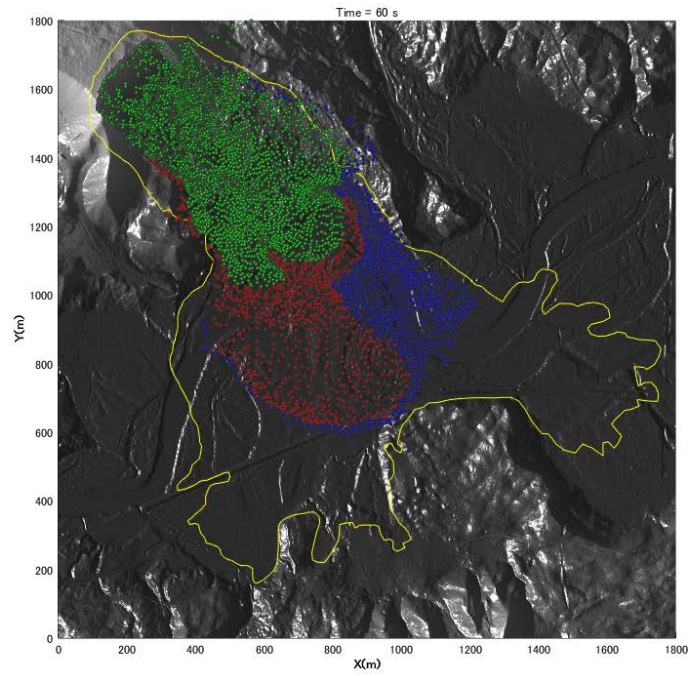
(b) t = 25 s
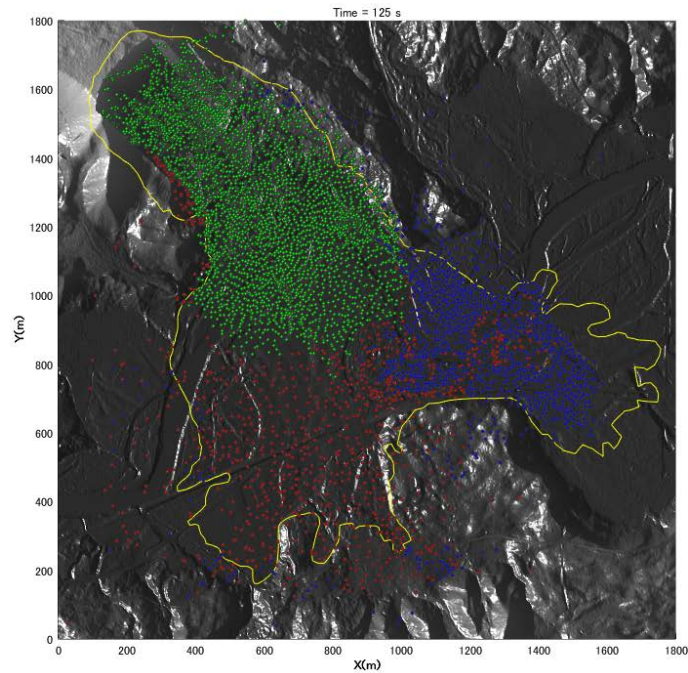
(c) t = 40 s

(d) t = 50 s

(e) t = 60 s

(f) t = 125 s

Figure K-22. *DA-MPM* result for Scenario 1: (a) t = 0 s, (b) t = 25 s, (c) t = 40 s, (d) t = 50 s, (e) t = 60 s, (f) t = 125 s.

Scenario 2 (Hypothetical 2014 SR-530 landslide without the 2006 debris field)

The results of the 3D runout analyses of a hypothetical 2014 SR-530 landslide without the 2006 debris field are shown in Figure K-23.

M1 and M2 landslides are represented by the blue and red material points. M3 landslide represented by the green material points is initiated at 25 seconds. Furthermore, the yellow solid line indicates the estimated flow extent of the 2014 SR-530 landslide event given in the GEER report (Keaton et al., 2014).
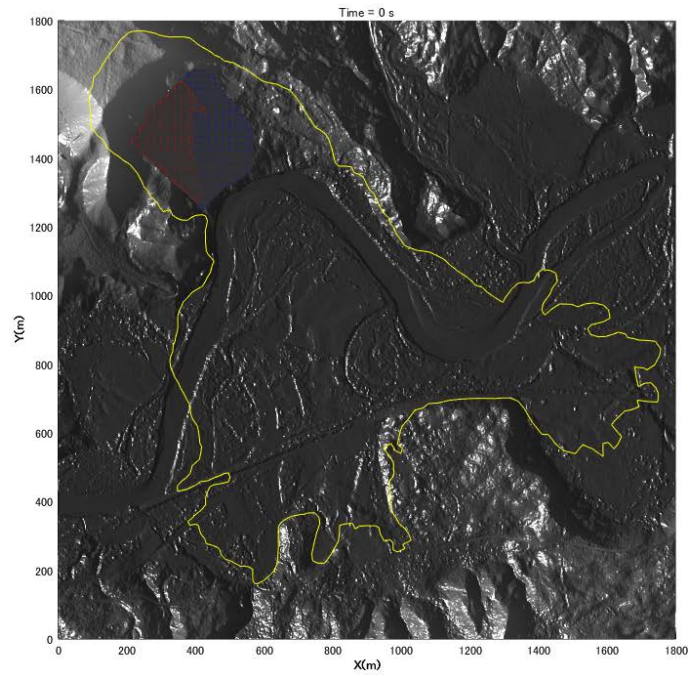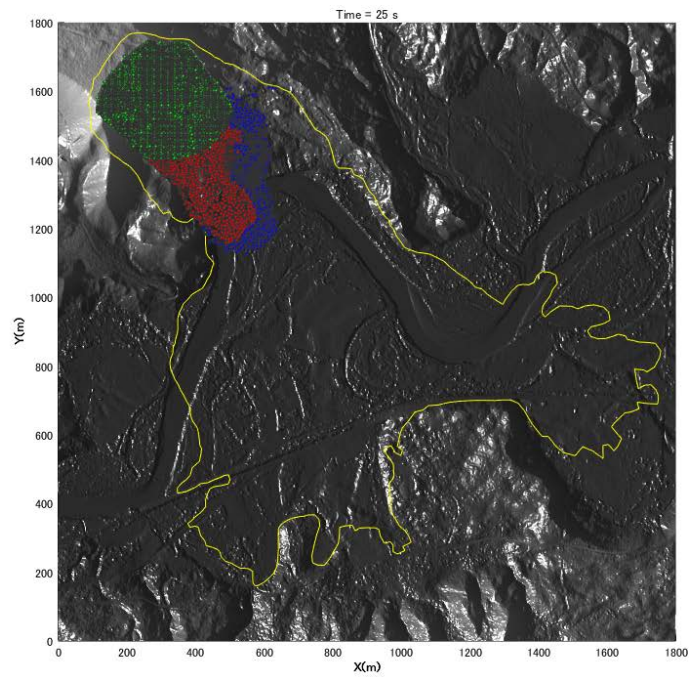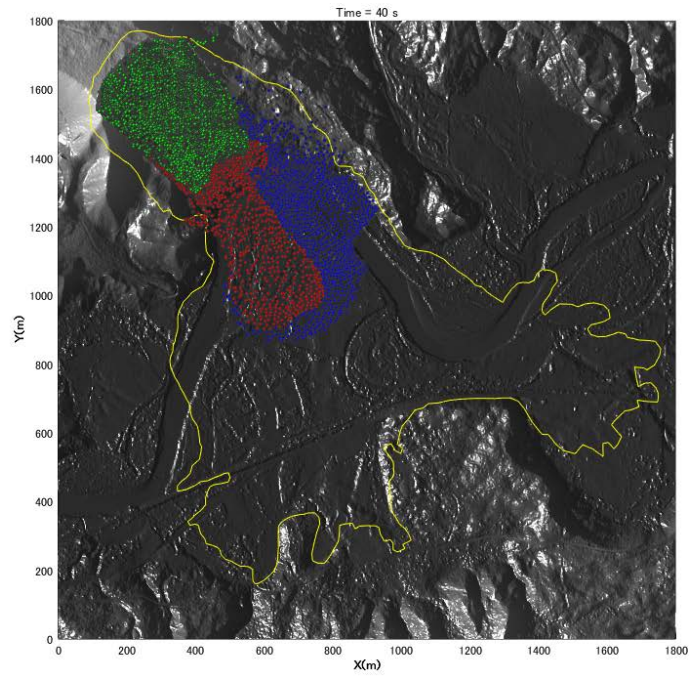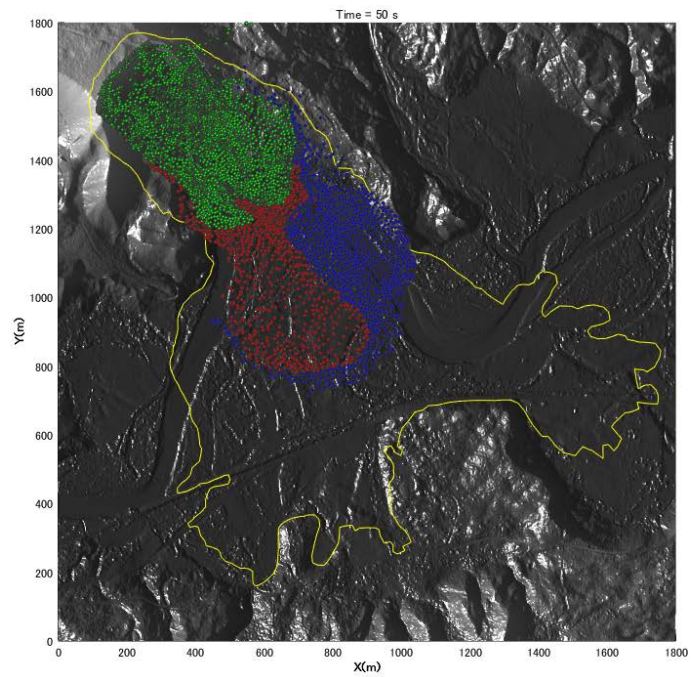
(a) t = 0 s
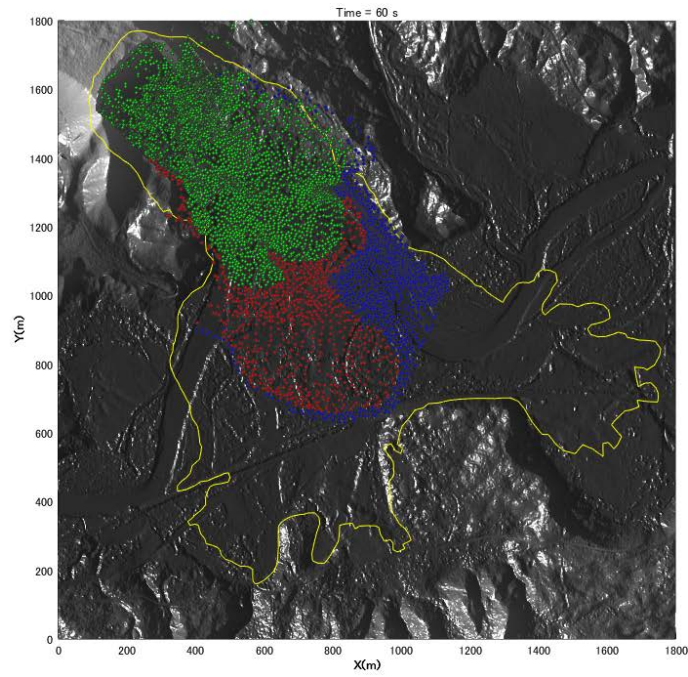
(b) t = 25 s
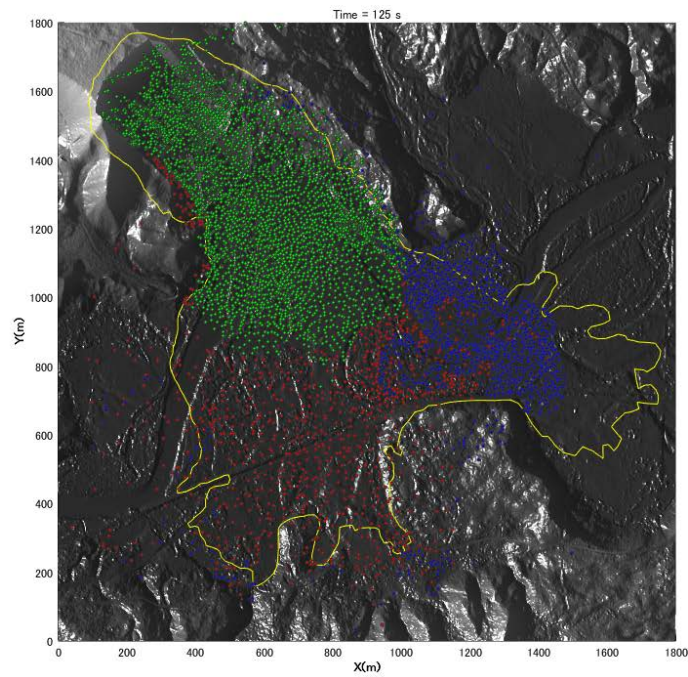
(c) t = 40 s

(d) t = 50 s

(e) t = 60 s

(f) t = 125 s

Figure K-23. *DA-MPM* result for Scenario 2: (a) t = 0 s, (b) t = 25 s, (c) t = 40 s, (d) t = 50 s, (e) t = 60 s, (f) t = 125 s.

In the Scenario 1 case, the spreading pattern of the material points after t = 125 seconds is in general similar to the extent of the final spreading observed in the field, which is shown by the yellow line in Figure K-22. This indicates that the undrained shear strength values evaluated from the plane strain analysis runout simulations presented in the previous sections can be adopted to produce reasonable behavior of the 2014 SR-530 landslide with the depth-averaged analysis. Furthermore, the movement pattern with time is similar to that reported in Iverson and George (2016) even though a direct comparison of results was not attempted in this study.

The Scenario 2 case simulates the runout behavior when the debris material modeled in Scenario 1 is removed, and the North Fork of the Stillaguamish River is placed in its pre-January 2006 Hazel landslide position. The simulation results in Figure K-23 show that the temporal and spatial runout behavior of the Scenario 2 case is similar to that of the Scenario 1 case, which is shown in Figure K-22. In particular, the runout extent and spreading pattern at t = 125 seconds are similar in both cases.

7.4 Findings

The depth-averaged runout model that was generally consistent with the plane strain runout model of the SR-530 landslide was calibrated to capture the observed general characteristics and runout distance of the 2014 SR-530 landslide. This calibrated depth-averaged runout model was rerun with only one change relative to the 2014 SR-530 landslide model (i.e., the 2006 debris field located between the toe of the landslide and the North Fork of the Stillaguamish River was removed) to investigate the potential effects of the absence of the 2006 debris field at the bottom of the slide. The simulated runout behavior of the hypothetical case where there is no debris field below the toe of the 2014 SR-530 landslide is similar to the simulated runout behavior of the actual 2014 SR-530 landslide case. Removal of the debris field does not change the calculated results appreciably. The presence or absence of the debris field is found to be relatively unimportant in these runout analyses.

8. References

Abe, K., Soga, K., and Bandara, S. (2014). "Material Point Method for Coupled Hydromechanical Problems." *Journal of Geotechnical and Geoenvironmental Engineering* Vol. 140, No. 3, 04013033.

Andersen, S., & Andersen, L. (2010). "Modelling of landslides with the material-point method." *Computational Geosciences*, *14*(1), 137–147.

Bandara, S. and Soga, K. (2015). "Coupling of soil deformation and pore fluid flow using material point method." *Computers and Geotechnics*, Vol. 63, 199-214.

Denlinger, R. P., & Iverson, R. M. (2004). "Granular avalanches across irregular three-dimensional terrain: 1. Theory and computation." Journal of Geophysical Research, 109(F1), F01014.

Hungr, O., & McDougall, S. (2009). "Two numerical models for landslide dynamic analysis." Computers & Geosciences, 35(5), 978–992.

Imran, J., G. Parker, J. Locat, & H. Lee (2001). "1d numerical model of muddy subaqueous and subaerial debris flows." *Journal of hydraulic engineering*, 127(11), 959–968.

Iverson, R. M., D. L. George, K. Allstadt, M. E. Reid, B.D. Collins, J.W. Godt, C.M. Cannon,

C.S. Magirl, R.L. Baum, & J.A. Coe. (2014). "Landslide mobility and hazard: implications of the 2014 Oso disaster," *Earth and Planetary Science Letters*, 412, 197-208.

Iverson, R.M. & George, D.L. (2014). "A depth-averaged debris-flow model that includes the effects of evolving dilatancy, I. Physical basis." *Proc. R. Soc. A*, 470, pp. 20130819.

Iverson, R.M. & George, D.L. (2016) "Modelling landslide liquefaction, mobility bifurcation and the dynamics of the 2014 Oso disaster." *Geotechnique*, Vol. 66, 175-187.

Keaton, J.R. et al. (2014). "The 22 March 2014 Oso Landslide, Snohomish County, Washington. s.l.", Geotechnical Extreme Events Reconnaissance (GEER) Report GEER-036; doi:10.18118/G6V884.

Kobayashi, T., Soga, K. and Dimmock, P. (2015). "Numerical analysis of submarine debris flows based on critical state soil mechanics." *Frontiers in Offshore Geotechnics III - 3rd International Symposium on Frontiers in Offshore Geotechnics*, ISFOG 2015, 975-980

Mazzanti, P. & Bozzano, F. (2009). "An equivalent fluid/equivalent medium approach for the numerical simulation of coastal landslides propagation: theory and case studies." *Natural Hazards and Earth System Science,* 9(6), 1941–1952.

Pastor, M., Quecedo, M., Gonzalez, E., Herreros, M. I., Merodo, J. A. F., & Mira, P. (2004). "Simple approximation to bottom friction for Bingham fluid depth integrated models." Journal of Hydraulic Engineering", 130, 149-155.

Savage, S. B. & Hutter, K. (1991). "The dynamics of avalanches of granular materials from initiation to runout. Part I: Analysis." *Acta Mech.* 86, 201–223.

Soga, K., Alonso, E., Yerro, A., Kumar, K., & Bandara, S. (2015). "Trends in large-deformation analysis of landslide mass movements with particular emphasis on the material point method." *Géotechnique*, *66*(3), 248–273.

Sulsky, D., Chen, Z., & Schreyer, H. L. (1994). "A particle method for history-dependent materials." *Computer Methods in Applied Mechanics and Engineering*, *118*(1–2), 179–196

Sulsky, D., Zhou, S.-J. & Schreyer, H. L. (1995). "Application of a particle-in-cell method to solid mechanics." *Computer Physics Communications* 87(1), 236–252.

Yerro, A., Alonso, E., & Pinyol, N. (2015). "The material point method for unsaturated soils." *Géotechnique*, *65*(3), 201–217.

Yerro, A., Pinyol, N. M., & Alonso, E. E. (2015). "Internal Progressive Failure in Deep-Seated Landslides." *Rock Mechanics and Rock Engineering*, 1–16.

Zabala, F., & Alonso, E. E. (2011). "Progressive failure of Aznalcóllar dam using the material point method." *Géotechnique*, *61*(9), 795–808.

APPENDIX L

J. David Rogers Declaration

**STATE OF WASHINGTON
KING COUNTY SUPERIOR COURT**

RYAN M. PSZONKA, et al.,	
Plaintiffs,	No. 14-2-18401-8 SEA
v.	DECLARATION OF J. DAVID
SNOHOMISH COUNTY, et al.,	ROGERS IN SUPPORT OF STATE'S SECOND MOTION FOR SUMMARY
Defendants.	JUDGMENT

TIM WARD, et al.,	
Plaintiffs,	
v.	
SNOHOMISH COUNTY, et al.,	No. 14-2-29255-4 SEA
Defendants.	

GREGORY REGELBRUGGE, et al.,	
Plaintiffs,	
v.	No. 15-2-01672-5 SEA
STATE OF WASHINGTON, et al.,	
Defendants.	

RANDI LESTER, et al.,	15-2-02098-6KNT
Plaintiffs,	

DECLARATION OF J. DAVID ROGERS   1

ATTORNEY GENERAL OF WASHINGTON
Torts Division
7141 Cleanwater Drive SW
PO Box 40126
Olympia, WA 98504-0126
(360) 586-6300

1 v.

2 SNOHOMISH COUNTY, et al.,

3   Defendants.

4   I, J. DAVID ROGERS, declare as follows:

5   1. I am over the age of eighteen, am competent to testify and have personal knowledge of

6   the matters stated below.

7   2. I hold the Karl F. Hasselmann Chair in Geological Engineering in the Department of

8   Geosciences and Geological and Petroleum Engineering at the Missouri University of

9   Science & Technology. I have 35 years of experience in evaluating the stability of

10   natural slopes, embankments, stream channels, highways and hydraulic structures.

11   Between 1979 and 2001, I managed over 500 projects in the western United States,

12   Hawaii, Taiwan, the Philippines and the Middle East. I have served as principal

13   investigator for scientific research funded by the National Science Foundation, U.S.

14   Geological Survey, Federal Highway Administration, Department of Defense and the

15   California and Missouri Departments of Transportation. Much of my research over the

16   past 15 years has focused on regional landslide hazard mapping, in the United States,

17   Ethiopia, Pakistan, and Nepal. I have also studied long-runout landslides in California,

18   Colorado, Alaska, Wyoming, Montana, Washington, Pakistan, and Papua New Guinea.

19   I have served on a number of panels, including the National Academies panel on

20   'Levees and the National Flood Insurance Program,' the Technical Advisory

21   Committee on Regional Geologic Studies and Slope Stability Modeling for the

22   California Geological Survey, and the Building Codes and Dam Safety Committees of

23   the Association of Environmental & Engineering Geologists.

DECLARATION OF J. DAVID ROGERS   2

ATTORNEY GENERAL OF WASHINGTON
Torts Division
7141 Cleanwater Drive SW
PO Box 40126
Olympia, WA 98504-0126
(360) 586-6300

3. In May 2015, the Court granted the State's request for time in which to conduct a geotechnical study of the SR530 Landslide to better understand the cause of the event. This study is currently ongoing. The geotechnical study includes (a) geologic field mapping; (b) geotechnical soil borings to examine soil stratigraphy and location of the landslide's basal surface of rupture (defined in Exhibit T) (c) geotechnical laboratory testing to determine engineering properties of the soils; (d) monitoring of groundwater levels; (e) installation of slope inclinometers to monitor subsurface movements within and adjacent to the landslide mass; and (f) rain gages to correlate precipitation events with groundwater fluctuations on Whitman Bench and within the SR530 Landslide mass.

4. I have direct, first-hand knowledge of the site, having spent several days at the site (starting in the summer of 2014 and continuing through the present), traversing Whitman Bench, Headache Creek basin, the body of the landslide, and the lower portions of the landslide, north and south of the Stillaguamish River. Our site-specific geotechnical exploration program consisted of 12 geotechnical soil borings with near continuous soil sampling, ranging in depths from about 100 ft to 600 ft; three Cone Penetration Tests (CPTs) ranging in depth from 20 ft to 100 ft; one standpipe to facilitate manual water level readings; installation of over 30 vibrating wire piezometers to monitor groundwater levels within specific horizons; and installation of five (5) inclinometers to monitor slope movements over time. I have personally been onsite during execution of this program. I have personally walked the Headache Creek drainage, observing the seeps emanating from the Whitman Bench, seeps emanating

1   from Headache Creek basin into the old Hazel Landslide area (at approximately El.

2   +500 ft), active ponding within the landslide complex (between El. +280 ft and +500

3   ft), and exposures of the pre-glacial "Olympia" sands at the western and eastern

4   margins of the 2014 landslide. I have engaged in regular meetings with other members

5   of the State's expert witness team who have actively participated in the geotechnical

6   exploration program since May 2015, as well as periodic teleconferences during the

7   geotechnical exploration program to address unexpected conditions, proposed

8   modifications, and review of preliminary results.

9

10   5. It should be noted that the Hazel Landslide is different from the SR530 Landslide event

11   of March 22, 2014. As shown in Exhibit U, the pre-existing Hazel Landslide was

12   constrained to the eastern portion of the SR530 Landslide, and had been active, at a

13   minimum, for decades. It emanated from a much lower elevation profile (its upper

14   surface being near El. + 700 ft), and consisted primarily of prehistoric landslide debris

15   from an older, much larger, landslide movement. The SR530 Landslide occurred west

16   of and included the Hazel Landslide, with its upper surface at a much higher elevation

17   (~El. +890 ft). The majority of the impacted soils were intact prior to the failure of

18   March 22, 2014, not having experienced any pervious disturbance. These two

19   landslides appear to have different footprints, different soil compositions, different

20   groundwater regimes, and different causal mechanisms.

21

22   6. The Crib Wall and Settling Pond were installed following movements of the Hazel

23   landslide in January 2006, where material slid down into the North Fork of the

24   Stillaguamish River, forcing the channel to the south about ~700 feet (Exhibit V). The

Crib Wall alignment ranged in elevation from a high point of approximately El. + 274 ft to a low of approximately El. +268 ft (based on the 2013 Aerial LiDAR). At this time, the river surface was approximately El. +260 ft. The Settling Pond was situated at approximately El. + 268 ft (Exhibit W).

7. There are three potential impacts of the 2006 Crib Wall on subsequent slope stability: (1) elevating groundwater levels within the 2014 SR530 Landslide mass, so as to decrease the stability of the slope; (2) increasing flow velocities of the Stillaguamish River so as to exacerbate bank erosion which would undermine the toe of surface rupture; and (3) the Crib Wall provided lateral support of the slope by creating a 'toe berm' that acted as a 'door stop' to keep the hillside propped up. The Settling Pond only has one potential impact on stability, which is the potential to elevate groundwater levels within the toe area of the 2014 SR530 Landslide, thereby decreasing the stability of that mass.

8. While the geotechnical study work is currently underway, I have collected and/or reviewed site-specific data that eliminates the Stillaguamish River Crib Wall and Settling Pond as potential contributors to exacerbating, causing, or in any way triggering the failure of the SR530 Landslide. This data includes:

    a. SR530 Landslide Surface of Rupture – The soil borings performed on the body of the landslide (Exhibit X) located the 2014 surface of rupture, which exhibited a pattern and geometry consistent with the observed ground features. The collar elevation of soil boring EB-04si-15 was at a ground elevation of +538.3 ft, with the surface of rupture located at a depth of 134.5 ft (El. +403.8 ft). The collar

DECLARATION OF J. DAVID ROGERS   5   ATTORNEY GENERAL OF WASHINGTON
Torts Division
7141 Cleanwater Drive SW
PO Box 40126
Olympia, WA 98504-0126
(360) 586-6300

elevation of soil boring EB-12si-15 was at a ground elevation of +439.2 ft, with

the surface of rupture located at a depth of approximately 119 ft (El. +320.2 ft).

The collar elevation of soil boring EB-09si-15 was at a ground elevation of

+380.2 ft, with the surface of rupture located at a depth of approximately 40 ft

(El. +340.2 ft). This field data establishes that the lowest elevation of the

surface of rupture is El. +320 ft; which is more than 40 ft above the top of the

Crib Wall and over 50 ft above the Settling Pond.

b. SR530 Landslide Surface of Rupture Disconnected From Crib Wall and Settling

Pond – The location of the 2014 landslide surface of rupture above El. +320 ft

eliminates any physical connection from channel scour at the Crib Wall,

saturated soils contained within the Settling Pond, or drainage channels flowing

into the Settling Pond. This physical separation also eliminates any

destabilizing effects associated with erosion/scour along the Crib Wall. The

2006 debris field slowed the rate of erosion of material from the main body of

the 2006 Hazel Landslide, as the materials stabilized themselves through natural

drainage and vegetation. The 2006 debris field also served to slow the northerly

migration of the river channel, which had the potential to destabilize the Hazel

slide, as it then existed.

c. Permeable "Olympia" Sands beneath Surface of Rupture– The 2014 SR530

Landslide surface of rupture is underlain by fine-grained, cross-bedded sand.

This sand was encountered in EB-04-15, EB-09-15, EB-12-15, and H-1vwp-14

(which was performed by WSDOT in October of 2014. The sand is also visible

in exposures on the west and east margins of the 2014 landslide complex. Instruments installed in H-1vwp-14 suggests that the groundwater level is situated at approximately El. +280 ft (Exhibit Y); which is the same elevation as the Stillaguamish River at this time. This establishes a regional groundwater level within the permeable fine-grained sands that generally corresponds to the surface elevation of the river (after the 2014 landslide). It also establishes a groundwater gradient within the "Olympia" sand that appears to be less than one (1) percent. In order for groundwater to be elevated up to the landslide's basal surface of rupture, a groundwater gradient of more than nine (9) percent would be required. A gradient of this magnitude would be wholly unsupportable due to the permeability of the "Olympia" sands and lack of confinement on the western and eastern margins, which would naturally tend to drain any elevated groundwater pressures.

d. <u>Lacustrine clay overlying the "Olympia" Sand</u> – An extensive deposit of lacustrine clay (Clay) overlies the "Olympia" sands from approximately El. +310 ft to El. +600 ft. The Clay is essentially impermeable compared to the sand, and any surface water, from precipitation or seepage, tends to be perched <u>on top of</u> the clay, or forms ponds of water lying on top of the clay. Retrogressive slumping and slump-earthflow slides from the old Hazel slide extended down slope to the Stillaguamish River and have been documented as far back as 1952 (Exhibit Z). A review of the 1952 map prepared by Shannon & Associates clearly maps springs ("Slide Creek" and "Mud Flow Creek")

flowing from the slide area down to the North Fork of the Stillaguamish River.

A review of imagery available from 2003 shows active discharge from the Hazel Landslide mass into the river. Following the January 2006 Hazel Landslide and construction of the Crib Wall and Settling Pond, evidence of surface flow and formation of a sediment delta in the western corner of the slide (into the Settling Pond) are easily observed. Following the SR530 Landslide in March of 2014, which fully displaced and removed both the Crib Wall and Settling Pond, surface water and active ponding can still be observed on the main body of the landslide. The 1952, 2003, and 2014 images demonstrate that drainage from the slide into the Stillaguamish River appear to be linked to the groundwater characteristics of the active Hazel Landslide, and were not the result of construction of the Crib Wall and/or the Settling Pond, as surface water and ponding was present before and after construction of the Crib Wall and Settling Pond in the late summer of 2006 (Exhibit AA).

9. Exhibit BB shows a summary of the 2014 SR530 Landslide's basal surface of rupture, as determined from our geotechnical exploration and field mapping of exposed outcrops to date. The lowest elevation of this failure surface is El. +310 ft to +320 ft, which places the surface of rupture well above any of the debris associated with the 2006 Hazel Landslide, the Settling Pond, or the Crib Wall. Groundwater would need to be elevated to more than the height of a three story building in order to influence the surface of rupture. Even with active surface flow and standing pools of water within the slide mass (similar to conditions following the 2006 Hazel Landslide), an extreme

water rise is not supported by instrumentation installed at the site today, which suggests groundwater levels within the permeable "Olympia" sands track closely with the river flow levels. Additionally, as illustrated in Exhibit BB the Crib Wall is located more than 600 feet from the 2014 SR530 surface of rupture, so any erosion/scour at the Crib Wall would have had no effect on the stability of the SR530 Landslide mass.

10. The virgin rupture surface of the 2014 SR530 landslide exited the slope at the toe of surface of rupture (Exhibits T and BB). From this point, the mobilized slide debris would have dropped approximately 30 vertical feet, over the erosional escarpment excavated into the "Olympia" sands. The contact between the moving mass of landslide debris is commonly referred to as a "surface of separation" (Exhibit T), which denotes the contact as a structure formed subsequent to the initial movement along a basal surface of rupture. The surface of rupture is the bounding discontinuity controlling any back-analysis of the 2014 landslide mass, as the ground lying south of the surface of separation was infilled and buried as the debris translated across this low-lying area (Exhibit BB).
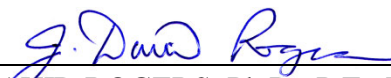
11. In summary, the data collected to date, through this site-specific geotechnical exploration program, eliminates the Stillaguamish River Crib Wall and Settling Pond as potential contributors to causing/triggering the failure of the SR530 Landslide. None of the three potential Crib Wall impacts {(1) elevating groundwater levels above the landslide's basal surface of rupture so as to decrease the stability of the slope; (2) increasing flow velocities of the Stillaguamish River so as to exacerbate bank undercutting and erosion; (3) the Crib Wall provides support for the slope by creating a

‘toe berm’ that acts as a ‘door stop’ to keep the hillside propped up} or the potential impact of the Settling Pond elevating groundwater levels above the landslide's basal surface of rupture so as to decrease the stability of the slope are feasible. The suite of available physical evidence demonstrates that these potential impacts are not pertinent.

12. This declaration is a simplification of the data acquired and analyses that I performed and would be prepared to present at trial.

I declare under penalty of perjury under the laws of the State of Washington, that the foregoing is true and correct.

DATED this 5th day of November, 2015, in Rolla, Phelps County, Missouri.

_____
J. DAVID ROGERS, Ph.D., P.E., P.G., C.E.G., C.HG.

DECLARATION OF J. DAVID ROGERS   10   ATTORNEY GENERAL OF WASHINGTON
Torts Division
7141 Cleanwater Drive SW
PO Box 40126
Olympia, WA 98504-0126
(360) 586-6300

PROOF OF SERVICE

I certify that I served a copy of this document on all parties or their counsel of record on the date below as follows:

☒ Electronic Mail

Counsel for Pszonka Plaintiffs:

Guy Michelson	gmichelson@corrcronin.com
Emily Harris	eharris@corrcronin.com
Dave Edwards	dedwards@corrcronin.com
	lnims@corrcronin.com
	elesnick@corrcronin.com

Counsel for Ward Plaintiffs:

Corrie Yackulic	corrie@cjylaw.com
	dianna@cjylaw.com
	clerk@cjylaw.com
John Phillips	jphillips@jphillipslaw.com
Michael Madderra	mmadderra@jphillipslaw.com
	kharrison@jphillipslaw.com
	hhoffman@jphillipslaw.com

Counsel for Regelbrugge Plaintiffs:

Karen Willie	kwillie@tmdwlaw.com
	williewaterlaw@outlook.com
Toby Marshall	tmarshall@tmdwlaw.com
Janay Ferguson	jferguson@tmdwlaw.com
	jboschen@tmdwlaw.com
	hhair@tmdwlaw.com
	filing@tmdwlaw.com

Counsel for Lester Plaintiffs:

Darrell Cochran	darrell@pcvalaw.com
Loren Cochran	loren@pcvalaw.com
	ksnyder@pcvalaw.com
	laura@pcvalaw.com

1

ATTORNEY GENERAL OF WASHINGTON
Torts Division
7141 Cleanwater Drive SW
PO Box 40126
Olympia, WA 98504-0126
(360) 586-6300

Counsel for Defendant Snohomish County:

Joseph Genster	joseph.genster@co.snohomish.wa.us
Michael Held	mheld@co.snohomish.wa.us
	steven.beard@co.snohomish.wa.us
Timothy G. Leyh	timl@calfoharrigan.com
Randall Thomsen	randallt@calfoharrigan.com
Kristin Ballinger	kristinb@calfoharrigan.com
	lynnv@calfoharrigan.com
	susiec@calfoharrigan.com
	kelliemc@calfoharrigan.com

Counsel for Defendant Grandy Lake Associates:

Elaine Spencer	elaine.spencer@millernash.com
Diane Meyers	diane.meyers@millernash.com
Vanessa Wheeler	vanessa.wheeler@millernash.com
Madeline Engel	madeline.engel@millernash.com
	donna.cauthorn@millernash.com
	dlizabeth.anderson@millernash.com
	kristine.couden@millernash.com

Co-Counsel for Defendants State of Washington:

Robert Christie	bob@christielawgroup.com
Ann Trivett	ann@christielawgroup.com
Haley Moore	haley@christielawgroup.com
	salim@christielawgroup.com

I certify under penalty of perjury under the laws of the state of Washington that the foregoing is true and correct.

DATED this ⟨6th⟩ day of November, 2015, at Tumwater, Washington.

DIANE HOOSIER
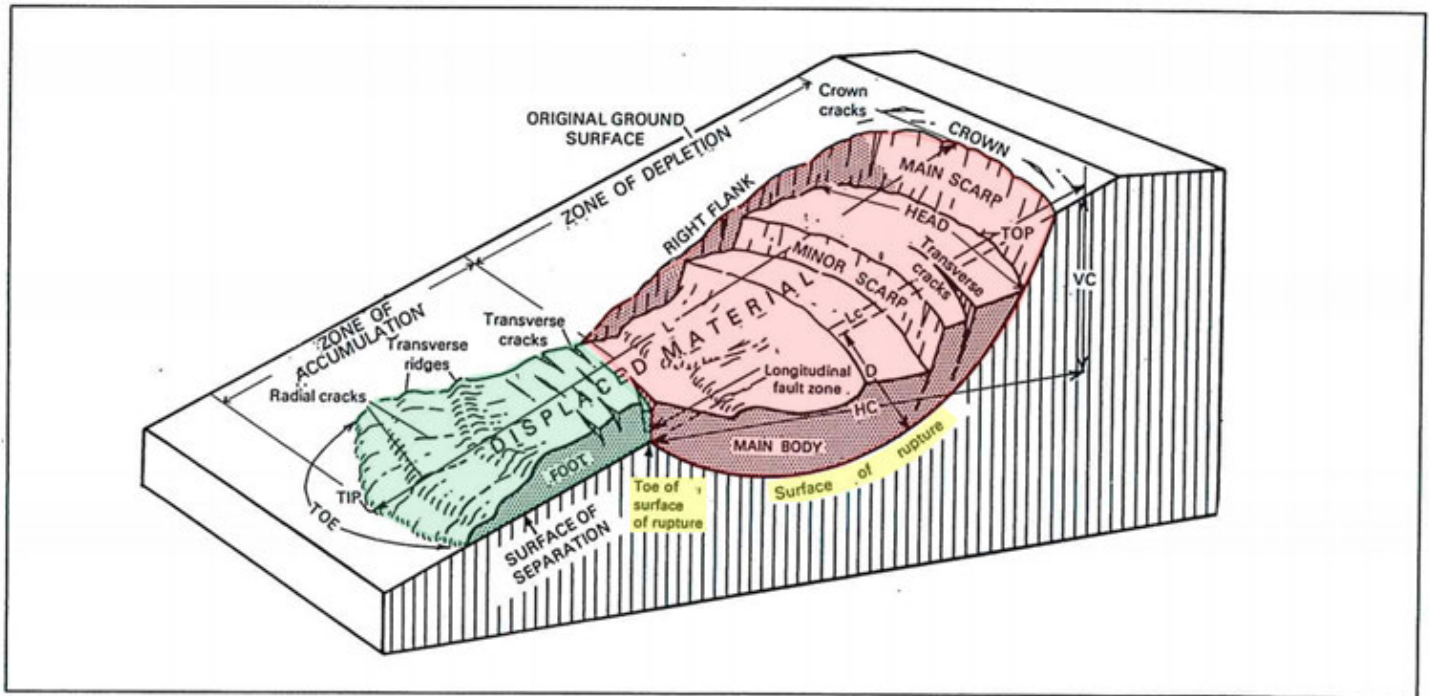
Table 3-3
Definitions of Landslide Features

NUMBER	NAME	DEFINITION
1	Crown	Practically undisplaced material adjacent to highest parts of main scarp
2	Main scarp	Steep surface on undisturbed ground at upper edge of landslide caused by movement of displaced material (13, stippled area) away from undisturbed ground; it is visible part of surface of rupture (10)
3	Top	Highest point of contact between displaced material (13) and main scarp (2)
4	Head	Upper parts of landslide along contact between displaced material and main scarp (2)
5	Minor scarp	Steep surface on displaced material of landslide produced by differential movements within displaced material
6	Main body	Part of displaced material of landslide that overlies surface of rupture between main scarp (2) and toe of surface of rupture (11)
7	Foot	Portion of landslide that has moved beyond toe of surface of rupture (11) and overlies original ground surface (20)
8	Tip	Point on toe (9) farthest from top (3) of landslide
9	Toe	Lower, usually curved margin of displaced material of a landslide, most distant from main scarp (2)
10	Surface of rupture	Surface that forms (or that has formed) lower boundary of displaced material (13) below original ground surface (20); mechanical idealization of surface of rupture is called *slip surface* in Chapter 13
11	Toe of surface of rupture	Intersection (usually buried) between lower part of surface of rupture (10) of a landslide and original ground surface (20)
12	Surface of separation	Part of original ground surface (20) now overlain by foot (7) of landslide
13	Displaced material	Material displaced from its original position on slope by movement in landslide; forms both depleted mass (17) and accumulation (18); it is stippled in Figure 3-4
14	Zone of depletion	Area of landslide within which displaced material (13) lies below original ground surface (20)
15	Zone of accumulation	Area of landslide within which displaced material lies above original ground surface (20)
16	Depletion	Volume bounded by main scarp (2), depleted mass (17), and original ground surface (20)
17	Depleted mass	Volume of displaced material that overlies surface of rupture (10) but underlies original ground surface (20)
18	Accumulation	Volume of displaced material (13) that lies above original ground surface (20)
19	Flank	Undisplaced material adjacent to sides of surface of rupture; compass directions are preferable in describing flanks, but if left and right are used, they refer to flanks as viewed from crown
20	Original ground surface	Surface of slope that existed before landslide took place

Exhibit T

2006 LiDAR

SR530 Landslide

Hazel Landslide

legend

Elevation (ft) NAVD88

900.000ft
700.000ft
500.175ft
500.000ft
352.443ft
351.221ft
350.000ft
343.111ft
260.000ft

Exhibit U

Legend
— 2003 River Margin
— CribWall
▨ Pond

250 125 0 250 Feet

Legend
— 2003 River Margin
— CribWall
▨ Pond

250 125 0 250 Feet

Exhibit V

El.+800 ft

El.+700 ft

El.+600 ft

El.+500 ft

El.+400 ft

El.+300 ft

Crib Wall
(El.+268 to +274 ft)

Landslide Debris

Pond
(El.+268 ft)

Exhibit W

Geotechnical Exploration Points

EB-11-15

EB-08-15

EB-01-15

EB-10-15

EB-02-15

EB-06-15

H-1vwp-14

EB-03-15

EB-05-15

EB-04si-15; CPT17-15; EB-14-15

EB-12si-15; CPT16-15; H15-15

EB-09si-15; H13-15; CPT19-15

250   0   250   500   750   1000 ft
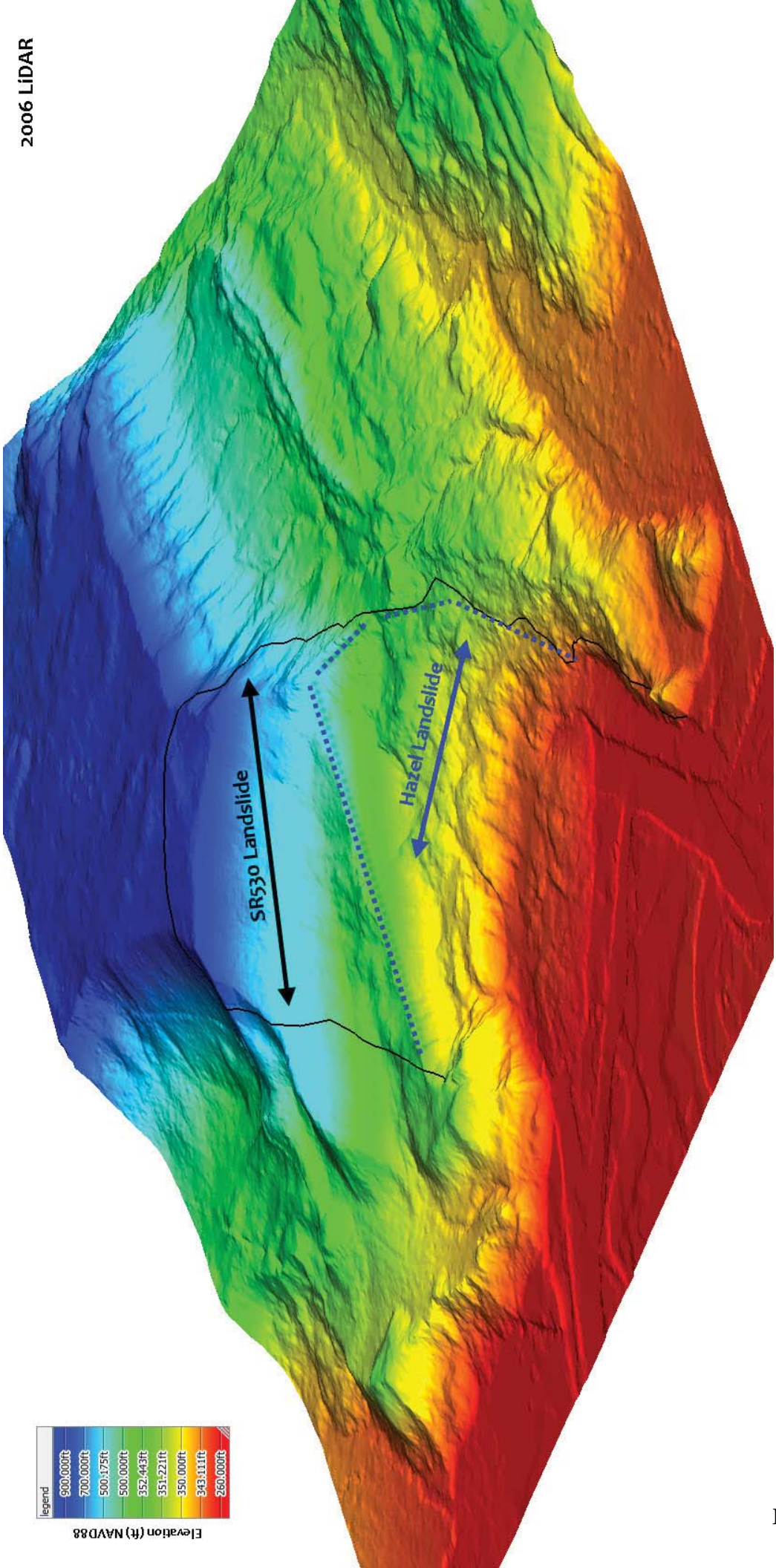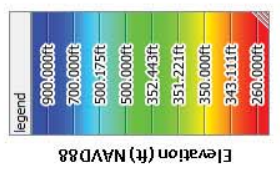
Exhibit X

Piezometer H-1vwp-14 @ depth=625 ft

Exhibit Y

STATE OF WASHINGTON
DEPARTMENT OF GAME

PLAN OF SLIDE AREA
NEAR HAZEL, WASH.
NORTH FORK STILLAGUAMISH RIVER

W. D. SHANNON & ASSOC. ENGINEERS
SEATTLE, WASHINGTON

SCALE IN FT.

DR. BY: R.H.E.
CH. BY: W.L.S.
DATE: FEB. 14, 1952

PLATE 2

LEGEND

—— Spring
⌇⌇⌇⌇ Steep Slope
⌢⌢⌢⌢ Edge of Wooded area

NOTES

Topography traced from map prepared by State of Washington Department of Game, "Fifteen Acre Topography Stillaguamish River Slide", "Topography Surveys made by Department of Game, October–December 1951. Arbitrary B.M. at 7.0.00 established at Elev. 300.00
For Sections 1-1 through 2-2, see Plate 3

SLIDE AREA 1
SLIDE AREA 2
SLIDE AREA 3

STILLAGUAMISH RIVER

HADAPSH CREEK

Proposed Diversion of Headach Creek S=0.005

Area Being Logged Sep–Dec., 1951

Logging Road

Proposed Diversion Ditch S=0.005

Mud Flow December 1951

Gravel Bar

Brush and Hardwoods

Logging Trail

TYPICAL SECTION "6-6"

Present ground surface
Asphalt Membrane with 6" cover where ditch is located in sand or sand gravel.
1½:1 slopes
10'
15 Min

SECTION "5-5"
TYPICAL

Present Ground surface

LOG OF BORINGS

B-1   B-2   B-3   B-4

* Indicates water lost during boring.
Number in column on right are no. of blows required to drive sampling pipe one foot, using 140 lb. hammer falling 30 inches

Exhibit Z

WA DNR NW C 2003

Water Flow

Water Flow/
Delta

Legend
2003 River Margin
CribWall
Pond

SR530_RGB_OrthoMosaic_05012014

Pond

Pond

Pond

Pond

Pond

Water Flow/
Delta

Legend
2003 River Margin
CribWall
Pond

300 150   0   300 Feet

LOG of BORINGS

RIVER

STILLAGUAMISH

Water Flow

Water Flow

Snohomish County 2007 Tiles

Water Flow

Water Flow/
Delta
Pond

Legend
2003 River Margin
CribWall
Pond

Exhibit AA

LiDAR Survey
- - - - 2003
——— 2013
——— 2014

Crib Wall (2014)

Settling Pond (2014)

Groundwater would need to rise the height of a 3-story building to reach the surface of rupture.

2014 Toe of Surface of Rupture

EB-09si-15

2014 Toe of Surface of Rupture

Settling Pond (2014)

Crib Wall (2014)

EB-09si-15

Pre-Landslide Ground Surface

2014 Surface of Rupture

EB-12si-15

EB-04si-15

2014 Post-Landslide Ground Surface

Regional Groundwater within "Olympia" Sands

Lacustrine Clay (low permeability)

Fine-Grained "Olympia" Sands (permeable)

H-1vwp-14

VWP@625ft

Elevation (ft) NAVD88

Horizontal Distance (ft)

Legend

Exhibit BB

APPENDIX M

Standard of Care

1   In summary Judgement dated May 11th, 2106 [NO. 14-2-18401-8 SEA], Judge Rogoff stated,

2

3   "The Court declines to allow this case to go forward based on the State's involvement in the

4   cribwall/pond project on any theory other than landowner liability."

5

6   This brings rise to the question of the standard of care that a landowner should employ in a case where

7   another party proposes to construct civil works on the landowner's property. Although the standard of

8   care can vary significantly, depending on the size of the project and its footprint on the landowners land,

9   the basic level of standard of care for a modest size project such as the cribwall and pond constructed by

10   the project owner, the Stillaguamish Nation, would include review of the credentials of the designer,

11   possibly the credentials of the construction company, a check to see that the appropriate permits as

12   necessary were obtained, and some level of review of whether the project owner had sufficient funds to

13   complete the project.

14

15   For a modest size project such as the cribwall and pond, a check to see that the designer and the

16   designer's firm were licensed to practice engineering in the State of Washington is sufficient review of

17   the designer's credentials.   The purpose of engineering licensure is to ensure the public that the

18   individuals and firms practicing engineering in the state meet a minimum standard of competence, and

19   will engage in practice within the bounds of statute and engineering ethics. Design of the Crib Wall and

20   Sediment Pond on the North bank of the Stillaguamish River opposite the Steelhead Haven

21   neighborhood was done by GeoEngineers, Inc., an engineering firm that was first licensed for the

22   practice of engineering in the State of Washington on December 12, 1980, and is still licensed. Based on

23   project documents reviewed for this report, the designer of the 2006, post-2006 Hazel Landslide cribwall

24   design was Tracy Drury, a professional engineer in the employ of GeoEngineers who was licensed as a

25   Professional Engineer on June 29, 2004.

26

27   Construction of the Cribwall required a permit from the Washington Department of Fish and Wildlife,

28   and the Army Corps of Engineers, and review by the Department of Ecology to ascertain whether the

29   project would require an individual water quality certification or a Coastal Zone Management

30   consistency determination.   The Washington Department of Fish and Wildlife Hydraulics Project

31   Approval for the project was issued on July 26, 2006, and signed by Ginger Holser, Habitat Biologist.

32   The Army Corps of Engineers Authorization was received in the form of a letter dated August 3, 2006

33   from Susan Glenn, Project Manager of the North Application Review Section, USACE. A letter from the

34   Department of Ecology informing the Stillaguamish Nation that neither an individual water quality

35   certification nor a Coastal Zone Management consistency determination would be required was dated

36   August 7, 2006, and signed by Rebekah R. Padgett, Federal Permit Manager.

37

38